Nonlinear mixed-effects modelling of drug-drug interactions between antiretroviral therapy and tuberculosis treatment

By

Allan Kengo

A Thesis Presented for the Degree of

DOCTOR OF PHILOSOPHY

in the Division of Clinical Pharmacology

Department of Medicine

UNIVERSITY OF CAPE TOWN

Supervisor: Professor Paolo Denti

Co supervisor: Doctor Juan Eduardo Resendiz Galvan

June 2025

Contributions to the field

This thesis includes some of the following contributions to the field of pharmacometrics and clinical pharmacology.

Full-length original articles

1. **Kengo A,** Gausi K, Nabisere R, Musaazi J, Buzibye A, Omali D, Aarnoutse R, Lamorde M, Dooley KE, Sloan DJ, Sekaggya-Wiltshire C, Denti P. 2023. Unexpectedly low drug exposures among Ugandan patients with TB and HIV receiving high-dose rifampicin. Antimicrob Agents Chemother 67:e00431-23. https://doi.org/10.1128/aac.00431-23
2. **Kengo A**, Nabisere R, Gausi K, Musaazi J, Buzibye A, Omali D, Aarnoutse R, Lamorde M, Dooley KE, Sloan DJ, Denti P, Sekaggya-Wiltshire C. 2023. Dolutegravir pharmacokinetics in Ugandan patients with TB and HIV receiving standard- versus high-dose rifampicin. Antimicrob Agents Chemother 67:e00430-23. https://doi.org/10.1128/aac.00430-23
3. **Kengo A,** Resendiz-Galvan JE, Najjemba L, Mugerwa H, De Nicolo A, D'Avolia A, Atoyebi S, Wiesner L, Svensson EM, Waitt C, Denti P. (2024). Model-based evaluation of the interaction between ritonavir-boosted atazanavir and rifampicin in Ugandan adults with HIV. (*Submitted to British Journal of Clinical Pharmacology*)
4. **Kengo A,** Nabeemeeah F, Denti P, Sabet R, Okyere-Manu G, Abraham P, Weisner L, Mosala MH, Tshabalala S, Scholefield J, Resendiz-Galvan JE, Martinson NA, Variava E. 2024. Assessing potential drug-drug interactions between clofazimine and other frequently used agents to treat drug-resistant tuberculosis. Antimicrob Agents Chemother68:e01583-23. https://doi.org/10.1128/aac.01583-23.

The author also contributed to the following articles.

5. Sekaggya-Wiltshire C, Nabisere R, Musaazi J, Otaalo B, Aber F, Alinaitwe L, Nampala J, Najjemba L, Buzibye A, Omali D, Gausi K, **Kengo A**, Lamorde M, Aarnoutse R, Denti P, Dooley KE, Sloan DJ. Decreased Dolutegravir and Efavirenz Concentrations With Preserved Virological Suppression in Patients With Tuberculosis and Human Immunodeficiency Virus Receiving High-Dose Rifampicin. Clin Infect Dis. 2023 Feb 8;76(3):e910-e919. http://doi:10.1093/cid/ciac585 PMID: 35861296; PMCID: PMC10226740.
6. De Nicolò, A., Palermiti, A., Mugerwa, H., Nakabuye, S., Namusanje, J., Kobusingye, J., Odoch, D., Lamorde, M., **Kengo, A.**, Denti, P., Gausi, K., Maartens, G., McIlleron, H., Wiesner, L., Khoo, S., Waitt, C., & D'Avolio, A. (2025). Intracellular Penetration of Atazanavir, Ritonavir and Dolutegravir With Concomitant Rifampicin: A Dose Escalation Study. Clinical Pharmacology & Therapeutics. https://doi.org/10.1002/cpt.3572

Scientific conference abstracts

1. **Allan Kengo**, Juan Eduardo Resendiz-Galvan, Letisha Najjemba, Henry Mugerwa, Amedeo de Nicolò, Antonio D'Avolio, Shakir Atoyebi (5), Lubbe Wiesner (1), Elin M. Svensson, Catriona Waitt, Paolo Denti. Population pharmacokinetic analysis of the drug interaction between ritonavir-boosted atazanavir and rifampicin. 32nd Population Approach Group Europe (PAGE) meeting, Rome, Italy, 26-28 June 2024.
2. **Allan Kengo**, Kamunkhwala Gausi, Ruth Nabisere, Joseph Musaazi, Allan Buzibye, Daniel Omali, Rob Aarnoutse, Mohammed Lamorde, Kelly E. Dooley, Derek James Sloan, Christine Sekaggya-Wiltshire, Paolo Denti. Unexpectedly low drug exposures

among Ugandan patients with TB and HIV receiving high-dose rifampicin. 31st Population Approach Group Europe (PAGE) meeting, A Coruna, Spain, 27 – 30 June 2023.

3. **Allan Kengo**, Kamunkhwala Gausi, Ruth Nabisere, Joseph Musaazi, Allan Buzibye, Rob Aarnoutse, Mohammed Lamorde, Kelly E. Dooley, Derek James Sloan, Paolo Denti, Christine Sekaggya-Wiltshire. Dolutegravir pharmacokinetics in patients receiving standard and higher doses of rifampicin. 3rd World Conference on Pharmacometrics (WCOP), Cape Town, South Africa, 29 March – 1 April 2022.

Declaration of work

I, **Allan Kengo**, hereby declare that the work on which this dissertation/thesis is based is my original work (except where acknowledgements indicate otherwise) and that neither the whole work nor any part of it has been, is being, or is to be submitted for another degree in this or any other university. Chapters three, four, five and six of this thesis have been published or are under review in an international journal and contents remain unchanged from the printed versions except where formatting was required to maintain consistency in the thesis. All co-authors gave their written consent to include the publications as part of a PhD.

I empower the university to reproduce for the purpose of research either the whole or any portion of the contents in any manner whatsoever.

Signature: **Date:** 27-06-2025

Declaration on the Inclusion of Publications in a PhD Thesis

"I confirm that I have been granted permission by the University of Cape Town's Doctoral Degrees Board to include the following publication(s) in my PhD thesis, and where co-authorships are involved, my co-authors have agreed that I may include the publication(s):"

1. **Kengo A,** Gausi K, Nabisere R, Musaazi J, Buzibye A, Omali D, Aarnoutse R, Lamorde M, Dooley KE, Sloan DJ, Sekaggya-Wiltshire C, Denti P. 2023. Unexpectedly low drug exposures among Ugandan patients with TB and HIV receiving high-dose rifampicin. Antimicrob Agents Chemother 67:e00431-23. https://doi.org/10.1128/aac.00431-23
2. **Kengo, A**., Nabisere R, Gausi K, Musaazi J, Buzibye A, Omali D, Aarnoutse R, Lamorde M, Dooley KE, Sloan DJ, Denti P, Sekaggya-Wiltshire C. 2023. Dolutegravir pharmacokinetics in Ugandan patients with TB and HIV receiving standard- versus high-dose rifampicin. Antimicrob Agents Chemother 67:e00430-23. https://doi.org/10.1128/aac.00430-23
3. **Kengo A**, Resendiz-Galvan JE, Najjemba L, Mugerwa H, De Nicolo A, D'Avolia A, Atoyebi S, Wiesner L, Svensson EM, Waitt C, Denti P. (2024). Model-based evaluation of the interaction between ritonavir-boosted atazanavir and rifampicin in Ugandan adults with HIV. (Submitted for publication)
4. **Kengo A**, Nabeemeeah F, Denti P, Sabet R, Okyere-Manu G, Abraham P, Weisner L, Mosala MH, Tshabalala S, Scholefield J, Resendiz-Galvan JE, Martinson NA, Variava E.2024.Assessing potential drug-drug interactions between clofazimine and other frequently used agents to treat drug-resistant tuberculosis. Antimicrob Agents Chemother68:e01583-23. https://doi.org/10.1128/aac.01583-23

Signature: **Date:** 27-06-2025

Student name: Allan Kengo **Student number:** KNGALL003

Acknowledgements

I would like to extend my profound gratitude to everyone who has supported me throughout my academic journey and the completion of this thesis.

Foremost, my deepest appreciation goes to my supervisor, **Prof. Paolo Denti.** Your expertise, patience, and guidance have shaped this research in ways I could not have imagined. Your mentorship not only elevated the quality and relevance of this work but also instilled in me the values and skills essential to becoming a more thoughtful and independent researcher. I am equally grateful to my co-supervisor, **Dr Juan Eduardo Resendiz Galvan**, whose invaluable guidance and critical feedback continuously challenged me to refine and improve this work. Together, your dedication and belief in my potential have left an indelible mark on my professional growth.

This research was made possible by the generous financial support of **VirTUAL**, a clinical trials consortium that was funded by the European Union through the European and Developing Countries Clinical Trials Partnership-2 (EDCTP2, grant RIA2016MC-1606-VirTUAL). Additionally, I am grateful to the University of Cape Town's ICTs High Performance Computing team whose advanced computational resources and facilities greatly improved the efficiency and feasibility of my research.

I am fortunate to have worked alongside exceptional and supportive colleagues and peers in the Pharmacometrics Modelling Group of the Division of Clinical Pharmacology at the University of Cape Town. To **Dr Kamunkhwala Gausi**, who co-supervised my earlier project, and **Dr Aida Nakayiwa Kawuma**, who was always willing to review drafts and offer constructive feedback—your support has been invaluable, both personally and professionally.

Finally, I am forever indebted to my family. To my wife, **Ritah Nansamba**, whose unwavering love and support provided me with strength and balance throughout this journey, and who

happily took on countless responsibilities to ensure I could fully commit to my research. To my parents, **Mr.** and **Mrs. Mbulamuko**, who have been my lifelong role models, always encouraging me to strive beyond obstacles and limitations. Your faith in me has been my anchor.

Thank you all for your encouragement, guidance, and support, without which this thesis would not have been possible.

Abstract

Nonlinear mixed-effects modelling of drug-drug interactions between antiretroviral therapy and tuberculosis treatment

Human immunodeficiency virus (HIV) remains a significant global health challenge that affected approximately 39 million individuals in 2022, with majority residing in Africa. Among people with HIV (PWH), co-infection with tuberculosis (TB) is a leading cause of death. However, the concurrent treatment of HIV and TB often results in drug-drug interactions (DDIs), mediated by especially by rifampicin, a key component of the TB regimen and potent enzyme and transporter inducer. These DDIs may compromise treatment safety and efficacy, potentially leading to therapeutic failure and increased risk of drug resistance.

In this thesis, we utilized non-linear mixed effects modelling and data from studies in PWH and healthy volunteers to characterise DDIs between first- and second-line antiretroviral (ARV) and anti-TB drugs. Additionally, we performed simulations to assess treatment target attainment following current dosing recommendations in PWH.

Our pharmacokinetic model of standard- and high-dose rifampicin in PWH identified lower bioavailability of the top-up capsule formulation as the cause of lower-than-expected drug exposures in participants on high-dose rifampicin. Furthermore, the reduced dolutegravir exposures in participants on concurrent high-dose rifampicin, compared to those on the standard-dose, were attributed to reduced bioavailability rather than enhanced clearance. Notably, our simulations demonstrated that doubling the dosing frequency of dolutegravir effectively counteracted the DDI with both standard- and high-dose rifampicin.

Secondly, we characterized the DDI between ritonavir-boosted atazanavir (ATV/r) and rifampicin, both in plasma and within peripheral blood mononuclear cells (PBMCs). Rifampicin increased the clearance of ATV/r by threefold, and doubling the dosing frequency of ATV/r was

sufficient to counteract this interaction and restore treatment target attainment. Notably, rifampicin did not affect atazanavir equilibration or accumulation in PBMCs, suggesting that plasma studies can reliably reflect intracellular processes. We also applied our model to an external dataset, estimating a twofold decrease in atazanavir clearance, likely due to ritonavir co-administration.

Lastly, we found clofazimine, a second-line drug resistant TB (DR-TB) drug, to increase the clearance of levofloxacin by 15% but not affect the pharmacokinetics of cycloserine, linezolid, or isoniazid. This confirmed that clofazimine can be safely co-administered with other DR-TB drugs, as it poses minimal risk of significant DDIs.

In conclusion, non-linear mixed effects modelling can be used to evaluate DDIs, and we recommend its incorporation in routine dose optimization and therapeutic drug monitoring programs to enhance treatment outcomes.

Table of contents

List of tables

List of equations

List of figures

List of abbreviations and acronyms

3TC: Lamivudine, 22
ABC: Abacavir, 22
AIDS: Acquired Immune Deficiency Syndrome, 17
ART: Antiretroviral therapy, 17
ATV: Atazanavir, 23
AUC: Area under the curve, 27
AZT: Zidovudine, 22
BCRP: Breast cancer resistance protein, 26
BID: Twice daily, 108
BOV: Between-occasion variability, 88
BSV: Between-subject variability, 88
BVV: Between visit variability, 88
CCR5: Chemokine receptor 5, 20
CI: Confidence interval, 103
CV: Coefficient of variation, 103
CYP: Cytochrome P450, 26
DDIs: Drug drug interactions, 25
DNA: Deoxyribonucleic acid, 19
DTG: Dolutegravir, 24
EFV: Efavirenz, 23
env: Envelope, 19
FDC: Fixed dose combination, 77
FFM: fat-free mass, 111
FOCEI: First order condition estimation with interaction, 91
FTC: Emtricitabine, 22
gp: Glycoprotein, 19
HIV: Human Immunodeficiency Virus, 17
HPLC: High performance liquid chromatography, 79
INSTIs: Integrase strand inhibitors, 22
IQR: Interquartile range, 96
JCRC: Joint Clinical Research Center, 80
LLOQ: Lower limit of quantification, 79
LPV: Lopinavir, 23
NAT: N-acetyltransferase, 58
NCA: Non compartmental, 86
NLME: Nonlinear mixed effects, 87
NNRTIs: Non-nucleoside reverse transcriptase inhibitors, 22
NRTIs: Nucleoside reverse transcriptase inhibitors, 22
NVP: Nevirapine, 23
OFV: Objective function value, 91
PA-IC90: Protein adjusted 90% inhibitory concentration, 29
PBMCs: Peripheral blood mononuclear cells, 131

Chapter 1: Introduction

1.1.0 Global burden of HIV

In global public health, a few challenges are as significant as Human Immunodeficiency Virus (HIV), the virus that causes the worldwide Acquired Immune Deficiency Syndrome (AIDS) epidemic. In 2022, there were about 1.3 million newly infected with HIV globally, bringing the total number of people with the virus to nearly 39 million (UNAIDS, 2023a). In the same year, about 630,000 people were reported to have died due to AIDS-related causes worldwide (UNAIDS, 2023a). Although Sub-Saharan Africa (SSA) is home to just 10% of the world's population, it sadly bears more than two-thirds of the global HIV burden (UNAIDS, 2023a). Notably, women and girls represented 77% of all new infections in 2022 (UNAIDS, 2023a), with South Africa recording the highest prevalence (18%) and hosting the world's largest antiretroviral treatment program (UNAIDS, 2019, 2022).

The adoption of highly effective combination antiretroviral therapy (ART) has played a crucial role in the global fight against HIV, greatly lowering the risk of progression to severe disease and associated mortality (UNAIDS, 2023a; Walensky et al., 2006). This progress has been further strengthened by increased awareness of HIV infection and the widespread uptake of mass testing initiatives, which have been crucial in identifying new cases and linking affected individuals to essential care and support programs (Kumah et al., 2023). Consequently, new infections and AIDS-related deaths have declined by approximately 59% and 69%, respectively, from their previous peak levels (UNAIDS, 2023a).

1.1.1 HIV disease

Most of the global HIV/AIDS cases are attributed to the more pathogenic HIV-1 virus strain (Deeks et al., 2015). In contrast, HIV-2, the other strain that shares a closer genetic relationship with the simian immunodeficiency virus, is mostly prevalent in Western Africa (Brunton & Bjorn, 2022). While both HIV-1 and HIV-2 generally respond to most antiretroviral (ARV) therapies, certain classes of drugs, like the non-nucleoside reverse transcriptase inhibitors, are ineffective against HIV-2 (Brunton & Bjorn, 2022).

The most common way HIV spreads is through exchange of bodily fluids, including blood, semen, vaginal fluids and breast milk from infected individuals (Moir et al., 2011). Other less frequent transmission routes include needle stick injuries (Abadie et al., 2024) and exposure to infected blood or blood products via transfusion (Savarit et al., 1992). HIV transmission may also occur from mother-to-child in utero via the placenta, during labour and delivery through exposure to maternal blood and bodily fluids, or postpartum through breastfeeding (Ladner et al., 2013; Moir et al., 2011).

Upon transmission, HIV rapidly replicates, peaking at 2-4 weeks and causing a transient reduction in peripheral CD4+ T-lymphocytes. This is a hallmark of acute HIV infection (Moir et al., 2011). During this phase, HIV ribonucleic (RNA) concentrations surge, and individuals often experience nonspecific symptoms like fever, fatigue, and muscle aches (Brunton & Bjorn, 2022; Lin et al., 2019). Over time, a quasi-steady state is reached, known as the "set point," determined by the balance between the individual immune response and viral pathogenicity (Brunton & Bjorn, 2022; Deeks et al., 2015). Without treatment, the host CD4+ T-lymphocyte count continues to decline steadily, often falling below 200 cells/mm^3 of peripheral blood. This decline is known to increase

the risk of catching opportunistic infections and other health complications, eventually progressing to AIDS, which is defined by marked increase in susceptibility to infections and cancers (Brunton & Bjorn, 2022; Lin et al., 2019).

Understanding HIV's structural components and life cycle has paved way to the development of targeted pharmacological therapies (Palmisano & Vella, 2011). The mature virion of HIV has a spherical shape, with an internal nucleocapsid surrounded by an envelope made up of a lipid bilayer derived from the host cell (Seitz, 2016). Embedded within the envelope are two glycoproteins (Env), gp120 and gp41, which are critical for initiating the infection process. Gp120 facilitates attachment to host cells, while gp41 mediates the fusion process necessary for viral entry (Zhu et al., 2006).

Inside the viral core, a cone-shaped protein shell encloses two RNA genomes and associated proteins (Seitz, 2016). The HIV genome consists of three primary reading frames: Gag, Pol, and Env. Gag encodes the structural polyproteins that form the virion, while Pol encodes essential enzymes such as reverse transcriptase, protease, and integrase. Env, the third frame, encodes the transmembrane proteins necessary for cell binding and entry (Brunton & Bjorn, 2022).

HIV's life cycle includes several key stages, namely, binding, fusion, reverse transcription, integration, replication, assembly, and budding. The virus begins by attaching to CD4 receptors on immune cells such as T-helper cells, macrophages, and dendritic cells via the Env glycoprotein (Brunton & Bjorn, 2022). Additionally, co-receptors like the chemokine receptor CCR5 or CXCR4, found on macrophage-lineage cells, are required for successful viral entry (Greene & Peterlin, 2002).

Following binding to the host cell, the virus fuses with its membrane via the gp41 component of the Env protein, allowing its RNA to enter the host cell's cytoplasm. Here, reverse transcription occurs, where the viral RNA is converted into DNA by the reverse transcriptase enzyme, resulting in a transient RNA-DNA duplex. This conversion is error-prone, leading to a variety of viral clones even within a single individual (Stevenson, 2003). Subsequently, the newly formed viral DNA is incorporated into the host chromosome by the viral integrase enzyme (Greene & Peterlin, 2002).

The integrated viral DNA may remain quiescent or produce viral RNA and proteins as the cell divides until activation (Brunton & Bjorn, 2022). When actively dividing, the structural proteins assemble around the full-length genomic RNA, forming a nucleocapsid, which buds off from the host cell membrane, incorporating envelope proteins clustered in cholesterol-rich lipid rafts. These budding events yield new enveloped HIV particles containing two complete single-stranded RNA genomes (Greene & Peterlin, 2002).

During the process of budding, HIV protease plays a crucial role in enzymatically cleaving long chains of polypeptides into mature viral proteins (Deeks et al., 2015). It processes the Gag and Gag-Pol polyproteins, generating functional proteins like protease, reverse transcriptase, and integrase (Deeks et al., 2015; Lv et al., 2015). This cleavage is essential for the virus to become infectious and fully active. Over time, continuous viral replication depletes essential lymphocytes, undermining immune function and driving the progression of HIV disease (Stevenson, 2003).

1.1.2 Treatment of HIV infection

A comprehensive understanding of HIV's life cycle and pathogenesis has been critical in identifying potential pharmacological targets, driving the development and approval of new ARV

drugs (Desai et al., 2012). Over time, HIV treatment strategies have advanced from single-drug therapy using zidovudine (AZT) to more effective regimens combining multiple ARVs (Desai et al., 2012). Modern ART combinations integrate drugs targeting various phases of the HIV life cycle and have significantly improved disease management (Castellino et al., 2013). The widespread adoption of ART has also improved patients' quality of life by improving their immune function and effectively mitigating the morbidity and mortality that was associated with HIV infection (Desai et al., 2012). Furthermore, early initiation of ART has had the important public health benefit of reducing HIV-1 transmission rates through sexual contact (Cohen et al., 2011).

Currently, there are at least six ARV classes comprising over 25 approved drugs designed to target four key viral components essential for HIV replication: the host receptor, reverse transcriptase, integrase, and protease (Brunton & Bjorn, 2022). These drugs work collectively to inhibit different stages of the viral life cycle. The primary classes of ARVs include nucleoside reverse transcriptase inhibitors (NRTIs), non-nucleoside reverse transcriptase inhibitors (NNRTIs), protease inhibitors (PIs), integrase strand transfer inhibitors (INSTIs), fusion inhibitors, and chemokine co-receptor antagonists.

NRTIs were the pioneering class of ARVs approved for HIV treatment and remain important components of first-line ART (Desai et al., 2012). These drugs act as analogues of natural nucleosides/nucleotides and inhibit reverse transcriptase by incorporating into viral DNA and terminating its synthesis (Deeks et al., 2015). Despite their efficacy, NRTIs present certain drawbacks, such as a low genetic barrier to resistance and potential side effects including bone marrow toxicity and mitochondrial damage (Desai et al., 2012). Currently recommended NRTIs include tenofovir disoproxil fumarate (TDF), tenofovir alafenamide fumarate (TAF), abacavir,

lamivudine (3TC), and emtricitabine. Older NRTIs like AZT and stavudine are largely obsolete due to metabolic complications like lactic acidosis, hepatic steatosis, anaemia, and lipoatrophy (Deeks et al., 2015).

NNRTIs function by binding to a distinct site on the reverse transcriptase enzyme, causing conformational changes that inhibit its activity (Brunton & Bjorn, 2022; Deeks et al., 2015). Unlike NRTIs, NNRTIs do not require intracellular activation and are ineffective against HIV-2 (Brunton & Bjorn, 2022). Common NNRTIs include efavirenz (EFV) and nevirapine (NVP), though their use has declined due to adverse effects. EFV is associated with central nervous system toxicity and an elevated risk of depression (Deeks et al., 2015). NVP was widely used during pregnancy and in newborns, but its popularity has also declined because of associated risk of fatal cutaneous hypersensitivity and hepatotoxicity (Desai et al., 2012). Newer NNRTIs include etravirine, doravirine, rilpivirine and delavirdine.

PIs are peptide-like chemicals that inhibit the HIV protease enzyme, preventing the formation of mature, functional viral proteins and blocking a critical step in the virus's replication cycle (Brunton & Bjorn, 2022; Deeks et al., 2015). When combined with two NNRTIs, PIs are highly effective and have high genetic barrier to resistance development (Deeks et al., 2015; Desai et al., 2012). Examples include saquinavir, indinavir, ritonavir (RTV), nelfinavir, amprenavir, fosamprenavir, lopinavir, atazanavir (ATV), tipranavir, and darunavir. However, their use is often limited by long-term side effects such as metabolic disorders like lipodystrophy, and cardio-/cerebro-vascular complications (Lv et al., 2015). Due to their rapid liver metabolism and subsequent first-pass effect, PIs are often co-administered with pharmacologic boosting agents (enzyme inhibitors) like low-dose RTV or its analogue, cobicistat (Deeks et al., 2015).

INSTIs inhibit viral integrase, preventing the insertion of HIV DNA into the host cell genome (Deeks et al., 2015). The integrase enzyme facilitates two key processes: the removal of a GT-dinucleotide from viral DNA (3’ processing) and the formation of covalent bonds between host and viral DNA (strand transfer) (Brunton & Bjorn, 2022; Smith et al., 2021). INSTIs have leapfrogged NNRTIs and PIs as the preferred choice for initial ART due to their superior therapeutic index (Deeks et al., 2015; Pommier et al., 2005). This is largely due to the absence of a host-cell equivalent to viral integrase, ensuring that INSTIs are less likely to interfere with human cellular processes, thus limiting their potential toxicity (Brunton & Bjorn, 2022; Pommier et al., 2005). Currently available INSTIs include raltegravir, dolutegravir (DTG), elvitegravir, bictegravir, and cabotegravir.

Entry inhibitors block the processes involved in HIV fusion and entry into host cells. This category includes chemokine receptor antagonists such as maraviroc and fusion inhibitors like enfuvirtide (Brunton & Bjorn, 2022). Maraviroc binds to the CCR5 receptor, preventing gp120 binding in CCR5-tropic HIV strains, and its proper use requires prior testing to confirm the absence of CXCR4-tropic viruses (Deeks et al., 2015). Enfuvirtide is a synthetic peptide derived from the gp41 that has limited use due to high production costs and the need for twice-daily subcutaneous administration (Brunton & Bjorn, 2022). Recently novel classes of ARVs have been developed, introducing new mechanisms of action against HIV-1. These include fostemsavir, a CD_4 attachment inhibitor (Heidary et al., 2024) and lenacapavir a long-acting capsid inhibitor (Naga & Kumar, 2024).

1.1.3 Drug-drug interactions

Given the complexity of ARV regimens, people living with HIV frequently face the risk of drug-drug interactions (DDIs). DDIs occur when medications influence each other's efficacy or safety,

either by altering drug concentrations (pharmacokinetics) or modifying their effects (pharmacodynamics) (Gabay & Spencer, 2021; Pai et al., 2006). Pharmacokinetic interactions typically involve changes in absorption, metabolism, or elimination, while pharmacodynamic interactions may produce additive, synergistic, or antagonistic pharmacological effects (Snyder et al., 2012). The likelihood of DDIs increases with polypharmacy, when multiple drugs are administered inevitably, like during the simultaneous management of HIV and tuberculosis (TB) (Gabay & Spencer, 2021).

1.1.3.1 HIV and TB drug interactions.

Understanding, predicting, and mitigating DDIs presents significant challenges for drug developers and clinicians, particularly in treating HIV and associated co-morbidities like TB (Devanathan et al., 2019). The burden of simultaneously treating multiple diseases is often unavoidable in SSA, where the HIV prevalence frequently overlaps with other infectious diseases (Gwitira et al., 2018). Consequently, the prescription of complex drug regimens becomes necessary, demanding careful drug selection to minimize the risk of unwanted DDIs (Piscitelli & Rodvold, 2005).

Managing HIV and TB concurrently poses significant challenges, particularly due to interactions between rifampicin—a key TB drug—and ARVs (World Health Organization, 2023). Rifampicin induces cytochrome P450 (CYP) enzymes, notably CYP3A and CYP2C, as well as drug transporters such as P-glycoprotein and breast cancer resistance protein (BCRP) (Niemi et al., 2003). This induction reduces the concentrations of ARVs metabolized by these pathways. For instance,

rifampicin significantly decreases the exposure of TAF by 55% and ATV by over 75% (Department of Health and Human Services, 2018).

Dose adjustments are often necessary to mitigate rifampicin's effects. For example, doubling the dosing frequency of DTG (Dooley et al., 2013, 2020) and ritonavir-boosted ATV to twice-daily (BID) can successfully restore their plasma concentrations when administered with rifampicin (Gausi et al., 2024). Likewise, maraviroc doses may need to be increased to 600 mg twice daily unless a CYP3A inhibitor is co-administered (Department of Health and Human Services, 2018). Conversely, isoniazid, another TB drug, inhibits CYP450 enzymes and can elevate concentrations of certain drugs like carbamazepine and diazepam (Arbex et al., 2010). Additionally, due to its inhibition of monoamine oxidase, isoniazid may cause adverse reactions when taken with tyramine-rich foods like red wine and cheese (Arbex et al., 2010).

Addressing and managing these interactions requires careful planning and monitoring by healthcare professionals to optimize treatment outcomes and minimize adverse drug reactions (ADRs) for individuals with HIV and TB.

1.1.4 Pharmacology of dolutegravir

DTG is a second-generation INSTI (Rathbun et al., 2014; Smith et al., 2021) widely recommended as part of first line ART for HIV-1 by the World Health Organization (WHO) (ViiV Healthcare, 2021; World Health Organization, 2021a). Additionally, its combination with either rilpivirine or lamivudine may replace existing ART regimens in adults who have suppressed HIV on stable therapy for at least six months (Gibas et al., 2022; ViiV Healthcare, 2021). DTG-containing ART regimens have gained worldwide acceptance because of the drug's safety, superior efficacy (Van

Lunzen et al., 2012), tolerability, and convenient once-daily (QD) dosing schedule (Cottrell et al., 2013; Scarsi et al., 2020).

DTG inhibits HIV integrase and blocks the integration of viral DNA into the host genome, a critical step in viral replication. It binds on to the enzyme's active site and effectively halts the viral strand transfer process (Min et al., 2010; Smith et al., 2021; Taha et al., 2015). Once bound to integrase enzyme, the dissociative half-life of dolutegravir could be as long as 71 hours (Hightower et al., 2011). This prolonged interaction with the nucleoprotein complex is thought to be a significant contributor to its distinctive high barrier to genetic resistance (DeAnda et al., 2013). DTG is very potent against HIV-1 in peripheral blood mononuclear cells and was found to have a protein adjusted 90% inhibitory concentration (PA-IC_{90}) of about 0.064 mg/L (Min et al., 2010). Although not properly investigated, the *in vivo* minimum trough concentration (C_{trough}) target for DTG is widely considered to be 0.3 mg/L. This was largely derived from the median C_{trough} of the smallest dose (10 mg QD) of dolutegravir investigated in earlier dose determination studies reported by Zhang et al. and Van Lunzen et al. (Van Lunzen et al., 2012; Zhang et al., 2015).

The recommended adult dose of DTG when used in ART combinations of treatment-naive and -experienced patients is 50 mg QD (ViiV Healthcare, 2021; World Health Organization, 2021a). Its dosing frequency may be doubled administered alongside enzyme inducers like rifampicin (Dooley et al., 2013; World Health Organization, 2021a). Similarly, if a treatment-experienced patients is suspected or confirmed to harbor HIV strains with INSTI-associated resistance substitutions, doubling the dosing frequency is also recommended (ViiV Healthcare, 2021). DTG is also conveniently formulated in child friendly 5mg dispersible tablets that can be administered based on weight (ViiV Healthcare, 2021).

1.1.4.1 Absorption

DTG absorption is rapid upon oral administration (Min et al., 2010), resulting in peak concentrations 2 to 3 hours after the dose (ViiV Healthcare, 2021). Food increases the extent of DTG absorption, with high fat-containing meals augmenting its area under the concentration curve (AUC) by 66% (Song et al., 2012). Notably, treatment guidelines do not specify a preference regarding DTG intake with or without food as this was considered moderate and clinically unsignificant (ViiV Healthcare, 2021). DTG exposure increases in a less than dose proportional manner (Min et al., 2010; ViiV Healthcare, 2021), and this may be an indication that its absorption is saturable (Wang et al., 2019). Although the absolute bioavailability of DTG has not been determined, Castellino et al. (Castellino et al., 2013) estimated that over 70% of the oral dose could be absorbed.

1.1.4.2 Distribution

DTG exhibits extensive (~99%) plasma protein binding (ViiV Healthcare, 2021) onto albumin and alpha-1 acid glycoprotein (Rathbun et al., 2014). It readily distributes to many body parts, including the central nervous system where concentrations mirror unbound plasma levels (Letendre et al., 2014). DTG also appreciably distributes into semen (Imaz et al., 2016), breast milk (Dickinson et al., 2021a) and crosses the blood-placenta barrier (Schalkwijk et al., 2016).

1.1.4.3 Metabolism and elimination

DTG metabolism occurs primarily through glucuronidation (19%) by UGT-1A1, with minor contributions from CYP3A4-mediated (7.9%) oxidation and glutathione substitution (1.8%) (Castellino et al., 2013; ViiV Healthcare, 2021). DTG is a substrate for transport proteins like P-glycoprotein and BCRP (ViiV Healthcare, 2021). About 64% of the oral dose is excreted unchanged

in faeces, while 31% is eliminated as metabolites in urine (ViiV Healthcare, 2021), representing both unabsorbed material and biliary secretion of the drug (Castellino et al., 2013). The drug's elimination half-life is approximately 14 hours (ViiV Healthcare, 2021), with steady-state concentrations reached after five daily doses (Min et al., 2010).

1.1.4.4 Adverse drug reactions

DTG is well tolerated compared to other ARV medication (Deeks et al., 2015; Taha et al., 2015; Van Lunzen et al., 2012). Most of the reported adverse effects of DTG like nausea, diarrhoea, and sleep disturbances, are neither considered serious and nor associated with DTG blood levels (Taha et al., 2015; Van Lunzen et al., 2012). Neuropsychiatric events like headache, dizziness, depression, and insomnia are rare but noteworthy (Scarsi et al., 2020). DTG-based ART was initially associated with neural tube defects when used around the time of conception, prompting caution during pregnancy (Scarsi et al., 2020; ViiV Healthcare, 2021). However, more recent surveillance data has provided evidence to the contrary (Gill et al., 2025).

DTG use has been associated with reversible mild increase in serum creatinine that is due to inhibition of the renal organic cation transporter (OCT2), involved in tubular creatinine secretion (Brunton & Bjorn, 2022; ViiV Healthcare, 2021). Emerging concerns include rare cases of impaired glucose control (Hirigo et al., 2022; Namara et al., 2022) and weight gain, particularly when combined with TDF (Hirigo et al., 2023; Huszar et al., 1997). The mechanism behind weight gain remains debated, though recent evidence suggests it does not involve significant MC4 receptor inhibition (McMahon et al., 2020).

1.1.4.5 Interactions

DTG has minimal effects on major drug-metabolizing enzymes and transporters, reducing the likelihood of significant DDIs (Cada et al., 2014; Podany et al., 2020; ViiV Healthcare, 2021). However, it inhibits OCT2 and the multidrug and toxin extrusion transporter-1 (Cada et al., 2014; Reese et al., 2013; ViiV Healthcare, 2021), increasing exposure of substrate drugs like metformin and dofetilide (Song et al., 2016). Chelation interactions with divalent and trivalent metal cations (e.g., calcium and iron supplements) can reduce DTG absorption, and can be mitigated by appropriately timing administration of the two drugs (Song et al., 2015; ViiV Healthcare, 2021).

Metabolic inducers like rifampicin decrease dolutegravir exposure, necessitating dose adjustments (Dooley et al., 2013; Kawuma et al., 2022). Conversely, certain PIs like ritonavir-boosted ATV counteract the effects of CYP3A4 inducers, maintaining dolutegravir efficacy (Song et al., 2011).

1.1.4.6 Resistance

Drug resistance can be defined as the capacity of a pathogen to avoid destruction by the drug (Brunton & Bjorn, 2022). The commonest mechanisms by which drugs develop resistance to medications include alteration of drug targets, reduction in drug accumulation and inactivation (or activation failure) of the drug (Hughes & Andersson, 2015; Santajit & Indrawattana, 2016).

DTG has a high genetic barrier to resistance compared to earlier INSTIs like raltegravir (Cottrell et al., 2013). This may be partly due to its flexible structure which allows for effective binding even in the presence of mutation induced target alterations (Cottrell et al., 2013). Furthermore, DTG demonstrates prolonged binding to its target, and this reduces viral replication that could

potentially generate additional mutations (Hightower et al., 2011). While resistance-associated treatment failures remain rare, ongoing vigilance is essential given the adaptive nature of HIV (ViiV Healthcare, 2021) and widespread use of DTG in resource-limited settings.

1.1.5 Pharmacology of atazanavir

ATV is a second-generation azapeptide inhibitor of HIV-1 protease approved for treatment of HIV infection (FDA & CDER, 2003). It binds to the HIV-1 protease enzyme and prevents maturation of viral particles by inhibiting the processing of gag and gag-pol precursor polyproteins (Busti et al., 2004). This blockade results in the release of immature and non-infectious virions (Dewolf et al., 2000).

With a PA-IC_{90} of 0.014 mg/L (FDA & CDER, 2003; Gausi et al., 2024), ATV is among the most potent PIs, and its exposure can even be enhanced further by co-administration with RTV (Dewolf et al., 2000; Gianotti & Lazzarin, 2007). ATV's widespread use in resource-limited settings is attributed to its superior safety profile, extended half-life allowing for QD dosing, and a unique resistance profile (Busti et al., 2004; FDA & CDER, 2003; Gianotti & Lazzarin, 2007; Havlir & O'marro, 2004).

Ritonavir-boosted ATV (ATV/r) is a common component of the preferred WHO second-line ART regimen (FDA & CDER, 2003; World Health Organization, 2021b). Recommended adult dosage for ATV/r is 300/100 mg. For paediatric patients, the doses vary: 150/100 mg for those weighing 15–20 kg and 200/100 mg for those between 20 and 40 kg (FDA & CDER, 2003). Although not extensively studied, a C_{trough} greater than 0.15 mg/L has been used for therapeutic drug monitoring of ATV (Back et al., 2006).

1.1.5.1 Absorption

ATV is rapidly absorbed following oral administration, with peak plasma concentrations observed approximately 2.5 hours post-dose (Busti et al., 2004; FDA & CDER, 2003). Its pharmacokinetics are nonlinear, as dose increases beyond the 200–800 mg range yield more-than-proportional increases in drug exposure. Steady-state concentrations are achieved within 4 to 5 days, with an accumulation factor of about 2.3 (FDA & CDER, 2003).

Food significantly enhances ATV absorption, increasing AUC by 70% and peak concentrations by 57% compared to fasting conditions (FDA & CDER, 2003). This effect is attributed to bile salt secretion, which promotes solubilization of lipophilic drugs (Kis et al., 2014). Additionally, coadministration of ATV/r with food reduces variability in its pharmacokinetics (FDA & CDER, 2003). As a substrate for transport proteins like P-glycoprotein and the organic anion transporting polypeptide, ATV's bioavailability can be increased by their inhibition (Kis et al., 2013).

The aqueous solubility and gut permeability of ATV is sensitive to changes in gut pH (FDA & CDER, 2003; Kis et al., 2014). Acidic environments reduce its P-glycoprotein-mediated efflux, enhancing drug absorption (Kis et al., 2014). Conversely, drugs such as proton pump inhibitors and antacids, which elevate gut pH, decrease ATV plasma concentrations and should be avoided during ATV therapy (FDA & CDER, 2003; Kis et al., 2014).

1.1.5.2 Distribution

ATV exhibits moderate plasma protein binding (~86%), with equal affinities for albumin and alpha-1 acid glycoprotein (Busti et al., 2004). Its binding profile remains stable across varying drug concentrations (FDA & CDER, 2003. ATV distributes significantly to various tissues, with evidence

showing significant penetration into the central nervous system and semen (Busti et al., 2004; FDA & CDER, 2003).

1.1.5.3 Metabolism and elimination

ATV undergoes extensive liver metabolism, primarily mediated by CYP3A4/5, yielding three metabolites that mainly lack activity against HIV or enzyme inhibiting properties (Alvarellos et al., 2018; FDA & CDER, 2003). It also competitively inhibits CYP3A and UGT1A1, resulting in a benign elevation of unconjugated bilirubin (Havlir & O'marro, 2004). At the initial 400 mg once daily dose, ATV exhibits a half-life of approximately 6 hours, which increased to over 11 hours when administered as 300 mg boosted with RTV (Busti et al., 2004; FDA & CDER, 2003).

ATV is primarily eliminated by biliary route resulting in 79% of the drug being eliminated mainly as metabolites in faeces (FDA & CDER, 2003). Dose adjustments are generally unnecessary except in cases of severe hepatic impairment, where data remain inconclusive (Busti et al., 2004; FDA & CDER, 2003).

1.1.5.4 Adverse drug reactions

ATV/r is generally well tolerated (FDA & CDER, 2003; Gianotti & Lazzarin, 2007), and results in much fewer side effects than other PIs (Busti et al., 2004). The most common adverse effect is asymptomatic hyperbilirubinemia, attributed to UGT inhibition by ATV (FDA & CDER, 2003; Gianotti & Lazzarin, 2007). This condition affects fewer than 2% of patients and rarely necessitates discontinuation (FDA & CDER, 2003).

Other rare adverse reactions include gastrointestinal disturbances (nausea, vomiting, diarrhoea), headache, rash, and peripheral neuropathy (Busti et al., 2004; FDA & CDER, 2003). Dyslipidemia

has been observed with ATV, but it occurs at lower rates compared to other PIs, such as darunavir, and may have limited clinical significance (FDA & CDER, 2003; Gianotti & Lazzarin, 2007).

1.1.5.5 Interactions

ATV, as a substrate of CYP3A4 and inhibitor of both CYP3A and UGT1A1, exhibits extensive DDIs (FDA & CDER, 2003). At higher doses, ATV has also been shown to inhibit the p-glycoprotein transporter (Busti et al., 2004). Co-administration with drugs metabolized by these enzymes can lead to altered drug levels and increased risk of adverse effects. Concomitant use of ATV with medications like midazolam, triazolam, ergot derivatives, cisapride, and pimozide is contraindicated due to potential toxicity (Busti et al., 2004).

Data about the interaction between TDF with ATV is conflicting. Mirochnick eta al. found TDF coadministration to be associated with reduced ATV AUC and trough concentration in pregnancy (Mirochnick et al., 2011). This effect of TDF on ATV AUC was also reportedly found by Taburet et al. in treatment-experienced patients (Taburet et al., 2004). However, a larger matched drug interaction study amongst patients at steady state found no significant interaction between TDF and ritonavir-boosted ATV (Von Hentig et al., 2007). TDF is an oral prodrug of tenofovir, a NRTI that is neither a substrate nor inducer of most CYP isoenzymes except CYP1A and CYP2B (Kearney et al., 2004). Tenofovir does not alter the functioning of the p-glycoprotein transporter (Kearney et al., 2004). Current guidelines recommend that when given with TDF, ATV should always be boosted with RTV (FDA & CDER, 2003).

1.1.5.6 Resistance

Studies on HIV-1 resistance reveal that mutations such as I84V, I50L, N88S, A71V, and M46I are associated with reduced susceptibility to ATV (FDA & CDER, 2019). These mutations, often linked to changes in protease cleavage sites, do not confer resistance to other PIs and may even enhance susceptibility to some (Busti et al., 2004; FDA & CDER, 2003). Despite ATV's unique resistance profile, cross-resistance to non-boosted ATV remains a concern in cases of multi-PI resistance (Busti et al., 2004).

1.1.5.7 Pharmacokinetic boosting of atazanavir

Pharmacokinetic boosting involves deliberately co-administering a drug with another that inhibits its metabolism, thereby increasing its plasma concentration and possibly enhancing its efficacy (Deeks, 2014). This has been successfully applied through the co-formulation of PIs with RTV or cobicistat, both of which inhibit their metabolism, enabling the use of lower, less frequent doses while maintaining efficacy (Deeks, 2014; Hull & Montaner, 2011). Besides enhancing patient adherence through less frequent dosing, pharmacokinetic boosting also prevents resistance development by maintaining consistently high plasma drug exposures (Loos et al., 2022).

1.1.5.7.1 Ritonavir

RTV was one of the first four HIV PIs approved for combination use in ART for HIV treatment (Hsu et al., 1998). It is a peptidomimetic inhibitor of HIV-1 protease that disrupts the viral life cycle by preventing the processing of the gag-pol precursor protein. This inhibition halts the production of mature infectious HIV particles, leading to the release of immature, non-infectious virions (FDA & CDER, 2019). When it was used to treat HIV-1, the recommended dose of RTV was 600 mg BID for adults and 350-400 mg/m^2 of body surface area for paediatric patients (FDA & CDER, 2019).

The early utilization of RTV as a standalone component of ART encountered significant challenges. RTV had poor systemic bioavailability because of its high first-pass metabolism by CYP3A and efflux by P-glycoprotein into bile (Loos et al., 2022). To achieve therapeutic efficacy, doses exceeding 1000 mg per day were required, resulting in frequent gastrointestinal side effects and elevated risks of other drug toxicities (FDA & CDER, 2019; Loos et al., 2022). Moreover, high-dose RTV was linked to interactions with the pregnane-X receptor (PXR) signalling pathway, inducing multiple CYP enzymes, UGT, and P-glycoprotein, leading to an even more complex drug interaction profile (Loos et al., 2022). Furthermore, RTV monotherapy often led to the rapid emergence of resistance and diminished efficacy (Loos et al., 2022).

RTV strongly inhibits CYP3A, with an IC_{50} of 0.034 µM (~0.0245 mg/L), as shown by Loos et al. in 2022, based on its effect on testosterone 6β hydroxylation (Hsu et al., 1998; Loos et al., 2022). Unlike ketoconazole, RTV is a suicide inhibitor of the CYP3A and P-glycoprotein in the gut and liver (Loos et al., 2023). This means that when RTV disables CYP3A, its activity will only be restored after new enzyme synthesis which typically takes a couple of days (Loos et al., 2022). Although there is no universal agreement on the duration of this recovery period, Katzenmaier et al. estimated CYP3A activity to return after 3 days of discontinuing RTV (Katzenmaier et al., 2011).

Several mechanisms have been suggested to explain the irreversible inhibition of CYP3A by RTV. These include: (I) formation of a metabolic intermediate complex; (II) strong attachment of unchanged RTV to the heme iron; (III) destruction of heme; and finally, (IV) establishment of a covalent bond between RTV's reactive intermediate and the CYP3A polypeptide (Loos et al., 2022). Among the mentioned mechanisms, those involving the creation of a reactive or metabolite intermediate that subsequently remains bound to the active site, impeding further

interaction with new substrate molecules, constitute mechanism-based inactivation (Loos et al., 2022).

This inhibition results in increased absorption and reduced metabolism of coadministered CYP3A substrates like ATV (Alvarellos et al., 2018; Hull & Montaner, 2011). For example, when ATV is coadministered with RTV, its pharmacokinetics is notably improved, and variability is reduced. Consequently, low dose RTV (typically 100 mg), or its analogue cobicistat (Deeks, 2014), are co-formulated with ATV and PIs to leverage their "pharmacokinetic boosting" effects. Prescribing ATV alone is strongly discouraged and only reserved for specific circumstances aiming to reduce pill burden, enhance treatment adherence, or mitigate RTV-induced toxicities (Alvarellos et al., 2018).

Absorption: RTV exhibits an estimated absolute bioavailability between 60% and 80% in humans (Hsu et al., 1998). When administered with food, liquid RTV formulations showed a 23% reduction in peak concentrations and a 7% decrease in AUC (FDA & CDER, 2019; Hsu et al., 1998).

Distribution: Approximately 99% of RTV binds to plasma proteins, including albumin and alpha-1 acid glycoprotein (Hull & Montaner, 2011). This high binding capacity is not saturable within therapeutic concentration ranges and remains unaffected by salicylate, ibuprofen, or clarithromycin (Hull & Montaner, 2011).

Metabolism and elimination: RTV is primarily metabolized by CYP3A with minor contribution of CYP2D6 (FDA & CDER, 2019). Its main metabolite, the isopropyl-thiazole oxidation product (M2), retains comparable antiviral activity to the parent compound (FDA & CDER, 2019; Hsu et al., 1998). Following oral administration, 86% of the drug is recovered in faeces, with 34% excreted

as unchanged drug (FDA & CDER, 2019; Hsu et al., 1998). RTV exhibits a half-life of 3 to 5 hours, induces its own metabolism, and reaches steady-state concentrations after approximately two weeks of continuous dosing (Hsu et al., 1998).

Adverse drug reactions and interactions: RTV's adverse effects commonly include gastrointestinal symptoms (diarrhoea, nausea, vomiting, and abdominal pain), neurological disturbances, skin rash, and fatigue/asthenia (FDA & CDER, 2019). Due to its enzyme inhibiting properties, RTV interacts with most substrates of CYP3A especially those with high intrinsic clearance and significant first-pass metabolism (Hsu et al., 1998). This necessitates careful dose adjustment and monitoring when RTV is combined with most medications.

1.2.0 Global burden of tuberculosis

Despite significant global efforts, TB remains a major public health threat and a leading cause of illness and death worldwide. The WHO's 2024 global TB report reveals that roughly 10.8 million individuals were diagnosed with TB in 2023, with an estimated 1.25 million deaths, making it the leading cause of death worldwide (World Health Organization, 2024).

TB is caused by the bacillus *Mycobacterium tuberculosis* (*M. tuberculosis*), which spreads through airborne droplets when individuals with active TB expel bacteria by coughing or other respiratory activities (Raja, 2004a; World Health Organization, 2024). Global estimates suggest that about one-quarter of the world's population is infected with the latent form of TB (Cohen et al., 2019; Houben & Dodd, 2016). While TB can affect anyone, the highest burden was found in adult men, constituting 55% of the estimated global cases in 2023.

1.2.1 TB Disease

TB primarily affects the lungs (pulmonary TB) but may also spread to other parts of the body (extrapulmonary TB). Common symptoms of active pulmonary TB include persistent coughing, chest pain, weight loss, fever, and night sweats (Brunton & Bjorn, 2022). Although only a small proportion of infected individuals develop active TB, those with risk factors such as HIV, malnutrition, alcohol use disorder, smoking, or diabetes face a much higher likelihood of disease progression (Raja, 2004b).

M. tuberculosis is a slow-growing acid-fast bacillus that primarily spreads through the respiratory route. Transmission occurs when airborne droplets containing the bacteria are inhaled by another person (Raja, 2004b). Once inhaled, the bacilli settle in the distal alveoli, where they are engulfed

by immune cells like macrophages (Philips & Ernst, 2012; Raja, 2004b). Different immune cells, such as neutrophils and dendritic cells, may also migrate to the site and ingest the mycobacteria, potentially influencing the course of infection (Philips & Ernst, 2012).

Phagocytic immune cells contain dense granules that fuse with phagosomes to degrade engulfed material (Armstrong & Hart, 1971; Philips & Ernst, 2012). However, *M. tuberculosis* can inhibit phagosome-lysosome fusion by releasing substances that block maturation, allowing it to access nutrients and evade the hostile lysosomal environment (Armstrong & Hart, 1971; Philips & Ernst, 2012; Raja, 2004b). This enables *M. tuberculosis* to acquire nutrients like iron via recycling endosomes while evading the acidic, degradative environment of the lysosome (Philips & Ernst, 2012). The bacillus also employs additional immune evasion strategies, such as interfering with antigen presentation, neutralizing reactive oxygen species, and escaping from lysosomal compartments (Raja, 2004b).

Once inside macrophages, *M. tuberculosis* replicates and attracts more macrophages to the site of infection, forming aggregates that mark the early stages of granuloma development (Philips & Ernst, 2012). This recruitment leads to aggregation and organization, marking the initial stages of granuloma formation. Upon host cell death, the bacilli are released and ingested by surrounding macrophages, enabling bacterial spread (Philips & Ernst, 2012). Some infected macrophages migrate to other tissues, initiating secondary infections, while others remain in granulomas, resisting immune elimination (Philips & Ernst, 2012).

In latent infections, the bacteria within granulomas may exist in a dormant or controlled replicative state, contained by the immune system (Raja, 2004b). Breakdown of this immune

containment can trigger reactivation, leading to tissue necrosis and disease progression (Raja, 2004b).

1.2.2 Treatment of tuberculosis

Tuberculosis, a disease that has afflicted humanity for centuries, underwent a transformation with the discovery of antibiotics in the mid-20th century (Murray et al., 2015). The discovery of streptomycin and para-amino salicylic acid (PAS) marked the beginning of effective TB treatment (Murray et al., 2015; Schatz et al., 2005; Todd M, 1953). Initially, using these drugs individually resulted in adverse effects and drug resistance. However, subsequent combination of the two drugs proved more effective and was adopted (Murray et al., 2015). The later discovery of isoniazid, a more potent and less toxic drug, led to the development of a triple therapy regimen involving isoniazid, PAS, and streptomycin (Murray et al., 2015).

The WHO currently recommends a 6-month treatment regimen for drug-susceptible TB, consisting of rifampicin, isoniazid, pyrazinamide, and ethambutol (WHO, 2024). Treatment is divided into two phases: an intensive 2-month phase with all four drugs, followed by a 4-month continuation phase with rifampicin and isoniazid (WHO, 2024).

Despite its effectiveness, TB treatment is lengthy and complex, posing challenges for both patients and healthcare systems globally (World Health Organization, 2022b). Patient adherence, critical to preventing drug resistance, is often hindered by drug toxicity and interactions, particularly in individuals co-treated for conditions like HIV (Arbex et al., 2010; Laurenzi et al., 2007). The emergence of drug-resistant TB strains remains the greatest obstacle to global TB eradication efforts (World Health Organization, 2022a).

1.2.2.1 Drug resistant tuberculosis

Drug-resistant TB (DR-TB) arises when *M. tuberculosis* becomes resistant to one or more standard TB treatments (World Health Organization, 2022a). A common form is rifampicin-resistant TB (RR-TB), characterized by resistance to rifampicin alone. When the bacilli resist both rifampicin and isoniazid, the condition is termed multi-drug-resistant TB (MDR-TB). Extensively drug-resistant TB (XDR-TB) involves resistance to rifampicin, isoniazid, one fluoroquinolone (levofloxacin or moxifloxacin), and at least one Group A drug bedaquiline or linezolid (World Health Organization, 2022a).

Resistance can be intrinsic or acquired. Intrinsic resistance may result from *M. tuberculosis'* structural features, such as its thick cell wall, which impedes drug entry, or mutations affecting key transport proteins (Heidary et al., 2022). Acquired resistance, however, arises from genetic mutations that alter drug targets, reduce drug binding affinity, or inhibit drug activation (Heidary et al., 2022). These mutations, though random, can become widespread when selective pressure from prolonged drug exposure favours resistant strains (Singh et al., 2020; Smith et al., 2012). Factors such as patient non-compliance (Nguyen, 2016; Smith et al., 2012), suboptimal drug regimens, or variations in patient pharmacokinetics also contribute to resistance development (Denti, Wasmann, Francis, et al., 2022).

In 2023, the WHO estimated that 3.2% of all new TB cases and 16% of previously treated TB cases were either MDR-TB or RR-TB (World Health Organization, 2024). Treating these forms of TB poses substantial challenges due to prolonged treatment durations, higher costs, and lower success rates (Heidary et al., 2022; World Health Organization, 2024). Treatment regimens are

often more toxic and require strict adherence, impacting patient quality of life (Heidary et al., 2022).

To standardize treatment, the WHO categorizes DR-TB drugs into groups: Group A includes levofloxacin, moxifloxacin, bedaquiline, and linezolid; Group B comprises clofazimine and cycloserine/terizidone; Group C contains ethambutol, delamanid, pyrazinamide, imipenem/meropenem, amikacin/streptomycin, ethionamide/prothionamide, and PAS (World Health Organization, 2022a). When possible, treatment regimens should include all Group A agents and at least one Group B agent. Group C drugs are used when necessary to complete the regimen (World Health Organization, 2022a).

Current preferred treatments for MDR TB include the 6-month BPaLM regimen—comprising bedaquiline, pretomanid, linezolid, and moxifloxacin—due to its promising efficacy and improved compliance rates (Van Deun et al., 2010; World Health Organization, 2022a). Alternatively, a 9-month regimen is recommended for patients with confirmed rifampicin resistance but no fluoroquinolone resistance (World Health Organization, 2022a).

1.2.3 Pharmacology of rifampicin

Rifampicin is a semisynthetic antibiotic derivative of rifamycin SV, originally isolated from *Streptomyces mediterranei* (Brunton & Bjorn, 2022; FDA & CDER, 2010). It binds to the beta subunit of bacterial RNA polymerase, forming a stable complex that blocks RNA elongation, ultimately causing bacterial cell death (Brunton & Bjorn, 2022). Rifampicin remains a cornerstone of modern active TB treatment and prevention therapy due to its potent activity against both replicating and dormant forms of *M. tuberculosis* (Gumbo et al., 2007; World Health Organization, 2024).

1.2.3.1 Resistance

Most cases of rifampicin resistance arise primarily from mutations in the beta subunit of mycobacterial RNA polymerase, particularly the Ser531Leu substitution, which reduces drug binding affinity (Goldstein, 2014). These mutations result in varying degrees of resistance, underscoring the complex nature of rifampicin resistance (Wehrli, 1983).

1.2.3.2 Absorption

Rifampicin is rapidly absorbed on an empty stomach, reaching peak plasma levels within 2-4 hours after oral administration (Acocella, 1978). Acidic conditions significantly enhance absorption, while co-administration with food or alkaline substances like sodium bicarbonate reduce bioavailability (Acocella, 1978; FDA & CDER, 2010). First-pass metabolism in the liver plays a central role in rifampicin's pharmacokinetics, with dose escalation beyond 600 mg yielding a more than proportional increase in drug exposure due to metabolic saturation (Acocella, 1978) Saturation of this process results in a more than dose-proportional increase in the drug’s exposure when the rifampicin dose is escalated from the therapeutic 600 mg dose (Acocella,

1978). Upon repeated administration, autoinduction of metabolism reduces drug exposure, stabilizing after approximately 21 days (Chirehwa et al., 2016a).

1.2.3.3 Distribution

Rifampicin distributes widely across body tissues and fluids, including cerebrospinal fluid, and binds approximately 88% to plasma proteins, predominantly albumin (Alghamdi et al., 2018). Its unbound fraction diffuses freely into tissues, maintaining therapeutic activity.

1.2.3.4 Metabolism and elimination

The liver metabolizes rifampicin through deacetylation into desacetylrifampicin, an active metabolite, which is excreted in bile and urine (Acocella, 1978). Following a single 600 mg dose, the elimination half-life is approximately 3.4 hours, extending to 5 hours at higher doses. However, with repeated administration, half-life decreases to 2-3 hours due to autoinduction (FDA & CDER, 2010).

1.2.3.5 Enzyme induction and drug interactions

Rifampicin is known to induce metabolizing enzymes including its own, a process known as auto-induction (Gorski, 2003). This process is mediated through binding and activation of an orphan nuclear receptor called PXR (Bolt, 2004). The rifampicin-PXR complex forms a heterodimer with the retinoid X receptor, which then binds to a DNA response element. This results in increased DNA transcription of genes that encode several transport proteins and metabolizing enzymes (Niemi et al., 2003). As a result, rifampicin reduces the efficacy of numerous drugs, including oral midazolam, simvastatin, and PIs, by accelerating their metabolism.

1.2.3.6 High dose rifampicin

To address the persistence of *M. tuberculosis* and shorten TB treatment duration, higher doses of rifampicin have been explored (Dickinson & Mitchison, 1981; Philips & Ernst, 2012). Boeree *et al*. demonstrated that increasing the dose of rifampicin to 35 mg/kg reduced time to sputum culture conversion from 62 to 48 days compared to the standard 10 mg/kg dose (Boeree et al., 2017a). Other studies have also supported the efficacy and relative safety of doses exceeding 20 mg/kg, particularly in severely ill patients (Seijger et al., 2019; Wasserman et al., 2021). The implementation of higher-dose rifampicin in routine care remains subject to regulatory and economic considerations.

1.2.3.7 Adverse effects

The therapeutic use of rifampicin has been associated with gastrointestinal disturbances like nausea, vomiting, and diarrhoea, as well as hepatotoxicity and thrombocytopenia (FDA & CDER, 2010). Less frequent effects include dizziness, headaches, and fatigue.

1.2.4 Pharmacology of Isoniazid

Isoniazid (isonicotinyl hydrazine, INH) is an important antimycobacterial agent predominantly used in combination therapies for treatment of drug-susceptible TB (FDA & CDER, 2016a; Klein et al., 2016; World Health Organization, 2022b). Administered at a standard adult dose of 300 mg, INH exhibits potent bactericidal activity against replicating intracellular and extracellular *M. tuberculosis* (FDA & CDER, 2016a). It has the highest early bactericidal activity among TB drugs, achieving an initial kill rate of greater than 90% of *M. tuberculosis* within the first 48 hours of treatment (Donald & Diacon, 2008; Mitchison, 2000). INH is also indicated for treatment of latent

TB, preventive TB therapy for high-risk populations, and some forms of DR-TB (World Health Organization, 2022b, 2022a).

1.2.4.1 Mechanism of action

INH is a pro-drug that passively diffuses into *M. tuberculosis* (Brunton & Bjorn, 2022). Within the cells, it is activated by catalase-peroxidase (KatG), an enzyme encoded by the mycobacterial *katG* gene. This activation produces reactive isonicotinoyl radicals (Argyrou et al., 2007), which interact with cellular pyridine nucleotide coenzymes (nicotinamide adenine dinucleotide (NAD) and nicotinamide adenine dinucleotide phosphate (NADP) to form isonicotinoyl-NAD(P) adducts (Argyrou et al., 2007). Among these adducts, the acyclic 4S isomer inhibits enoyl acyl carrier protein reductase (InhA) and β-ketoacyl-ACP synthase (KasA), thereby disrupting mycolic acid synthesis, an essential component of the mycobacterial cell wall (Argyrou et al., 2007; Brunton & Bjorn, 2022). This process leads to cell death. Additionally, the 4R isomer of the nicotinoylNADP adduct inhibits mycobacterial dihydrofolate reductase, interfering with nucleic acid synthesis (Argyrou et al., 2007). Other products of KatG-mediated activation like superoxide, hydrogen peroxide, and nitric oxide, may also contribute to the bactericidal effects of INH (Timmins & Deretic, 2006).

1.2.4.2 Resistance

Resistance to isoniazid mostly arises from spontaneous mutations in several mycobacterial genes, including *katG, inhA, kasA* and *ahpC* (Brunton & Bjorn, 2022; FDA & CDER, 2016a). These mutations can be rapidly selected and amplified by monotherapy. Mutations involving deletion or alteration of *katG*, particularly the serine-to-asparagine substitution at position 315, are the

most prevalent in clinical isolates and confer high-level resistance (Brunton & Bjorn, 2022; Vilchèze & Jacobs, 2014).

Overexpression of *inhA* and compensatory mutations in the *ahpC* promoter region, which enhance bacterial survival under oxidative stress, are associated with low-level resistance (Brunton & Bjorn, 2022). Additional mechanisms, such as changes in drug activator expression, redox imbalances, drug inactivation, and efflux pump activation, have also been proposed as contributors to INH resistance (Vilchèze & Jacobs, 2014).

1.2.4.3 Absorption

INH is rapidly and completely absorbed (Weber & Hein, 1979), with peak plasma concentrations reached within 1-2 hours (Klein et al., 2016; Weber & Hein, 1979). Absorption primarily occurs in the small intestine and remains largely unaffected by partial surgical resections of the gastrointestinal tract (Klein et al., 2016). However, concomitant use of antacids delays gastric emptying (Weber & Hein, 1979). Similarly, food, particularly sugar-containing meals, can convert INH to less absorbable hydrazone derivatives (Klein et al., 2016; Weber & Hein, 1985).

1.2.4.4 Distribution

INH is extensively distributed throughout body fluids and tissues (FDA & CDER, 2016a). It has very low plasma protein binding (Weber & Hein, 1979) of about 14% (Alghamdi et al., 2018). The drug readily crosses the blood-brain barrier, achieving therapeutic concentrations in the cerebrospinal fluid (Donald, 2010). INH also appreciably penetrates lung tissue, pleural fluid, and caseous lesions (Weber & Hein, 1985). Furthermore, it crosses the placenta and is minimally excreted in breast milk (Singh et al., 2008; Weber & Hein, 1985).

1.2.4.5 Metabolism and excretion

Metabolism of INH predominantly occurs in the liver and intestines (FDA & CDER, 2016a; Weber & Hein, 1979), through *N*-acetylation, catalysed by *N*-acetyltransferase-2 (NAT2), which converts INH to N-acetylisoniazid (AcINH) (Klein et al., 2016). AcINH undergoes further biotransformation to isonicotinic acid and monoacetylhydrazine. Isonicotinic acid is conjugated with glycine and excreted via the kidneys, while monoacetylhydrazine is converted to diacetylhydrazine (Weber & Hein, 1979). Approximately 80% of INH and its metabolites are excreted in urine, with about 10% eliminated through faeces (FDA & CDER, 2016; Klein et al., 2016; Weber & Hein, 1979).

1.2.4.5.1 Pharmacogenetics of isoniazid and acetylator status

The *NAT2* gene, which encodes NAT2 enzyme, exhibits significant polymorphism, resulting in three major acetylator phenotypes: slow, intermediate, and rapid (McDonagh et al., 2014). Variability in NAT2 function is attributed to single nucleotide polymorphisms (SNPs) that affect enzyme stability, substrate affinity, or proteasome degradation targeting (McDonagh et al., 2014; Weber & Hein, 1985).

Although there are many more identified SNPs, Hein and Doll recently used a four-SNP genotype panel of rs1801279 (191G>A), rs1801280 (341T>C), rs1799930 (590G>A), and rs1799931 (857G>A) to infer NAT2 acetylator phenotype with high accuracy (Hein & Doll, 2012). Participants were categorized as rapid acetylators if they were homozygous for the common allele of all four SNPs (i.e., GG, TT, GG, GG, respectively). Those who were heterozygous for only one of the four SNPs were categorized as intermediate acetylators, and those who were heterozygous for two or more SNPs, or homozygous for the variant allele for any of the SNPs, were categorized as slow acetylators (Hein & Doll, 2012; McDonagh et al., 2014).

The elimination half-life of INH exhibits bi-modal distribution, ranging from 35 to 110 minutes in rapid acetylators and 110 to 400 minutes in slow acetylators (Weber & Hein, 1979).

1.2.4.6 Adverse drug reaction

The most frequent ADRs to INH are neurologic and hepatic in nature (FDA & CDER, 2016a). Peripheral neuropathy, characterized by paraesthesia in extremities, is the commonest neurotoxic effect, particularly at high INH doses. It occurs more frequently in malnourished, diabetic, or alcoholic patients, as well as in slow acetylators (FDA & CDER, 2016a; Klein et al., 2016). Other neurotoxic manifestations include seizures, memory impairment, optic neuropathy, and toxic psychosis, often resembling symptoms of vitamin B6 deficiency. These effects can be mitigated by co-administration of vitamin B6/pyridoxine (FDA & CDER, 2016a).

Hepatotoxicity is the other major ADR to INH, manifesting as elevated serum transaminase levels, bilirubinaemia, jaundice, and, in severe cases, hepatitis (FDA & CDER, 2016a). Hepatic side effects typically emerge within the first three months of treatment and are often self-limiting, though some cases necessitate drug discontinuation (FDA & CDER, 2016a).

1.2.4.7 Interactions

INH inhibits several CYP enzymes, histaminase, and monoamine oxidase (Self et al., 1999). This inhibition can lead to food-drug interactions with tyramine- and histamine-rich foods, such as cheese and red wine, causing symptoms like headache, flushing, and hypotension (FDA & CDER, 2016a; Self et al., 1999).

Due to its CYP inhibition properties, INH increases serum concentrations and toxicity risks of drugs such as phenytoin and carbamazepine at standard doses, and theophylline and warfarin at higher

doses (Self et al., 1999). Although primarily recognized as a CYP inhibitor, INH also induces CYP2E1, contributing to the generation of toxic metabolites from acetaminophen (FDA & CDER, 2016a; Self et al., 1999).

1.2.5 Pharmacology of clofazimine

Clofazimine is a lipophilic substituted riminophenazine dye with notable anti-inflammatory and anti-mycobacterial properties (FDA & CDER, 2016b; Islam et al., 2023). Initially used for leprosy treatment alongside rifampicin and dapsone (Mirnejad et al., 2018), its role in TB management gained renewed interest after Van Deun *et al.* demonstrated its efficacy in shorter MDR-TB regimens (Van Deun et al., 2010). The WHO currently classifies clofazimine as a Group B drug for second-line DR-TB therapy (World Health Organization, 2022a).

1.2.5.1 Mechanism of action

Clofazimine exerts antimycobacterial effects by targeting bacterial membranes, disrupting respiration, and ion transport systems (FDA & CDER, 2016b). Its redox cycling generates reactive oxygen species such as superoxide and hydrogen peroxide (FDA & CDER, 2016b; Mirnejad et al., 2018). Additionally, it stimulates bacterial phospholipase A2, releasing toxic lysophospholipids that impair membrane integrity and K+ uptake (FDA & CDER, 2016b; Islam et al., 2023; Mirnejad et al., 2018). The drug may also bind selectively to DNA guanine, interfering with DNA functions in *M. tuberculosis*, and potentially disrupting some M. tuberculosis DNA functions (Mirnejad et al., 2018).

1.2.5.2 Resistance

Although not fully understood, clofazimine resistance has been linked to mutations in the Rv0678, Rv1979c, and Rv1453 genes (Islam et al., 2023; Sonnenkalb et al., 2023). Mutations in Rv0678, which regulates the mmpS5/L5 efflux pump, lead to pump overexpression and increased resistance to clofazimine and bedaquiline (Poulton et al., 2022; Sonnenkalb et al., 2023). Additionally, mutations in the *pepQ* gene are implicated in efflux-mediated resistance (Brunton & Bjorn, 2022).

1.2.5.3 Absorption

Clofazimine shows variable oral absorption, estimated at around 20%, which can be enhanced to approximately 70% by a microcrystalline suspension formulation (Holdiness, 1989). Absorption is also increased by a high-fat meal and decreased when taken with orange juice or antacids (Nix et al., 2004). Peak plasma levels are typically achieved (FDA & CDER, 2016b; Holdiness, 1989).

1.2.5.4 Distribution

Because of its high lipophilicity, clofazimine accumulates in fatty tissue (Holdiness, 1989). It can also be engulfed by macrophages and cells of the reticuloendothelial system throughout the body (FDA & CDER, 2016b). Clofazimine crystals were found predominantly in the mesenteric lymph nodes, adrenals, subcutaneous fat, liver, bile, gall bladder, spleen, small intestine, muscles, bones, and skin. It does not cross an intact blood brain barrier in therapeutically significant concentrations (Holdiness, 1989). Clofazimine also binds to alpha- and beta-lipoproteins in serum and negligibly to gamma-globulin and albumin (FDA & CDER, 2016b).

1.2.5.5 Metabolism and excretion

Clofazimine undergoes limited metabolism, with three urinary metabolites identified: one from hydrolytic dehalogenation and two from glucuronidation (Holdiness, 1989). Clofazimine is retained in the body for long and is excreted slowly, primarily as unchanged drug in faeces (Holdiness, 1989). A pharmacokinetic model proposed by Abdelwahab *et al.* (Abdelwahab, Wasserman, et al., 2020) described clofazimine disposition via a three-compartment pharmacokinetic model, reporting a shorter half-life (30 hours) than earlier estimates of 70 hours.

1.2.5.6 Adverse drug reactions

Common side ADRs to clofazimine include skin, mucosal, and body fluid discoloration, gastrointestinal disturbances, and gastric intolerance (FDA & CDER, 2016b). Clofazimine deposition in the gastrointestinal tract may cause bleeding and obstruction. Prolonged QT intervals, linked to inhibition of the hERG K+ channel (Wallis, 2016), pose a risk of fatal arrhythmias such as torsades de pointes (Abdelwahab, Court, et al., 2021), regular necessitating ECG monitoring.

1.2.5.7 Interactions

Clofazimine is a moderate-to-strong inhibitor of CYP3A4/5 and weakly inhibits CYP2C8 and CYP2D6 (Sangana et al., 2018). It strongly inhibits membrane transporters like P-glycoprotein and breast cancer resistance protein (Te Brake et al., 2016). Despite reports of the above interactions, clinical evidence of significant clofazimine induced DDIs remains limited.

1.2.6 Pharmacology of levofloxacin

Levofloxacin is the more active and efficacious isomer of fluoroquinolone antibiotic ofloxacin (FDA & CDER, 2018; Fish & Chow, 1997; Ji et al., 1995). Levofloxacin is classified by the WHO as Group A drugs, recommended for MDR-TB unless resistance is identified (World Health Organization, 2022a).

1.2.6.1 Mechanism of action

Levofloxacin inhibits bacterial DNA replication and transcription by attaching to the A subunit of the type II topoisomerase enzyme, DNA gyrase, and blocking DNA replication (Fish & Chow, 1997). At higher concentrations, it also disrupts topoisomerase IV activity, further impairing bacterial DNA processes (Brunton & Bjorn, 2022). Levofloxacin greatly penetrates cells and is effective against both gram-positive and gram-negative bacteria Fish & Chow, 1997).

1.2.6.2 Resistance

Resistance primarily arises from chromosomal mutations that alter DNA gyrase and diminish its affinity for the drug (Van Bambeke et al., 2005). Mutations, mostly due to transcription error, in the *gyrA*, *gyrB*, *parC*, and *parE* genes clustered in the quinolone resistance-determining region, contribute greatly to development of resistance to fluroquinolones (Van Bambeke et al., 2005). Additional mechanisms include decreased membrane porin expression and upregulated efflux pumps, which lower intracellular drug concentrations. Mutations in the *norA* gene are linked to increased fluroquinolone efflux in staphylococci (Wimer et al., 1998).

1.2.6.3 Absorption

Levofloxacin is well absorbed orally, bioavailability reaching 99% (FDA & CDER, 2018; Wimer et al., 1998). Peak plasma concentrations occur between 1 and 2 hours after an oral dose (Fish & Chow, 1997). Coadministration of levofloxacin with food results is slower absorption and lower peak concentrations without significant changes in the extent of absorption (Fish & Chow, 1997).

1.2.6.4 Distribution

Levofloxacin distributes rapidly and widely into most body tissues including breast milk and the blood-placenta barrier. The two important exceptions to this excellent penetration are the central nervous system and aqueous humour where concentrations achieved may be insufficient to treat infections (Fish & Chow, 1997). It effectively penetrates phagocytic cells and is therefore active against intracellular pathogens. Approximately 38% binds to plasma proteins, predominantly albumin (Fish & Chow, 1997).

1.2.6.5 Metabolism and excretion

Levofloxacin undergoes limited metabolism in humans, with 87% excreted as unchanged drug in urine and 4% in faeces (FDA & CDER, 2018). Its clearance involves both glomerular filtration and tubular secretion, necessitating dosage adjustments in patients with renal impairment (Wimer et al., 1998). Less than 5% of levofloxacin is eliminated as the desmethyl- and N-oxide metabolites in urine (Fish & Chow, 1997) and its terminal half-life is about 7.6 hours (FDA & CDER, 2018).

1.2.6.6 Adverse drug reaction

Levofloxacin is generally well tolerated, with gastrointestinal symptoms such as nausea, diarrhoea, vomiting, and abdominal pain being the most common. Central nervous system

effects, though less frequent than with other fluoroquinolones, include anxiety, agitation, and nervousness. The drug may increase seizure risk and should be avoided in susceptible individuals (FDA & CDER, 2018; Fish & Chow, 1997).

1.2.6.7 Interactions

Multivalent cation containing products like antiacid, and supplements chelate levofloxacin and result in decreased absorption by up to 50% and should not be taken within 2 hours of an oral dose (FDA & CDER, 2018). Cimetidine and probenecid reduce renal clearance, slightly increasing drug exposure, though the clinical impact is limited (FDA & CDER, 2018; Fish & Chow, 1997). Minor interactions with theophylline, warfarin, and digoxin may may warrant monitoring for toxicity (FDA & CDER, 2018; Fish & Chow, 1997).

1.2.7 Pharmacology of linezolid

Linezolid is a synthetic antibiotic and the first member of the oxazolidinone class (Hashemian et al., 2018). It is highly effective against gram-positive bacteria, including strains resistant to standard treatments, such as streptococci, staphylococci, and enterococci (Stalker & Jungbluth, 2003). The WHO recommends linezolid as a Group A drug for DR-TB management (World Health Organization, 2022a).

1.2.7.1 Mechanism of action

Linezolid uniquely targets the bacterial ribosome, a crucial apparatus for initiation of protein synthesis (FDA & CDER, 2013; Stalker & Jungbluth, 2003). It inhibits bacterial protein synthesis by binding to the 23S ribosomal RNA of the 50S subunit, preventing the formation of a functional 70S initiation complex (FDA & CDER, 2013; Hashemian et al., 2018). This disruption interferes

with tRNA binding and halts bacterial translation. The drug is bacteriostatic against enterococci and staphylococci but bactericidal for streptococci (FDA & CDER, 2013).

1.2.7.2 Resistance

Linezolid's unique mechanism of action limits cross-resistance with other antibiotics (FDA & CDER, 2013). Resistance to linezolid is linked to a point mutation in the 23S rRNA, specifically the substitution of thymine for guanine at position 2576 (FDA & CDER, 2013; Hashemian et al., 2018). In staphylococci, resistance may also arise through the *cfr* gene, which encodes a methyltransferase enzyme and can be transferred between bacteria via plasmids (FDA & CDER, 2013).

1.2.7.3 Absorption

Linezolid has nearly 100% bioavailability after oral administration, with peak concentrations reached within 1 to 2 hours (FDA & CDER, 2013). Although a high-fat meal may delay absorption and reduce peak concentrations by 17%, the overall AUC mostly remains unchanged (Dryden, 2011). Additionally, antacids containing magnesium and aluminium hydroxide do not impact the pharmacokinetics of linezolid and can be safely used concurrently (Dryden, 2011).

1.2.7.4 Distribution

Linezolid distributes well to highly perfused tissues (FDA & CDER, 2013), and its volume of distribution is approximately equivalent to the volume of total body water (Stalker & Jungbluth, 2003). It exhibits relatively low protein binding (~31%), which is concentration-dependent (FDA & CDER, 2013; Stalker & Jungbluth, 2003).

1.2.7.5 Metabolism and excretion

Linezolid undergoes minimal metabolism, mainly through morpholine ring oxidation, producing two inactive metabolites: aminoethoxyacetic acid (via CYP2J2 and CYP4F) and hydroxyethyl glycine (via non-enzymatic oxidation) (FDA & CDER, 2013). Its plasma elimination half-life is approximately 3.4 to 7.4 hours (Dryden, 2011).

Approximately 84% of the administered dose of linezolid is excreted in urine, with 30% as unchanged linezolid, 40% as hydroxyethyl glycine, and 10% as aminoethoxyacetic acid (Dryden, 2011; FDA & CDER, 2013). Faecal excretion is minimal, with no parent drug recovered and only small amounts of the metabolites detected (Dryden, 2011; FDA & CDER, 2013).

1.2.7.6 Adverse drug reaction

The most common ADRs to linezolid are diarrhoea, nausea, and vomiting (Dryden, 2011). Linezolid is also associated with peripheral and ocular neuropathy, thrombocytopenia, anaemia, hyperlactatemia, and reticulocytopenia. Anaemia is attributed to the drug's direct effect on bone marrow red cell production (Hashemian et al., 2018).

1.2.7.7 Interactions

As a reversible, nonselective inhibitor of monoamine oxidase, linezolid may cause life-threatening serotonin toxicity when combined with other monoamine oxidase inhibitors such as phenelzine or isocarboxazid (Hashemian et al., 2018).

1.2.8 Pharmacology of cycloserine / terizidone

Cycloserine (D-4-amino-3-isoxazolidone) is a broad-spectrum antibiotic produced by *Streptococcus orchidaceous* (Brunton & Bjorn, 2022; Lowther et al., 2010). Terizidone is a

derivative of cycloserine and consists of two cycloserine molecules combined with terephthalic dialdehyde (Zítková & Toušek, 1974). After administration, it rapidly undergoes pre-systemic hydrolysis, converting back into cycloserine, through which it primarily exerts its pharmacological activity. Terizidone is favoured over its parent drug due to its improved tolerability and toxicity profile (Mulubwa & Mugabo, 2019). Both are classified as Group B drugs in the WHO-recommended DR-TB regimen (World Health Organization, 2022a).

1.2.8.1 Mechanism of action

Cycloserine is structural analogue of D-alanine, a critical component of the peptide chains that cross-link the polysaccharide chains in peptidoglycan (Azam & Jayaram, 2016; Brunton & Bjorn, 2022). It inhibits two critical enzymes: L-alanine racemase, which converts L-alanine to D-alanine, and D-alanine:D-alanine ligase, which forms the peptidoglycan precursor D-alanyl-D-alanine (Brunton & Bjorn, 2022; Prosser & De Carvalho, 2013).

1.2.7.2 Resistance

The molecular target and mode of action of cycloserine distinguish it from other antibiotic classes, preventing cross-resistance with other antibiotics (Prosser & De Carvalho, 2013. Resistance is linked to mutations in the *alr* gene, which encodes alanine racemase (Brunton & Bjorn, 2022). Recent findings by Chen *et al*. suggest that D-cycloserine resistance mechanisms are complex and potentially involve genes associated with lipid metabolism, stress response, and methyltransferase (Chen et al., 2017).

1.2.7.3 Absorption

Cycloserine is rapidly absorbed (70–90%) after oral administration (Neon Healthcare Ltd, 2023), reaching peak plasma concentrations within 45 minutes on an empty stomach. However, a fatty meal may delay attainment of peak concentrations to over 3 hours (Brunton & Bjorn, 2022).

1.2.7.4 Distribution

Cycloserine exhibits minimal binding to plasma proteins and extensively distributes throughout various tissues and bodily fluids, including cerebrospinal fluid, amnionic fluid and breast milk. Additionally, it readily crosses the placental barrier, resulting in foetal blood concentrations equivalent to those in the maternal circulation (Neon Healthcare Ltd, 2023).

1.2.7.5 Metabolism and excretion

Terizidone is hydrolysed in the GI tract to cycloserine and terephthalaldehyde (Zítková & Toušek, 1974). Notably, there is no evidence of in vivo antimicrobial activity of terephthalaldehyde. Approximately 35% of cycloserine is metabolized into unspecified metabolites. Up to 70% of an administered dose is excreted unchanged in the urine within 24 hours. Accumulation can occur in renal failure patients and cause toxicity (Brunton & Bjorn, 2022). The half-life of cycloserine ranges from 8 to 12 hours (Neon Healthcare Ltd, 2023).

1.2.7.6 Adverse drug reaction

Neuropsychiatric symptoms are prevalent among patients receiving cycloserine, affecting approximately 50% of individuals on a daily dosage of over 1 gram. Manifestations of these symptoms vary widely, ranging from minor complaints like headache and drowsiness to severe conditions including psychosis, seizures, and suicidal ideations (Brunton & Bjorn, 2022).

1.2.7.7 Interactions

Alcohol particularly increases the risk of seizure in patients taking cycloserine and because of this, other treatment options should be considered in patients with a history of epilepsy and depression (Neon Healthcare Ltd, 2023).

1.3 Study Justification

Despite continued global efforts to curb the HIV pandemic, both new infections and AIDS-related fatalities remain persistently high (UNAIDS, 2023b). In SSA, the situation is worsened is worsened by concurrent prevalence of other infectious diseases like malaria and TB, with TB standing out as a leading cause of death among people living with HIV (UNAIDS, 2023b). For individuals co-infected with TB and HIV, prompt and simultaneous treatment initiation is essential for improving survival rates and enhancing quality of life (Odone et al., 2014; Salim, 2010; The INSIGHT START Study Group, 2015).

The challenge becomes more complex in cases involving drug-resistant TB, which requires treatment with second-line medications often associated with increased adverse effects (Shean et al., 2013). Treatment regimens for both HIV and TB rely on combinations of three or more carefully selected drugs to maximize effectiveness, minimize toxicity, and limit the emergence of resistant strains (Mitchison, 2005; Scourfield et al., 2011). Since these treatments are administered over long periods, maintaining adherence is crucial to achieving successful outcomes (Singh et al., 1999; Paterson et al., 2000).

A significant challenge in managing TB and HIV coinfection lies in the drug-drug interactions between the medications used for each condition. These drugs often affect each other's

pharmacokinetics due to overlapping and opposing effects on metabolic enzymes (Mukonzo et al., 2019). For instance, rifampicin, a key drug for treating drug-susceptible TB, is known to potently induce CYP enzymes, which can reduce the exposure of co-administered drugs (Niemi et al., 2003). Moreover, higher doses of rifampicin have been investigated to improve TB outcomes and shorten treatment duration which may further complicate pharmacokinetic interactions (Boeree et al., 2017b). Consequently, when combined with ARV drugs like DTG and PIs, dose adjustments are required to sustain effective drug levels and therapeutic efficacy (Dooley et al., 2013, 2020; Gausi et al., 2024).

Given the need to maintain therapeutic drug exposure during HIV-TB co-treatment, accurately quantifying the extent and effects of drug-drug interactions becomes critical. This evaluation is essential to assess the adequacy of current treatment strategies and to support evidence-based approaches for optimizing co-treatment outcomes.

1.4 Aim

The overall aim of this thesis is to use population pharmacokinetic modelling to characterize drug-drug interactions between antiretroviral and anti-TB medication to optimize their concurrent use in people with HIV.

Objectives

1. To describe the population pharmacokinetics of standard- and high-dose rifampicin when taken with dolutegravir- or efavirenz-based ART.
2. To investigate the effect of high-dose rifampicin and UGT1A1 polymorphism on dolutegravir pharmacokinetics and simulate treatment target attainment in different rifampicin dosing strategies.
3. To characterize the drug-drug interaction between rifampicin and ritonavir-boosted atazanavir and simulate the probability of target attainment with different regimen scenarios.
4. To investigate the pharmacokinetic interactions between clofazimine and isoniazid, linezolid, levofloxacin, and cycloserine in adults with DR TB.

Chapter 2: Methodology

2.1 Study designs and data description

2.1.1 SAEFRIF study

SAEFRIF stands for Pharmacokinetics, **SA**fety/tolerability, and **EF**ficacy of high-dose **RIF**ampicin in TB-HIV co-infected patients on efavirenz- or dolutegravir-based ART. It was a randomised, open-label, phase IIb clinical trial carried out among TB patients coinfected with HIV attending an outpatient clinic in Kampala, Uganda. Participant recruitment was carried out at the Infectious Disease Institute of Makerere University, and ethical approval was obtained from the Joint Clinical Research Center research and ethics committee (JC2218) in Kampala, Uganda (Nabisere et al., 2020).

Participants: The study recruited newly diagnosed TB patients with HIV. The main inclusion criteria included adults aged 18 years or older, with confirmed diagnoses of HIV and drug-susceptible TB. Female participants were excluded if they were pregnant or refused birth control during the study period. Individuals with decompensated liver disease as indicated by abnormal liver function tests, or poor renal function, defined as a glomerular filtration rate less than 50 ml/minute, were also excluded.

Study procedures: Upon recruitment, participants were randomised to take anti-TB regimens containing either the high- (35 mg/kg) (35RHZE) or the standard- (10 mg/kg) dose rifampicin (10RHZE). All other anti-TB drugs (isoniazid, ethambutol, and pyrazinamide) were given at their standard dose for weight bands using the fixed dose combination (FDC) tablets supplied by the

National TB Control Program. Participants in the 35RHZE arm had their rifampicin doses supplemented by 300 mg rifampicin capsules to complement that in the FDC.

Two weeks after starting TB treatment, ART-naïve participants were started on ART and randomly assigned the recommended first-line regimens containing either dolutegravir or efavirenz, together with tenofovir and lamivudine. Those who were already on ART at enrolment continued the same ART regimen. The dose of participants in the dolutegravir arm was doubled to 50 mg twice daily by administering an additional 50 mg dolutegravir-only tablet in the morning, in addition to the nightly dose taken with the rest of their ART.

At the end of the intensive phase of TB treatment, all participants were given the standard continuation phase treatment of isoniazid and rifampicin. The dolutegravir dose was restored to the standard 50 mg once-daily dose two weeks after the discontinuation of rifampicin containing TB treatment. Participants were also assessed for toxicities at each visit, and TB and HIV treatment outcomes were evaluated at the end of TB treatment at week 24.

Pharmacokinetic sampling: Blood sampling for PK analysis was performed six weeks after initiation of TB treatment as is illustrated below in Figure 1. During the study visit, participants came to the clinic in the morning after an overnight fast. Intake of the TB drugs and the morning dose of dolutegravir was observed.

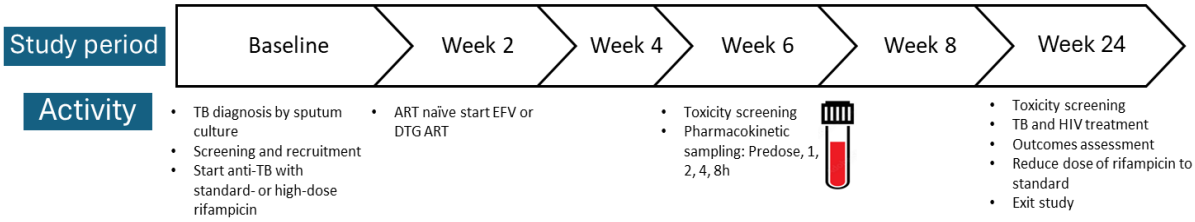

Figure 1: SAEFRIF study design

Blood samples to measure rifampicin and dolutegravir concentrations were drawn just before drug intake (0 h), and at 1-, 2-, 4-, and 8-hours after intake of the anti-TB drugs. These blood samples were immediately placed in a dark cooler box and transported to the laboratory within 30 minutes of collection. The samples were then centrifuged, aliquoted, batched, and frozen at -80 ^{0}C until quantification of the drug concentration was carried out.

Drug assays: Dolutegravir concentrations were determined at Infectious Disease Institute Translational Laboratory, by reverse phase high performance liquid chromatography (HPLC) mass spectrometry using a modified version of a previously published method (Bennetto-Hood et al., 2014). The assay was validated, and the lower limit of quantification (LLOQ) was 0.05mg/L while the upper limit was 10 mg/L. The inter-day precision (percent coefficient of variation [CV%]) based on quality control samples was between 1.8% and 10.88%, and accuracy (percent bias) was between –1.0% and 10.0%.

Total plasma rifampicin concentrations were analysed by validated high-performance liquid chromatography with ultraviolet detection (HPLC-UV), at the same laboratory. Analysis was carried out on an LC-2010C HT system (Shimadzu, Kyoto, Japan), equipped with a controller, a quaternary gradient pump, an ultraviolet detector, an autosampler, a column oven, an on-line

degasser and was remotely operated by class VP software. The assay was internally validated and performed well in an external international quality control (QC) programme; accuracy of the QC samples ranged from 94% to 102% depending on the concentration, and the intra- and inter-assay CV% ranged from 2.9 to 3.6% and 3.4 to 4.8% respectively. The calibration curve for rifampicin in plasma covered a range from 0.25 to 15 mg/L. Samples with concentrations above the upper limit of quantitation were diluted with blank plasma before re-analysis.

2.1.2 DERIVE study

DERIVE is an acronym for **D**ose **E**scalation study to determine the pharmacokinetics of Atazanavir administered with **RI**fampicin to HI**V** positive adults on s**E**cond-line ART regimen with suppressed HIV-1 viral load. It was an open-label, single-arm, doe-escalation study (NCT04121195, EDCTP) with ethical approval from; the Joint Clinical Research Center (JCRC) Ethics Committee, National Drug Authority, and Uganda National Council of Science and Technology.

Participants: Study participants were enrolled from the outpatient clinic of JCRC located in Kampala, Uganda. Adults with HIV aged 18 to 65 years, who had been receiving a second-line ART regimen containing ATV/r and two NRTIS for at least six months, were recruited. Participants were excluded if their liver enzymes and renal function were not in the normal range. Other exclusion criteria included patients with active TB, detected by X-Ray or clinical history/examination, hepatitis B, or on concomitant medication known to interact with study drugs. Women who were breast feeding, pregnant or not on effective contraception were also excluded from the study.

Study procedures: Upon recruitment, standard doses of NRTIs were maintained throughout the study. Treatment was open-label and study drugs were administered for 42 days and in five different study periods. The first 7 days after enrolment comprised period 1 and steady-state

pharmacokinetic sampling (PK1) was carried out on the last day. From day 8, participants' regimens were supplemented with 600 mg of rifampicin once daily and 50 mg of dolutegravir twice daily to prevent the development of drug resistance due to potentially sub-therapeutic levels of atazanavir. A follow-up pharmacokinetic evaluation was conducted after 14 days on day 21 (PK2). Subsequently, the dose of ATV/r was increased to the PBPK model-predicted dose of 300/100 mg twice daily (Montanha et al., 2022), and another pharmacokinetic evaluation was carried out one week later, on day 28 (PK3). Following the third pharmacokinetic visit, the rifampicin dose of the participants was doubled to 1200 mg once daily for an additional seven days, with a final pharmacokinetic evaluation conducted on day 35 (PK4). Rifampicin was then discontinued, and the ATV/r reduced to 300/100 mg once daily. However, the dolutegravir 50 mg twice-daily dose was continued for an additional two weeks until day 49 to allow the residual effect of rifampicin to diminish. Participants were monitored for safety up to day 60, at which point they exited the study. Figure 2 below illustrates the study design of the DERIVE study.

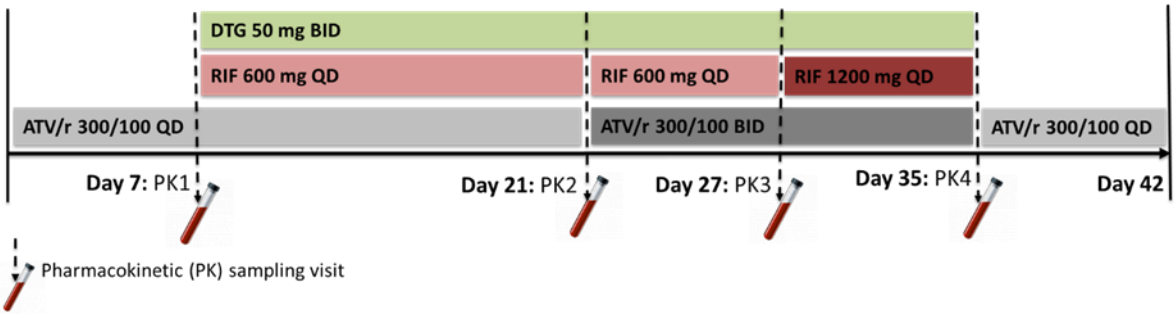

Figure 2: DERIVE study design

Pharmacokinetic sampling: During each of the pharmacokinetic visits, participants received study medications in the morning after fasting overnight for at least 8 hours. A total of 4 mL blood samples were collected just before dosing and 0.5-, 1-, 2-, 4-, 6-, 8-, and 12-hours post observed dose. An additional 24-hour sample was collected during PK1, and all trough (24 and 12h) samples

were collected in duplicate. The blood samples were immediately centrifuged at 1900g to separate plasma and stored at −80°C until being shipped for assay.

Drug assays: All samples were transferred for assay to the Clinical Pharmacokinetics Laboratory in the Division of Clinical Pharmacology of the University of Cape Town. Rifampicin assay was carried out by High-performance liquid chromatography with tandem mass spectrometry detection. The calibration range was 0.117–30.0 mg/L, with inter-day accuracy 101–107%, and precision coefficient of variation (%CV) 2.70–13.7.

A validated multiplex assay was utilized to analyse the plasma concentrations of atazanavir and ritonavir. This assay involved liquid-liquid extraction followed by high-performance liquid chromatography with tandem mass spectrometry detection. During validation, the calibration ranges were as follows: 0.030 mg/L (LLOQ) to 10.0 mg/L for atazanavir and dolutegravir, and 0.005 to 2.50 mg/L for ritonavir. The accuracy and precision of the low, medium, and high-quality controls ranged between 99.7% and 109%, with a coefficient of variation below 8.80%.

2.1.3 ISA-DRPK study

The **I**ndia-**S**outh **A**frica **D**rug **R**esistance **P**harmacokinetic study was a non-interventional, prospective cohort study among DR-TB patients who were about to begin clofazimine-based treatment. This study took place at the Klerksdorp/Tshepong Hospital Complex in North West Province, South Africa, and received ethics approval from the Human Research Ethics Committee of the University of Witwatersrand (REF: 171115B).

Participants: Eligible participants were newly diagnosed, adults with confirmed pulmonary DR-TB scheduled to start clofazimine-containing therapy. Given clofazimine's delayed onset of action, the attending physician evaluated whether delaying its administration for the first two weeks of

treatment would pose a significant risk to the patient. If such a risk was identified, the patient was excluded from the study. Additional exclusion criteria included pregnancy, isoniazid mono-resistance, a poor prognosis at enrolment, prior treatment with bedaquiline or clofazimine within the last two years, and refusal to undergo HIV testing.

Study procedure: Study participants were hospitalized for the initial two weeks of treatment, during which they received their DR-TB medications under direct observation, accompanied by a meal. The daily oral dosages were: 100 mg for clofazimine, 450/600 mg for high-dose isoniazid, 600 mg for linezolid, 750/1000 mg for levofloxacin, and 750 mg for terizidone.

Pharmacokinetic sampling: Pharmacokinetic sampling was done on day 14 (visit 1). Subsequently, clofazimine was added to their regimen, and a second pharmacokinetic sampling (visit 2) was conducted 21 days later. At both visits 1 and 2, blood samples for pharmacokinetics evaluation were collected just before dosing and at 2, 4, 6, 8, and 10 hours after the observed dose, as summarised in the Figure 3 below.

After collection, blood samples were immediately placed on ice, transferred to an on-site laboratory, and centrifuged at 1500G to separate the plasma. The plasma was aliquoted and stored at –80°C until it was batched and transferred for analysis at the University of Cape Town's Division of Clinical Pharmacology laboratory.

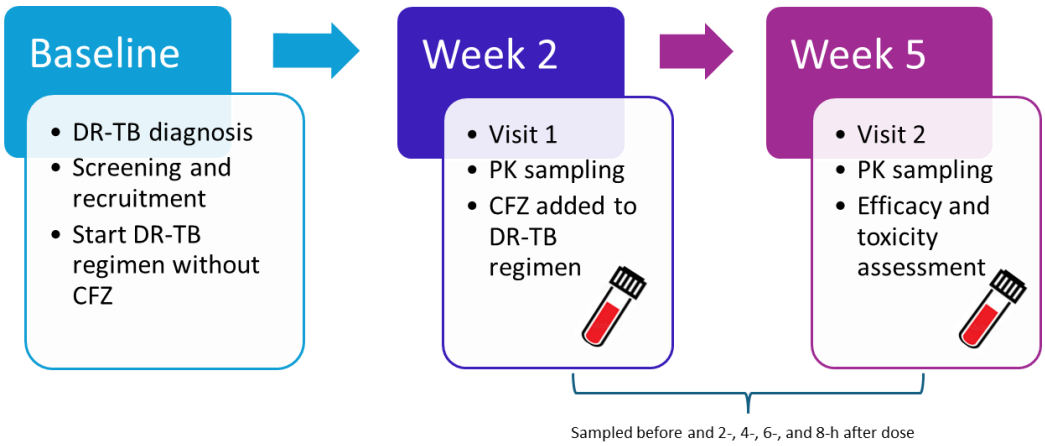

Figure 3: ISA-DRPK study design

Drug assays: In the initial participants, visit 2 samples were tested for clofazimine, with additional drugs assayed opportunistically based on the participants' prescribed regimens. Concentrations of pyrazinamide and ethambutol were not measured due to their unlikely interaction with clofazimine (Arbex et al., 2010). Similarly, bedaquiline was not included due to its long terminal half-life (Khoshnood et al., 2021) and slow accumulation, complicating data interpretation between the two study visits. Plasma concentrations were quantified using previously validated liquid chromatography-tandem mass spectrometry assays with the following LLOQ: 0.00781 mg/L for clofazimine (Abdelwahab, Wasserman, et al., 2020), 0.105 mg/L for isoniazid (Abdelwahab, Leisegang, et al., 2020), 0.100 mg/L for linezolid (Abdelwahab, Wasserman, et al., 2021), 0.0781 mg/L for levofloxacin (Denti et al., 2018), and 0.313 mg/L for cycloserine (Court et al., 2018). Other details are presented in Table 1 below.

Table 1: Inter-day accuracy, precision ranges and lower limits of quantification of the pharmacokinetic analysis methods for the assayed drugs in the ISA-DRPK study.

Drug analyzed	Range of inter-day accuracy (%)	Range of precision (%)	LLOQ (mg/L)
Clofazimine	102 – 103	2.50 – 5.00	0.00781
Isoniazid	95.3 – 100	5.70 – 6.50	0.105
Linezolid	90.1 – 98.1	3.50 – 3.60	0.100
Levofloxacin	94.5 – 98.6	2.40 – 3.00	0.0781
Cycloserine	89.9 – 97.0	3.30 – 15.3	0.313

LLOQ; lower limit of quantification.

NAT2 Phenotype: Additional consent for genetic studies was obtained. Genomic DNA was isolated as previously described (Longmire et al., 1987), and genotyping was performed using Sanger sequencing of the NAT2 gene following amplification with the primers 5’ ATTAACTGACATTCTTGAGC 3’ and 5’ GCACATAAGTTGATAATTAG 3’. Acetylator status was assigned based on the genotype of four single nucleotide polymorphisms (SNPs): rs1801279 (c.191G>A), rs1801280 (c.341T>C), rs1799930 (c.590G>A), and rs1799931 (c.857G>A) (Gausi et al., 2021; Hein & Doll, 2012). Participants were categorized as rapid acetylators if they were homozygous for the common allele of all four SNPs (GG, TT, GG, GG). Those heterozygous for only one of the SNPs were categorized as intermediate acetylators, and those heterozygous for two or more SNPs, or homozygous for the variant allele for any SNP, were categorized as slow acetylators (Gausi et al., 2021; McDonagh et al., 2014).

2.2 Data analysis

2.2.1 Exploratory data analysis

Study data was made available in multiple spread sheets obtained from information collected using study case report forms. A comprehensive data management and manipulation process was then conducted, which included compiling, cleaning, and formatting the raw data files into an analysis-ready dataset using R software (Andy Bunn, 2008; Crawley, 2010). During this process, the data was also explored by generating graphical and tabular summaries to investigate informational content relative to potential models to be evaluated. This data exploration highlighted important trends, identified outliers and extreme values that required prior exclusion, and determined potential covariates.

2.2.2 Pharmacometrics

Pharmacometrics is a field of clinical pharmacology where drug and disease characteristics are quantified using mathematical and statistical models, to aid efficient drug development, regulatory decision-making and provide guidelines for drug dose optimization (FDA, 2021; Gobburu, 2010). It involves developing models to characterize, understand, and predict a drug's pharmacokinetic, pharmacodynamic, and biomarker-outcome behaviour (Barrett et al., 2008).

Pharmacokinetics is the study and characterization of the time course of drug absorption, distribution, metabolism, and elimination, as well as their relationship to the intensity and time course of therapeutic and adverse effects (Burton, 1986). Pharmacokinetics has also been described as what the body does to the drug. Conversely, pharmacodynamics is the study of the biochemical and physiological effects of drugs on the body, their mechanisms of action, and the

relationship between drug concentration and effects (Maxwell, 2024). This has also been referred to as what the drug does to the body.

Population pharmacokinetics

Population pharmacokinetics (PopPK) is the study of variability in plasma drug concentrations between individuals in a population when standard doses are administered (Aarons, 1991). Variability in the pharmacokinetics can arise due to demographic, pathologic or therapeutic characteristics of individuals and may in turn affect the drug's dose-response relationship (Aarons, 1991; Holford & Sheiner, 1982). PopPK analysis seeks to identify significant predictors of drug exposure and pharmacokinetics, and to determine the necessary dose adjustments to maintain optimal drug exposure that ensures the best therapeutic outcome.

Unlike the traditional non-compartmental (NCA) approaches like the two-stage approach that summarizes individual pharmacokinetic parameters, PopPK modelling involves studying the entire population together (Menger, 2006; Wright, 1998). NCA analysis relies on straightforward mathematics, making it easy to implement. However, it necessitates more intensive sampling and strict adherence to study design (Owen & Fiedler-Kelly, 2014). Additionally, NCA has limited flexibility in describing complex kinetics and predicting unobserved scenarios (Wright, 1998).

Nonlinear mixed-effects modelling

Nonlinear mixed effects (NLME) modelling is a tool used to account for different levels of variability in PopPK data (Menger, 2006). Nonlinearity in NLME models arises because dependent variables, such as drug concentration, change in a nonlinear manner with respect to independent variables, like time (Mould & Upton, 2013). Mixed-effects modelling involves the parameterization of models to include fixed effects (parameters that remain constant across

individuals) and random effects (parameters that vary across individuals) (Mould & Upton, 2013). A NLME PopPK model comprises three major aspects, namely the structural model, stochastic model, and covariate model.

2.2.2.1 Structural model

The structural model aims to describe the typical time course of the response/dependent variable. The structural elements of a PopPK model, such as clearance and volume, are represented by fixed effect parameters, usually designated Greek letter THETA (θ_n), where n is an integer index defining a particular element in the vector of all THETA parameters in the model (Owen & Fiedler-Kelly, 2014).

For pharmacokinetic data, the structural model should satisfactorily describe the typical plasma concentration-time profile of the drug within the observed population. In the case of pharmacodynamic data, an appropriate model should explain how the drug exposure or concentration effects changes in relevant response/biomarker over time. For example, the structural model for a one-compartment pharmacokinetic model with first-order absorption and elimination (Figure 2) may be mathematically defined by Equation 1 below (Owen & Fiedler-Kelly, 2014).

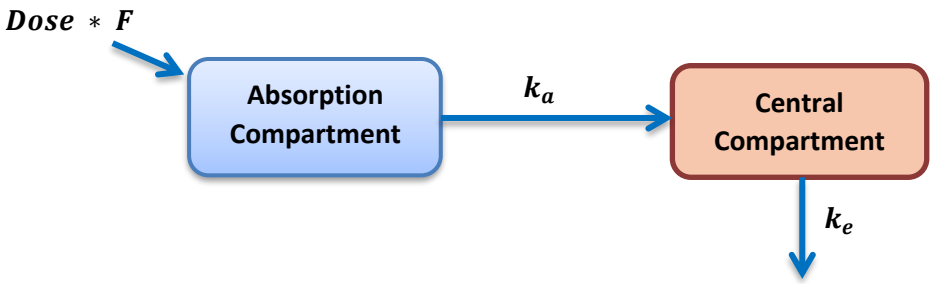

Figure 4: One compartment model with first order absorption and elimination

$$\boldsymbol{C_{pred,i} = \frac{k_a * F * Dose}{V\,(k_a - k_e)}\left(e^{-k_e * t_i} - e^{-k_a * t_i}\right)}$$

Equation 1: One-compartment model with first-order absorption and elimination

where k_a is the first-order absorption rate constant, V is the volume of distribution, k_e is the first-order elimination rate constant, and F is the bioavailability. $C_{pred,i}$ represents the model-predicted concentration/observation at the i^{th} time point following the administration of a single dose ($Dose$).

2.2.2.2 Statistical model

The statistical component of a PopPK model describes variability in the structural model (Mould & Upton, 2013). Variability in PopPK models can be characterised with random effect parameters that quantify the magnitude of unexplained variability in parameters (Level 1), and the error in model predictions (Level 2) (Owen & Fiedler-Kelly, 2014).

Level 1 random effects describe the magnitude of the difference in parameter values between subjects (i.e., between-subject variability, BSV) or between occasions (doses) within the same subject (i.e., between-occasion variability, BOV) (Owen & Fiedler-Kelly, 2014; Mould & Upton, 2013). Some datasets may also support the inclusion of between visit variability (BVV) which accounts for parameter differences across different study visits of an individual that may not be captured by the ones described above.

Level 1 random effects in the model are generally denoted by the Greek letter ETA (η), and the vector containing an individual subject's estimates of these random errors is termed as the ETA vector ($\eta_{i,n}$), where i denotes a particular individual and n is an index variable representing a specific element (parameter) of the vector. Level 1 parameters of the population are assumed to

follow a normal distribution with a mean of zero and a standard deviation of OMEGA (ω_n). The Level 1 random parameter that is estimated in most PopPK models is the variance, ω_n^2, which is the square of the standard deviation (Owen & Fiedler-Kelly, 2014). For example, if clearance (fixed effect) is denoted $THETA\ (1)$ and its Level 1 random error is $ETA\ (1)$, it follows that the model predicted clearance of any individual subject would be written as shown in Equation 2, below:

$$\boldsymbol{CL\ = THETA\ (1) * EXP\ (ETA(1))}$$

Equation 2: An expression of the fixed and random effects of clearance (CL)

Since the random effects are assumed to arise from a log-normal distribution, the variance estimate is also in the log-domain. Equation 3 below is then used to convert the variance to coefficient of variation, CV%, which in the same magnitude/domain as the THETA values (Mould & Upton, 2013).

$$\boldsymbol{CV\%} = \sqrt{\boldsymbol{\exp(\omega^2) - 1}} * \boldsymbol{100\%}$$

Equation 3: Percentage coefficient of variation

Level 2 random effects describe the magnitude of unexplained differences between the predicted and observed values of the dependent variable, after controlling for other sources of variability (Owen & Fiedler-Kelly, 2014; Mould & Upton, 2013. This error is also called the residual unexplained variability (RUV) and may arise from multiple sources including errors in sample collection, assay variability and model misspecification (Mould & Upton, 2013).

In any PopPK model, the difference between observed (C_{obs}) and model-predicted (C_{pred}) plasma concentration, at time t, in the i^{th} individual, is the RUV and can be calculated as shown in Equation 4:

$$\boldsymbol{C_{obs}(t)_i = C_{pred}(t)_i \pm \varepsilon_i}$$

Equation 4: Residual unexplained variability

where ε_i is RUV which is also assumed to be normally distributed with a mean of zero and standard deviation of SIGMA, σ. Level 2 random effects are usually reported as variance, which is the square root of the SIGMA, (σ^2) (Owen & Fiedler-Kelly, 2014; Mould & Upton, 2013).

2.2.2.3 Covariate model

A covariate is an independent variable that may contain information on the variability in a parameter of interest (Joerger, 2012). Covariates may include variables that change over time (time-variant), such as age and weight, or constants like the patient's sex or race.

Covariate models in PopPK explain variability in pharmacokinetic parameters that can be predicted by subject characteristics (Mould & Upton, 2013). Covariate analysis involves screening for participant characteristics which when included may reduce unexplained variability in pharmacokinetic parameters. Incorporation of these covariates in models may explain variability and facilitate dose adjustment decision. This helps identify patient subpopulations at risk of toxicity or therapeutic failure, and hence facilitating lifesaving therapeutic adjustments (Joerger, 2012).

Covariates can be categorical, such as sex and race, or continuous, such as age and weight. A categorical covariate can also be created by combining two or more characteristics into a composite covariate. The relationship between parameters and covariates is typically expressed and interpreted relative to reference value of the covariate.

Various functional forms can be explored to describe the relationship between a covariate and a model parameter of interest. Categorical covariate effects can be introduced into the PopPK

model by assigning a different factor for each subgroup. Conversely, continuous covariates may be included using various functional forms depending on the shape of their relationship with the parameter of interest. These functional forms include linear, power, Emax, exponential or “broken stick” functions as described by Mould and Upton (Mould & Upton, 2013).

2.2.2.4 Software

PopPK analyses in this this thesis were performed using the first order condition estimation with interaction (FOCEI) or stochastic approximation expectation maximization methods (SAEM) in NONMEM 7.5.1 (Beal, Boeckmann and Sheiner, 2017). FOCEI estimates the model parameters by minimizing an objective function value (OFV) using maximum likelihood estimation. The OFV is expressed as minus twice the log of the likelihood which is a singe number that provides the overall summary of how closely the model predictions match the data (Mould & Upton, 2013). On the other hand, the SAEM method includes stochastic estimation which refines estimates partially iterative “trial and error” (Mould & Upton, 2013).

Other software that were used to support model development in NONMEM include Perl-speaks-NONMEM (PsN) v5.2, Pirana v3.0.0, and Xpose in RStudio (Keizer et al., 2013).

2.2.2.5 PopPK model development

The general procedure of developing a PopPK model to estimate pharmacokinetic parameters of a given drug typically began by identifying a suitable structural model. This involved sequentially testing various disposition models, such as one-, two-, or three-compartment model, with either linear or nonlinear / semi-mechanistic (liver) elimination. To describe drug absorption, first-order absorption with or without a lag was initially tested. More complex models, such as the transit

compartment model of absorption, were then considered whenever necessary (Savic et al., 2007).

The variability in the model was accounted for by testing different random effects at various levels. To account for Level 1 random effects, we tested variability at the subject, occasion (each dose), or visit (each pharmacokinetic sampling visit) levels, assuming these followed lognormal distribution. RUV was included to characterize Level 2 random errors using either additive, proportional, or combined error models (Mould & Upton, 2013).

Potential covariates were identified based on prior knowledge, biological plausibility, study design and objectives, as well as exploration of raw data plots. Initially, the effect of body size on disposition parameters was accounted for with allometric scaling, using different descriptors of body size like total body weight or fat-free mass (Anderson & Holford, 2008; Holford & Anderson 2017). Subsequently plausible covariates were added to the model in stepwise approach (Wählby et al., 2002).

The model development process was guided by assessing the change in the objective function value (ΔOFV) for nested models or the Akaike information criterion for non-nested models (Mould & Upton, 2013). The ΔOFV was assumed to follow χ2-distribution, with a drop of 3.84 in OFV being significant at $p<0.05$ for one additional parameter (1 degree of freedom, df). Additionally, model development decisions were informed by examining a series of diagnostic plots like the goodness of fit plots, and visual prediction checks (VPCs).

The VPC is a key model evaluation tool used for model external validation in PopPK modelling. It involves simulating multiple datasets using the final model, with variability introduced through

stochastic sampling from the OMEGA (interindividual variability) and SIGMA (residual error) matrices (Joel & Fiedler-Kelly, 2014). The distributions of simulated predictions are then compared to observed data using summary statistics (e.g., medians and prediction intervals), allowing assessment of the model's ability to reproduce key features of the observed data (Holford & Karlsson, 2005). Physiological plausibility and clinical relevance of the results were also considered during model development. Finally, model parameter uncertainty and confidence intervals were mostly estimated by using sampling importance resampling (Dosne et al., 2016).

Chapter 3: Unexpectedly low drug exposures among Ugandan patients with TB and HIV receiving high dose rifampicin.

3.1 Abstract

We characterized the pharmacokinetics of standard- and high-dose rifampicin in Ugandan adults with tuberculosis and HIV taking dolutegravir- or efavirenz-based ART. A liver model with saturable hepatic extraction adequately described the data and the increase in exposure between high and standard doses was 4.7-fold. This was lower than what previous reports of dose-exposure nonlinearity would predict and was ascribed to 38% lower bioavailability of the rifampicin only top up formulation compared to the fixed-dose combination.

3.2 Introduction

Rifampicin is an essential component of the first-line treatment of drug-susceptible tuberculosis (Bonnett et al., 2017a) that has a dose-dependent bactericidal effect (Te Brake et al., 2021). It undergoes hepatic extraction, which displays saturation kinetics even at the current 10 mg/kg dose (Acocella, 1978) and induces its own and other drug-metabolizing enzymes and transporters (Chen & Raymond, 2006; Niemi et al., 2003). Promising results support increasing rifampicin dose beyond the current clinical practice, as this may reduce time to sputum conversion (Boeree et al., 2015; Velásquez et al., 2018) and support shorter treatment regimens (Boeree et al., 2015, 2017b), possibly enhancing adherence and improving treatment outcomes (Mitchison, 2005; Svensson et al., 2020). Although the efficacy and safety of high-dose rifampicin in the intensive treatment phase has been reported (Cresswell et al., 2021; Sekaggya-Wiltshire et al., 2022; Wasserman et al., 2021), there is limited information about its clinical pharmacokinetics and

interaction with co-administered antiretroviral therapy (ART). We described the population pharmacokinetics of standard- and high-dose rifampicin when taken with dolutegravir- or efavirenz-based ART.

3.3 Methods / results / discussion

Data were available from an approved study (SAEFRIF: NCT03982277) conducted in Kampala, Uganda (Nabisere et al., 2020). Participants with tuberculosis and HIV were randomized to receive a standard 10 (10RHZE) or higher 35 mg/kg (35RHZE) rifampicin dose, alongside standard doses of isoniazid, pyrazinamide, and ethambutol. In the 35RHZE arm, the Macleods (Macleods, India) FDC was topped up with Rifacos (Cosmos, Kenya) (Table 5) rifampicin-only capsules (RifCaps) to make 35 mg/kg (Sekaggya-Wiltshire et al., 2022). ART-experienced participants continued their treatment while ART-naïve participants were started on medication, doubling the dose of dolutegravir as per guidelines (World Health Organization, 2021). After 6 weeks of tuberculosis treatment, pharmacokinetic samples were drawn at pre-dose, 1-, 2-, 4-, and 8-h following an observed dose (Sekaggya-Wiltshire et al., 2022). Rifampicin concentrations were quantified using a previously reported HPLC method with LLOQ and upper limits of quantification of 0.25 and 15 mg/L, respectively (Cresswell et al., 2021).

Nonlinear mixed-effects modelling with stochastic approximation expectation maximization method was implemented, in NONMEM (v7.5.0) (Beal, Boeckmann, and Sheiner, 2017), to perform population pharmacokinetic analysis of the rifampicin data (Mould & Upton, 2013). One- and two-compartment models with first-order absorption (with lag time or transit compartments) and elimination were considered. A previously published well-stirred liver-model with saturated hepatic extraction (Chirehwa et al., 2016b) (Figure 6) was tested, fixing the liver

volume (V_H), hepatic blood flow (Q_H), and the free rifampicin plasma concentration fraction to literature values of 1 L, 90 L/h (Zhu et al., 1999), and 0.2 (Acocella, 1978), respectively.

Considering an occasion to be the period from one dose to the next, log-normally distributed BOV and BSV were tested, as were additive and/or proportional residual error models. Allometric scaling of clearance and volume parameters (Holford & Anderson, 2017), alongside other covariates like age and rifampicin dose/formulation were tested. Improvement in OFV, goodness-of-fit plots, and the VPC guided model development (Mould & Upton, 2013). The final model was used to estimate rifampicin maximum concentration (C_{max}), the 24-h AUC (AUC_{0-24}) and make simulations of unobserved dosing scenarios. Data will be made publicly available upon publication and upon request for peer review.

Of the 111 (62% male) participants in the pharmacokinetic phase of the SAEFRIF study (Sekaggya-Wiltshire et al., 2022), 54 (49%) received 35RHZE, 63 (57%) were ART-experienced, and 53 (48%) were on efavirenz. Their median (interquartile range, [IQR]) age and weight were 36 (31-43) years and 53 (47-60) kg, respectively. These characteristics were balanced between study arms and are presented below in Table 3. 77 (14%) of the 538 samples were below the LLOQ and predominantly pre-dose.

A 1-compartment model with first-order absorption via transit compartments (ΔOFV = -18.7, 1 degree of freedom [df], P<0.001 compared with lag time), and elimination was initially fit to the data. It predicted a 48% slower clearance for the 35HRZE cohort (ΔOFV = -22.7, 1 df, P<0.001) compared with the 10HRZE cohort, which was consistent with saturation.

A previously published well-stirred liver model with saturable hepatic extraction (Chirehwa et al., 2016b) was then applied and it fit the 10RHZE but not 35RHZE data (ΔOFV = -20.3, 1 df, P<0.021).

The best explanation that our model found for the lower-than-expected exposure in the 35RHZE arm was 38% lower bioavailability of the top up RifCaps versus the FDC (ΔOFV = -35.1, 1 df, P<0.001). Allometric scaling by fat-free mass (ΔOFV = -32.7) best fit the data, and there was no difference between the rifampicin pharmacokinetics in participants on dolutegravir- and efavirenz-based ART. The final model estimated a maximum intrinsic clearance ($CL_{int,max}$) of 133 (109-165) L/h and Michaelis-Menten constant (k_m) of 8.00 (5.32-10.9) mg/L (Table 4), and the VPC in Figure 5 shows an adequate fit.

Rifampicin AUC_{0-24} and C_{max} (IQR) for the 10RHZE cohort were estimated to be 32.3 (28.7-36.7) mg·h/L and 8.1 (6.6-9.2) mg/L, respectively, and were like previous reports (Boeree et al., 2017b; Chirehwa et al., 2016b Corresponding values for the 35RHZE cohort were 153 (138-175) mg·h/L and 25.2 (21.4-26.9) mg/L, respectively. This 4.7-fold increase (Table 2) in AUC_{0-24} of the high-dose cohort was lower than the 6.8- to 8.93-fold increase reported by other studies (Boeree et al., 2015, 2017b; Cresswell et al., 2021; Wasserman et al., 2021), despite receiving the same 35 mg/kg dose and the certificate of analysis of our top up formulation showing acceptable quality. Cases of inferior rifampicin formulations have been reported (McIlleron et al., 2002, 2016a; Moses et al., 2013; Sekaggya-Wiltshire et al., 2019), and McIlleron et al. partly attributed this to less favourable drug absorption (McIlleron et al., 2016b).

Rifampicin is a Biopharmaceutic Classification System class II (low solubility and high permeability) drug (Gordon L. et al., 1995) and is therefore not a candidate of waivers for in vivo bioequivalence studies (FDA et al., 2017). It shows pH-dependent solubility which affects absorption from the gut and is known to adsorb to other pharmaceutical excipients (Panchagnula & Agrawal, 2004) which results in different rates and extent of absorption of pharmaceutically

equivalent solid oral formulations. When the top-up RifCaps and FDC in the 35RHZE cohort were assumed to be bioequivalent, the median (IQR) AUC_{0-24} was predicted to increase to 230 (160-334) mg·h/L, representing a more in-line 7.2-fold increase from that of the 10RHZE.

Our model validates the utility of previously described rifampicin models of saturable hepatic extraction and predicts a similar concentration at which saturation happens (Chirehwa et al., 2016b; Denti et al., 2022). We also confirm previous reports that steady-state rifampicin pharmacokinetics is not affected by concomitant dolutegravir- / efavirenz-based ART (Bhatt et al., 2014; McIlleron et al., 2012). As the advantages of high-dose rifampicin in tuberculosis treatment emerge and the use of top-up rifampicin-only formulations becomes common, stringent bioequivalence studies are recommended to ensure achievement of targeted rifampicin exposures.

Table 2: Comparative exposures of high-dose rifampicin reported by different studies.

STUDY												
Characteristic	**RifT (13)**		**LASER-TBM (13)**		**Boeree et al. (7)**		**Boeree et al. (8)**		**Chirehwa et al. (18)**	**Current study**		
Day of pharmacokinetic sampling	Day 2		Day 3		Day 14		Week 4		Week 4	Week 6		
Rifampicin dose (mg/kg)	10	**35**	10	**35**	10	**35**	10	**35**	10	10	**35**	35*
Number of participants (n)	20	**21**	17	**15**	8	**15**	123	**63**	61	54	**57**	-
Brand name of rifampicin formulation	Macleods	Macleods + Rifadin	Rifafour	Rifafour + Rimactane / Eremfat	Rifafour	Rifafour + Rifadin	Rimcure	Rimcure + Svizera	Rifafour / Antib-4	Macleods	Macleods + Rifacos	Macleods + bioequivalent RifCaps
Coadministered ART regimen	DTG/TDF/3TC		AZT/TDF/EFV -3TC/FTC/ABC		No ART†		No ART†		EFV/3TC/AZT	AZT/TDF/DTG/EFV-3TC/FTC/ABC		
Weight (kg) Median (IQR/range) ‡	50 (45-55)	**51 (50-55)**	64 (54-77)	**60 (53-80)**	56.9 (47-50)	**57.0 (41-74)**	54 (49-59)	**52 (47-59)**	55.2 (34-90)	51.7 (46-60)	**53.0 (47-60)**	-
Age (yr) Median (IQR/range) ‡	34 (27-36)	**32.5 (27-39)**	38 (34-47)	**41 (36-45)**	27.5 (19-49)	**37.0 (21-59)**	34 (26-41)	**33 (23-40)**	32 (18-47)	38 (32-43)	**34 (30-42)**	-
AUC_{0-24} (mg·h/L) Geometric mean/median	42.9	**327**	42.9	**295**	26.3	**235**	24.2	**170**	39.3	32.3	**153**	230
(-fold change) in AUC_{0-24} ®	-	**7.6**	-	**6.9**	-	**8.9**	-	**7.0**	-	-	**4.7**	**7.1**
C_{max} (mg/L) Geometric mean/median	6.04	**29.3**	6.9	**34.7**	7.4	**35.2**	5.8	**26.7**	6.9	8.07	**25.2**	38.2
(-fold change) in C_{max} ®	-	**4.9**	-	**5.0**	-	**4.8**	-	**4.6**	-	-	**3.2**	**4.7**

AUC_{0-24}, 24-h area under the curve; C_{max}, maximum concentration; IQR, interquartile range; ART, antiretroviral; TDF, tenofovir diphosphate; 3TC, lamivudine; DTG, dolutegravir; EFV, efavirenz; AZT, zidovudine; FTC, emtricitabine; ABC, abacavir; RifCaps, Top up rifampicin-only formulation.

* This is the 35mg/kg dose assuming bioequivalence of the fixed dose combination and top-up rifampicin-only formulation (RifCaps).

®The fold change presented is a ratio of the geometric means/medians of the parameter of the high to standard-dose rifampicin cohorts.

†ART regimen of participants with HIV was withheld for the period of the trial or not reported.

‡We present IQR/range as presented in the original publication.

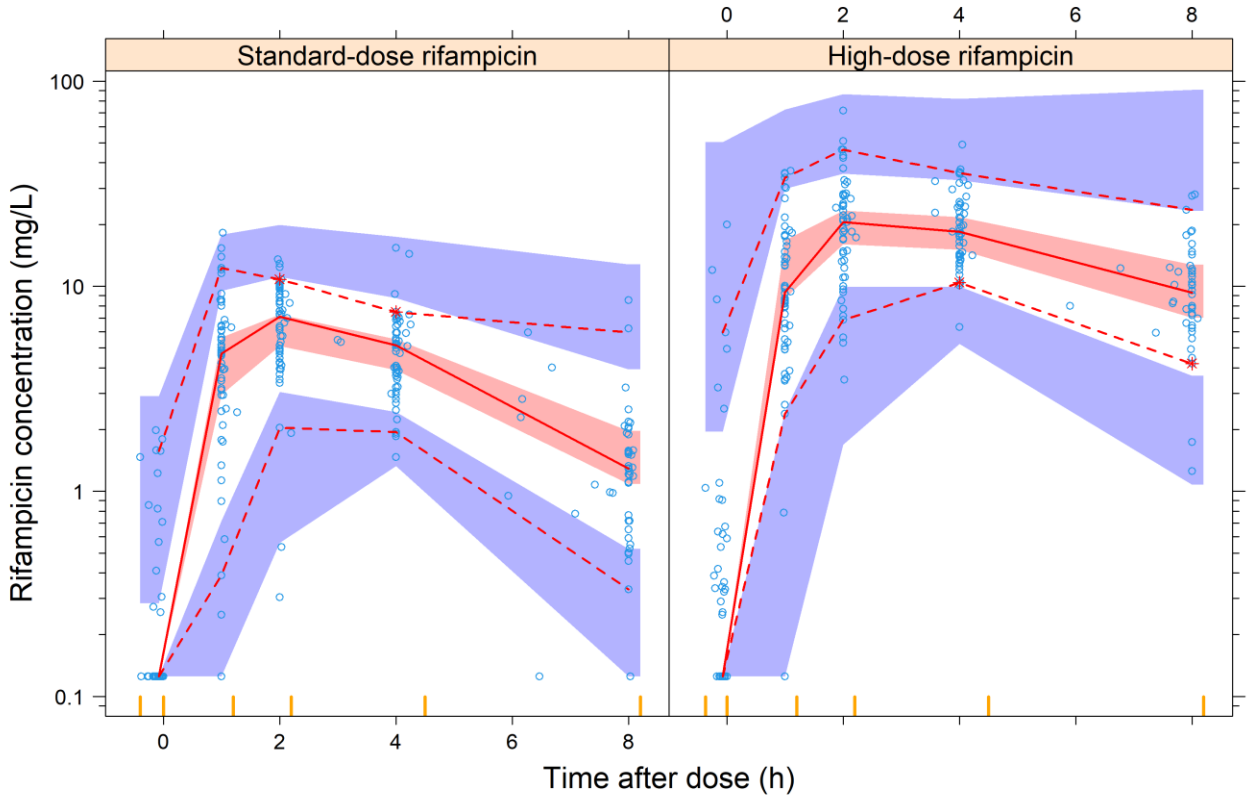

Figure 5: Visual predictive check stratified by rifampicin dose.
The solid and dashed lines represent the 50th, 5th, and 95th percentiles of the observed data (open circles), while the shaded areas represent the model-predicted 95% confidence intervals

3.4 Supplementary material

Results

Table 3: SAEFRIF study participant characteristics

Characteristic	Rifampicin dose		Total
	10 mg/kg	35 mg/kg	
Number of participants (%) [a]	57 (51)	54 (49)	111 (100)
Male (%) [a]	35 (51)	34 (49)	69 (62)
Age (yr) [b]	38 (32 – 43)	34 (30 – 42)	36 (31 – 43)
Height (cm) [b]	162 (157 – 172)	164 (160 – 172)	163 (158 – 172)
Weight (kg) [b]	52 (46 – 60)	54 (48 – 54)	53 (47 – 60)
Fat-free mass (kg) [b]	42 (36 – 48)	43 (37 – 48)	42 (36 – 48)
Participants on efavirenz (%) [a]	29 (55)	24 (45)	53 (48)
Antiretroviral therapy experienced (%) [a]	32 (51)	31 (49)	63 (57)

[a] Data presented as number (percent).
[b] Data presented as median (interquartile range, IQR)

Table 4: Pharmacokinetic parameter values for rifampicin in adults with tuberculosis and HIV infection

Parameter	Typical value (95% CI) [b]	Variability as CV% [c] (95% CI) [b]
Maximum intrinsic clearance, $CL_{int,max}$ (L/h) [a]	133 (109 – 165)	BSV: 25.0 (12.2 – 31.9)
Michaelis-Menten constant, k_m (mg/L)	8.00 (5.32 – 10.9)	
Volume of distribution, V (L) [a]	45.2 (38.6 – 48.7)	
Hepatic volume, V_H (L) [a]	1 fixed	
Hepatic blood flow rate, Q_H (L/h) [a]	90 fixed	
Unbound fraction of rifampicin, f_u (fraction)	0.2 fixed	
Absorption rate constant, k_a (/h)	1.76 (1.04 – 2.39)	BOV: 85.0 (49.6 – 110)
Mean transit time (h)	0.505 (0.299 – 0.669)	BOV: 88.1 (59.0 – 121)
Number of transit compartments (n)	16.8 (11.4 – 21.5)	
Relative bioavailability, F (fraction) [d]	1 fixed	BOV: 27.0 (20.8 – 32.1)
Change in F of top-up rifampicin capsules (%)	-38.4 (-48.6 – -26.0)	
Scaling factor for BOV of data from unobserved dosing (-fold) [e]	2.82 (1.71 – 3.29)	
Proportional error (%)	21.3 (18.0 – 25.0)	
Additive error (mg/L)	0.05, fixed to 20% of LLOQ	

All the parameters refer to a typical 53 kg person in the study whereas the hepatic flow and volume are for a typical 70 kg adult.

[a] This parameter has been adjusted by allometric scaling, and the values reported here refer to a subject with a fat-free mass (FFM) of 42 kg. i.e., for subject i: $\mathrm{CL_i} = \mathrm{TVCL} \cdot \left(\frac{\mathrm{FFM_i}}{42}\right)^{\frac{3}{4}}$ and $\mathrm{V_i} = \mathrm{TVV} \cdot \left(\frac{\mathrm{FFM_i}}{42}\right)$.

$\mathrm{FFM} = \frac{\mathrm{WHS_{max}} \cdot \mathrm{HT}^2 \cdot \mathrm{WT}}{\mathrm{WHS_{50}} \cdot \mathrm{HT}^2 + \mathrm{WT}}$, where: HT, height; WT, weight; WHS_{50} and WHS_{max} are sex dependent parameters (Holford & Anderson, 2017).

[b] The values in the parentheses are empirical 95% confidence interval (CI) generated from sampling importance resampling (SIR).

[c] The parameter variability was included either as between-subject variability (BSV) or between-occasion variability (BOV), assuming a lognormal distribution. It is reported here as the percent coefficient of variation (CV) calculated as $\%\mathrm{CV} = \sqrt{\omega^2} \times 100$.

[d] This is the relative bioavailability of the standard-dose rifampicin fixed dose combination administered.

[e] This is a multiplicative factor increasing the BOV of absorption parameters for pre-dose concentrations following an unobserved dose. LLOQ, lower limit of quantification.

Table 5: Details of the brands of rifampicin formulations used in the SAEFRIF study.

Drug	Brand name	Manufacturer	Batch number
Fixed dose combination (RHZE)	Macleods	Macleods, India	NRG937A
Fixed dose combination (RHZE)	Macleods	Macleods, India	NRG8187A
Rifampicin capsules	Rifacos	Cosmos, Kenya	81223
Rifampicin capsules	Rifacos	Cosmos, Kenya	90967

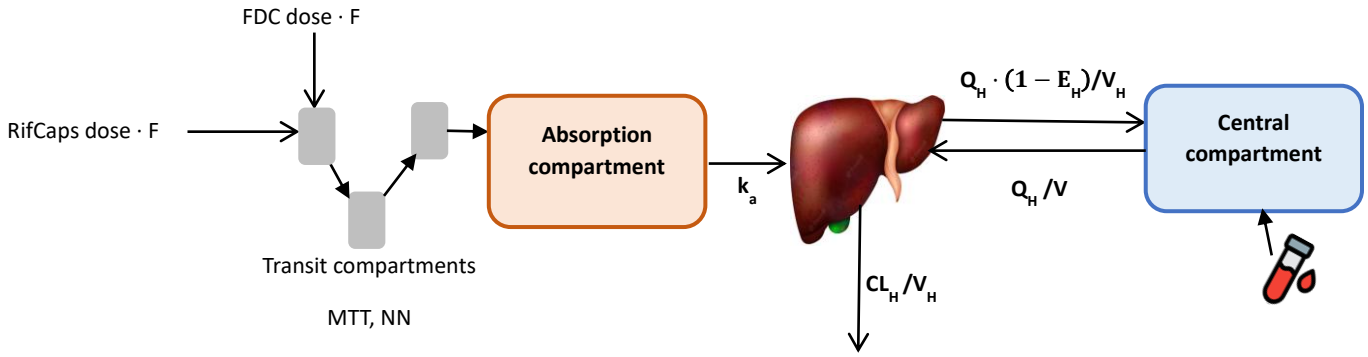

$$CL_H = Q_H \cdot E_H \qquad (1) \qquad E_H = \frac{CL_{int} \cdot fu}{CL_{int} \cdot fu + Q_H} \qquad (2) \qquad CL_{int} = \frac{CL_{int.max} \cdot k_m}{C_H + k_m} \qquad (3)$$

Figure 6: Schematic representation of the rifampicin model.
V, volume of observation compartment; MTT, mean transit time; NN, number of transit compartments; k_a, absorption rate constant; V_H, liver volume; Q_H, hepatic plasma flow rate; CL_{int}, intrinsic clearance; $CL_{int,max}$, maximum CL_{int}; k_m, Michaelis-Menten constant; F, relative bioavailability; fu, fraction of unbound rifampicin in plasma; FDC, fixed dose combination; RifCaps, top-up rifampicin only formulation.

Chapter 4: Dolutegravir pharmacokinetics in Ugandan patients with TB and HIV receiving standard- versus high-dose rifampicin.

4.1 Abstract

Higher rifampicin doses may improve tuberculosis treatment outcomes. This could however exacerbate the existing drug interaction with dolutegravir. Moreover, the metabolism of dolutegravir may also be affected by polymorphism of UGT1A1, a gene that codes for uridine diphosphate glucuronosyltransferase. We used population pharmacokinetic modelling to compare the pharmacokinetics of dolutegravir when coadministered with standard- versus high-dose rifampicin in adults with tuberculosis and HIV and investigated the effect of genetic polymorphisms. Data from the SAEFRIF trial, where participants were randomized to receive first-line tuberculosis treatment with either standard- 10 mg/kg or high-dose 35 mg/kg rifampicin, alongside antiretroviral therapy were used. The dolutegravir model was developed with 211 plasma concentrations from 44 participants. The median (IQR) rifampicin AUC in the standard- and high-dose arms were 32.3 (28.7-36.7) and 153 (138-175) mg·h/L, respectively. A 1-compartment model with first-order elimination and absorption through transit compartments best described dolutegravir pharmacokinetics. For a typical 56 kg participant, we estimated a clearance, absorption rate constant, and volume of distribution of 1.87 L/h, 1.42 h^{-1}, and 12.4 L, respectively. Each 10 mg·h/L increase in the AUC of coadministered rifampicin from 32.3 mg·h/L led to a 2.3 (3.1-1.4) % decrease in dolutegravir bioavailability. Genetic polymorphism of UGT1A1 did not significantly affect dolutegravir pharmacokinetics. Simulations of trough dolutegravir concentrations show that the 50 mg twice-daily regimen attains both the primary and secondary

therapeutic targets of 0.064 and 0.3 mg/L, respectively, regardless of the dose of coadministered rifampicin, unlike the once-daily regimen.

4.2 Introduction

Thanks to its superior efficacy, safety, and high genetic barrier to resistance (Cottrell et al., 2013; DeAnda et al., 2013; Hightower et al., 2011), dolutegravir-based combination ART was rolled out as first-line treatment for HIV infection (World Health Organization, 2021b). Dolutegravir is an integrase strand transfer inhibitor, mainly metabolized by UGT, but also a substrate of CYP3A4 and P-glycoprotein (Castellino et al., 2013; Min et al., 2010). UGT1A1, the gene that codes for UGT, is polymorphic (Z. Chen et al., 2014; Vukovic et al., 2018) and increase in the number of TA_n repeats in its promoter region from TA_6 (UGT1A1*1) to TA_7 (UGT1A1*28) results in reduced activity (Gammal et al., 2016). This has been associated with increased dolutegravir exposure (Chen et al., 2014) and higher incidence of neuropsychiatric adverse events (Yagura et al., 2017). Rifampicin is a key first-line drug for drug-susceptible TB (Dickinson & Mitchison, 1981), a common comorbidity among people with HIV (World Health Organization, 2021). Early initiation and coadministration of ART during TB treatment is recommended, and their efficacy and tolerability are important (World Health Organization, 2021b). Increasing the daily rifampicin dose from 10 to 35 mg/kg has been investigated as a potential component of strategies to shorten TB treatment duration (Boeree et al., 2015, 2017a; Cresswell et al., 2021; Seijger et al., 2019; Sekaggya-Wiltshire et al., 2022; te Brake et al., 2021) and improve efficacy (Boeree et al., 2017a; Bun Ng et al., 2015; Svensson et al., 2020).

Rifampicin, though, is an inducer of CYP3A4, UGT, P-glycoprotein (Bolt, 2004; Niemi et al., 2003), and significantly lowers dolutegravir's exposure (Cottrell et al., 2013). Consequently, the dose of

dolutegravir must be doubled from 50 mg once- (QD) to twice-daily (BID) (Dooley et al., 2013, 2020) when coadministered with rifampicin. Currently, the PA-IC_{90} of HIV-1 (0.064 mg/L) is considered the primary therapeutic target dolutegravir trough concentration (C_{trough}) (Cottrell et al., 2013; Min et al., 2010). The geometric mean C_{trough} of the least efficacious dose in the SPRING-1 trial (Van Lunzen et al., 2012; Zhang et al., 2015) of 0.3 mg/L has also been adopted as a secondary target.

Non-compartmental analysis of data from the **S**afety/tolerability, **A**nd **EF**ficacy of high-dose **RIF**ampicin (SAEFRIF) trial (Nabisere et al., 2020) showed a decrease in dolutegravir C_{trough} of participants who received 35 mg/kg compared to those on standard-dose of rifampicin (Sekaggya-Wiltshire et al., 2022). Using population pharmacokinetic modelling, we investigated the effect of high-dose rifampicin and UGT1A1 polymorphism on dolutegravir pharmacokinetics. We also performed simulations to predict target attainment in a large cohort of in silico individuals using different dosing strategies.

4.3 Methods

4.3.1 Study design. SAEFRIF was a clinical trial conducted at the Infectious Diseases Institute of Makerere University in Kampala, Uganda. Pharmacokinetic data were collected from enrolled participants with TB and HIV who received efavirenz- or dolutegravir-based ART (Nabisere et al., 2020). The protocol was approved by a local research and ethics committee, registered at clinicaltrials.gov (NCT03982277) and all participants provided written informed consent.

A detailed description of the design and inclusion/exclusion criteria of SAEFRIF has been reported (Nabisere et al., 2020; Sekaggya-Wiltshire et al., 2022). Newly diagnosed adults with TB and HIV were randomized to either receive 10 mg/kg (10RHZE) or 35 mg/kg (35RHZE) rifampicin dose-

containing regimen in the intensive phase of TB treatment. ART-naïve participants were randomly assigned to start either dolutegravir- or efavirenz-based ART, two weeks into TB treatment, while those already on ART continued with their existing medications. The TB treatment consisted of RHZE programmatic Macleods (Macleods, India) fixed-dose combination (FDC) and top up Rifacos (Cosmos, Kenya) rifampicin-only capsules in the 35RHZE arm (Kengo et al., 2023). The dolutegravir dose was doubled to 50 mg BID during and up to two weeks after completion of TB treatment. Participants were excluded if they were pregnant, had rifampicin-resistant TB, or impaired liver/renal function.

4.3.2 Specimen collection and processing. Pharmacokinetic sampling was done after at least 4 weeks of ART. An observed dose of ART and anti-TB medication was given, and blood samples drawn at pre-dose, then 1-, 2-, 4- and 8-hours post dose. The samples were centrifuged within 30 minutes of collection, and plasma stored at -80 ^{0}C until bioanalysis.

Dolutegravir plasma concentrations were determined by reverse-phase HPLC-mass spectrometry using a previously published method with modifications (Bennetto-Hood et al., 2014). The assay was calibrated over a range of 0.05 (LLOQ) to 10 mg/L with inter- and intra-day precision of 8.2 to 10.9% CV and 1.9 to 7.5% CV, respectively. Quality control samples were prepared and stored at concentrations of 0.06, 0.6, and 6 mg/L, and based on their analysis, the bias (% relative error) ranged from 1.0 to 10.0%.

DNA was extracted from the participant's blood samples, using QIAmp DNA mini kit (QIAGEN) following the manufacturer's protocol with minor modifications. DNA quantification and quality control were done using the NanoDrop 2000c (ThermoScientific). Polymerase chain reaction (PCR) targeting the UGT1A1 gene was performed using primer sets. The success of the

amplification was determined, and following confirmation of amplification, the amplicons were cleaned for Sanger sequencing using ExoSAP-IT™ (Applied Biosystems). Cycle sequencing chain termination PCR was then set up with the forward primer. The cycle sequencing products were then cleaned up and sequenced. The variants were called from the Sanger traces using a mutation surveyor.

4.3.3 Pharmacokinetic analysis. Population pharmacokinetic modelling of dolutegravir plasma concentrations was performed using NONMEM software (v7.5.0) (Beal, Boeckmann, and Sheiner, 2017). PsN (v5.2.6) was used to execute various model development and evaluation methods. Pirana (v3.0.0) was used to track model development and Xpose4, together with RStudio (v1.4.1106), used to perform model diagnostics and post-modelling analysis (Keizer et al., 2013). Several structural models were tested to describe the pharmacokinetics of dolutegravir; one- and two-compartment models with first-order elimination and absorption with or without lag time or a chain of transit compartments (Savic et al., 2007). We also tested elimination using a well stirred liver model (Cherkaoui-Rbati et al., 2017; Yang et al., 2007). Log-normally distributed BOV was tested on absorption parameters whereas BSV was tested on disposition parameters (Karlsson & Sheiner, 1993). A combined proportional and additive error was used to model residual unexplained variability (Mould & Upton, 2012), with lower bound of the additive component fixed to 20% of the LLOQ (0.05 mg/L). Concentrations below the LLOQ (0.05 mg/L) were imputed to LLOQ/2, except for consecutive values during the elimination phase which were excluded from the fit as described in Beal's M6 method (Beal, 2001; Denti et al., 2016).

Allometric scaling by total body weight or fat-free mass (FFM) (Holford & Anderson, 2017; Janmahasatian et al., 2005), was applied to account for body size effects on disposition

parameters, with exponents on clearance and volume fixed to 0.75 and 1, respectively (Anderson & Holford, 2008). To investigate the effect of the dose of coadministered rifampicin, 2 different approaches were tested. First, the effect was tested categorically (i.e., 10RHZE vs 35RHZE) and then continuously using rifampicin 24-hour area under the concentration curve (AUC_{0-24}) determined separately (Kengo et al., 2023). Other covariates like UGT1A1 genotype and age were also investigated. Model development was guided by evaluation of change in minimum value of OFV and inspection of diagnostics plots like the VPC. The changes (Δ) in OFV were assumed to follow a chi-square distribution whereby, for hierarchical models, a ΔOFV of at least 3.84 points was considered significant at $P<0.05$ for 1 degree of freedom (df). Sampling importance resampling procedure was used to assess parameter uncertainty and generate 95% CI (Dosne et al., 2016; PSN 5.3.0, 2019). The final model was used to estimate participants' steady-state dolutegravir AUC_{0-12} for comparison with previous reports.

4.3.4 Simulations. We used the final dolutegravir model estimates to perform Monte Carlo simulations to evaluate proportions of individuals who would attain treatment targets. The targets used were a C_{trough} above the PA-IC_{90} and 0.3 mg/L (Min et al., 2010; Van Lunzen et al., 2012). A suitable dataset was generated using demographic characteristics of 1225 participants with TB from pharmacokinetic studies carried out in West Africa and South Africa as described previously (Chirehwa et al., 2020). The different dosing scenarios simulated were: dolutegravir 50 mg QD or BID, with standard- or high-dose rifampicin containing TB regimen. With our model we also explored a scenario of higher rifampicin exposures in the 35RHZE. Data will be made publicly available upon publication and upon request for peer review.

4.4 Results

4.4.1 Study participants. Of 111 participants in the pharmacokinetic phase of the SAEFRIF study, 58 (52%) were randomized to the dolutegravir arm. Of these, 14 (5 on 10RHZE and 9 on 35RHZE) were not included in the pharmacokinetic analysis because they were considered non-adherent to medication. Their exclusion did not significantly change participant characteristics as shown by Table 9 in the supplement materials.

A total of 211 dolutegravir plasma concentrations from 44 (76%) participants were used to develop the pharmacokinetics model: 28 (64%) were male and 19 (43%) received 35RHZE. Their median (inter-quartile range, IQR) weight and age were 56 (47-61) kg and 36 (31-43) yr., respectively (Table 6). Rifampicin pharmacokinetic data were analysed separately (Kengo et al., 2023), and the median (IQR) rifampicin AUC_{0-24} for the standard- and high-dose cohorts were 32.3 (28.7-36.7) and 153 (134-175) mg·h/L, respectively. Of note, the high-dose exposures were lower than previously reported and this was attributed to lower relative bioavailability of the top-up rifampicin-only formulation used together with the RHZE FDC. Using the model to adjust for this effect and predict exposures assuming full bioequivalence of the 2 formulations, the median rifampicin AUC_{0-24} (IQR) was 230 (160-334) mg·h/L.

4.4.2 UGT genotypes: Of the 44 participants included in the dolutegravir pharmacokinetic analysis, 9 (20%) were not genotyped because of failed DNA amplification. Results were therefore available for 35 individuals: 3 (7%) were heterozygous for UGT1A1*36 $(TA)_5$, 19 (43%) were homozygous for UGT1A1*1 $(TA)_6$, 11 (25%) were heterozygous for UGT1A1*28 $(TA)_7$, and 2 (5%) were homozygous for UGT1A1*28 $(TA)_7$ (Table 6).

4.4.3 Dolutegravir pharmacokinetic model: Dolutegravir pharmacokinetics was adequately characterized by a 1-compartment model with first-order elimination and absorption through a series of transit compartments (ΔOFV = -6.5, 1 degree of freedom (df), p=0.011 compared to lag). A second compartment did not improve the model fit and neither did the well-stirred liver model (Table 10). Clearance and volume were best allometrically scaled (Holford & Anderson, 2017) by FFM (ΔOFV = -3.96) and normalized to the median FFM of 43 kg. A 1.56-fold scaling factor on the BOV of absorption parameters was added to account for the uncertainty in dosing information (ΔOFV = -5.2, 1 df, p=0.023).

When investigating the effect of high-dose rifampicin by comparing study arms, participants on 35RHZE were found to have 31% decreased dolutegravir bioavailability (ΔOFV = -6.9, 1 df, p=0.009) compared to those on 10RHZE. When the effect was tested on clearance, a 17% increase was detected but the model fit was worse (ΔOFV = -4.02, 1 df, p=0.046). A model including both effects was not better than having the effect on bioavailability alone (ΔOFV = -0.40, 1 df, p=0.527). Alternatively, we tested the rifampicin effect on dolutegravir bioavailability as a continuous covariate using the individual values of rifampicin AUC_{0-24}. This produced better improvement in the model fit (ΔOFV=-12.1, 1 df, p<0.001) and predicted that, for each 10 mg·h/L increase in AUC_{0-24} of rifampicin from the median 10RHZE AUC_{0-24} (32.3 mg·h/L), dolutegravir bioavailability would reduce by 2.3% (3.1-1.4). This continuous effect of rifampicin AUC_{0-24} on dolutegravir bioavailability is presented in Figure 9 and was preferred in the final model as it provides an opportunity to predict the effect of the interaction within therapeutic exposures of rifampicin.

UGT1A1 genotype effects were neither statistically significant on dolutegravir clearance nor bioavailability when tested separately. UGT1A1*28 was associated with a non-significant 6%

increase in bioavailability (ΔOFV=-0.394, 2 df, p=0.821), resulting in similar dolutegravir exposures.

The VPC (Figure 8) shows that the final model adequately described the data as median, 5th and 95th percentiles all fell within their respective model predicted 95% CI. The estimated typical values of clearance and volume of dolutegravir were 1.87 L/kg and 12.4 L, respectively (Table 7). The terminal half-life of dolutegravir was estimated to be 4.41 and 4.49 h in the 10RHZE and 35RHZE arms, respectively. The geometric mean (IQR) of the model-derived dolutegravir $AUC_{0\text{-}12,}$ and C_{trough} for participants in the 10RHZE arm were 21.6 (18.8-24.2) mg·h/L and 1.07 (0.866-1.47) mg/L, respectively. These values decreased to 15.2 (13.6-16.0) mg·h/L and 0.744 (0.527-1.00) mg/L in the 35RHZE arm.

4.4.4 Simulations. Results of the simulations, displayed in Figure 9, show predicted C_{trough} after different dosing strategies. With the 50 mg BID dolutegravir regimen, everyone (99% in 35RHZE arm) attained the PA-IC_{90} and 0.3 mg/L. The proportion who attained 0.3 mg/L reduced to 92% when higher 35RHZE exposures were given. When dolutegravir 50 mg QD with rifampicin was administered, 92% and 18% of simulated population in the 10RHZE arm attained the PA-IC_{90} and 0.3 mg/L targets, respectively. These proportions reduced to 83% and 8%, respectively, in the 35RHZE cohort. When the higher 35RHZE rifampicin exposure was tested, only 65% and 2% attained PA-IC_{90} and 0.3 mg/L target, respectively.

4.5 Discussion

We developed a population pharmacokinetic model to describe the effect of standard- versus high-dose rifampicin on dolutegravir pharmacokinetics in adults with TB and HIV and performed simulations to demonstrate how different doses of rifampicin affect exposure across different

weight bands. We found that rifampicin coadministration lowers dolutegravir bioavailability but doubling its dose to 50 mg BID is sufficient to maintain exposures above therapeutic targets, even when high-dose rifampicin exposures were higher than what we observed. We could not find an effect of UGT1A1 gene polymorphism on dolutegravir pharmacokinetics.

We found that increasing rifampicin exposure affects dolutegravir bioavailability and that this relationship was best described in our data using a linear function (Figure 7). Each 10 mg·h/L increase in the $AUC_{0\text{-}24}$ of coadministered rifampicin decreased dolutegravir bioavailability by 2.3%, thus causing a 31% decrease between the typical patient on 10RHZE and 35RHZE in our study. When trying to extrapolate what this reduction would be at rifampicin concentrations reported in other studies of high-dose rifampicin (AUC of 230 mg·h/L), the reduction was 45%. Because of the direct relationship between bioavailability and AUC (Rescigno, 2000), rifampicin coadministration is predicted to similarly effect dolutegravir AUC. This finding is consistent with the fact that rifampicin is an inducer of drug metabolizing enzymes (Niemi et al., 2003) and previous findings that rifampicin coadministration lowers dolutegravir exposure (Dooley et al., 2013, 2020; Kawuma et al., 2022).

To contextualise our results and compare them with previous studies, we summarized them and previous findings in Table 8. As previously reported, dolutegravir $AUC_{0\text{-}24}$ of the 10RHZE arm was lower than that achieved with 50 mg QD in absence of rifampicin (Zhang et al., 2015) and comparable to previous reports where dolutegravir was coadministered BID with rifampicin (Dooley et al., 2013). A further reduction in dolutegravir $AUC_{0\text{-}24}$ was observed in the high-dose rifampicin cohort, and this was attributed to reduced bioavailability of dolutegravir, and not increased clearance and this is evident in terminal elimination phase of the VPC. This is an

interesting observation that may be due to maximal induction of hepatic enzyme activity that has been reported at standard doses of rifampicin (Acocella, 1978; Xu et al., 2011). Possibly, maximal induction may not have been achieved in the gut with standard doses and higher rifampicin doses resulted in additional induction of gut enzymes and/or transport proteins, causing more pre-systematic elimination of dolutegravir (Castellino et al., 2013; Cottrell et al., 2013; Niemi et al., 2003).

As consensus builds about the most appropriate clinical dolutegravir therapeutic target, the 50 mg BID dose maintained C_{trough} above the higher 0.3 mg/L target, irrespective of rifampicin dose in the coadministered anti-TB regimen. Conversely, the 50 mg QD dose was predicted to achieve C_{trough} generally lower than 0.3 mg/L, but mostly above the PA-IC_{90} of 0.064 mg/L, at least when rifampicin is coadministered at 10 mg/kg. Consistent with this, recent findings in Botswana showed that participants who took the once-daily dolutegravir 50 mg dose with a standard dose rifampicin-containing anti-TB regimen achieved viral suppression like those whose dolutegravir dose was doubled (Modongo et al., 2019). This seems to point towards the validity of the lower target. Moreover, dolutegravir has a long dissociative half-life from viral integrase of about 71 hours (Hightower et al., 2011), which may provide protection against drug concentrations temporarily falling below the PA-IC_{90}. Taking all this into perspective, it seems plausible that the efficacy of dolutegravir could be maintained at lower concentrations than currently targeted, and this question deserves further investigation.

A one-compartment model adequately described dolutegravir pharmacokinetics, like that reported by Zhang et al. (Zhang et al., 2015), Barcelo et al. (Barcelo et al., 2019), and Parant et al. (Parant et al., 2019). This however deviates from the two-compartment model that was reported

by Kawuma et al. (Kawuma et al., 2021), and Dickinson et al. (Dickinson et al., 2021b). This divergence in structural model may be due to differences in study design and sampling schedule, since in the latter studies all participants were sampled over 24 hours after dose, whereas those in our study were sampled over 8 hours. Dolutegravir clearance in the 10RHZE cohort was more than twice as high as that reported in studies of dolutegravir alone (average of 0.92 L/kg) (Barcelo et al., 2019; Dooley et al., 2013; Kawuma et al., 2021; Zhang et al., 2015). This level of induction is in line with findings from other studies where the drug was coadministered with standard doses of rifampicin (Barcelo et al., 2019; Dooley et al., 2013; Kawuma et al., 2022).

Dolutegravir exposure during rifampicin cotreatment was also found to be similar in participants with or without the less functional UGT1A1*28 allele, deviating from previous reports without rifampicin where differences were observed (Yagura et al., 2017). This may be due to our limited sample size, or that in the presence of the strong enzyme inducer like rifampicin, genotype is no longer a meaningful influencer of dolutegravir exposure. Interestingly, UGT1A1*1 was the most prevalent allele in our study population, in contrast with previous findings reporting UGT1A1*28 as the most common allele in the Ugandan population (Horsfall et al., 2011).

Our study had limitations. We used a parallel design because the intensive phase of TB treatment, during which we conducted the study, could not allow enough time for steady-state induction to be achieved between one rifampicin dose and the other. We did not include participants taking dolutegravir without rifampicin but try to remedy this by comparing our results with previous studies where dolutegravir was given alone. The rifampicin plasma concentrations observed in the 35RHZE arm were unexpectedly lower (Kengo et al., 2023) but we explored what would happen at higher rifampicin exposures using model-based simulations. Whereas the relationship

between rifampicin exposure and dolutegravir bioavailability may be saturable like many physiologic reactions, we use a linear function which represents a worst-case scenario and demonstrate that dolutegravir exposures would be okay regardless. Finally, the sample size of our study was limited, and it may not have been large enough for us to draw conclusions about the effect of genetic polymorphism on dolutegravir pharmacokinetics.

In conclusion, increasing the rifampicin dose in the anti-TB regimen from the current 10 to 35 mg/kg reduces the bioavailability of concomitant dolutegravir. However, despite further reduction in dolutegravir exposure due to a higher rifampicin dose, doubling the dolutegravir dose to 50 mg BID maintains its C_{trough} above therapeutic targets.

Table 6: Baseline characteristics of participants in the SAEFRIF study

Characteristic [a]	**Rifampicin regimen**		**Total**
	10RHZE	**35RHZE**	
Number of participants, n (%)	25 (56)	19 (43)	44 (100)
Male, n (%)	16 (64)	12 (63)	28 (64)
Age (yr.)	33 (29 – 43)	37 (34 – 44)	36 (31 – 43)
Height (cm)	162 (158 – 171)	163 (160 – 170)	162 (158 – 171)
Weight (kg)	56 (47 – 61)	56 (47 – 61)	56 (47 – 61)
Fat-free mass (kg)	44 (37 – 50)	42 (40 – 48)	43 (38 – 50)
Antiretroviral experience, n (%)	20 (68)	15 (79)	32 (73)
UGT1A1 genotype, n (%)			
*1/*36	1 (4)	2 (11)	3 (7)
*1/*1	13 (52)	6 (32)	19 (43)
*1/*28	5 (20)	6 (32)	11 (25)
*28/*28	1 (4)	1 (5)	2 (5)
Unknown	5 (20)	4 (20)	9 (20)

[a] Data are expressed as median (interquartile range, IQR) or number (percent). 35HRZE is the arm that received 35mg/kg of rifampicin containing an anti-TB regimen, while 10RHZE is the arm that took 10 mg/kg of rifampicin.

Table 7: Pharmacokinetic parameter values for dolutegravir in adults living with HIV who have TB co-infection

Parameter	Typical value (95% CI) [b]	Variability as CV% [c] (95% CI) [b]
Clearance, CL (L/h) [a]	1.87 (1.63 – 2.15)	BSV: 13.5 (3.36 – 25.5)
Volume of distribution, V (L) [a]	12.4 (10.2 – 14.6)	
Absorption rate constant, k_a (h^{-1})	1.41 (0.918 – 2.18)	BOV: 105 (74.4 – 140)
Mean transit time (h)	0.58 (0.386 – 0.723)	BOV: 47.7 (33.8 – 94.3)
Number of transit compartments (n)	21.3 (6.10 – 42.7)	
Relative bioavailability, F (fraction) [d]	1 FIXED	BOV: 41.2 (32.7 – 53.7)
Effect of a 10 mg·h/L increase in rifampicin $AUC_{0\text{-}24}$ on F, RIF_F (%) [d]	-2.29 (-3.14 – -1.38)	
Scaling factor for BOV of pre-dose occasion (-fold) [f]	1.56 (1.08 – 2.21)	
Proportional error (%)	10.0 (6.83 – 14.5)	
Additive error (mg/L)	0.205 (0.111 – 0.279)	

This parameter has been adjusted by allometric scaling and the values reported here refer to a subject with a fat-free mass of 43 kg i.e., for subject i:

$\mathbf{CL_i} = \mathbf{TVCL} \cdot \left(\frac{\mathbf{FFM_i}}{\mathbf{43}}\right)^{\frac{3}{4}}$ and $\mathbf{V_i} = \mathbf{TVV} \cdot \left(\frac{\mathbf{FFM_i}}{\mathbf{43}}\right)$

[b]The values in the parentheses are empirical 95% confidence interval (CI) obtained by sampling importance resampling.

[c]The pharmacokinetic parameter variability was included either as between-subject variability (BSV) or between occasion variability (BOV), assuming a log-normal distribution. It is reported here as the percent coefficient of variation (CV) calculated as: $\%\mathbf{CV} = \sqrt{\boldsymbol{\omega}^{\mathbf{2}}} \times \mathbf{100}$

[d]The relative bioavailability was dependent on the $AUC_{0\text{-}24}$ of rifampicin. The reference value of 1 refers to bioavailability of the typical participant in the 10 mg/kg study arm, with rifampicin $AUC_{0\text{-}24}$ of 32.3 mg·h/L. The effect (RIF_F) is presented for every 10 mg·h/L increase in rifampicin $AUC_{0\text{-}24}$ ($RIFAUC_i$) from 32.3 mg·h/L: $\mathbf{F_i} = \mathbf{TVF} + \mathbf{RIF_F} \cdot \left(\frac{\mathbf{RIFAUC_i - 32.3}}{\mathbf{10}}\right)$

[f]This is a multiplicative factor increasing the BOV of absorption parameters for pre-dose concentrations following an unobserved dose

Table 8: Comparison of dolutegravir pharmacokinetic parameters with other studies.

Study	Studies in people living with HIV					Studies in healthy volunteers			
	SAEFRIF (This study)		**SPRING-1** (Zhang et al., 2015)	**SHCS** (Barcelo et al., 2019)		**NCT01231542** (Dooley et al., 2013)		**RADIO** (Wang et al., 2019)	
Dolutegravir 50 mg regimen	BID	BID	OD	OD	BID	OD	BID	OD	OD
Rifampicin dose (mg/kg)	10 (10RHZE)	35 (35RHZE)	0	0	10	0	10	0	10
Number of participants	25	19	563	521		11	9	14	
Median weight (kg)	56	60	75	73		79	83	79	
African ancestry (%)	100	100	12	0		67	10	14	
$AUC_{0\text{-}24}$ (mg·h/L) [¥] Geometric mean (IQR)	43.6 (37.6–48.4)	30.4 (27.2–32.0)	53.8 (49.6–58.2)	49.0 (25.1–102)	29.8 (14.7–58.1)	29.8 (14.7–58.1)	32.1 (29.5–34.6)	42.6 (39.7–45.5)	
C_{trough} (mg/L) Geometric mean (IQR)	1.07 (0.866–1.47)	0.744 (0.527–1.00)	1.17 (1.04–1.33)	1.08 (0.269–3.19)	0.424 (0.054–1.45)	0.55 (0.464–0.689)	0.67 (0.590–0.750)	1.06 (0.745–1.51)	0.156 (0.115–0.214)
Oral clearance (CL/F) for a 70-kg participant (L/h) [‡]	2.21	3.51	0.901	0.91	2.38	1.37	2.06	0.96[†]	2.19[†]

IQR, interquartile range; F, bioavailability; BID, twice-daily; OD, once-daily; 10RHZE, standard-dose rifampicin; 35RHZE, high-dose rifampicin; C_{trough}, trough concentration, i.e., either C_{12} or C_{24}, depending on the dosing frequency.

[¥]Dolutegravir $AUC_{0\text{-}24}$ were calculated by doubling $AUC_{0\text{-}12}$ for BID dosing.

‡Calculated by adjusting for weight with allometry whenever the typical participant was not 70 kg.

†Clearance value not reported in original publication but derived here for purpose of comparison using the formula AUC = Dose/Clearance

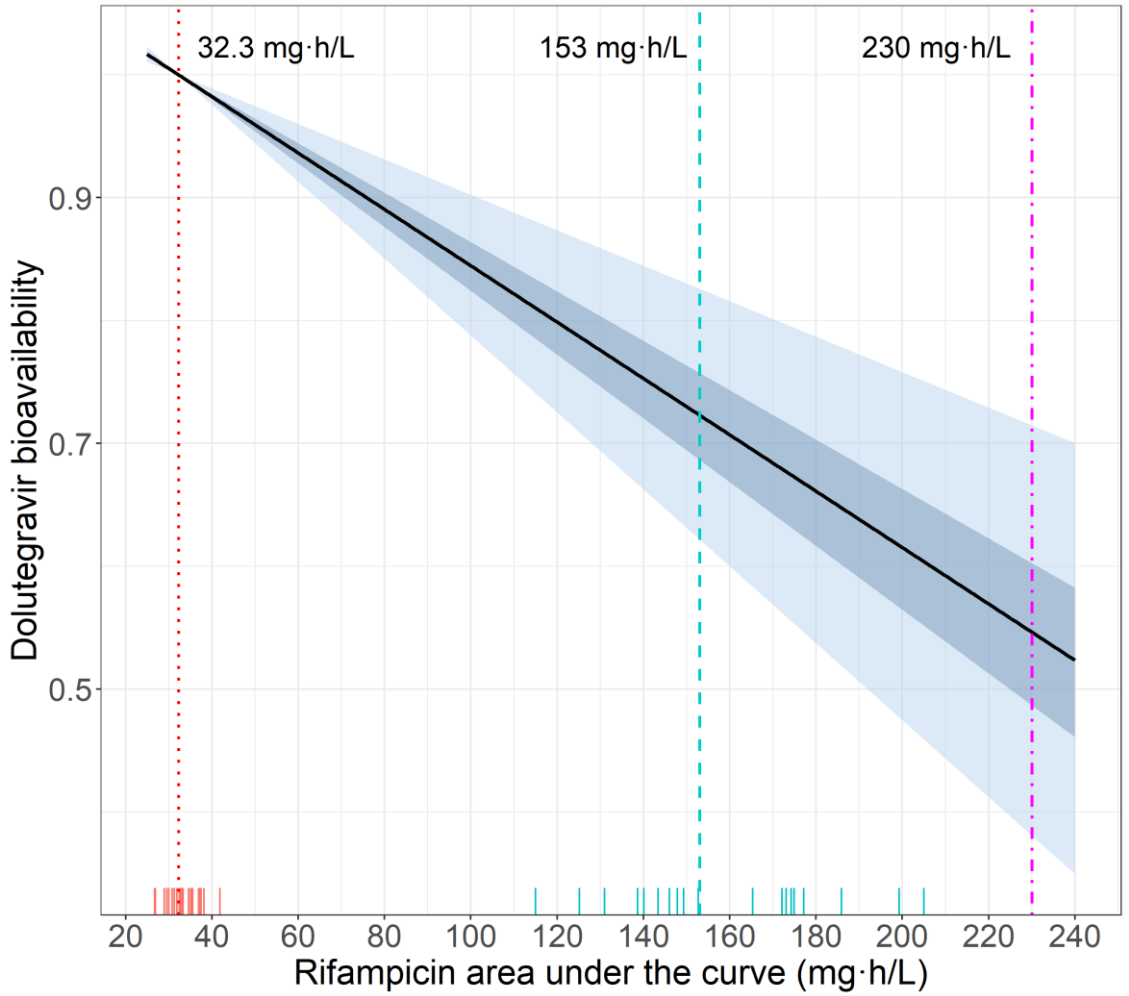

Figure 7: A function of dolutegravir bioavailability versus 24-h area under the curve ($AUC_{0\text{-}24}$) of coadministered rifampicin. $\mathbf{F_i} = \mathbf{TVF} + \mathbf{RIF_F} \cdot \left(\frac{\mathbf{RIFAUC_i - 32.3}}{\mathbf{10}}\right)$. The dotted (red) and dashed (blue) vertical lines represent the median $AUC_{0\text{-}24}$ of the standard- and observed high-dose arms of the study. The dash-dot (purple) vertical line is the median $AUC_{0\text{-}24}$ of the predicted high-dose cohort assuming bioequivalence of the two rifampicin formulations (top-up rifampicin-only formulation and fixed dose combination). The shaded areas represent the 50th and 90th confidence intervals of the predicated dolutegravir bioavailability.

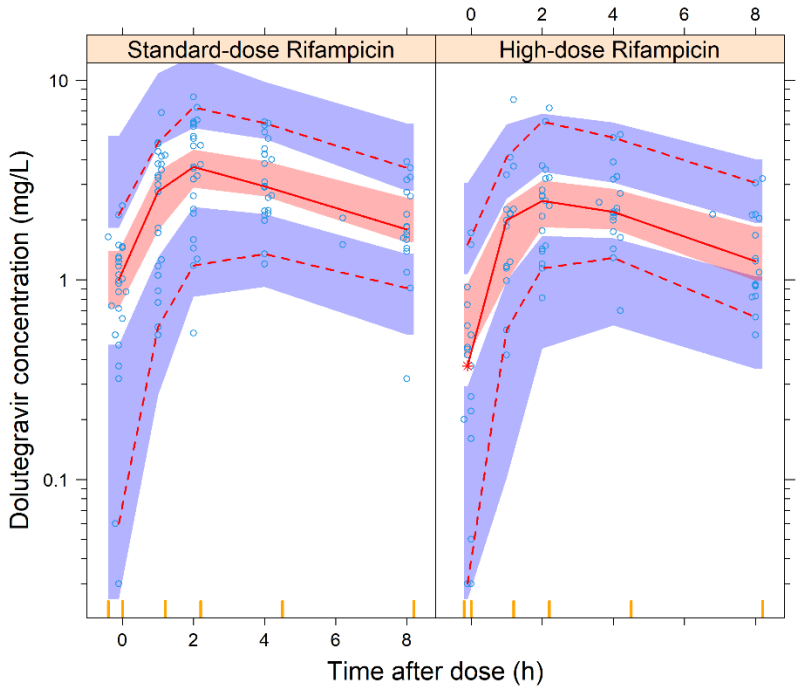

Figure 8: Visual predictive check of the dolutegravir stratified by rifampicin dose.
The open circles represent observed data. The solid and dashed lines represent the 50th, 5th and 95th percentiles of the observed data. The shaded areas represent the model-predicted 95% confidence intervals for the same percentiles.

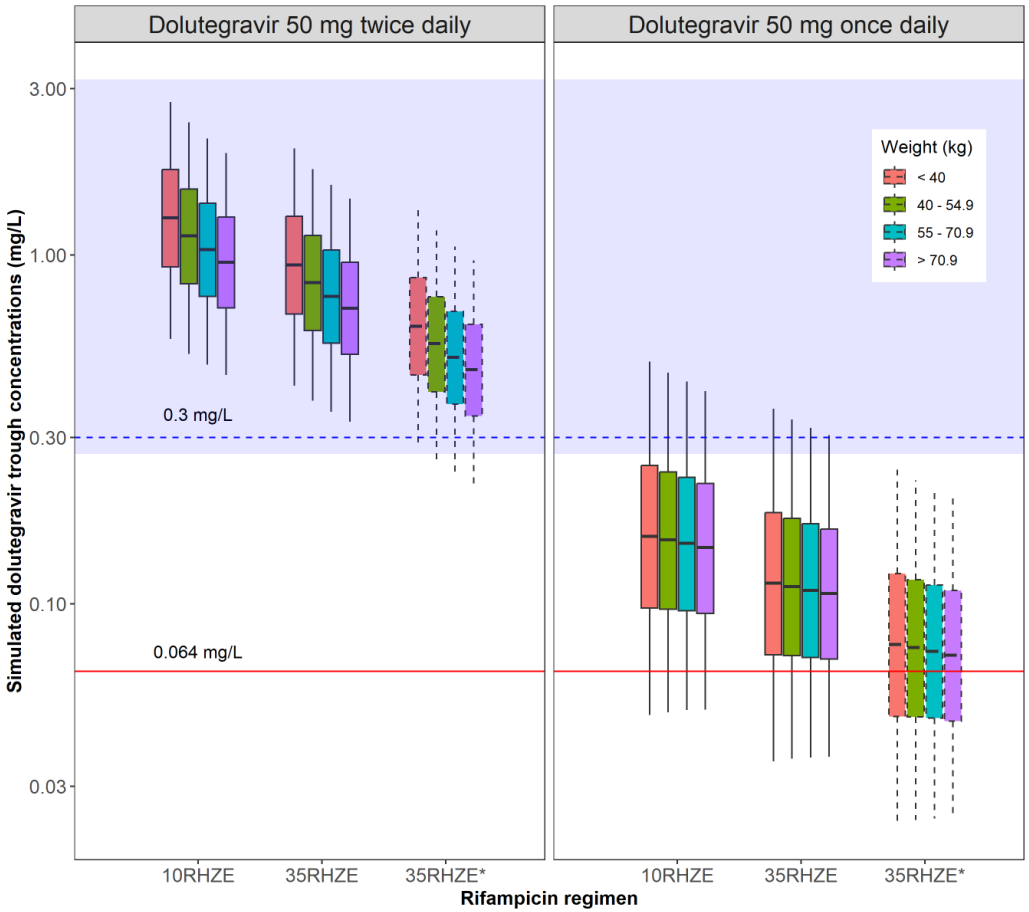

Figure 9: Simulated trough dolutegravir concentrations of participants in different weight bands10RHZE and 35RHZE represent participants receiving 10 and 35 mg/kg rifampicin dose containing anti-TB regimen, respectively.
35RHZE* (dashed) represents simulated trough concentration when the 2 formulations used in the 35RHZE cohort were assumed to be bioequivalent. Left panel: Trough concentrations of dolutegravir achieved after 12 hours when participants are given a twice-daily 50 mg dose. Right panel: Trough concentrations of dolutegravir achieved after 24 hours when participants are given a once daily 50 mg dose. The solid and dotted horizontal lines represent target dolutegravir trough concentrations of 0.064 mg/L and the 0.3 mg/L. The shaded region (0.269-3.19) mg/L represents the range of trough concentrations achieved in participants with HIV taking dolutegravir 50 mg once daily without rifampicin (Barcelo et al., 2019).

4.6 Supplementary materials

Results

Table 9: Participant characteristics (all participants randomized to dolutegravir)

Characteristic [a]	Rifampicin regimen		Total
	10RHZE	35RHZE	
Participants, n (%)	29 (50)	29 (50)	58 (100)
Male, n (%)	20 (69)	19 (66)	39 (67)
Age (yrs.)	36 (30 – 43)	36 (33 – 44)	37 (32 – 43)
Height (cm)	162 (158 – 171)	164 (161 – 175)	163 (159 – 172)
Weight (kg)	52 (46 – 61)	54 (47 – 61)	53 (47 – 61)
Fat-free mass (kg)	43 (37 – 49)	44 (40 – 50)	43 (38 – 49)
Antiretroviral experience, n (%)	20 (69)	19 (66)	39 (67)
UGT1A1 genotype, n (%)			
*1/*36	2 (7)	4 (14)	6 (10)
*1/*1	15 (52)	12 (41)	27 (47)
*1/*28	5 (17)	7 (24)	12 (21)
*28/*28	2 (7)	1 (3)	3 (5)
Unknown	5 (17)	5 (17)	10 (17)

[a] Data expressed as median (inter-quartile range; (IQR)) or number (percent). 35HRZE is the arm that took 35mg/kg of rifampicin containing anti-TB regimen while 10RHZE is the arm that took 10 mg/kg of rifampicin.

Table 10: The minimum objective values of objective function (OFV) of major models of dolutegravir

Model ID	Description	-2Log Likelihood (OFV)	Parent model	ΔOFV	df	p - value	Significance at α = 0.05
1	1st order absorption and elimination	310.3					
2	+ BOV in bioavailability, F	179.1	1	-131.2	1*	< 0.0001	Yes
3	+ BSV in clearance, CL	165.9	2	-13.2	1*	0.00028	Yes
4	+ BOV in in absorption rate constant, ka	140.5	3	-25.4	1*	< 0.0001	Yes
5	+ Absorption lag time	113.3	4	-27.2	1	< 0.0001	Yes
6	+ BOV in lag time	100.2	5	-13.1	1*	0.00030	Yes
7	+ Scaling of BOV of unobserved dosing	95.0	6	-5.2	1	0.02258	Yes
8	+ 2 compartment model	95.1	7	0.01	2	0.92034	No
9	+ Transit compartment absorption	88.5	7	-6.50	1	0.01079	Yes
10	+ Rifampicin dose on DTG F	81.6	9	-6.90	1	0.00862	Yes
11	+ Rifampicin dose on DTG CL	84.5	9	-4.00	1	0.04550	Yes
12	+ Rifampicin dose on DTG CL and F	81.2	10	-0.40	1	0.52709	No
13	+ Rifampicin AUC_{RIF} on DTG F	76.4	9	-12.1	1	0.000504	Yes

DTG, dolutegravir; BSV, between subject variability; BOV, between occasion variability; F, bioavailability; CL, clearance; AUC_{RIF}, 24 h area under the curve of rifampicin.

*This is a random effect and may have less degrees of freedom (Delattre et al., 2014).

Chapter 5: Model-based evaluation of the interaction between ritonavir-boosted atazanavir and rifampicin in Ugandan adults with HIV

5.1 Abstract

Background: Concomitant treatment of tuberculosis (TB) and human immunodeficiency virus (HIV) is complicated by drug-drug interactions (DDI). This analysis aimed to characterize the DDI between ritonavir-boosted atazanavir (ATV/r) and rifampicin in plasma and peripheral blood mononuclear cells (PBMC).

Methods: DERIVE study (NCT04121195) recruited Ugandan adults with HIV (not TB) on ATV/r-based second line antiretroviral therapy, and collected intensive plasma and PBMC pharmacokinetic samples during four visits: (i) standard dose ATV/r 300/100 mg QD, (ii) same ATV/r regimen adding rifampicin 600 mg QD, (iii) doubling ATV/r to BID with rifampicin 600 mg QD, and (iv) ATV/r 300/100 mg BID with rifampicin increased to 1200 mg QD. ATV/r plasma and PBMC concentrations were analysed with population pharmacokinetic modelling in NONMEM.

Results: Twenty-six participants (23 female) were enrolled, with median age and weight of 44 years and 67 kg, respectively. A two-compartment model with an effect compartment effectively described atazanavir concentrations in plasma and PBMC. Rifampicin increased atazanavir clearance threefold, while decreasing its bioavailability and absorption rate. Doubling dosing frequency of ATV/r largely mitigated the interaction with rifampicin, restoring the proportion of simulated participants achieving the targeted trough atazanavir concentration of 0.014 mg/L to 99%. Rifampicin did not affect the ratio of atazanavir concentration between PBMCs and plasma.

Conclusion: Metabolic induction by rifampicin accounts for the decrease in plasma exposure of ATV/r. Doubling the ATV/r dosing frequency to BID effectively mitigated this interaction. The plasma exposure of ATV/r mirrored that in PBMCs, suggesting that for these drugs, plasma concentrations provide a reliable reflection of site-of-action exposures.

What is already known about this subject:

- Ritonavir-boosted atazanavir is a WHO-preferred protease inhibitor used as second-line antiretroviral therapy in resource limited settings.
- The clinically significant drug-drug interaction between atazanavir and rifampicin has precluded its use in patients requiring treatment for tuberculosis.

What this study adds:

- This article uses population pharmacokinetics to describe the interaction between ritonavir-boosted atazanavir and rifampicin in Ugandan adults with HIV. The effect of the drug-drug interaction on atazanavir pharmacokinetic parameters is characterized in a model that is subsequently used to estimate the speed and extent of intracellular accumulation of the drug.

5.2 Introduction

Boosted protease inhibitors (bPI), combined with an appropriate nucleoside reverse-transcriptase inhibitor backbone, form the second-line antiretroviral therapy (ART) regimen recommended by the World Health Organization (World Health Organization, 2021b). Ritonavir-boosted atazanavir (ATV/r) is currently the most used bPI combination, owing to its tolerability, superior potency (Busti et al., 2004), simplified once-daily dosing (FDA & CDER, 2003; Havlir & O'marro, 2004; Swainston Harrison & Scott, 2005), and significantly reduced effects on lipid metabolism (Busti et al., 2004; Swainston Harrison & Scott, 2005) compared with others.

Atazanavir (ATV) is rapidly absorbed, and its bioavailability is enhanced by food (Alvarellos et al., 2018; FDA & CDER, 2003) but reduced by increased gastric pH (Havlir & O'marro, 2004). It is about 86% bound to plasma proteins (FDA & CDER, 2003), and a substrate of transporter proteins like p-glycoprotein (Kis et al., 2013). Atazanavir is metabolised by cytochrome P450 (CYP) 3A, an enzyme it also competitively inhibits (Busti et al., 2004; FDA & CDER, 2003) and is primarily eliminated by the liver through bile (Alvarellos et al., 2018; FDA & CDER, 2003). Its protein adjusted in-vitro 90% inhibitory concentration (PA-IC_{90}) against HIV-1 is 0.014 mg/L (FDA & CDER, 2003; Gausi et al., 2024), and a trough plasma concentration (C_{trough}) of 0.15 mg/L has previously been used as a target for therapeutic drug monitoring (Back et al., 2006).

Ritonavir was initially developed as a PI for therapeutic use but is now primarily used to enhance the pharmacokinetics of other drugs because it inhibits their metabolism (Hull & Montaner, 2011; Loos et al., 2022). It is an irreversible inhibitor of enzymes (FDA & CDER, 2019; Loos et al., 2022, 2023), which prevents them from metabolizing their substrates until new enzymes or cells are

produced (Loos et al., 2022). Ritonavir is approximately 99% bound to plasma proteins and is primarily metabolised by CYP3A4 (Loos et al., 2022), and partly by CYP2D6 (FDA & CDER, 2019; Hsu et al., 1998). Although its half-life is only 3-5 hours (FDA & CDER, 2019), ritonavir reaches steady-state concentrations after about 2 weeks of daily dosing, likely due to having some CYP3A4 induction properties (Hsu et al., 1998; Loos et al., 2023).

Rifampicin is crucial in treating drug-susceptible tuberculosis (TB) (Bonnett et al., 2017b; World Health Organization, 2024), a prevalent coinfection and leading cause of mortality among people living with HIV (World Health Organization, 2021b, 2024). Currently, there is no clear guidance on its concurrent use with ATV/r due to limited clinical data on the effects of their drug-drug interaction (DDI) (Niemi et al., 2003; Zhang et al., 2012a). Rifampicin strongly induces CYP3A and drug transporters (Chen & Raymond, 2006; Niemi et al., 2003), affecting ATV/r exposure (Gausi et al., 2024). Previous investigations of DDIs between rifampicin and other bPIs had mixed results. Rifampicin caused unacceptable hepatotoxicity in patients on ritonavir-boosted darunavir (Ebrahim et al., 2020), whereas it showed mixed results in healthy volunteers and patients on ritonavir-boosted lopinavir (Murphy et al., 2012). Recently, higher rifampicin doses (up to 35mg/ kg) have been found to result in more favourable treatment outcomes and to be well tolerated (Boeree et al., 2017b; Bun Ng et al., 2015; Sekaggya-Wiltshire et al., 2022).

A physiologically based pharmacokinetic model developed by Montanha *et al*. predicted that doubling the dosing frequency of ATV/r to 300/100 mg twice daily (BID) would effectively mitigate its interaction with rifampicin (Montanha et al., 2022). The regimen was subsequently evaluated in the DERIVE trial whose non-compartmental analysis (NCA) showed that the administration of BID ATV/r with rifampicin largely restored ATV C_{trough} (Gausi et al., 2024) and resulted in no cases

of hepatotoxicity. In this population pharmacokinetics analysis, we aimed to further characterize the effect of the rifampicin coadministration on the pharmacokinetic parameters of ATV/r. We sought to use intracellular concentrations to characterize the distribution of ATV/r into peripheral blood mononuclear cells (PBMCs) and investigate whether rifampicin affects drug concentrations at the site of action. We also simulated the probability of achieving therapeutic target C_{trough} with current treatment recommendations.

5.3 Methods

Study design and participants: Data were available from DERIVE (NCT04121195), an open-label, single arm, dose-escalation study conducted at the Joint Clinical Research Center (JCRC) in Uganda (Gausi et al., 2024). The study enrolled adults with undetectable HIV viral load (<50 copies/mL) and on ATV/r-based second line ART for at least 6 months. Participants were excluded if they were pregnant or breastfeeding, had coinfections like TB and hepatitis, or were taking medication known to interact with study drugs. The study was approved by the JCRC Ethics Committee (JC1819), the University of Liverpool Research Ethics Committee (Ref 5802) and the Uganda National Council for Science and Technology (HS2685). All participants provided voluntary written informed consent.

Sample collection and drug quantification: Pharmacokinetic sampling was conducted over four visits. During Visit 1 (Day 7 after recruitment), participants were still on ATV/r 300/100 mg once daily (QD). Afterward, rifampicin 600 mg QD and dolutegravir 50 mg twice daily (BID) were added to the regimen and Visit 2 sampling was carried out on Day 21. The dosing frequency of ATV/r was then increased to BID, with further sampling conducted during Visit 3 (Day 28). The rifampicin

dose was increased to 1200 mg once daily (QD) for one week. Sampling for Visit 4 was conducted on Day 35, prior to discontinuing rifampicin and resuming the standard QD ATV/r dose. Dolutegravir was maintained for an additional two weeks. Blood samples were collected for plasma separation at pre-dose, and 0.5-, 1-, 2-, 4-, 6-, 8-, and 12-hour post-dose during all visits, with an extra 24-hour sample during Visit 1. Separate trough samples for intracellular PBMC concentration assays were collected at visits (1, 3 and 4), and at 12 hours post-dose during visit 2.

Blood samples were centrifuged and stored at -80°C prior to shipment and assay at the University of Cape Town, where drug concentrations were measured using high-performance liquid chromatography with tandem mass spectrometry (HPLC MS/MS). The lower limits of quantification (LLOQ) were 0.030 mg/L for atazanavir and 0.005 mg/L for ritonavir (Gausi et al., 2024). A separate blood sample was collected in a cell preparation tube, for subsequent PBMC isolation by density gradient centrifugation (De Nicolò et al., 2020). Isolated PBMCs were stored at -80 ^{0}C and transferred to the University of Turin in Italy. PBMCs were counted using a previously described turbidimetric method (De Nicolò et al., 2024), and intracellular atazanavir and ritonavir concentrations assayed using HPLC MS/MS (De Nicolò et al., 2025; De Nicolò et al., 2020) (LLOQ: 0.015 mg/L (De Nicolò, et al., 2020; Focà et al., 2017). More details are presented in the supplementary file.

Additional atazanavir data (without ritonavir) were available from the ACTG A5213 study, which enrolled healthy adult volunteers in the USA (Acosta et al., 2007). Atazanavir was administered with or without rifampicin in three periods: 300 mg BID for 8 days (Period 1), 300 mg BID with rifampicin 600 mg QD for 11 days (Period 2), and 400 mg BID with rifampicin 600 mg QD for 8

days (Period 3) (Acosta et al., 2007). Pharmacokinetic sampling was conducted at the end of each period, with blood collected 15 minutes pre-dose and at 1-, 2-, 3-, 4-, 5-, 6-, 8-, 10-, 12-, and 24-hours post-dose. Plasma samples were analyzed at the University of Alabama using HPLC with UV detection (LLOQ: 0.025 mg/L) (Acosta et al., 2007).

Pharmacokinetic analysis: Population pharmacokinetic analysis was done in NONMEM v7.5.1 (Beal, Boeckmann, and Sheiner, 2017) using first-order conditional estimation with eta-epsilon interaction. PsN (Lindbom et al., 2004) and Pirana were used in the modelling process while the Xpose4 package in R via RStudio was used for model diagnostics (Keizer et al., 2013).

Ritonavir and atazanavir pharmacokinetic models were separately developed using DERIVE data. We tested one- and two-compartment disposition models with linear elimination, and delayed absorption modelled by a lag time or series of transit compartments. PBMC concentrations were modelled using a hypothetical effect compartment connected to the central compartment of the plasma model. An equilibration half-life ($t_{1/2}$) and a pseudo-partition coefficient (PPC) were used to parameterize the rate of drug entry into the PBMC compartment and its accumulation ratio between the PBMC and plasma, respectively (Figure 14, supplementary file).

Considering each administered dose as a separate occasion, we tested log-normally distributed BOV (Karlsson & Sheiner, 1993) on all absorption parameters. BSV (Mould & Upton, 2013) and BVV were similarly tested on clearance to describe its variance across individuals and study visits, respectively. RUV was modelled with a combined additive and proportional error model (Mould & Upton, 2013), fixing the additive error to at least 20% of the corresponding LLOQ.

Concentrations below LLOQ (BLQ) were included by imputing 50% of the LLOQ and inflating their additive component of the RUV by LLOQ/2 (Beal, 2001).

Total body weight or fat-free mass (FFM) (Janmahasatian et al., 2005) were tested to apply allometric scaling (Holford & Anderson, 2017) to all clearance and volume parameters. Various approaches were tested to model rifampicin and ATV/r interactions. Ritonavir and rifampicin AUCs were evaluated as continuous covariates, and study visits/rifampicin dosing regimen as categorical covariates. A joint atazanavir-ritonavir model like that by Zhang *et al.* (Zhang et al., 2012b) modelling was also tested. A covariate was retained in the model if its addition resulted in a drop in objective function value (ΔOFV) of more than 3.84, which was considered significant at $P<0.05$ (Mould & Upton, 2013).

Model performance was also assessed using goodness-of-fit plots, a visual predictive check (VPC), and sampling importance resampling (Dosne et al., 2016). Monte Carlo simulations were used to estimate the probability of achieving atazanavir treatment targets (C_{trough} higher than 0.014 mg/L (FDA & CDER, 2003) or 0.15 mg/L (Back et al., 2006). Exposure was estimated for different dosing regimens using a reference cohort of 1,225 in-silico individuals based on demographic data from previous African HIV/TB studies (Chirehwa et al., 2020). To evaluate the role of ritonavir in the interaction with rifampicin, we evaluated the final ATV/r model with the additional ATV-only data from the A5213 study, allowing re-estimation of some absorption parameters.

Data availability statement: The datasets generated and analyzed in this study may be made available by the corresponding author upon request, subject to suitable access agreements.

5.4 Results

Study participants and data: The study enrolled 26 participants (88% female), with median age and weight of 44 years and weight 67 kg, respectively. All participants were taking lamivudine and 17 (65%), 8 (31%), and 1 (4%) were also on tenofovir disoproxil fumarate (TDF), zidovudine, and abacavir, respectively, as shown in Table 11. Concentrations in 857 plasma samples were included in the analysis, of which 28 (3%) atazanavir and 20 (2%) ritonavir samples were below the quantification limit (BLQ). External atazanavir data (355 samples) was available from the ACTG A5231 study which enrolled 13 (8 male) participants with median age and weight of 30 years and 75 kg, respectively (Table 13, supplementary file).

Table 11: Participant baseline characteristics

Characteristic [a]	
Participants, n	26
Female, n	23 (88)
Black African, n	23 (100)
Participants living with HIV, n	26 (100)
Age, years	44 (23 – 61)
Weight, kg	67 (50 – 75)
Fat-free mass, kg	41.0 (37.9 – 41.9)
Body mass index, kg/m^2	26.1 (19.9 – 31.6)
Height, m	1.59 (1.48 – 1.86)
ART baseline drug, n (%)	
TDF	17 (65)
AZT	8 (31)
ABC	1 (4)

[a] The characteristics are presented as number (%) or median (range).
TDF, tenofovir disoproxil fumarate; AZT, Zidovudine; ABC, Abacavir; BMI, body mass index

Atazanavir model: Atazanavir plasma data were best described by a two-compartment model (ΔOFV = -202, P<0.001, compared to one¬ compartment model) with transit compartment absorption (ΔOFV = 21, P<0.001, compared to lag time) and first-order elimination. The typical

(95% confidence interval) atazanavir clearance was 7.57 L/h (6.30–9.03) when standard dose ATV/r was given OD without rifampicin. A VPC of the model fit is shown in Figure 10.

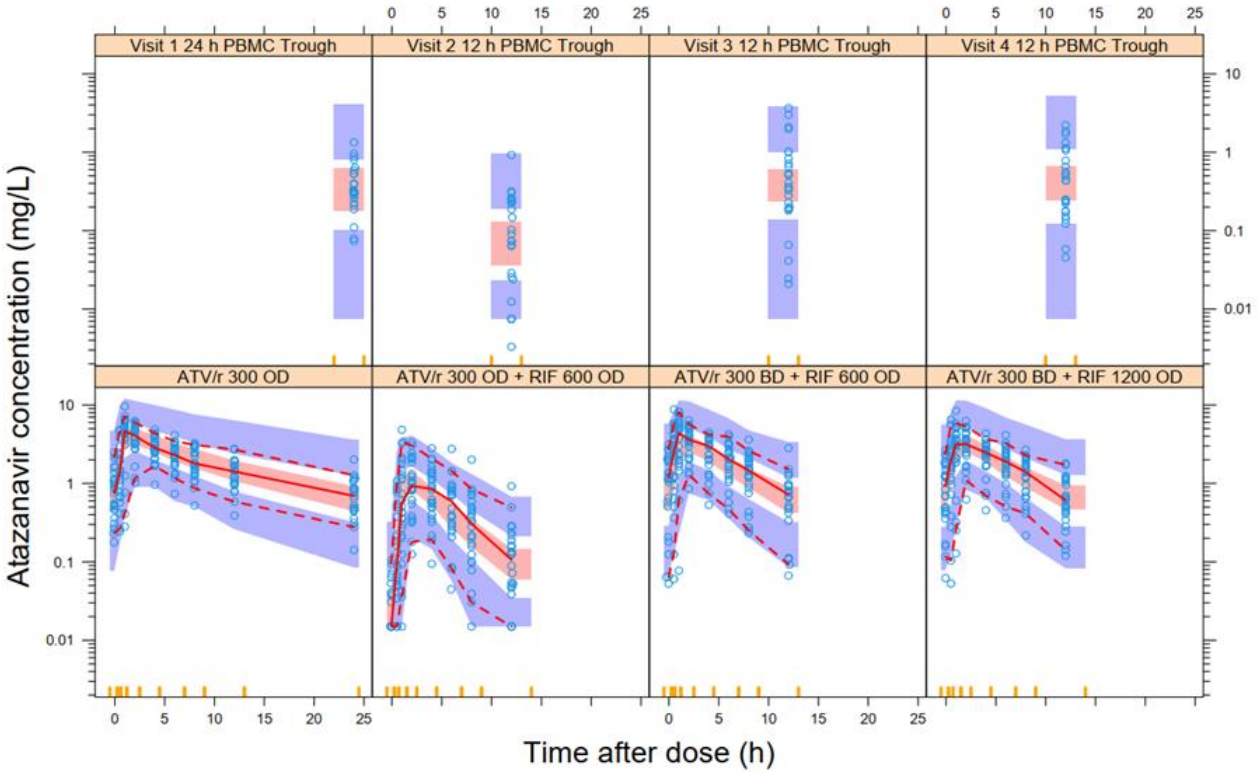

Figure 10: Visual predictive check of plasma (bottom) and intracellular (top) atazanavir concentrations versus time.
The red solid and dashed lines represent the 5th, 50th, and 95th percentiles of the observed data (open blue circles), while the shaded areas represent the model-predicted 95% confidence intervals for the same percentiles. ATV/r- ritonavir boosted atazanavir; PBMC, peripheral blood mono nuclear cells.

Ritonavir model: Ritonavir plasma pharmacokinetics was characterized by a two-compartment model (ΔOFV = -271, P<0.001, compared to one-compartment) and absorption through transit compartments (ΔOFV = -52, P<0.001 compared to lag time) (Figure 11). The typical clearance of ritonavir was 9.67 L/h (8.51–11.6) when administered as ATV/r without rifampicin. Clearance and volume parameters of both drugs were allometrically scaled by FFM, and other parameter estimates are presented in Table 12.

Rifampicin data were acceptably characterised by fitting a previously published 1-compartment model with saturation of elimination via a liver compartment (Chirehwa et al., 2016a; Kengo et al., 2023). The parameters of the model were re-estimated and presented in Table 14 while a VPC is shown in Figure 15.

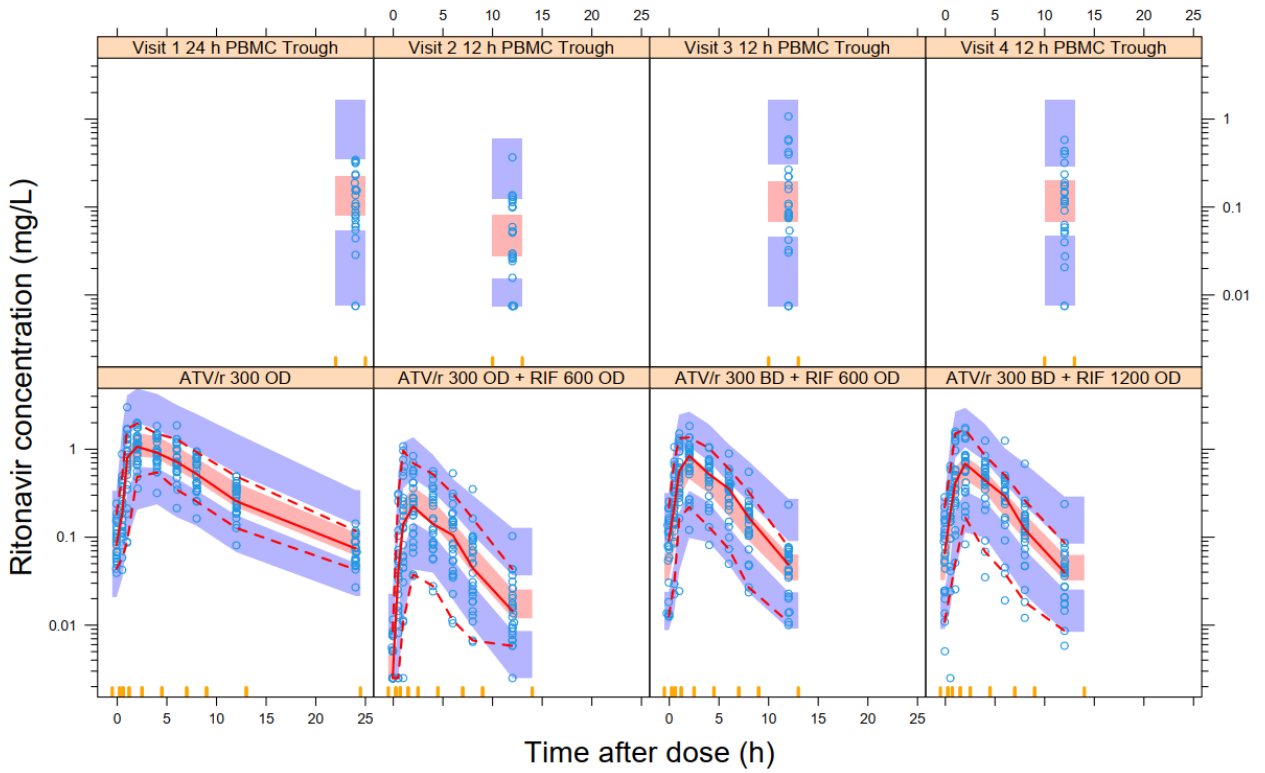

Figure 11: Visual predictive check of plasma (bottom) and intracellular (top) ritonavir concentrations versus time
The red solid and dashed lines represent the 5th, 50th, and 95th percentiles of the observed data (open blue circles), while the shaded areas represent the model-predicted 95% confidence intervals for the same percentiles. ATV/r- ritonavir boosted atazanavir; RIF, rifampicin; PBMC, peripheral blood mononuclear cells

Interactions between drugs: There was a strong correlation between ritonavir and atazanavir clearance and absorption parameters (Figures 17 and 18). Attempts to fit a ritonavir-based inhibition for atazanavir led to limited improvement in model fit and reduced parameter

precision. Similarly, including rifampicin AUC to explain inter-visit differences in atazanavir clearance did not provide more benefit over considering each dosing regimen as its own category. Atazanavir: Adding rifampicin to the standard ATV/r regimen, increased atazanavir clearance by 3-fold (2.7–3.6) (ΔOFV = -122, *P*<0.001) and reduced its bioavailability and absorption rate by 53% (62–40) (ΔOFV = -47, *P*<0.001) and 67% (78–56) (ΔOFV = -19, *P*<0.001), respectively. Doubling the dosing frequency of ATV/r to BID with standard dose rifampicin, restored atazanavir bioavailability and reduced the rifampicin induction of its clearance to 2-fold (1.8–2.3). There was no significant effect of increasing rifampicin dose on atazanavir clearance or bioavailability, and TDF affected neither atazanavir clearance (ΔOFV = -0.64, *P*=0.424) nor bioavailability (ΔOFV = -2.66, *P*=0.103). Ritonavir: Rifampicin increased ritonavir clearance by 2-fold (1.95–2.31) (ΔOFV = -163, P<0.001) and decreased its bioavailability to 31% (25–41) (ΔOFV = -63, P<0.001). Doubling the dosing frequency of ATV/r partially restored ritonavir bioavailability to 66% (54–89) (ΔOFV = -8, P=0.005), and increasing the rifampicin dose had no further effect on ritonavir pharmacokinetics.

PBMC concentrations: The atazanavir PBMC concentrations were linked to the central plasma compartment by a distributional equilibration half-life ($t_{1/2}$) of 0.963 h (0.546-1.51) and plasma-to-PBMC PPC of 0.653 (0.538-0.797), neither of which were affected by rifampicin. For ritonavir, the $t_{1/2}$ and PPC were 1.40 h (1.38-1.63) and 1.68 (0.643-1.75), respectively. The other model parameters are presented in the Table 12.

Additional atazanavir data: The final atazanavir model, developed with DERIVE data, was applied to the A5231 dataset. We made the following adjustment to our model to account for the differences between the two studies. Firstly, A5231 was found to have slower absorption compared to DERIVE (MTT was 2.5-fold (2.3–3.2) longer, ΔOFV = -81, *P*<0.001). Additionally, the

clearance of atazanavir in all PK visits of A5231 was 2-fold (1.9–2.3) higher compared to when ATV/r was given without rifampicin in Visit 1 of the DERIVE study (ΔOFV = -93, *P*<0.001). Finally, a significant 55% (64–46) reduction in atazanavir bioavailability was observed when rifampicin was coadministered with atazanavir (Period 2 and 3) (ΔOFV = -63, *P*<0.001). A VPC and other model parameter estimates are presented in Figure 19 and Table 15**,** respectively, of the supplementary file.

Simulations of atazanavir trough plasma concentrations: Figure 12 and figure 16 (Supplementary file) present a summary of the predicted atazanavir C_{trough} and are under the curve (AUC), respectively, attained when ATV/r was dosed QD without rifampicin and then QD or BID with rifampicin. When ATV/r was administered QD alone, all (100%) simulated individuals attained a C_{trough} greater than the PA-IC90 (0.014 mg/L) and 95.4% also attained the higher 0.15 mg/L target. When given with rifampicin, the proportion of participants whose C_{trough} was above the PA-IC90 and 0.15 mg/L dropped to 72.8% and 2.83%, respectively. In the 3rd scenario when the dosing frequency of ATV/r was doubled in the presence of standard dose rifampicin, the proportion of simulated participants who attained a C_{trough} greater than the PA-IC90 and 0.15 mg/L were restored to 99% and 94%, respectively. Figure 13 shows the simulated atazanavir exposure of the typical individual in the 3 dosing scenarios.

Table 12: Table of ritonavir and atazanavir pharmacokinetic model parameter estimates

Parameter	Typical parameter estimates (95% CI [b])	
	Ritonavir	**Atazanavir**
Clearance, CL (L/h) [a]	9.67 (8.51 – 11.6)	7.57 (6.42 – 9.06)
Fold-change in CL for ATV/r QD + RIF (-fold)	2.12 (1.95 – 2.31)	3.05 (2.67 – 3.45)
Fold-change in CL ATV/r BID + RIF (-fold)	-	2.03 (1.82 – 2.25)
Volume of distribution (central compartment) (L) [a]	55.4 (46.3 – 69.1)	77.5 (69.3 – 88.7)
Inter compartmental clearance (L/h) [a]	1.56 (1.17 – 2.15)	3.13 (2.34 – 4.31)
Volume of distribution (peripheral compartment) (L) [a]	70.1 (39.7 – 125)	42.1(26.6 – 79.0)
Bioavailability, F (fraction)	1 Fixed	1 Fixed
Change in F for ATV/r QD + RIF (%)	-68.8 (-75.2 – -58.5)	-52.5 (-62.5 – -41.4)
Change in F for ATV/r BID + RIF (%)	-33.3 (-46.6 – -10.9)	-
Absorption rate constant, ka (/L)	1.02 (0.864 – 1.27)	6 Fixed
Change in ka due to RIF (%)	-	-67.3 (-76.2 – -53.2)
Mean absorption transit time, MTT (h)	0.483 (0.428 – 0.545)	0.499 (0.429 – 0.574)
Transit compartments, NN (n)	12.3 (6.64 – 17.7)	10 Fixed
Additive error (plasma) (mg/L)	0.001 Fixed	0.006 Fixed
Proportional error (plasma) (%)	25.6 (24.1 – 27.8)	19.8 (18.2 – 21.1)
Variability (% CV) [c]		
Between subject variability in clearance	16.4 (12.3 – 21.8)	27.6 (19.7 – 36.7)
Between visit variability in clearance	-	17.5 (14.4 – 24.5)
Between occasion variability (BOV) in ka	82.3 (67.3 – 99.1)	97.9 (80.8 - 125)
BOV in MTT	43.6 (37.7 – 51.6)	59.4 (49.3 – 73.6)
BOV in F	55.5 (48.1 – 63.8)	48.2 (40.7 – 53.6)
Scaling factor on BOV for unobserved dose (-fold change) [d]	-	1.63 (1.26 – 2.10)
Peripheral blood mono-nuclear cell (PBMC)		
Equilibration half-life, t1/2 (h)	1.40 (1.38 – 1.63)	0.963 (0.546 – 1.51)
Pseudo-partition coefficient, PPC (.)	1.68 (0.643 – 1.75)	0.653 (0.538 – 0.797)
Proportional error PBMC (%)	51.4 (42.9 – 61.1)	74.9 (62.4 – 92.0)
Additive error PBMC (mg/L)	0.003 Fixed	0.003 Fixed

[a] All clearance and volume parameters for atazanavir and ritonavir were allometrically scaled using fat-free mass. The values reported here refer to a typical participant with a weight of 67 kg and fat-free mass of 42 kg.

[b] Parameter uncertainty was determined by sampling importance resampling to obtain the 95% confidence interval (CI).

[c] Variability in these parameters was modelled as either between-subject (BSV), between-occasion (BOV), or between-visit (BVV) variability. It was assumed to be log-normally distributed and is reported here as the percent coefficient of variation (%CV) calculated by $\%CV = \sqrt{\omega^2} \times 100$.

[d] Multiplicative factor increasing the BOV of absorption parameters (absorption rate constant, mean transit time, and bioavailability) for pre-dose concentrations following an unobserved dose.

QD, once daily; BID, twice daily; ATV/r, ritonavir-boosted atazanavir; RIF, rifampicin.

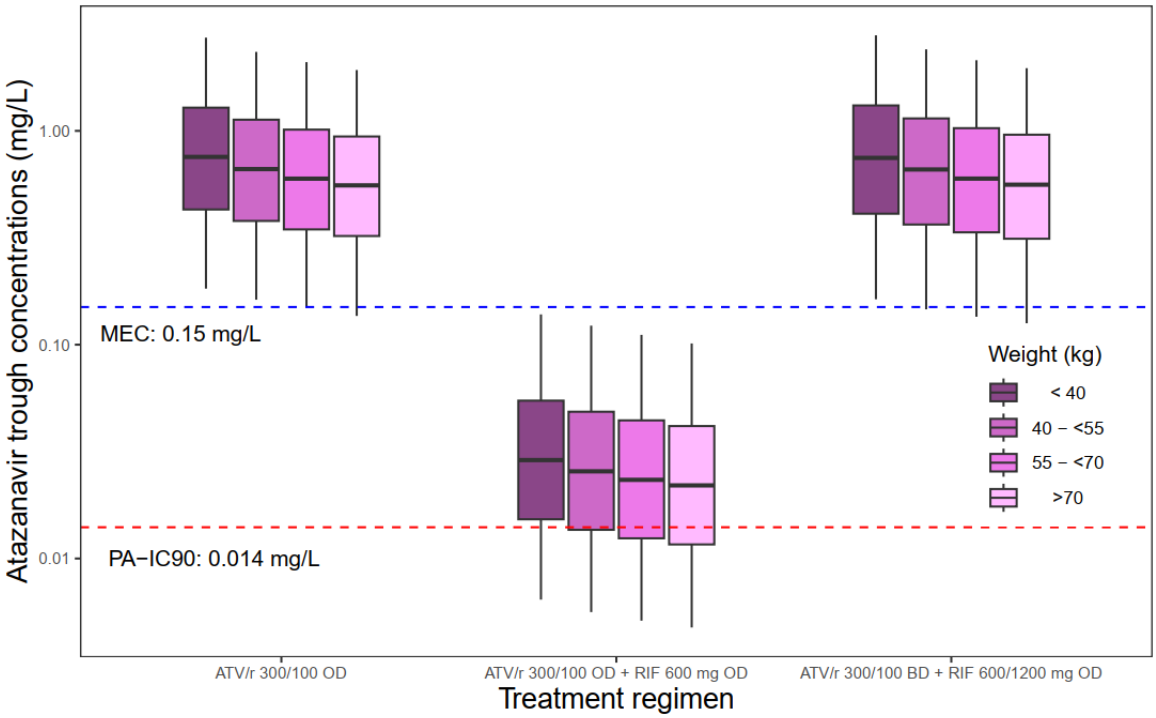

Figure 12: Simulated trough plasma atazanavir concentrations of participants (stratified by WHO weight bands) in different dosing scenarios.

The dashed lines represent atazanavir target trough concentrations of 0.15 mg/L (blue) and 0.014 mg/L (red), respectively. The first group of boxes represents the trough concentrations achieved during ATV/r OD. The boxes in the middle are the trough concentrations reached by the simulated individuals when rifampicin 600 mg OD is added to ATV/r OD. The third dosing scenario represents trough concentrations achieved when ritonavir boosted atazanavir is given twice daily with both 600 and 1200 mg of rifampicin. ATV/r- ritonavir boosted atazanavir; RIF, rifampicin; MEC, minimum efficacious concentrations; PA_IC90, protein adjusted 90% inhibitory concentration; MEC, minimum efficacious dose; OD, once daily; BD, twice daily.

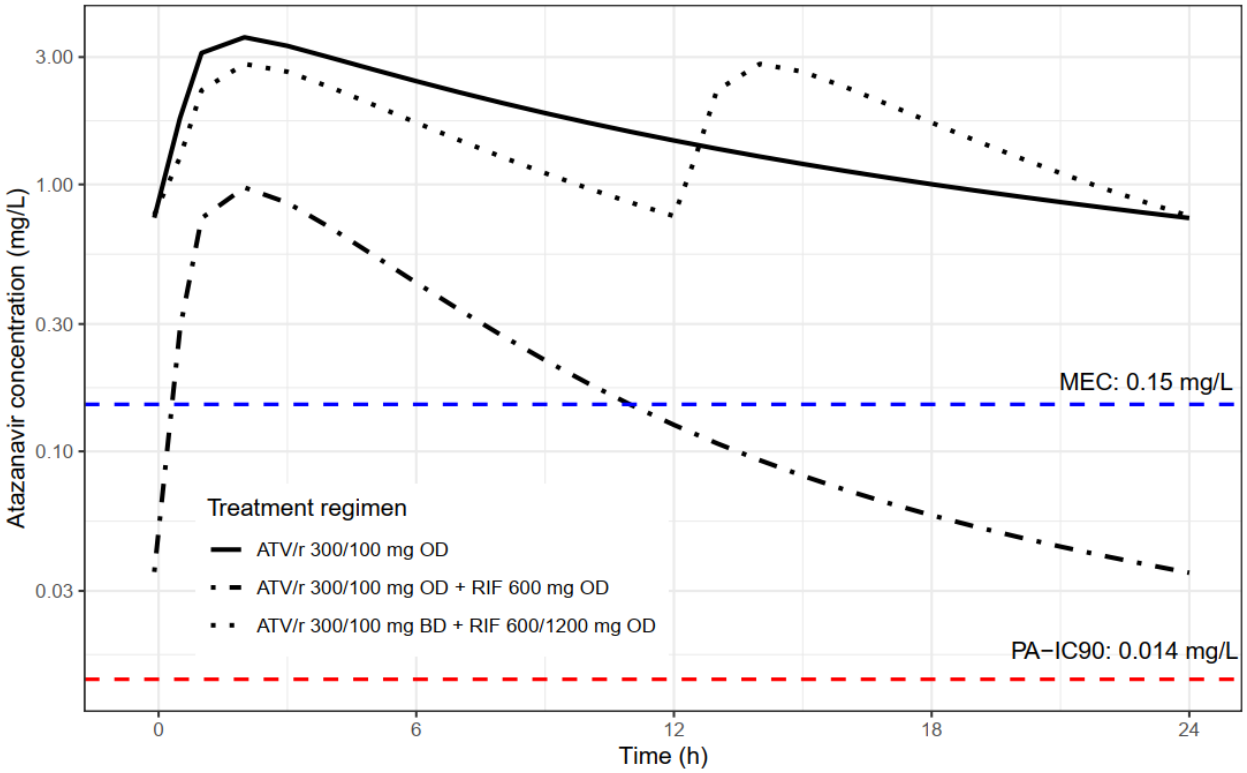

Figure 13: Atazanavir concentration versus time profiles of the typical 61 kg individual during the 3 different dosing scenarios. The solid curve represents exposure when the ATV/r is given alone in the standard regimen.

The dash-dot and the dotted lines represent exposure when standard and doubled the frequency doses of ATV/r are administered with rifampicin, respectively. The lower and upper horizontal dashed lines represent the protein adjusted 90% inhibitory concentration (PA IC90) and commonly used target trough atazanavir concentration (MEC), respectively.

5.5 Discussion

In this pharmacokinetic study, we modelled the effect of rifampicin on ATV/r pharmacokinetics in Ugandan HIV patients without TB. Rifampicin reduced atazanavir and ritonavir exposures by inducing their clearance and reducing bioavailability. Our simulations showed that doubling ATV/r dosing from QD to BID restores atazanavir exposure, achieving a comparable C_{trough} to standard ATV/r QD without rifampicin, which was confirmed by PBMC observations. No stronger interaction was observed with the higher rifampicin dose.

These findings are consistent with previous studies showing that rifampicin reduces the exposure of PIs by induction of CYP3A enzymes and transporters (Acosta et al., 2007; FDA & CDER, 2003, 2019; Ribera et al., 2007; Zhang et al., 2012a), through activation of the pregnane X receptor (Bolt, 2004; Fromm et al., 2000; Glaeser et al., 2005; Niemi et al., 2003). Although more complex models like a ritonavir-inhibition ATV model were explored, they did not provide more meaningful benefit over using visit or drug regimen as categorical covariates. This is likely because the interaction involves a shared clearance pathway for both drugs, making it difficult to distinguish causality from correlation, as illustrated in Figures 17 and 18. Moreover, both drugs also inhibit their own metabolism, and were administered at a constant ratio in all participants, further limiting our ability to characterize the ATV-ritonavir DDI within this dataset.

Our model found rifampicin to have a more pronounced effect on atazanavir clearance than ritonavir, but it caused greater reduction in ritonavir bioavailability. This is likely due to rifampicin's induction of gut CYP3A (Glaeser et al., 2005; Loos et al., 2023) and efflux transporters (Fromm et al., 2000; Greiner et al., 1999; Kim et al., 1998), which can delay drug absorption, as

previously reported for atazanavir (Kis et al., 2013) and digoxin (Greiner et al., 1999). When ATV/r dosing frequency was increased to BID, atazanavir's bioavailability was restored. Interestingly, this was not observed with the additional A5231 ATV-only data, suggesting that doubling the dosing frequency of ritonavir, and possibly not ATV, has a protective effect on ATV bioavailability when given with rifampicin. Moreover, we observed a twofold increase in atazanavir clearance compared to the DERIVE study, likely due to the absence of ritonavir's strong inhibitory effect (Eichbaum et al., 2013). In our study, a higher rifampicin dose did not further induce atazanavir clearance, possibly due to near-maximal enzyme induction at the standard dose (Mirochnick et al., 2011; Taburet et al., 2004).

Differences in rifampicin's effect on atazanavir and ritonavir may stem from their distinct metabolic pathways and interactions with CYP enzymes. Ritonavir's interaction with less inducible CYP2D6 (Farooq et al., 2016; Glaeser et al., 2005) may also make it less affected by rifampicin. Additionally, it binds differently to the CYP3A4 active site compared to atazanavir, leading to either metabolism or inhibition (Loos et al., 2022, 2023). This could make ritonavir less available for metabolism, resulting in less induction by rifampicin.

A two-compartment model provided a better fit for both drugs, with clearance estimates like previous studies (Foissac et al., 2011; Schipani et al., 2013). Like previously reported (Von Hentig et al., 2007), no significant interaction between TDF and ATV/r was observed in our study, contrasting with reports in pregnant women (Mirochnick et al., 2011) and pre-treated patients (Taburet et al., 2004). Despite inhibiting p-glycoprotein (Storch et al., 2007), TDF's interaction with atazanavir may be less significant in the presence of ritonavir, a stronger inhibitor.

Our model estimates of the intracellular accumulation of atazanavir and ritonavir are consistent with previous reports (De Nicolò et al., 2025.). The accumulation $t_{1/2}$ between plasma and PBMCs was estimated to be around 1 hour, differing from previously assumed instantaneous equilibration (Ngwalero et al., 2021; Ter Heine et al., 2010). Despite having limited PBMC sampling points, the precision of the $t_{1/2}$ estimate was confirmed through sensitivity analysis. This delay may reflect the time needed for drug molecules to cross cellular membranes. These findings suggest that plasma concentrations reliably indicate intracellular levels and drug activity at the PBMC site of action.

The study had several limitations. Participants were required to weigh between 50-75 kg, excluding more severely ill TB patients, and the sample was predominantly female, potentially limiting the detection of previously reported sex-related differences (Punyawudho et al., 2017; Venuto et al., 2014). Another study (NCT03923231) has been carried out to explore this interaction in participants with more extreme demographics. The fixed-dose ATV/r regimen limited our ability to describe ATV-RTV interaction with our data alone prompting the use of additional ATV-only data. The rifampicin dose was lower than the proposed 35 mg/kg (Boeree et al., 2015), which may affect results generalizability. Rifampicin was also administered alone, excluding other anti-TB drugs like isoniazid that may also affect CYP enzymes (Wen et al., 2002). Finally, intracellular ATV/r accumulation estimates were based on limited sampling and require further validation with more intensive data collection.

In conclusion, our findings provide insights into the mechanisms underlying the DDI between rifampicin and ATV/r, complementing previous non-compartmental analyses (Gausi et al., 2024). We also demonstrated that rifampicin does not affect the intracellular accumulation of atazanavir,

suggesting plasma levels accurately reflect drug activity at the site of action. Monte Carlo simulations support the suitability of BID dosing of ATV/r to overcome the DDI with rifampicin in HIV patients, consistent with safety data from the DERIVE trial (Gausi et al., 2024). The concurrent use of ATV/r-based ART and rifampicin-containing anti-TB regimens in individuals with HIV and TB should be further evaluated.

Acknowledgement: We are very grateful to the DERIVE study participants and clinical team at the Joint Clinical Research Center in Kampala, Uganda. We also extend our thanks to the Trial Steering Committee chaired by Ed Wilkins and comprising Cissy Kityo, Gary Maartens, Saye Khoo, Helen McIlleron and Regina Kamoga. Similarly, we appreciate the AIDS Clinical Trial Group A5231 study team for sharing their data which is partly presented in this manuscript. Computations were performed using facilities provided by the University of Cape Town's ICTS High Performance Computing team: hpc.uct.ac.za.

Funding: The DERIVE project was funded with support from the EDCTP2 program supported by the European Union (grant number RIA2016MC-1606-VirTUAL). Additionally, Allan Kengo received Ph.D. funding from the same source. Catriona Waitt is funded by Wellcome Clinical Research Career Development Fellowship 222075/Z/20/Z.

Principal Investigation (PI) statement: The authors confirm that the PI for this paper is Prof. Catriona Waitt and that she had direct clinical responsibility for patients.

Author contributions: A.K. drafted the manuscript and C.W. and P.D. designed the research. A.K., J.E.R.G., L.N., H.M., A.D.N., A.D.A., S.A., L.W., E.M.S., and P.D., performed the research and analysed the data. All authors reviewed and agreed on the final version of the manuscript.

Conflict of interest: The authors do not have any conflict of interest to declare.

5.6 Supplementary File

Methods

High-performance liquid chromatography with tandem mass spectrometry detection methods were developed and validated to assay rifampicin at the Division of Clinical Pharmacology, University of Cape Town. The calibration ranges were: 0.030 (LLOQ) – 10.0 mg/L for atazanavir, 0.005 (LLOQ) – 2.50 mg/L for ritonavir (Gausi et al., 2024). The calibration range for the rifampicin assay was 0.117 – 30.0 mg/L, with an inter-day accuracy of 101% – 107%. The precision, measured as coefficient of variation (%CV), ranged from 2.70% – 13.7%. A more detailed description of the method has been previously described (Abdelgawad et al., 2023; Gausi et al., 2024). PBMC concentrations were assayed with a previously described validated HPLC MS/MS method (D'Avolio et al., 2013; De Nicolò et al., 2020). The LLOQ for both drugs were 0.015 mg/L, and the accuracy ranged from 92.7 to 103.7% (De Nicolò et al., 2020; Focà et al., 2017).

Table 13: Baseline characteristics of participant in the A5231 study

Characteristic [a]	**A5231 Study**
Participants, n	13
Female, n	5 (38)
Black race, n	1 (8)
Participants living with HIV, n	None
Age, years	30 (23 – 48)
Weight, kg	75 (55 – 110)

[a] The characteristics are presented as number (%) or median (range).

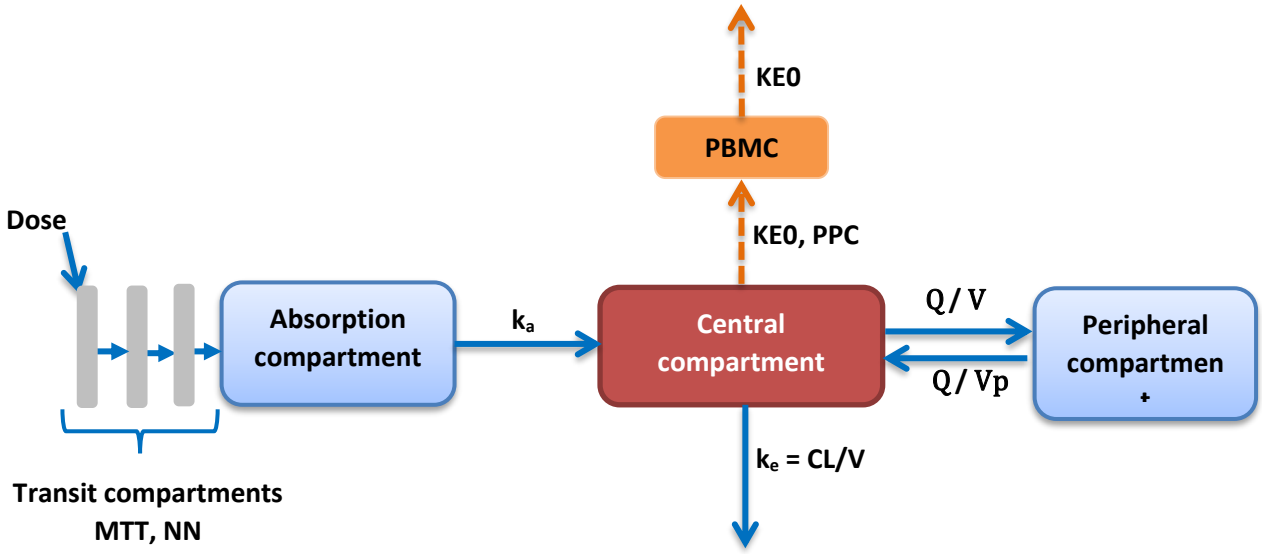

Figure 14: Schematic representation of the final ritonavir and atazanavir pharmacokinetic models The mean transit time (MTT) is the time the drug takes to traverse the series of transit compartments (NN) during its absorption; ka is the absorption rate constant; PBMC, peripheral blood mono nuclear cell; KE0, drug plasma-PBMC equilibration rate constant which describes how soon the change in plasma is reflected in the PBMC; PPC, the pseudo-partition coefficient which represents the ratio of drug in PBMC to the plasma. From the central compartment the drug equilibrates to a peripheral compartment with an intercompartmental clearance (Q) and peripheral volume (Vp). Ke is the elimination constant rate based on clearance (CL) and central volume (V).

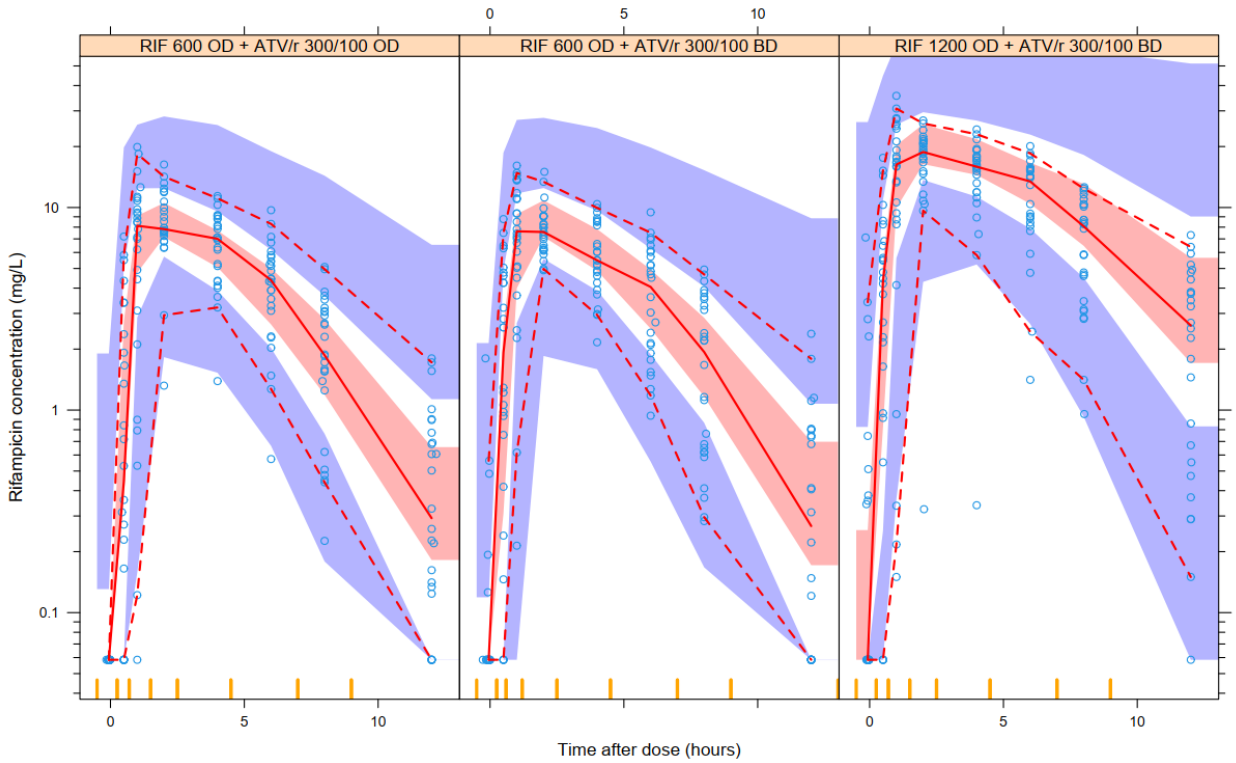

Figure 15: Visual predictive check of plasma rifampicin concentrations versus time.
The red solid and dashed lines represent the 10th, 50th, and 90th percentiles of the observed data (open blue circles), while the shaded areas represent the model-predicted 95% confidence intervals for the same percentiles. ATV/r- ritonavir boosted atazanavir; RIF, rifampicin; OD, once daily; BD, twice daily.

Table 14: Table of rifampicin model pharmacokinetic parameter estimates

Parameter	Typical parameter estimates (95% CI [b])
Clearance, CL (L/h) [a, e]	33.0 (27.2 – 40.8)
Michaelis-Menten constant, Km (L/h)	4.90 (3.82 – 6.23)
Volume of distribution (central compartment) (L)	44.7 (42.2 – 47.8)
Bioavailability, F (fraction)	1 (fixed)
Absorption rate constant, ka (/L)	2.40 (1.74 – 3.30)
Mean absorption transit time, MTT (h)	0.502 (0.447 – 0.558)
Transit compartments, NN (n)	20.3 (15.8 – 25.9)
Additive error (mg/L)	0.023 (fixed)
Proportional error (%)	18.6 (17.1 – 20.3)
Hepatic volume, V_H (L)	1 (fixed)
Hepatic blood flow rate, Q_H (L/h) [a]	90 (fixed)
Unbound fraction of rifampicin, f_u (fraction)	0.2 (fixed)
Variability (% CV) [c]	
Between subject variability in clearance	27.7 (22.1 – 35.2)
Between occasion variability (BOV) in F	22.0 (17.9 – 26.3)
BOV in ka	104 (85.3 – 136)
BOV in MTT	46.8 (40.0 – 56.8)
Scaling factor on BOV for unobserved dose (-fold change) [d]	2.54 (1.90 – 3.32)

All fixed parameters are estimates from DERIVE study population.

[a] All clearance and volume parameters for atazanavir and ritonavir were allometrically scaled using fat-free mass. The values reported here refer to a typical participant with a fat-free mass of 41 kg and total body weight of 67 kg.

[b] Values in parentheses are empirical 95% confidence intervals obtained by sampling importance resampling procedure.

[c] Variability in these parameters was modeled as either between-subject (BSV), between-occasion (BOV), or between-visit (BVV) variability. It was assumed to be log-normally distributed and is reported here as the percent coefficient of variation (%CV) calculated by $\%\boldsymbol{CV} = \sqrt{\boldsymbol{\omega^2}} \times \mathbf{100}$.

[d] Multiplicative factor increasing the BOV of absorption parameters (ka, MTT, and BIO) for pre-dose concentrations following an unobserved dose.

[e] Clearance calculated from maximum intrinsic clearance using the formular: $\boldsymbol{CL} = \boldsymbol{CL_{int.max}} \times \boldsymbol{f_u}$. where $CL_{int,max}$, maximum intrinsic clearance; f_u, unbound fraction of rifampicin in plasma.

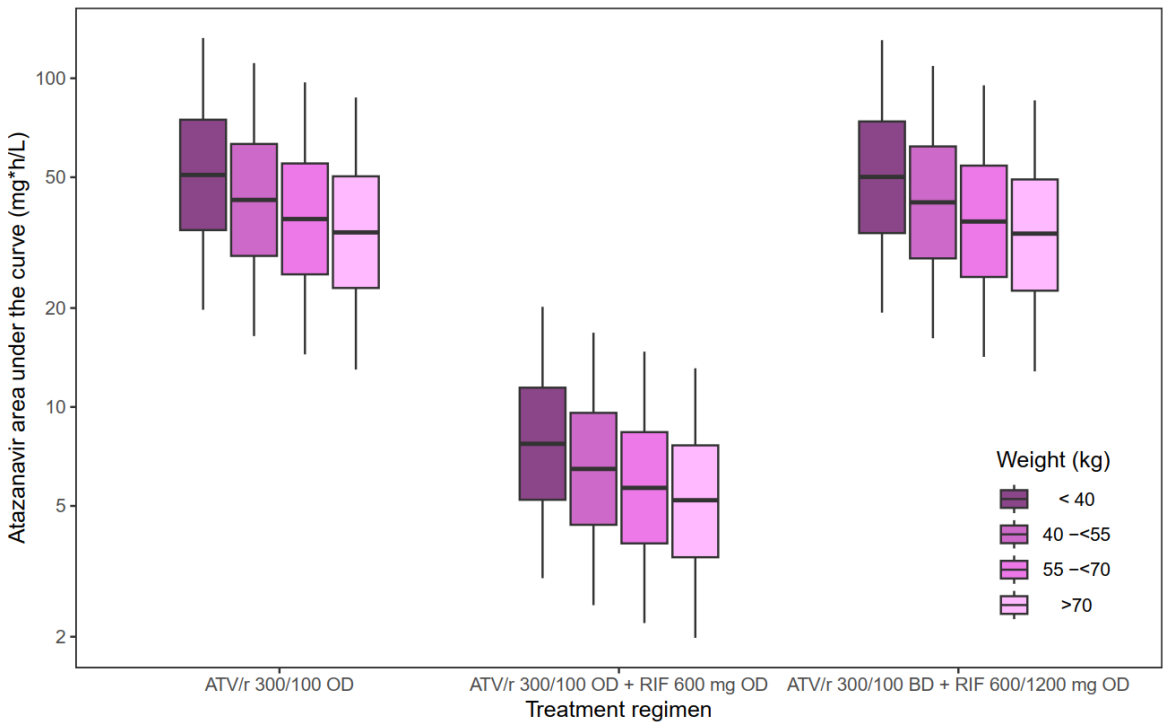

Figure 16: Simulated atazanavir plasma area under the curve (AUC) of participants (stratified in weight bands) in different atazanavir dosing scenarios.
ATV/r- ritonavir boosted atazanavir; RIF, rifampicin; OD, once daily; BD, twice daily.

Table 15: Table of atazanavir model pharmacokinetic parameter estimates from the ACTG A5231 data.

Parameter	Typical parameter estimates (95% CI [b])
Clearance, CL (L/h) [a]	7.55 (fixed)
Fold-change in CL due to absence of ritonavir (-fold)	2.13 (1.88 – 2.34)
Volume of distribution (central compartment) (L)	77.3 (fixed)
Inter compartmental clearance (L/h)	3.51 (fixed)
Volume of distribution (peripheral compartment) (L)	48.9 (fixed)
Bioavailability, F (fraction)	1 (fixed)
Change in F with rifampicin (%)	-55.3 (-64.0 – -46.2)
Absorption rate constant, ka (/L)	6 (fixed)
Change in ka with rifampicin (%)	-70.8 (fixed)
Mean absorption transit time, MTT (h)	1.38 (1.15 – 1.61)
Transit compartments, NN (n)	10 (fixed)
Additive error (mg/L)	0.005 (fixed)
Proportional error (%)	18.8 (fixed)
Variability (% CV) [c]	
Between subject variability in clearance	18.8 (13.7 – 24.4)
Between occasion variability (BOV) in ka	101 (fixed)
BOV in MTT	48.1 (36.9 – 63.4)
BOV in F	58.3 (46.4 – 73.5)
Scaling factor on BOV for unobserved dose (-fold change) [d]	1.7 (1.10 – 2.81)

All fixed parameters are estimates from DERIVE study population.

[a] All clearance and volume parameters for atazanavir and ritonavir were allometrically scaled using fat-free mass. The values reported here refer to a typical participant with a fat-free mass of 41 kg and total body weight of 67 kg.

[b] Values in parentheses are empirical 95% confidence intervals obtained by sampling importance resampling procedure.

[c] Variability in these parameters was modelled as either between-subject (BSV), between-occasion (BOV), or between-visit (BVV) variability. It was assumed to be log-normally distributed and is reported here as the percent coefficient of variation (%CV) calculated by $\%CV = \sqrt{\omega^2} \times 100.$

[d] Multiplicative factor increasing the BOV of absorption parameters (ka, MTT, and BIO) for pre-dose concentrations following an unobserved dose.

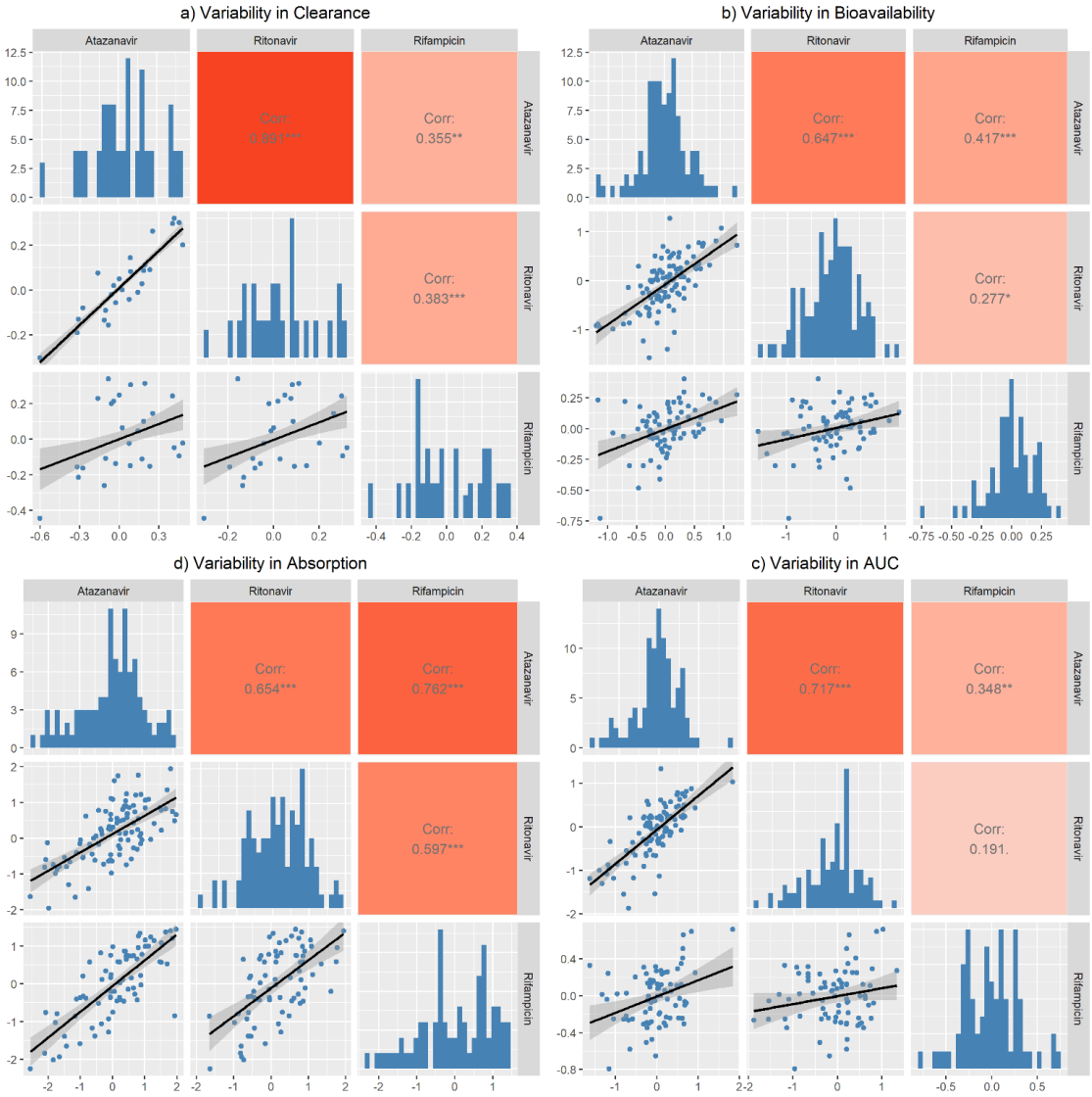

Figure 17: Correlation matrix of unexplained parameter variability

Parameter; A, clearance; B, bioavailability; C, absorption; and D, area under the curve from time 0 to infinity) of atazanavir, ritonavir and rifampicin. Only variability from the dosing occasion associated with the observed dose on the study visit was included.

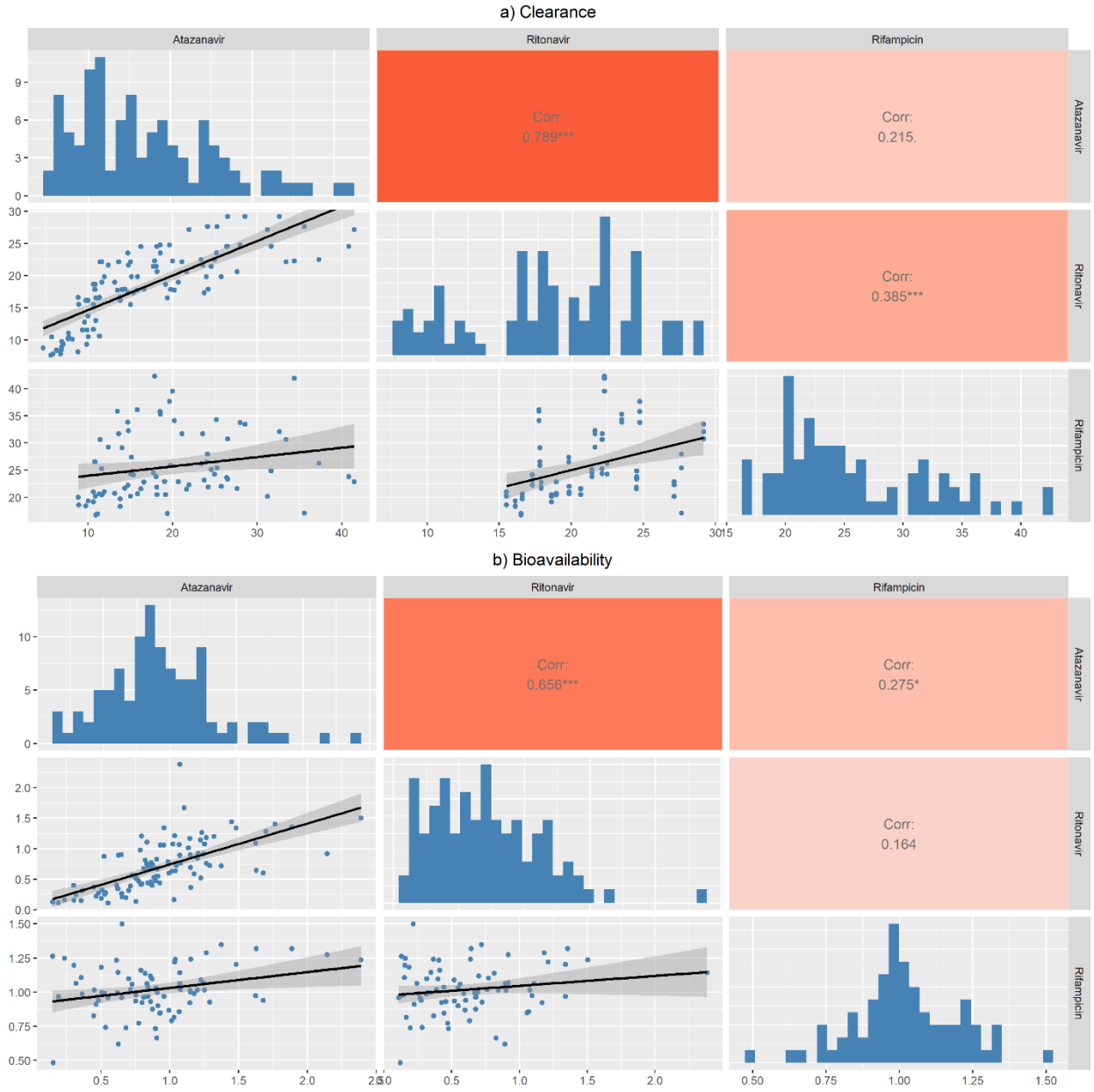

Figure 18: Correlation matrix of clearance and bioavailability of atazanavir, ritonavir and rifampicin

Only parameters from the dosing occasion associated with the observed dose on the study visit were included.

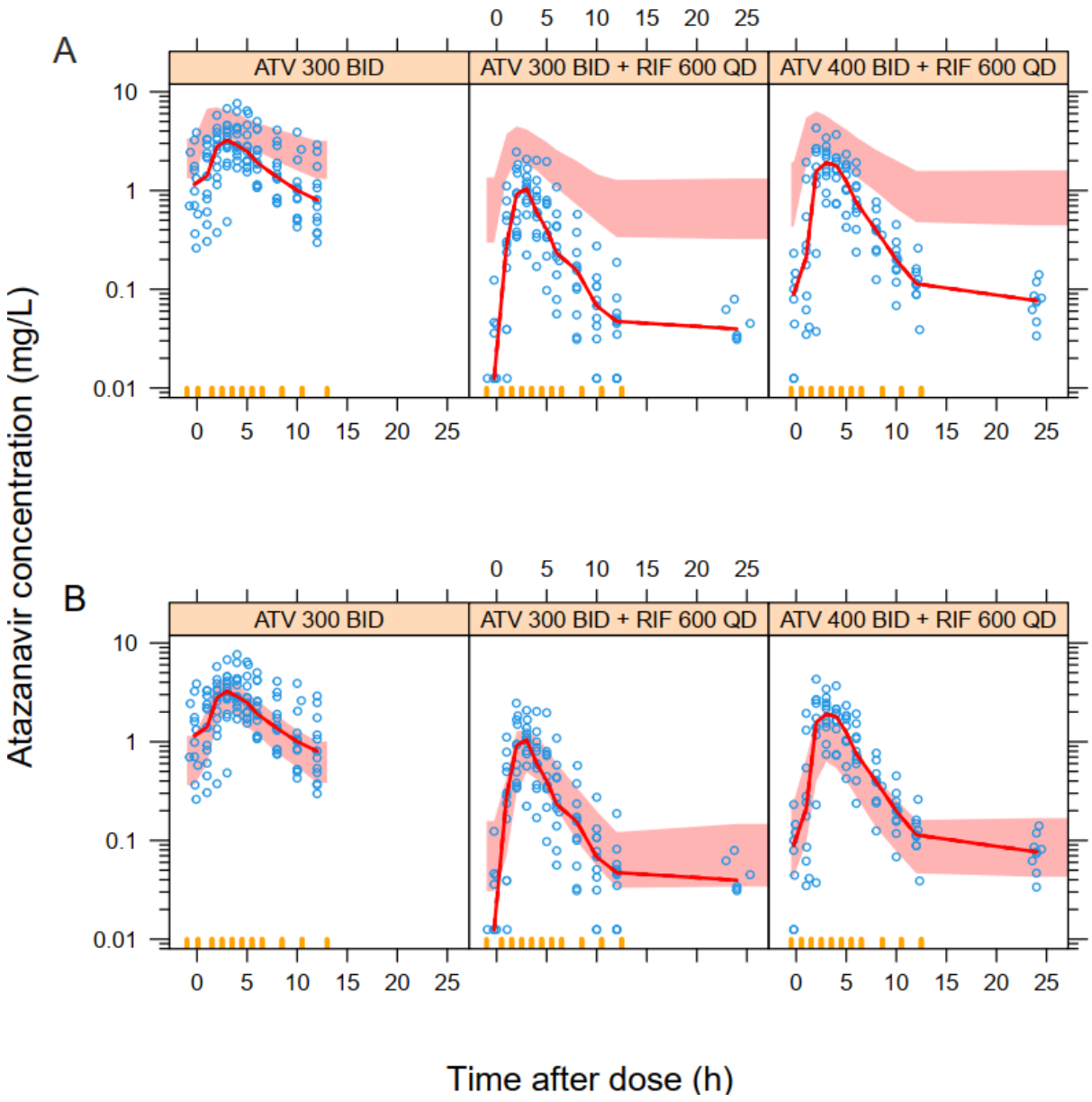

Figure 19: Visual predictive check of plasma atazanavir concentrations versus time
A; DERIVE model and B; after making changes in bioavailability (due to rifampicin) and clearance (due to absence of ritonavir inhibition). The atazanavir model developed with DERIVE study data was used to describe the exposures observed in the ACTG study (A5231) with factors describing the -fold change on absorption, bioavailability, and clearance. The solid lines represent the 50th percentile of the observed data (open circles), while the shaded areas represent the model-predicted 95% confidence intervals for the percentiles. ATV, atazanavir; RIF, rifampicin; BID, twice daily; QD, once daily.

Chapter 6: Assessing potential drug-drug interactions between clofazimine and other frequently used agents to treat drug-resistant tuberculosis.

6.1 Abstract

Clofazimine is included in drug regimens to treat rifampicin/drug-resistant tuberculosis (DR-TB), but there is little information about its interaction with other drugs in DR-TB regimens. We evaluated the pharmacokinetic interaction between clofazimine and isoniazid, linezolid, levofloxacin, and cycloserine, dosed as terizidone.

Newly diagnosed adults with DR-TB at Klerksdorp/Tshepong Hospital, South Africa, were started on the then-standard treatment, with clofazimine temporarily excluded for the initial 2 weeks. Pharmacokinetic sampling was done immediately before, and three weeks after starting clofazimine, and drug concentrations were determined using validated liquid chromatography-tandem mass spectrometry assays. The data were interpreted with population pharmacokinetics in NONMEM v7.5.1, to explore the impact of clofazimine coadministration and other relevant covariates on pharmacokinetics of isoniazid, linezolid, levofloxacin, and cycloserine.

Clofazimine, isoniazid, linezolid, levofloxacin, and cycloserine data were available for 16, 27, 21, 21, and 6 participants respectively. The median age and weight for the full cohort were 39 years and 52 kg, respectively. Clofazimine exposures were in the expected range and its addition to the regimen did not significantly affect the pharmacokinetics of the other drugs except levofloxacin, for which it caused a 15% reduction in clearance. *A posteriori* power size calculations predicted that our sample sizes had 97%, 90%, and 87% power at $P<0.05$ to detect a 30% change in clearance of isoniazid, linezolid and cycloserine, respectively. Although clofazimine increased the

area under the curve of levofloxacin by 19%, this is unlikely to be of great clinical significance and the lack of interaction with other drugs tested is reassuring.

6.2 Background

The surge in incidence of rifampicin/drug-resistant tuberculosis (DR-TB) is an obstacle to global efforts to eradicate TB (World Health Organization, 2022). Unlike its susceptible form, DR-TB is more challenging to manage and requires longer treatment duration (World Health Organization, 2021a). However, new regimens utilising novel and repurposed antimycobacterial agents have greatly reduced treatment duration (Van der Walt & Sizulu, 2018) and mortality attributed to DR-TB (Ndjeka et al., 2018).

Over the past decade there has been renewed interest in clofazimine, a fat-soluble riminophenazine dye that was initially used to treat leprosy (Gopal et al., 2013), partly because clofazimine-containing regimens showed potential to safely shorten the duration of DR-TB treatment (Stadler et al., 2023; Van Deun et al., 2010). Although clofazimine is not part of the current WHO-recommended BPaL/M regimen for DR-TB (World Health Organization, 2022a), it is categorized as a group B drug, used when levofloxacin/moxifloxacin, bedaquiline, or linezolid cannot (World Health Organization, 2022a). In 2019, the South African Department of Health recommended a shorter 9–11-month oral DR-TB regimen (Department of Health & RSA, 2019) comprising of bedaquiline, clofazimine, levofloxacin/moxifloxacin, linezolid, higher-dose isoniazid, pyrazinamide, and ethambutol. Terizidone was used whenever there was established fluoroquinolone resistance.

Clofazimine is highly lipophilic and exhibits significant duration-dependent accumulation in tissues like fat, muscle, and skin (Mirnejad et al., 2018), leading to relatively low serum

concentrations (Cholo et al., 2017). Little is known about its metabolism, and it is largely excreted unchanged (Holdiness, 1989). In vitro research suggests that clofazimine may inhibit some cytochrome enzymes (Sangana et al., 2018), and common membrane efflux transport proteins like P-glycoprotein and breast cancer resistance protein (BCRP) (Te Brake et al., 2016).

Isoniazid is an important component of drug-sensitive TB treatment (World Health organization, 2022) and is used at higher doses for DR-TB (Department of Health & RSA, 2019; World Health Organization, 2021a). Upon ingestion, isoniazid is rapidly absorbed, undergoes significant first-pass metabolism (Weber & Hein, 1979), and is eventually eliminated in urine (Klein et al., 2016; Weber & Hein, 1979). It is metabolized by NAT2 (Klein et al., 2016) which is encoded by a highly polymorphic *NAT2* gene (Boukouvala & Fakis, 2005). Polymorphism of the *NAT2* gene has been extensively studied, resulting in the phenotypic classification of populations into slow, intermediate, and rapid acetylators (Gausi et al., 2021; Klein et al., 2016; McDonagh et al., 2014; Weber & Hein, 1985), which are closely linked to isoniazid plasma concentrations.

Linezolid and levofloxacin are WHO-recommended Group A drugs for inclusion in DR-TB treatment regimens (World Health Organization, 2022a). Linezolid is an oxazolidinone antibiotic that is well absorbed upon oral administration (Hashemian et al., 2018), metabolized by cytochrome P450 2J2, 4F2, and 1B1 (Obach, 2022), and eliminated unchanged or as metabolites in urine (Hashemian et al., 2018). Levofloxacin is a broad-spectrum fluoroquinolone antibiotic used against many bacterial diseases (Wimer et al., 1998), including DR-TB (World Health Organization, 2022a). It is rapidly absorbed upon oral administration (Fish & Chow, 1997), and its absorption is affected by food (Fish & Chow, 1997) and chelating agents (FDA & CDER, 2018). Levofloxacin undergoes limited metabolism and is mainly excreted unchanged by the kidneys

through glomerular filtration and transporter mediated tubular secretion (Fish & Chow, 1997; Ikuko et al., 1997). Terizidone is a Group B drug for DR-TB (World Health Organization, 2022a) which is rapidly hydrolysed into cycloserine in the gut (Chirehwa et al., 2020; Zítková & Toušek, 1974). Cycloserine is a D-alanine analogue that interferes with bacterial cell wall synthesis by inhibiting L-alanine racemase and D-alanyl alanine synthetase enzymes (Azam & Jayaram, 2016). It is rapidly absorbed from the gut (Mulubwa & Mugabo, 2019), partly metabolized but mostly eliminated unchanged in urine (Neon Healthcare Ltd, 2023).

Safe use of clofazimine containing regimens requires an understanding of the nature and extent of pharmacokinetic interactions with co-administered DR-TB drugs. The aim of this study was to investigate the pharmacokinetic interactions between clofazimine and isoniazid, linezolid, levofloxacin, and cycloserine in adults with DR-TB.

6.4 Materials and methods

6.4.1 Participants and study treatments. We conducted a non-interventional, prospective cohort study among participants with DR-TB about to start clofazimine-based treatment, at Klerksdorp/Tshepong Hospital in North-West Province, South Africa. The study was approved by Human Research Ethics Committee of the University of Witwatersrand (REF: 171115B) and all participants provided written informed consent.

Newly diagnosed non-pregnant adults with confirmed pulmonary DR-TB, due to start clofazimine-containing treatment were recruited. As clofazimine has a delayed onset of action, the attending doctor assessed whether withholding it in the first two weeks of treatment would unduly harm the patient. If there was such an indication, patients were ineligible for inclusion. Other exclusion criteria were, isoniazid mono-resistance, poor prognosis at the time of

enrolment, bedaquiline or clofazimine treatment in the previous two years, and refusal to test for HIV.

All participants were hospitalised for the first two weeks of treatment, receiving their TB treatment under direct observation, routinely accompanied by a meal. The first pharmacokinetic sampling (visit 1) was done on day 14. Clofazimine was then added to the regimen of all participants and a second pharmacokinetic sampling (visit 2) was done 21 days later (Figure 24). At both visits, blood samples were drawn before, and then 2-, 4-, 6-, 8- and 10-hrs after the observed dose. The daily oral doses for the drugs were as follows: 100 mg for clofazimine, 450/600 mg for high-dose isoniazid, 600 mg for linezolid, 750/1000 mg for levofloxacin, and 750 mg for terizidone.

After collection, blood samples were immediately placed on ice, transferred to an on-site laboratory, and centrifuged at 1500G to separate plasma. The plasma was aliquoted and stored at -80^0C until batched-transfer for analysis at the University of Cape Town's Division of Clinical Pharmacology laboratory.

6.4.2 Drug assays. Visit 2 samples in the first participants were assayed for clofazimine and other drugs were assayed opportunistically depending on participants' prescribed regimens as summarized in Figure S1. Concentrations of pyrazinamide and ethambutol were not determined as they are unlikely to interact with clofazimine (Arbex et al., 2010). Similarly, bedaquiline was not investigated because its long terminal half-life (Khoshnood et al., 2021) and slow accumulation between the two study visits would make it difficult to interpret the data. Plasma concentrations were quantified using previously published validated liquid chromatography-tandem mass spectrometry assays; the LLOQ were 0.00781 mg/L for clofazimine (Abdelwahab,

Wasserman, et al., 2020), 0.105 mg/L for isoniazid (Abdelwahab, Leisegang, et al., 2020), 0.100 mg/L for linezolid (Abdelwahab, Wasserman, et al., 2021), 0.0781 mg/L for levofloxacin (Denti et al., 2018) and 0.313 mg/L for cycloserine (Court et al., 2018), as previously described. More details are presented in **Table 18** of supplementary materials.

6.4.3 NAT2 phenotype. Consent for genetic studies was obtained, and blood samples were collected to determine the NAT2 genotype of participants. Genomic DNA was isolated as previously described (Longmire et al., 1987), and genotyping was performed using sanger sequencing of the *NAT2* gene after amplification using the following primers: 5' ATTAACTGACATTCTTGAGC 3' and 5' GCACATAAGTTGATAATTAG 3'. Acetylator status was subsequently allocated based on the genotype of following four single nucleotide polymorphisms (SNPs): rs1801279 (c.191G>A), rs1801280 (c.341T>C), rs1799930 (c.590G>A), and rs1799931 (c.857G>A) (Gausi et al., 2021; Hein, 2009; Hein & Doll, 2012). Participants were categorized as rapid acetylators if they were homozygous for the common allele of all four SNPs (i.e., GG, TT, GG, GG, respectively). Those who were heterozygous for only one of the 4 SNPs were categorized as intermediate acetylators, and those who were heterozygous for two or more SNPs, or homozygous for the variant allele for any of the SNPs were categorized as slow acetylators (Gausi et al., 2021; McDonagh et al., 2014).

6.4.4 Pharmacokinetic modelling. Nonlinear mixed-effects modelling in the software NONMEM v7.5.1 (Beal, Boeckmann, and Sheiner, 2017) was used to analyse the data of all drugs. PsN v5.2.6, Pirana v3.0.0, and Xpose in RStudio were used to support model development (Keizer et al., 2013).

First, clofazimine exposures in the first 16 participants were evaluated by fitting their visit 2 clofazimine concentrations to a previously published model (Abdelwahab, Wasserman, et al., 2020) without estimation. Thereafter, suitable models were developed to characterize the pharmacokinetics of isoniazid, linezolid, levofloxacin, and cycloserine. One- and two-compartment disposition models with first-order absorption, and either lag or transit compartment absorption were evaluated (Savic et al., 2007). First-order elimination was explored for all drugs and a well-stirred liver model with hepatic extraction was tested for isoniazid (Gausi et al., 2021; Pang & Rowland, 1977).

To account for body size, allometric scaling with total body weight or FFM was evaluated on all clearance and volume parameters with fixed exponents of 0.75 and 1, respectively (Holford & Anderson, 2017). The effect of clofazimine co-administration was explored as a categorical covariate on clearance and bioavailability for all the drugs. Other previously reported covariates like NAT2 acetylator status for isoniazid, known drug interactions, and estimated creatinine clearance (Cockcroft and Gault formula (Cockcroft et al., 1976)) were also explored during the covariate analysis.

Random effects on pharmacokinetic parameters were added at different levels: BSV, BVV, and BOV (Karlsson & Sheiner, 1993), assuming a lognormal distribution. BOV was tested for all absorption parameters considering each dose as a separate occasion, while BVV was tested only on clearance between the two study visits. Residual unexplained variability was modelled by including both proportional and additive components, with the lower bound of the additive component constrained to at least 20% of LLOQ (Denti et al., 2018). Data below the LLOQ were

imputed to LLOQ/2 (47) as in Beal's M6 method (Beal, 2001), and the additive component of their residual error inflated by LLOQ/2 (Denti et al., 2018; Gausi et al., 2021).

Model development was guided by ΔOFV (Mould & Upton, 2013), which was assumed to follow chi-square distribution (for 1 df, ΔOFV>3.84 units was significant at P<0.05), and evaluation of goodness of fit (Figures S2.2.1-3) and individual plots (Karlsson & Savic, 2007; Nguyen et al., 2017). Final model performance was evaluated using visual predictive checks (Holford & Karlsson, 2005; Karlsson & Savic, 2007; Nguyen et al., 2017), and parameter precision was determined using sampling importance resampling (Dosne et al., 2016). Whenever no effect of clofazimine co-administration was found, *a posteriori* stochastic simulation and estimation (SSE) (SSE User Guide, 2018) was performed to estimate the power of our sample size. Briefly, each final model was modified by adding a 30% effect of clofazimine on clearance and used to simulate 1000 replicates of the study dataset. The input model (with effect) and an alternative (without effect) were fitted to the simulated datasets and the ΔOFV between the 2 models was evaluated for significance at α=0.05. The power of the sample size was then derived from the percentage of simulations in which the clofazimine effect was statistically significant.

6.3 Results

Study population. Data were available for 27 adult participants of whom 19 (70%) were men and 23 (85%) were living with HIV. Their median age and weight were 39 years, and 52 kg, respectively (Table 16), and their median estimated glomerular filtration rate (eGFR) was 89.3 mL/min. Visit 2 samples from 16 participants were assayed for clofazimine. All samples from 27 participants were assayed for isoniazid. Linezolid and levofloxacin concentrations were assayed for 21 participants,

and samples from 6 participants were assayed for cycloserine. For isoniazid, 5 (19%), 13 (48%), and 9 (33%) participants were categorized as slow, intermediate, and rapid acetylators, respectively.

Population pharmacokinetic analysis. Clofazimine data were adequately predicted by a previously published three-compartment disposition model (Abdelwahab, Wasserman, et al., 2020), without re-estimating any pharmacokinetic parameter. In keeping with the previous model, exposure reduced with increasing proportion body fat (Figure 20).

The typical parameter estimates for isoniazid, linezolid, and levofloxacin, and their 95% confidence intervals (95% CI) are presented in Table 17. A two-compartment model with first-pass effect through a liver compartment (Gausi et al., 2021) adequately described isoniazid data (Figure 21). Fixing the typical absorption parameters to literature values (Gausi et al., 2021), we estimated an intrinsic clearance of 12.2, 24.9, and 46.7 L/h for slow, intermediate, and rapid acetylators, respectively (change in objective function value [ΔOFV] = -39.0; 2 degrees of freedom [df]; P<0.001). Inclusion of allometric scaling by FFM on all disposition parameters improved the fit (ΔOFV=-1.42). BVV in clearance improved the model (ΔOFV=-14.2, 1 df, P<0.001), but the 10% decrease in clearance we found on visit 2 was not significant (ΔOFV=-3.52, 1 df, P=0.061).

Linezolid data were well described by a 1-compartment model with first-order elimination and absorption through transit compartments (ΔOFV=-108, 2 df, P<0.001) (Figure 22). With allometric scaling by FFM included on disposition parameters (ΔOFV=-4.82), we estimated a typical clearance and volume of 3.04 L/h and 38.7 L, respectively. BVV in clearance improved the model (ΔOFV=-32.4, 1 df, P<0.001) and we observed a non-significant (ΔOFV=-3.7, 1 df, P=0.054) 2%

decrease in clearance on visit 2. Additionally, a 1.6-fold increase in BOV of the absorption parameters of unobserved pre-doses (ΔOFV=-6.2, 1 df, P=0.013) significantly improved the model.

Levofloxacin data were well characterized by a 1-compartment model with first-order elimination and transit compartment absorption (ΔOFV =- 198, 2 df, P<0.001) (Figure 22), and the typical values of clearance and volume were 6.81 L/h and 98.5 L, respectively. Allometric scaling of disposition parameters by FFM improved the model (ΔOFV = -17.6). Renal function improved the fit (ΔOFV = -4.53, 1 df, P = 0.033), predicting a 4.70% (95% CI: 1.58–7.77) increase in levofloxacin clearance for every 10-mL/min increase in creatinine clearance from the median. At visit 2, when clofazimine was given, clearance was 15% (95% CI: 10–28) slower (ΔOFV = -10.7, 1 df, P = 0.001), and consequently the median AUC increased from 140 to 166 mg·h/L (Figure S3). A ~2-fold increase in variability of absorption parameters of the unobserved doses improved the model significantly (ΔOFV = -6.34, 1 df, P = 0.012), and so did BVV on clearance (ΔOFV = -4.3, 1 df, P = 0.038).

For cycloserine, we employed the 1-compartment model with first-order absorption and elimination split into renal and non-renal clearance developed by Chirehwa et al. (Chirehwa et al., 2020). While keeping all other parameters fixed, we re-estimated total clearance to account for differences between our dataset and the original model. This was not significant (ΔOFV = -2.16, 1 df, P = 0.142), and neither was estimating different clearances during the 2 study visits (ΔOFV = -2.21, 2 df, P = 0.331) (Figure 23).

For isoniazid, linezolid and cycloserine, simulations showed that our samples of 27, 21, and 6 participants had 97%, 90%, and 87% power, respectively, to detect a 30% decrease in clearance across the 2 study visits.

6.5 Discussion

This is the first study we are aware of that has assessed the pharmacokinetic interaction between clofazimine and other DR-TB drugs. We found a 19% increase in levofloxacin AUC during visit 2, when clofazimine was added to the DR-TB regimen. However, we found no effect for high-dose isoniazid, linezolid, or terizidone/cycloserine.

Clofazimine exposures in our cohort were in line with predictions by a model developed by Abdelwahab et al. (Abdelwahab, Wasserman, et al., 2020) in a similar population. Using this model, we confirmed the effect of body fat composition on clofazimine disposition by stratifying our data by proportion of body fat and showing that clofazimine plasma exposure reduces with increasing proportion of body fat. This is consistent with clofazimine's known high lipophilicity and extensive fat distribution (Abdelwahab, Wasserman, et al., 2020; Cholo et al., 2017; Stadler et al., 2023).

Our isoniazid model is structurally like the one by Gausi et al. (Gausi et al., 2021). We estimate comparable increases in intrinsic clearance for intermediate and rapid acetylators compared to slow acetylators, consistently with the trimodal pattern of isoniazid acetylation due genetic differences in NAT2 enzyme activity (Boukouvala & Fakis, 2005; Gausi et al., 2021; Klein et al., 2016; Weber & Hein, 1979, 1985). We did not find significant changes in isoniazid pharmacokinetics after addition of clofazimine to the DR-TB regimen. This is not unexpected,

since clofazimine has not been reported to affect NAT2 enzyme activity, the most important factor for isoniazid excretion (Arbex et al., 2010; Klein et al., 2016; Weber & Hein, 1979).

Our linezolid pharmacokinetics results are consistent with previous findings (Abdelwahab, Wasserman, et al., 2021; Resendiz-Galvan et al., 2023), and we found no statistically significant interaction with clofazimine. The absence of a pharmacokinetic interaction between linezolid and clofazimine is not unexpected as linezolid excretion has not been reported to be affected by clofazimine (Hashemian et al., 2018). Notably, we found slower absorption of linezolid than previously reported (Abdelwahab, Wasserman, et al., 2021; Resendiz-Galvan et al., 2023), most likely due to drug intake with a meal (Stalker & Jungbluth, 2003).

Like Canouï et al. and Sidamo et al., (Canouï et al., 2022; Sidamo et al., 2022), a one-compartment model adequately described our levofloxacin data. This differs from the two-compartment model found by Denti et al., and Garcia-Prats et al. (Denti et al., 2018; Garcia-Prats et al., 2019), probably due to different sampling schedules and study population. Our finding of a significant effect of creatinine clearance on levofloxacin clearance is in line with previous reports (Canouï et al., 2022; Fish & Chow, 1997; Wimer et al., 1998). We also found slower absorption of levofloxacin than has been previously reported (Denti et al., 2018; Garcia-Prats et al., 2019; Sidamo et al., 2022), likely due to a food effect (Fish & Chow, 1997; Wimer et al., 1998).

Interestingly, we found a statistically significant 15% reduction in levofloxacin clearance during visit 2 when clofazimine was added to the DR-TB regimen. Although, no precise mechanism has been elucidated for the interaction between levofloxacin and clofazimine, in vitro studies have shown that clofazimine may inhibit P-glycoprotein and BCRP (Te Brake et al., 2016), which may be

involved in the active tubular secretion of levofloxacin in the kidneys (FDA & CDER, 2018; Ikuko et al., 1997). These transporters are located along the apical membrane of kidney tubules (Drozdzik et al., 2021) and were found to efflux quinolone antibiotics into urine (Maeda et al., 2007; Ikuko et al., 1997). Their inhibition, as was found for ciprofloxacin (Landersdorfer et al., 2010), may be the reason behind this observed reduction in levofloxacin clearance when administered with clofazimine. The resulting increase in levofloxacin AUC, however, may not be of great clinical relevance as the exposures largely remained within the range of previous reports (FDA & CDER, 2018; Fish & Chow, 1997; Peloquin et al., 2008, 2018).

For terizidone/cycloserine, the model by Chirehwa et al. (Chirehwa et al., 2020) adequately described our data. The lack of a significant difference in total clearance across study visits, coupled with the fact that cycloserine is mostly cleared unchanged in urine (Chirehwa et al., 2020; Neon Healthcare Ltd, 2023), suggests minimal likelihood of a major pharmacokinetic interaction between cycloserine and clofazimine.

One limitation of our study was the opportunistic nature of sampling during study visits, lacking strict observance of dosing prior to the pharmacokinetic visits and restrictions on food intake following the observed dose. Consequently, there was greater uncertainty in the pre-dose concentrations, which we addressed by allowing for greater variability in absorption parameters of unobserved doses. Similarly, food ingestion predictably led to slower absorption of linezolid and levofloxacin amongst our cohort. However, this had minimal impact on our primary findings, as the clearance parameters closely aligned with previous reports.

The study's observational nature also resulted in a small sample size for terizidone as few participants in our cohort were on the long (terizidone-containing) regimen. We compensated for this by using a fixed literature model and only estimating separate clearance values for the two visits. Although simulations demonstrated acceptable power to rule out a large interaction, the results should be interpreted cautiously because the fixing of all pharmacokinetic parameters in the model maybe an over-simplification.

Secondly, due to budget constraints, fewer participant samples were analyzed for clofazimine. This however, had less consequence for the conclusions we draw about clofazimine as we only aimed to check if exposures in our cohort were in line with previous reports. Similarly, our sampling schedule did not include a 1-hour post dose sample and therefore was not sufficient to describe the rapid absorption of isoniazid. We mitigated this by fixing the typical absorption parameters to those reported by Gausi et al. (Gausi et al., 2021). Finally, because of the long half-life of clofazimine, it was not possible to design a cross-over study. Consequently, we cannot exclude that any differences in clearance between the 2 study visits may be due to factors other than the delayed introduction of clofazimine interaction, like patient clinical improvement.

In conclusion, our data provides reassuring evidence that clofazimine does not cause significant pharmacokinetic interactions with other drugs commonly co-prescribed for DR-TB.

Table 16: Baseline characteristics of participants in the ISA_DRPK study

Characteristic	Drug			
	Clofazimine	**Isoniazid**	**Linezolid / levofloxacin**	**Cycloserine**
Number of participants	16	27	21	6
Number (%) of male participants	10 (63)	19 (70)	13 (62)	4 (67)
Number (%) living with HIV	14 (88)	23 (85)	16 (76)	5 (83)
Median (range) age (yr)	40 (20 – 66)	39 (20 – 62)	39 (27 – 68)	39 (33 – 53)
Median (range) weight (kg)	52 (35 – 66)	53 (37 – 66)	52 (37 – 74)	53.4 (55 – 70)
Median (range) fat-free mass (kg)	39.5 (25.7 – 51.9)	44.2 (26.0 – 56.5)	41.5 (26.0 – 51.6)	42.0 (35.7 – 51.6)
Median (range) height (m)	1.65 (1.30 – 1.76)	1.67 (1.30 – 1.81)	1.64 (1.49 – 1.80)	1.64 (1.56 – 1.79)
Median (range) creatinine clearance (mL/min)[a]		89.3 (35.0 - 143)	81.8 (50.5 - 136)	96.5 (71.4 – 115)
Median dose (range) (mg/kg) [c]	1.90 (1.52 – 2.86)	10.0 (7.35 – 12.1)	11.5 (8.11 – 16.2) / 19.1 (13.5 – 26.3)	13.2 (10.7 – 17.6) [b]
Number (%) of participants with NAT2 acetylator status				
Slow		5 (19)		
Intermediate		13 (48)		
Rapid		9 (33)		

NAT2, N-acetyltransferase-2.

[a] Creatinine clearance was calculated using the Cockcroft and Gault formular (Cockcroft et al., 1976).

[b] The dose of terizidone (cycloserine) was split into 250, 500 mg in the morning and evening respectively.

[c] The weight normalized dose was calculated by dividing total daily dose of the drug by weight of participant.

Table 17: Table of model pharmacokinetic parameter estimates

Parameter	Typical parameter estimates (95% CI [c])		
	Isoniazid	**Linezolid**	**Levofloxacin**
Clearance (L/h) [a]	–	3.04 (2.74 – 3.87)	6.81 (6.05 – 7.63)
Intrinsic clearance (slow acetylators) (L/h) [a]	12.2 (9.53 – 14.5)	–	–
Intrinsic clearance (intermediate acetylators) (L/h) [a]	24.9 (19.0 – 27.0)	–	–
Intrinsic clearance (rapid acetylators) (L/h) [a]	46.7 (37.9 – 56.4)	–	–
Volume of distribution (central compartment) (L) [a]	57 (49.0 – 61.9)	38.7 (37.0 – 43.1)	98.5 (90.3 – 107)
Inter compartmental clearance (L/h)	1.70 (0.806 – 2.27)	–	–
Volume of distribution (peripheral compartment) (L) [a]	42.4 (9.88 – 52.9)	–	–
Bioavailability, F (fraction) [b]	1 (fixed) [d]	1 (fixed)	1 (fixed)
Absorption rate constant, ka (/L)	3.28 (fixed) [e]	1.14 (0.768 – 1.77)	2.05 (1.19 – 3.25)
Mean absorption transit time, MTT (h)	0.122 (fixed) [e]	0.928 (0.713 – 1.36)	1.32 (1.00 – 1.61)
Transit compartments, NN (n)	2.32 (fixed) [e]	12.6 (9.98 – 37.0)	15.7 (9.91 – 27.3)
Hepatic blood flow rate, QH (L/h) [a, f]	72.4 Fixed	–	–
Unbound fraction, fu (%) [f]	95 Fixed	–	–
Scaling factor on BOV for unobserved dose (-fold change) [h]	–	1.60 (1.07 – 2.67)	1.99 (1.40 – 2.92)
Effect of CL_{CR} (+10 mL/min change) on CL (%)	–	–	+4.70 (+1.58 – +7.77)
Effect of clofazimine on clearance (%)	–	–	-14.8 (-23.2 – -5.88)
Additive error (mg/L)	0.021, i.e., 20% LLOQ (fixed)	0.284 (0.142 – 0.596)	0.238 (0.121 – 0.375)
Proportional error (%)	24.4 (21.1 – 28.0)	7.31 (5.36 – 8.59)	4.97 (3.81 – 6.01)
Variability (% CV) [g]			
BSV in clearance	16.2 (8.10 – 26.1)	31.6 (13.2 – 41.5)	18.3 (13.2 – 24.0)
BVV in clearance	18.4 (11.5 – 25.0)	33.3 (25.4 – 49.2)	17.0 (9.69 – 22.0)
BOV in ka	94.3 (4.27 – 101)	104 (74.5 – 127)	118 (88.9 – 156)
BOV in MTT	129 (87.0 – 215)	73.8 (47.4 – 101)	44.4 (31.6 – 56.0)
BOV in F	47.5 (34.3 – 54.6)	12.4 (6.48 – 18.4)	21.5 (16.5 – 27.9)

[a] All clearance and volume parameters for isoniazid, linezolid and levofloxacin were scaled with allometric scaling based on fat-free mass. The values reported here refer to a typical participant with a fat-free mass of 42 kg and total body weight of 52 kg.

[b] Since only oral data was available, we set the typical bioavailability to the reference value of 1 and estimated variability around it.

[c] Values in parentheses are empirical 95% confidence intervals obtained by sampling importance resampling procedure.

[d] For isoniazid, the typical bioavailability reported is pre-hepatic.

[e] The typical values of the absorption parameters (ka, MTT, NN) of isoniazid have been fixed to those reported by Gausi et al. (Gausi et al., 2021).

[f] The isoniazid unbound fraction and hepatic flow rate were fixed to literature values (Gausi et al., 2021; Zhu et al., 1999). The hepatic flow rate reported here is for a typical participant with a fat-free mass 42 kg.

[g] Parameter variability was modeled as either between-subject (BSV), between-occasion (BOV), or between-visit (BVV) variability. Variability was assumed to be log-normally distributed and is reported here as the percent coefficient of variation (%CV) calculated by $\%CV = \sqrt{\omega^2} \times 100$.

[h] This is a multiplicative factor increasing the BOV of absorption parameters for pre-dose concentrations following an unobserved dose.

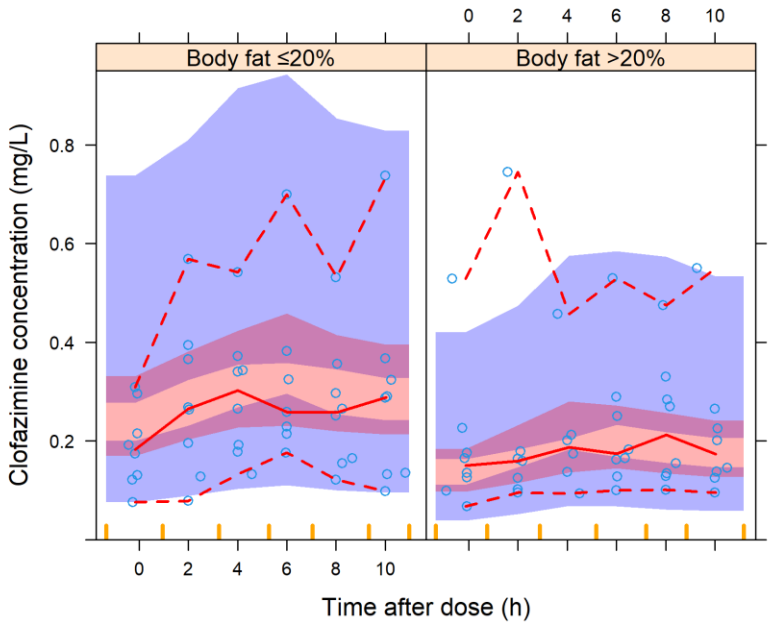

Figure 20: A visual predictive check (VPC) of clofazimine concentration versus time after dose, stratified by proportion of body weight that is fat.

The solid and dashed lines represent the 5th, 50th, and 95th percentiles of the observed data (open circles), while the shaded areas represent the model-predicted 95% confidence intervals for the same percentiles. Of note, this VPC was obtained without re-estimating parameters (maxeval=0 in NONMEM) which is like an external validation. CFZ, clofazimine.

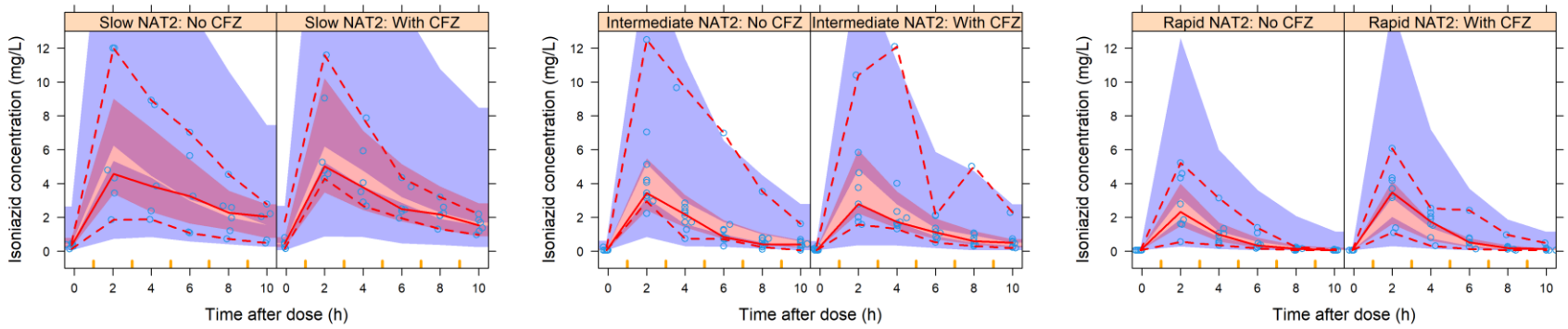

Figure 21: Visual predictive check of the isoniazid concentration versus time after dose, stratified by N-acetyltransferase-2 phenotype and study visit (with vs. without clofazimine).
The model without an effect of clofazimine fit all data on both study visits. The solid and dashed lines represent the 50th, 5th, and 95th percentiles of the observed data (open circles), while the shaded areas represent the model-predicted 95% confidence intervals for the same percentiles. NAT2, N-acetyltransferase activity; CFZ, clofazimine.

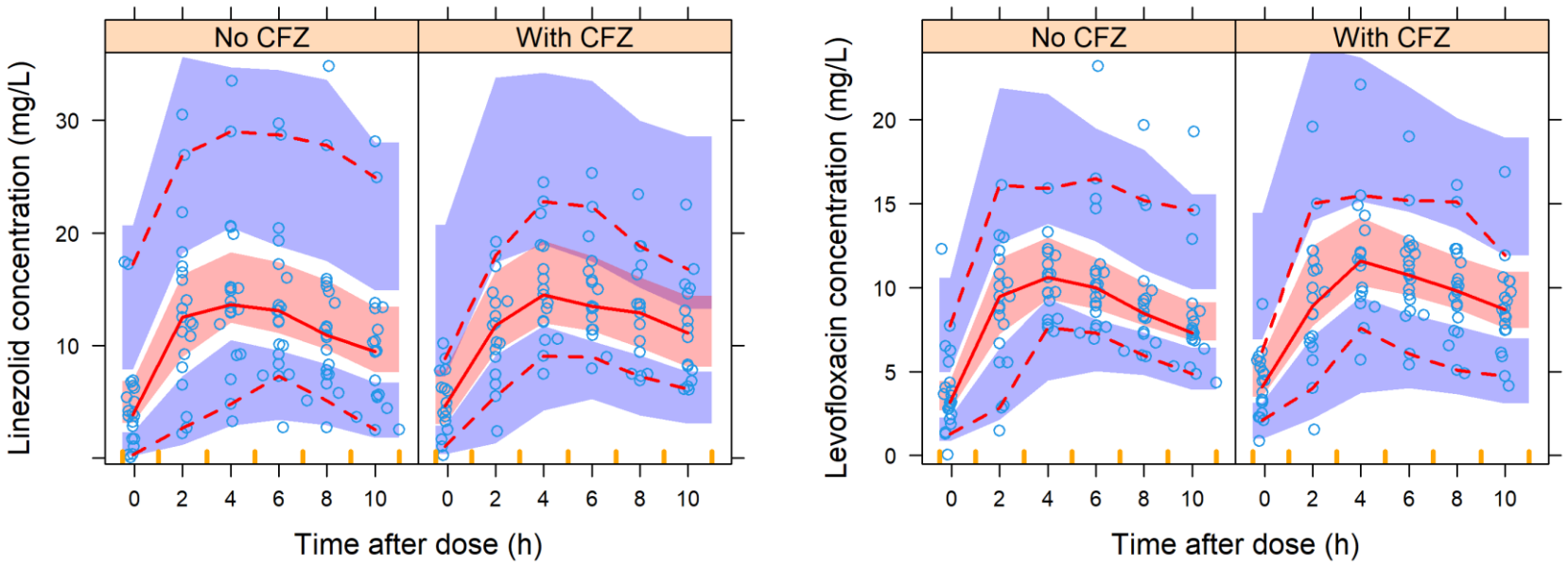

Figure 22: A VPC of the linezolid (left) and levofloxacin (right) concentration versus time after dose.
The solid and dashed lines represent the 50th, 5th, and 95th percentiles of the observed data (open circles), while the shaded areas represent the model-predicted 95% confidence intervals for the same percentiles. CFZ, clofazimine.

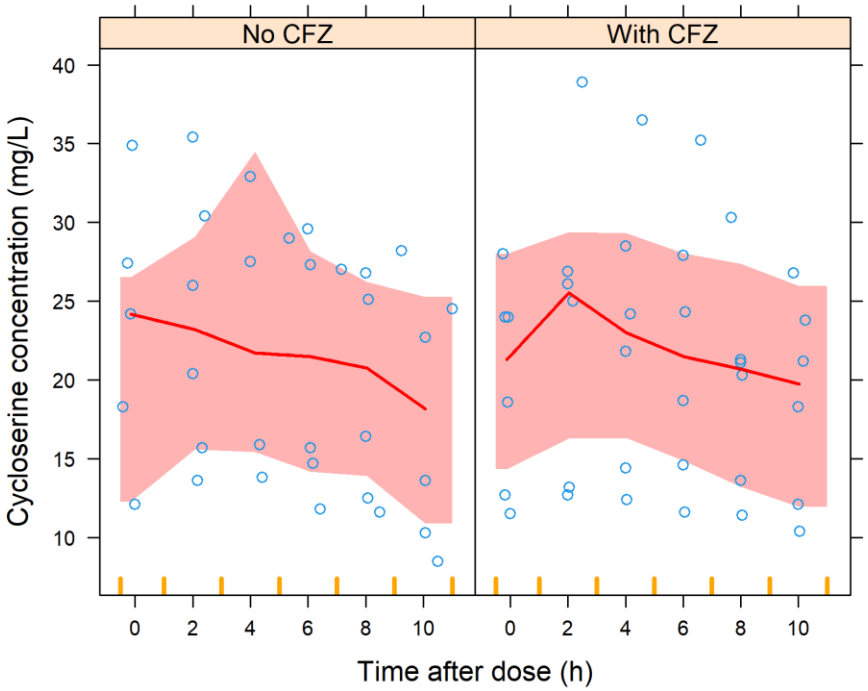

Figure 23: A VPC of cycloserine concentration versus time after dose (stratified by study visit).
The solid line represents the median of the observed data (open circles), while the shaded areas represent the model-predicted 95% confidence interval for median. CFZ, clofazimine.

6.6 Supplementary materials

Methods

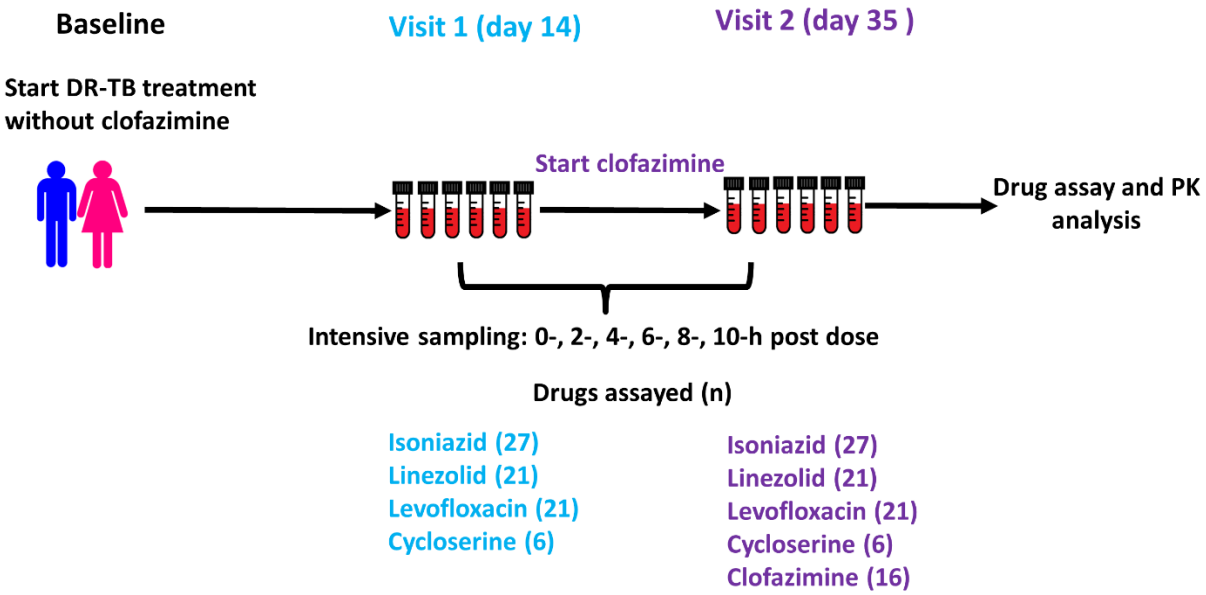

Figure 24: A schematic representation of study protocol showing the different study visits and what drugs were assayed from samples collected during the visits.

Drug assays.

Table 18: A table showing the inter-day accuracy, precision ranges and lower limits of quantification of the pharmacokinetic analysis methods for the assayed drugs.

Drug analyzed	Range of inter-day accuracy (%)	Range of precision (%)	LLOQ (mg/L)
Clofazimine	102 – 103	2.50 – 5.00	0.00781
Isoniazid	95.3 – 100	5.70 – 6.50	0.105
Linezolid	90.1 – 98.1	3.50 – 3.60	0.100
Levofloxacin	94.5 – 98.6	2.40 – 3.00	0.0781
Cycloserine	89.9 – 97.0	3.30 – 15.3	0.313

LLOQ; lower limit of quantification.

Results

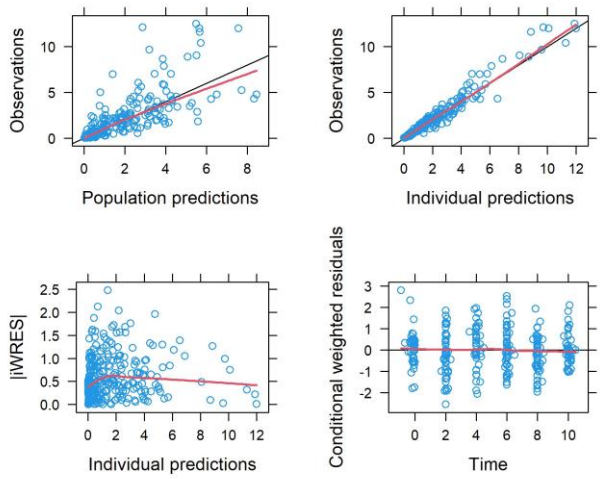

Figure 25: Basic goodness-of-fit plots for the Isoniazid model.
Scatter plot of (top left) observed concentration vs. population predicted values, (**top right**) observed concentration vs. individual predicted values, (**bottom left**) Individual weighted residuals vs. individual predictions and (**bottom right**) Conditional weighted residual vs. time. Each circle represents an individual data point from the respective analysis dataset.

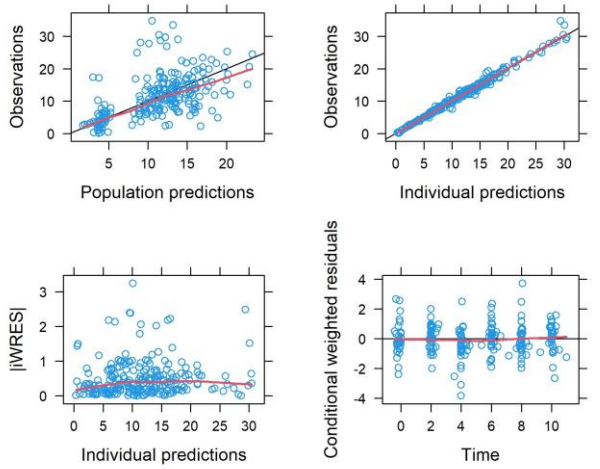

Figure 26: Basic goodness-of-fit plots for the linezolid model
Scatter plot of (**top left**) observed concentration vs. population predicted values, (**top right**) observed concentration vs. individual predicted values, (**bottom left**) Individual weighted residuals vs. individual predictions and (**bottom right**) Conditional weighted residual vs. time. Each circle represents an individual data point from the respective analysis dataset.

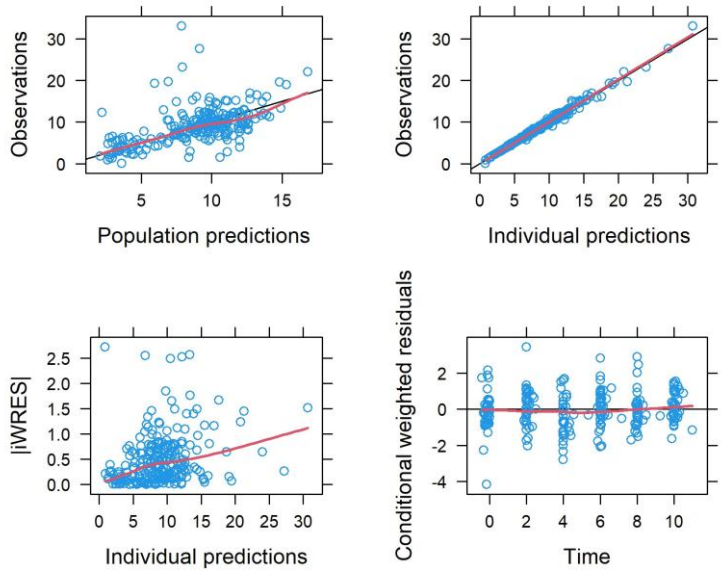

Figure 27: Basic goodness-of-fit plots for the levofloxacin model.
Scatter plot of (**top left**) observed concentration vs. population predicted values, (**top right**) observed concentration vs. individual predicted values, (**bottom left**) Individual weighted residuals vs. individual predictions and (**bottom right**) Conditional weighted residual vs. time. Each circle represents an individual data point from the respective analysis dataset.

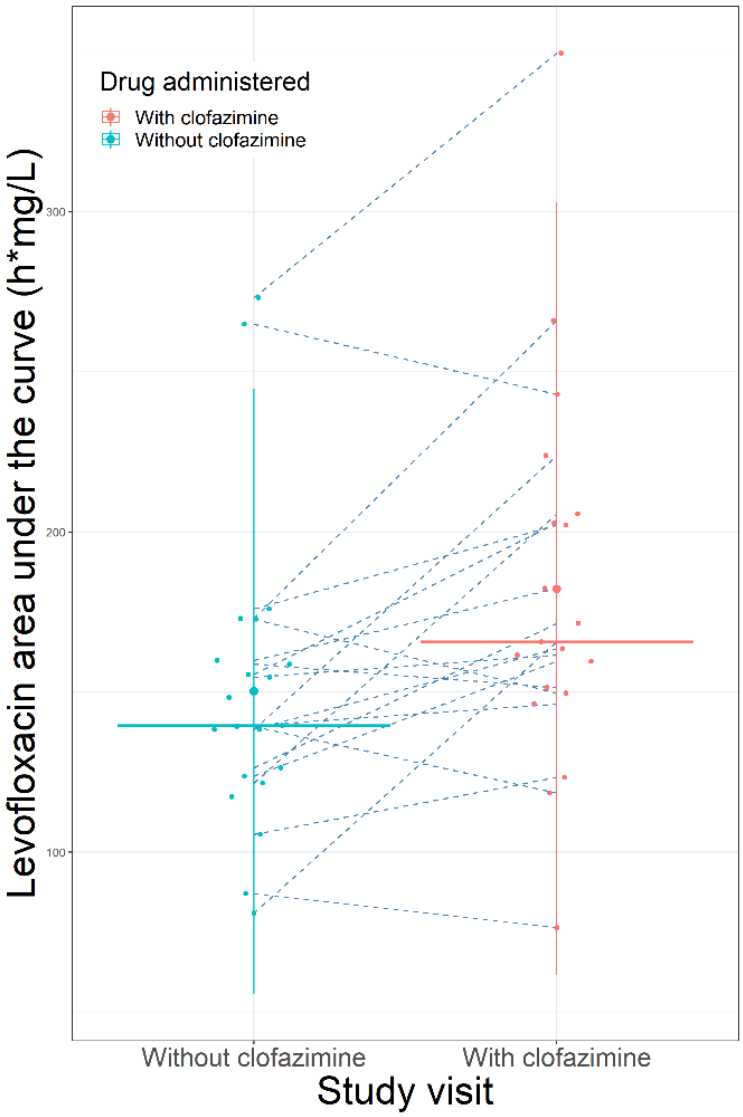

Figure 28: A bee swarm plot showing the change in levofloxacin area under the curve of participants before and after clofazimine was added to their drug-resistant TB regimen. Shrinkage in apparent between occasion bioavailability and between subject variability in clearance were 43% and 12% respectively.

Chapter 7: Discussion and conclusions

7.1 Overall Summary

One of the biggest challenges for drug developers and clinicians is understanding, predicting, and managing DDIs (Dartois & Rubin, 2022). Interactions between ARVs and anti-TB medications are among the most challenging and frequently encountered DDIs (Devanathan et al., 2019b). Optimizing HIV and TB treatment is important to prevent toxicity or sub-therapeutic drug exposure which could lead to the development of drug-resistant strains (Gardner et al., 2009).

The research presented in this thesis compliments existing knowledge on the nature and magnitude of pharmacokinetic DDIs between ARV and TB medications, possibly contributing to their further optimization. In **Chapter 1**, we introduce the challenges of HIV and TB, focusing on their prevalence, disease mechanisms, and current treatment guidelines. We discuss key pharmacokinetic aspects of the drugs covered in this thesis, emphasizing their role in managing TB and HIV, potential DDIs, and drug resistance profiles. Additionally, we highlight important aspects of DR-TB including underlying mechanisms and current treatment strategies. In **Chapter 2**, we describe how the data was collected and introduce PopPK modelling, highlighting how it is better than traditional non-compartmental pharmacokinetic analysis. We also describe the components of a PopPK model and give a general outline of the model developing process. This background supports the analyses and findings discussed in this thesis, showing how PopPK modelling is useful for studying pharmacokinetic DDIs in diverse populations and for predicting unobserved scenarios.

7.1.1 Pharmacokinetics of high-dose rifampicin: significance of the quality of rifampicin-only formulation

Non-linearity in the dose-exposure relationship of rifampicin due to saturation of its clearance has long been established (Chirehwa et al., 2016a). However, as reported in **Chapter 3,** we observed lower exposures of high-dose rifampicin in Ugandan patients, than what saturation of its clearance could predict. We found that this was most likely due to the lower bioavailability of the rifampicin-only top-up formulation than the standard fixed-dose combination. These findings underscore previously reported concerns about the lower quality and bioavailability of some generic TB drug formulations in resource-limited settings, possibly due to shortcomings in regulatory frameworks (McIlleron et al., 2002).

7.1.2 Dolutegravir interaction with standard- and high-dose rifampicin

When dolutegravir is co-administered with rifampicin, its dosing frequency is doubled to counteract the resulting DDI (Dooley et al., 2013, 2020). In **Chapter 4**, we found that increasing the rifampicin dose from 10 to 35 mg/kg further reduced dolutegravir exposure. Our model attributed this reduction to decreased dolutegravir bioavailability rather than increased clearance, likely due to the saturation of rifampicin's induction effect on hepatic enzymes (Acocella, 1978; Xu et al., 2011), in contrast to its continued impact on gut transporters and enzymes (Tsunoda et al., 1999).

Additionally, our simulations showed that doubling the dolutegravir dose was sufficient to restore treatment target attainment when administered with both standard- and high-dose rifampicin. This supports extending of existing dolutegravir dosing recommendations to include high-dose rifampicin.

7.1.2 Drug-drug interaction between dolutegravir and standard- vs. high-dose rifampicin:

When dolutegravir is co-administered with rifampicin, its dosing frequency is doubled to counteract the resulting DDI (Dooley et al., 2013, 2020). In **Chapter 4**, we found that increasing the rifampicin dose from 10 to 35 mg/kg further reduced dolutegravir exposure. Our model attributed this reduction to decreased dolutegravir bioavailability rather than increased clearance, likely due to the saturation of rifampicin's induction effect on hepatic enzymes (Acocella, 1978; Xu et al., 2011), in contrast to its continued impact on gut transporters and enzymes (Tsunoda et al., 1999).

Additionally, our simulations showed that doubling the dolutegravir dose was sufficient to restore treatment target attainment when administered with both standard- and high-dose rifampicin. This supports extending of existing dolutegravir dosing recommendations to include high-dose rifampicin.

7.1.3 Modelling the drug-drug interaction between ritonavir-boosted atazanavir and standard- vs. higher-dose rifampicin in plasma and PBMC

The interaction between rifampicin and PIs like ATV/r poses significant challenges in managing TB in patients on second-line ART. Attempts to co-administer these drugs previously resulted in toxicity (Decloedt et al., 2011; Ebrahim et al., 2020). In **Chapter 5**, we demonstrated that rifampicin reduces atazanavir and ritonavir plasma exposure by increasing their clearance and decreasing their bioavailability. Despite these effects, rifampicin did not appear to affect the rate of drug accumulation or steady-state concentrations of either drug in PBMCs.

Using external atazanavir-only data, we estimated ritonavir's protective effect on atazanavir clearance. Our analysis showed that doubling the dosing frequency of ritonavir, rather than atazanavir, restores atazanavir's exposure when combined with rifampicin. Furthermore,

twice-daily ATV/r dosing met treatment targets when co-administered with rifampicin, offering a potential strategy for managing TB in patients on second-line ART.

7.1.4 Drug-drug interaction between clofazimine and other frequently used agents to treat drug-resistant Tuberculosis: a case for clofazimine-based regimens.

In **Chapter 6**, we explored the potential effect of clofazimine on the pharmacokinetics of other anti-TB drugs. Clofazimine did not significantly impact the pharmacokinetics of isoniazid, linezolid, or cycloserine. However, concurrent clofazimine treatment was associated with a 15% reduction in clearance of levofloxacin, and a non-clinically significant 19% increase in its AUC. This is likely because clofazimine inhibits some kidney transporters (Te Brake et al., 2016) that may be essential for levofloxacin elimination (Ikuko et al., 1997). The absence of significant drug interaction between clofazimine and these drugs is reassuring for its continued use in DR-TB treatment regimens.

7.2 Cross cutting issues and future considerations

7.2.1 Role of clinical treatment targets

Drug concentrations are reliable predictors of treatment outcomes for anti-TB (Pasipanodya et al., 2013) and many ARV medications (Acosta et al., 2000). However, DDIs can alter drug concentrations, making their routine monitoring possibly critical for treatment outcome optimization. Consequently, several pharmacokinetic parameters have been adopted as markers of drug exposure, including the AUC, and the observed minimum (C_{min}) and maximum (C_{max}) concentrations. Values of these parameters have been proposed as targets above which patients are more likely to achieve treatment success. These therapeutic targets are often derived from in vitro experiments or earlier clinical trials and usually fall within a therapeutic window that maximizes the probability of efficacy and minimizes that of toxicity.

Most treatment targets for ARVs are based on C_{min}, which is attractive partly because it requires collecting and evaluating concentrations at one time point. However, C_{min} primarily depends on the drug's terminal half-life, and does not account for other important factors like drug absorption and the accuracy of information regarding the previous dose. Additionally, the C_{min} may be difficult to evaluate for drugs with a short half-life, as their later concentrations may shortly fall below the assays' limit of quantification.

Another challenge is that many treatment targets are adopted from in vitro or early-phase clinical data and based on non-compartmental analyses. Quite often, as is the case with dolutegravir (Van Lunzen et al., 2012), these targets are derived from the means or medians of exposure at the lowest dose found to be efficacious and may lack a mechanistic basis. To establish more sound clinical targets, model-based approaches that describe the pharmacokinetic-pharmacodynamic (PK/PD) relationship of drugs may be more informative. Using PK/PD modelling early in drug development could help set clearer clinical targets for routine use and managing drug interactions. This approach improves dosing, enhances safety and effectiveness, and supports better decisions throughout the drug's development and use.

7.2.2 Integration of PBPK into earlier studies of DDIs

Physiologically based pharmacokinetic (PBPK) modelling is another useful tool for predicting the extent of DDIs and suggesting dose modifications (Foti, 2024). PBPK models divide the human body into anatomically meaningful compartments that integrate properties of body organs, drugs, and demographic characteristics of a population into mathematical equations. These are then used to describe the absorption, distribution, metabolism and excretion of drugs (Montanha et al., 2022), simulate DDIs and identify potential corrective dose adjustments to inform later clinical trials.

PBPK modelling incorporates mechanistic information about the drug pharmacokinetic processes and hence predicts how drug exposure may be affected when they are affected. Consequently, PBPK models are used to simulate unobserved scenarios, including investigations of exposures in less studied populations, like pregnant women and patients with renal or liver disease. However, PBPK modelling requires specialized software and training, and it tends to describe the average individual without accounting for many potential sources of variability. Despite these limitations, PBPK modelling and simulation is a powerful tool for predicting initial doses prior to being administered to patients. When used alongside PopPK modelling, as demonstrated in Chapter 5, PBPK can contribute to an efficient predict-learn-confirm cycle in drug development and clinical research.

7.2.3 Role of quantification of enzyme biomarkers of enzyme induction

Endogenous biomarkers are naturally occurring molecules within the body whose concentrations are influenced by the activity of biological processes, enzymes, or transporters (Chu et al., 2018). Measuring the concentration of these substances in blood or urine offers an alternative way to study the level of activity of associated metabolic processes in vivo. Since most pharmacokinetic DDIs result from modulation of endogenous enzyme and transporter activity, endogenous biomarkers present a promising method for monitoring changes in metabolic process activity. This approach provides an alternative to evaluate DDIs without the need for artificial probes, such as midazolam.

One promising endogenous biomarker is 4β-hydroxycholesterol (4β-OHC), a metabolite of cholesterol formed by CYP3A4/5 (Diczfalusy et al., 2011). Subsequently, it has been demonstrated that treatment with known inducers of CYP3A activity results in increased concentration of 4β-OHC (Bodin et al., 2001). Conversely, known CYP3A inhibitors, like ATV/r, have been observed to reduce its concentration (Josephson et al., 2008). To account for

potential confounders, like inter- and intra-individual variability in cholesterol concentration, the ratio of cholesterol to 4β-OHC could be used to improve its reliability as a biomarker of CYP3A4/5 activity.

Given that CYP3A4/5 is the most abundant enzyme among cytochromes in the liver and gut wall and is responsible for the metabolism of most drugs processed by cytochromes, a specific biomarker like 4β-OHC could serve as a valuable monitor for potential DDIs. However, there are several limitations to consider when using endogenous biomarkers for enzyme induction quantification. First, endogenous biomarkers can be influenced by factors unrelated to drug metabolism, such as diet, disease states, and genetic polymorphisms. These possible confounders may introduce variability and make it challenging to attribute changes in biomarker levels solely to enzyme induction or inhibition. Additionally, the long half-life some biomarkers like 4β-OHC, may delay the detection of changes in enzyme activity, making them less suitable for assessing acute DDIs. Finally, while the ratio of cholesterol to 4β-OHC helps mitigate some variability, it may not fully account for all sources of fluctuation, potentially leading to less precise assessments of changes in enzyme activity. Despite these limitations, the quantification of endogenous biomarkers remains a promising approach for evaluating changes in enzyme/transporter activity and their role in DDIs. Future research and validation studies are needed to address these challenges and refine the use of these biomarkers in clinical and research settings.

7.3 Concluding remarks

Characterization of the nature and magnitude of DDIs amongst HIV and TB medications is crucial for maintaining the safety and efficacy of drug combinations, especially in low-income countries where newer alternatives are not readily available. In this thesis, we demonstrate

how population pharmacokinetic modelling can be used to quantify DDIs and identify what pharmacokinetic parameters are affected. We simulated unobserved dosing scenarios and confirmed the suitability of recommended dose modifications to overcome these DDIs. We also highlighted the importance of properly identified treatment targets and recommend inclusion of modelling techniques in their identification using early clinical trial data.

References

Aarons, L. (1991). Population pharmacokinetics: theory and practice. In J. clin. Pharmac (Vol. 32).

Abadie, R. B., Brown, E. M., Campbell, J. R., Alvarez, I. A., Allampalli, V., Ahmadzadeh, S., Varrassi, G., Shekoohi, S., & Kaye, A. D. (2024). Incidence and Risks of HIV Infection, Medication Options, and Adverse Effects in Accidental Needle Stick Injuries: A Narrative Review. Cureus. https://doi.org/10.7759/cureus.51521

Abdelgawad, N., Tshavhungwe, M., Rohlwink, U., McIlleron, H., Abdelwahab, M. T., Wiesner, L., Castel, S., Steele, C., Enslin, J., Thango, N. S., Denti, P., & Figaji, A. (2023). Population Pharmacokinetic Analysis of Rifampicin in Plasma, Cerebrospinal Fluid, and Brain Extracellular Fluid in South African Children with Tuberculous Meningitis. Antimicrobial Agents and Chemotherapy, 67(3). https://doi.org/10.1128/aac.01474-22

Abdelwahab, M. T., Court, R., Everitt, D., Diacon, A. H., Dawson, R., Svensson, E. M., Maartens, G., & Denti, P. (2021). Effect of Clofazimine Concentration on QT Prolongation in Patients Treated for Tuberculosis. https://journals.asm.org/journal/aac

Abdelwahab, M. T., Leisegang, R., Dooley, K. E., Mathad, J. S., Wiesner, L., Mcilleron, H., Martinson, N., Waja, Z., Letutu, M., Chaisson, R. E., & Denti, P. (2020). Population Pharmacokinetics of Isoniazid, Pyrazinamide, and Ethambutol in Pregnant South African Women with Tuberculosis and HIV. https://journals.asm.org/journal/aac

Abdelwahab, M. T., Wasserman, S., Brust, J. C. M., Dheda, K., Wiesner, L., Gandhi, N. R., Warren, R. M., Sirgel, F. A., Meintjes, G., Maartens, G., & Denti, P. (2021). Linezolid Population Pharmacokinetics in South African Adults with Drug-Resistant Tuberculosis. https://doi.org/10.1128/AAC

Abdelwahab, M. T., Wasserman, S., Brust, J. C. M., Gandhi, N. R., Meintjes, G., Everitt, D., Diacon, A., Dawson, R., Wiesner, L., Svensson, E. M., Maartens, G., & Denti, P. (2020). Clofazimine pharmacokinetics in patients with TB: Dosing implications. Journal of Antimicrobial Chemotherapy, 75(11), 3269–3277. https://doi.org/10.1093/jac/dkaa310

Acocella, G. (1978). Clinical Pharmacokinetics of Rifampicin. Clinical Pharmacokinetics, 3(2), 108–127. https://doi.org/10.2165/00003088-197803020-00002

Acosta, E. P., Kakuda, T. N., Brundage, R. C., Anderson, P. L., & Fletcher, C. V. (2000). Pharmacodynamics of Human Immunodeficiency Virus Type 1 Protease Inhibitors General Pharmacodynamic Principles. In Clinical Infectious Diseases (Vol. 30, Issue 2). https://academic.oup.com/cid/article/30/Supplement_2/S151/372252

Acosta, E. P., Kendall, M. A., Gerber, J. G., Alston-Smith, B., Koletar, S. L., Zolopa, A. R., Agarwala, S., Child, M., Bertz, R., Hosey, L., & Haas, D. W. (2007). Effect of concomitantly administered rifampin on the pharmacokinetics and safety of atazanavir administered twice daily. Antimicrobial Agents and Chemotherapy, 51(9), 3104–3110. https://doi.org/10.1128/AAC.00341-07

Alghamdi, W. A., Al-Shaer, M. H., & Peloquin, C. A. (2018). Protein Binding of First-Line Antituberculosis Drugs. https://doi.org/10

Alvarellos, M., Guillemette, C., Altman, R. B., & Klein, T. E. (2018). PharmGKB summary: Atazanavir pathway, pharmacokinetics/pharmacodynamics. Pharmacogenetics and Genomics, 28(5), 127–137. https://doi.org/10.1097/FPC.0000000000000331

Amidon Gordon L., Lennernas Hans, Shah Vinod P., & Crison John R. (1995). A Theoretical Basis for a Biopharmaceutical Drug Classification: The correlation of in Vitro drug product dissolution and in vivo bioavailability. Pharmaceutical Research, 12(3), 413–420. https://doi.org/10.1023/a:1016212804288.

Anderson B.J, & Holford N.H.G. (2008). Mechanism-Based Concepts of Size and Maturity in Pharmacokinetics. Annual Review of Pharmacology and Toxicology, 48(1), 303–332. https://doi.org/10.1146/annurev.pharmtox.48.113006.094708

Andy Bunn, M. K. (2008). An Introduction to dplR. Industrial and Commercial Training, 10(1), 11–18.

Arbex, M. A., Varella, M. de C. L., Siqueira, H. R. de, & Mello, F. A. F. de. (2010). Antituberculosis drugs: drug interactions, adverse effects, and use in special situations. Part 1: first-line drugs. Jornal Brasileiro de Pneumologia : Publicacao Oficial Da Sociedade Brasileira de Pneumologia e Tisilogia, 36(5), 626–640. https://doi.org/10.1590/s1806-37132010000500016

Argyrou, A., Vetting, M. W., & Blanchard, J. S. (2007). New insight into the mechanism of action of and resistance to isoniazid: Interaction of Mycobacterium tuberculosis enoyl-ACP reductase with INH-NADP. Journal of the American Chemical Society, 129(31), 9582–9583. https://doi.org/10.1021/ja073160k

Armstrong, J. A., & Hart, D. (1971). Response of cultured macrophages to Mycobacterium Tuberculosis, with observations on fusion of lysosomes with phagosomes. Journal of Experimental Medicine, 134(3), 713–740. https://doi.org/10.1084/jem.134.3.713

Azam, M. A., & Jayaram, U. (2016). Inhibitors of alanine racemase enzyme: a review. Journal of Enzyme Inhibition and Medicinal Chemistry, 31(4), 517–526. https://doi.org/10.3109/14756366.2015.1050010

Back, D., Gibbons, S., & Khoo, S. (2006). An Update on Therapeutic Drug Monitoring for Antiretroviral Drugs. Therapeutic Drug Monitoring, 28(3), 468–473. https://doi.org/10.1097/01.ftd.0000211825.57984.41

Barcelo, C., Aouri, M., Courlet, P., Guidi, M., Braun, D. L., Gü nthard, H. F., Piso, R. J., Cavassini, M., Buclin, T., Decosterd, L. A., & Csajka, C. (2019). Population pharmacokinetics of dolutegravir: influence of drug-drug interactions in a real-life setting. Journal of Antimicrobial Chemotherapy, 74(9), 2690–2697. https://doi.org/10.1093/jac/dkz217

Barrett, J. S., Fossler, M. J., Cadieu, K. D., & Gastonguay, M. R. (2008). Pharmacometrics: A Multidisciplinary Field to Facilitate Critical Thinking in Drug Development and Translational Research Settings. The Journal of Clinical Pharmacology, 48(5), 632–649. https://doi.org/10.1177/0091270008315318

Beal, S., Boeckmann, A. and Sheiner, L. (1989-2009). (2017). NONMEM User Guides. Icon Development Solutions, Elliot City. Manajemen Asuhan Kebidanan Pada Bayi Dengan Caput Succedaneum Di Rsud Syekh Yusuf Gowa Tahun, 4(December), 9–15.

Beal, S. L. (2001). Ways to Fit a PK Model with Some Data Below the Quantification Limit. Journal of Pharmacokinetics and Pharmacodynamics, 28(5).

Bennetto-Hood, C., Tabolt, G., Savina, P., & Acosta, E. P. (2014). A Sensitive HPLC-MS/MS Method for the Determination of Dolutegravir in Human Plasma. Journal of Chromatography. B, Analytical Technologies in the Biomedical and Life Sciences, 0, 225. https://doi.org/10.1016/J.JCHROMB.2013.11.054

Bhatt, N. B., Barau, C., Amin, A., Baudin, E., Meggi, B., Silva, C., Furlan, V., Grinsztejn, B., Barrail-Tran, A., Bonnet, M., & Taburet, A. M. (2014). Pharmacokinetics of rifampin and isoniazid in tuberculosis-hivcoinfected patients receiving nevirapine-or efavirenz-based antiretroviral treatment. Antimicrobial Agents and Chemotherapy, 58(6), 3182–3190. https://doi.org/10.1128/AAC.02379-13

Bodin, K., Bretillon, L., Aden, Y., Bertilsson, L., Broomé, U., Einarsson, C., & Diczfalusy, U. (2001). Antiepileptic drugs increase plasma levels of 4β-hydroxycholesterol in humans. Evidence for involvement of cytochrome P450 3A4. Journal of Biological Chemistry, 276(42), 38685–38689. https://doi.org/10.1074/jbc.M105127200

Boeree, M. J., Diacon, A. H., Dawson, R., Narunsky, K., Du Bois, J., Venter, A., Phillips, P. P. J., Gillespie, S. H., McHugh, T. D., Hoelscher, M., Heinrich, N., Rehal, S., Van Soolingen, D., Van Ingen, J., Magis-Escurra, C., Burger, D., Van Balen, G. P., & Aarnoutse, R. E. (2015). A dose-ranging trial to optimize the dose of rifampin in the treatment of tuberculosis. American Journal of Respiratory and Critical Care Medicine, 191(9), 1058–1065. https://doi.org/10.1164/rccm.201407-1264OC

Boeree, M. J., Heinrich, N., Aarnoutse, R., Diacon, A. H., Dawson, R., Rehal, S., Kibiki, G. S., Churchyard, G., Sanne, I., Ntinginya, N. E., Minja, L. T., Hunt, R. D., Charalambous, S., Hanekom, M., Semvua, H. H., Mpagama, S. G., Manyama, C., Mtafya, B., Reither, K., … Hoelscher, M. (2017b). High-dose rifampicin, moxifloxacin, and SQ109 for treating tuberculosis: a multi-arm, multi-stage randomised controlled trial. The Lancet Infectious Diseases, 17(1), 39–49. https://doi.org/10.1016/S1473-3099(16)30274-2

Bolt, H. M. (2004). Rifampicin, A Keystone Inducer of Drug Metabolism: From Herbert Remmer's Pioneering Ideas to Modern Concepts. Drug Metabolism Reviews, 36(3–4), 497–509. https://doi.org/10.1081/DMR-200033432

Bonnett, L. J., Ken-Dror, G., Koh, G. C. K. W., & Davies, G. R. (2017a). Comparing the Efficacy of Drug Regimens for Pulmonary Tuberculosis: Meta-analysis of Endpoints in Early-Phase Clinical Trials. Clinical Infectious Diseases, 65(1), 46–54. https://doi.org/10.1093/cid/cix247

Bonnett, L. J., Ken-Dror, G., Koh, G. C. K. W., & Davies, G. R. (2017b). Comparing the Efficacy of Drug Regimens for Pulmonary Tuberculosis: Meta-analysis of Endpoints in Early-Phase Clinical Trials. Clinical Infectious Diseases, 65(1), 46–54. https://doi.org/10.1093/cid/cix247

Boukouvala, S., & Fakis, G. (2005). Arylamine N-acetyltransferases: What we learn from genes and genomes. In Drug Metabolism Reviews (Vol. 37, Issue 3, pp. 511–564). https://doi.org/10.1080/03602530500251204

Brunton & Bjorn. (2022). Goodman and Gilman's The Pharmacological Basis of Therapeutics, 14th Edition. https://accessmedicine.mhmedical.com/content.aspx?bookid=3191&sectionid=265824603

Bun Ng, T., Kumar Dutta, N., Kumar, A., Hu, Y., Liu, A., Ortega-Muro, F., Alameda-Martin, L., Mitchison, D., & Coates, A. (2015). High-dose rifampicin kills persisters, shortens treatment duration, and reduces relapse rate in vitro and in vivo. https://doi.org/10.3389/fmicb.2015.00641

Burton, M. E. (1986). Introduction to Pharmacokinetics. Journal of Pharmacy Technology, 2(2), 67–73. https://doi.org/10.1177/875512258600200207

Busti, A. J., Hall, R. G., & Margolis, D. M. (2004). Atazanavir for the treatment of human immunodeficiency virus infection. In Pharmacotherapy (Vol. 24, Issue 12 I, pp. 1732–1747). https://doi.org/10.1592/phco.24.17.1732.52347

Cada, D., Levien, T., & Baker, D. (2014). Dolutegravir. Hospital Pharmacy, 49(2), 184–195. https://doi.org/10.1310/hpj4902-184

Canouï, E., Kerneis, S., Morand, P., Enser, M., Gauzit, R., Eyrolle, L., Leclerc, P., Contejean, A., Zheng, Y., Anract, P., Hirt, D., Treluyer, J. M., Bouazza, N., & Benaboud, S. (2022). Oral levofloxacin: population pharmacokinetics model and pharmacodynamics study in bone and joint infections. Journal of Antimicrobial Chemotherapy, 77(5), 1344–1352. https://doi.org/10.1093/jac/dkac031

Castellino, S., Moss, L., Wagner, D., Borland, J., Song, I., Chen, S., Lou, Y., Min, S. S., Goljer, I., Culp, A., Piscitelli, S. C., Savina A Glaxosmithkline, P. M., Park, R. T., Carolina, N., & Glaxosmithkline, ; (2013). Metabolism, Excretion, and Mass Balance of the HIV-1 Integrase Inhibitor Dolutegravir in Humans. https://doi.org/10.1128/AAC.00292-13

Chen, J., & Raymond, K. (2006). Roles of rifampicin in drug-drug interactions: underlying molecular mechanisms involving the nuclear pregnane X receptor. Annals of Clinical Microbiology and Antimicrobials, 5(1), 3. https://doi.org/10.1186/1476-0711-5-3

Chen, J., Zhang, S., Cui, P., Shi, W., Zhang, W., & Zhang, Y. (2017). Identification of novel mutations associated with cycloserine resistance in Mycobacterium tuberculosis. Journal of Antimicrobial Chemotherapy, 72(12), 3272–3276. https://doi.org/10.1093/jac/dkx316

Chen, S., St Jean, P., Borland, J., Song, I., Yeo, A. J., Piscitelli, S., & Rubio, J. P. (2014). Evaluation of the effect of UGT1A1 polymorphisms on dolutegravir pharmacokinetics. Pharmacogenomics, 15(1), 9–16. https://doi.org/10.2217/pgs.13.190

Chen, Z., Su, D., Ai, L., Jiang, X., Wu, C., Xu, Q., Wang, X., & Fan, Z. (2014). UGT1A1 sequence variants associated with risk of adult hyperbilirubinemia: A quantitative analysis. Gene, 552(1), 32–38. https://doi.org/10.1016/J.GENE.2014.09.009

Cherkaoui-Rbati, M. H., Paine, S. W., Littlewood, P., & Rauch, C. (2017). A quantitative systems pharmacology approach, incorporating a novel liver model, for predicting pharmacokinetic drug-drug interactions. PLoS ONE, 12(9). https://doi.org/10.1371/journal.pone.0183794

Chirehwa, M. T., Court, R., Kock, M. De, Wiesner, L., De Vries, N., Harding, J., Gumbo, T., Maartens, G., Warren, R., Denti, P., & Mcilleron, H. (2020). Population Pharmacokinetics of Cycloserine and Pharmacokinetic/Pharmacodynamic Target Attainment in Multidrug-Resistant Tuberculosis Patients Dosed with Terizidone. https://doi.org/10.1128/AAC

Chirehwa, M. T., Rustomjee, R., Mthiyane, T., Onyebujoh, P., Smith, P., McIlleron, H., & Denti, P. (2016a). Model-based evaluation of higher doses of rifampin using a semimechanistic model incorporating autoinduction and saturation of hepatic extraction. Antimicrobial Agents and Chemotherapy, 60(1), 487–494. https://doi.org/10.1128/AAC.01830-15

Cholo, M. C., Mothiba, M. T., Fourie, B., & Anderson, R. (2017). Mechanisms of action and therapeutic efficacies of the lipophilic antimycobacterial agents clofazimine and bedaquiline. Journal of Antimicrobial Chemotherapy, 72(2), 338–353. https://doi.org/10.1093/jac/dkw426

Chu, X., Liao, M., Shen, H., Yoshida, K., Zur, A. A., Arya, V., Galetin, A., Giacomini, K. M., Hanna, I., Kusuhara, H., Lai, Y., Rodrigues, D., Sugiyama, Y., Zamek-Gliszczynski, M. J., & Zhang, L. (2018). Clinical Probes and Endogenous Biomarkers as Substrates for Transporter Drug-Drug Interaction Evaluation: Perspectives From the International Transporter Consortium. Clinical Pharmacology and Therapeutics, 104(5), 836–864. https://doi.org/10.1002/cpt.1216

Cockcroft, D. W., Henry, M., & Ault, G. (1976). Prediction of Creatinine Clearance from Serum Creatinine1. In Nephron (Vol. 1).

Cohen, M. S., Chen, Y. Q., McCauley, M., Gamble, T., Hosseinipour, M. C., Kumarasamy, N., Hakim, J. G., Kumwenda, J., Grinsztejn, B., Pilotto, J. H. S., Godbole, S. V., Mehendale, S., Chariyalertsak, S., Santos, B. R., Mayer, K. H., Hoffman, I. F., Eshleman, S. H., Piwowar-Manning, E., Wang, L., … Fleming, T. R. (2011). Prevention of HIV-1 Infection with Early Antiretroviral Therapy. New England Journal of Medicine, 365(6), 493–505. https://doi.org/10.1056/nejmoa1105243

Cohen, Mathiasen VD, Schön T, & Wejse C. (2019). The global prevalence of latent tuberculosis: a systematic review and meta-analysis. European Respiratory Journal, 54(3), 1900655. https://doi.org/10.1183/13993003.00655-2019

Cottrell, M. L., Hadzic, T., & Kashuba, A. D. M. (2013). Clinical pharmacokinetic, pharmacodynamic and drug-interaction profile of the integrase inhibitor dolutegravir. Clinical Pharmacokinetics, 52(11), 981–994. https://doi.org/10.1007/s40262-013-0093-2

Court, R., Wiesner, L., Stewart, A., De Vries, N., Harding, J., Maartens, G., Gumbo, T., & McIlleron, H. (2018). Steady state pharmacokinetics of cycloserine in patients on terizidone for multidrug-resistant tuberculosis. International Journal of Tuberculosis and Lung Disease, 22(1), 30–33. https://doi.org/10.5588/ijtld.17.0475

Crawley, M. J. (2010). The R Book. In The R Book. https://doi.org/10.1016/b978-0-12-374507-1.00050-9

Cresswell, F. V, Meya, D. B., Kagimu, E., Grint, D., te Brake, L., Kasibante, J., Martyn, E., Rutakingirwa, M., Quinn, C. M., Okirwoth, M., Tugume, L., Ssembambulidde, K., Musubire, A. K., Bangdiwala, A. S., Buzibye, A., Muzoora, C., Svensson, E. M., Aarnoutse, R., Boulware, D. R., & Elliott, A. M. (2021). High-Dose Oral and Intravenous Rifampicin for the Treatment of Tuberculous Meningitis in Predominantly Human Immunodeficiency Virus (HIV)-Positive Ugandan Adults: A Phase II Open-Label Randomized Controlled Trial. Clinical Infectious Diseases, 73(5), 876–884. https://doi.org/10.1093/cid/ciab162

Dartois, V. A., & Rubin, E. J. (2022). Anti-tuberculosis treatment strategies and drug development: challenges and priorities. In Nature Reviews Microbiology (Vol. 20, Issue 11, pp. 685–701). Nature Research. https://doi.org/10.1038/s41579-022-00731-y

D'Avolio, A., Simiele, M., Calcagno, A., Siccardi, M., Larovere, G., Agati, S., Baietto, L., Cusato, J., Tettoni, M., Sciandra, M., Trentini, L., Di Perri, G., & Bonora, S. (2013). Intracellular accumulation of ritonavir combined with different protease inhibitors and correlations between concentrations in plasma and peripheral blood mononuclear cells. Journal of Antimicrobial Chemotherapy, 68(4), 907–910. https://doi.org/10.1093/jac/dks484

De Nicolò, A., Ianniello, A., Ferrara, M., Avataneo, V., Cusato, J., Antonucci, M., De Vivo, E., Waitt, C., Calcagno, A., Trentalange, A., Muccioli, G., Bonora, S., Perri, G. Di, & D'avolio, A. (2020). pharmaceuticals Validation of a UHPLC-MS/MS Method to Quantify Twelve Antiretroviral Drugs within Peripheral Blood Mononuclear Cells from People Living with HIV. Pharmaceuticals, 14(1), 12. https://doi.org/10.3390/ph1401

De Nicolò, A., Palermiti, A., Dispinseri, S., Marchetti, G., Trunfio, M., De Vivo, E., D'Avolio, A., Muscatello, A., Gori, A., Rusconi, S., Bruzzesi, E., Gabrieli, A., Bernasconi, D. P., Bandera, A., Nozza, S., & Calcagno, A. (2024). Plasma, intracellular and lymph node antiretroviral concentrations and HIV DNA change during primary HIV infection: Results from the INACTION P25 study. International Journal of Antimicrobial Agents, 64(2), 107200. https://doi.org/10.1016/j.ijantimicag.2024.107200

De Nicolò, A., Palermiti, A., Mugerwa, H., Nakabuye, S., Namusanje, J., Kobusingye, J., Lamorde, M., Kengo, A., Denti, P., Gausi, K., Marteens, G., Mcilleron, H., Wiesner, L., Khoo, S., Waitt, C., & D'avolio, A. (n.d.). Intracellular penetration of Atazanavir, Ritonavir and Dolutegravir with concomitant Rifampicin: a dose escalation study (Submitted manuscript). https://clinicaltrials.gov/ct2/show/NCT04121195

DeAnda, F., Hightower, K. E., Nolte, R. T., Hattori, K., Yoshinaga, T., Kawasuji, T., & Underwood, M. R. (2013). Dolutegravir Interactions with HIV-1 Integrase-DNA: Structural Rationale for Drug Resistance and Dissociation Kinetics. PLoS ONE, 8(10). https://doi.org/10.1371/journal.pone.0077448

Decloedt, E. H., McIlleron, H., Smith, P., Merry, C., Orrell, C., & Maartens, G. (2011). Pharmacokinetics of lopinavir in HIV-infected adults receiving rifampin with adjusted doses

of lopinavir-ritonavir tablets. Antimicrobial Agents and Chemotherapy, 55(7), 3195–3200. https://doi.org/10.1128/AAC.01598-10

Deeks. (2014). Cobicistat: A review of its use as a pharmacokinetic enhancer of atazanavir and darunavir in patients with HIV-1 infection. Drugs, 74(2), 195–206. https://doi.org/10.1007/s40265-013-0160-x

Deeks, S. G., Overbaugh, J., Phillips, A., & Buchbinder, S. (2015). HIV infection. Nature Reviews Disease Primers, 1. https://doi.org/10.1038/nrdp.2015.35

Delattre, M., Lavielle, M., Poursat, M.-A., & Poursat, M.-A. A. (2014). A note on BIC in mixed-effects models. Electronic Journal of Statistics, 8, 456–475. https://doi.org/10.1214/14-EJS890ï

Denti, P., Garcia-Prats, A. J., Draper, H. R., Wiesner, L., Winckler, J., Thee, S., Dooley, K. E., Savic, R. M., McIlleron, H. M., Simon Schaaf, H., & Hesseling, A. C. (2018). Levofloxacin population pharmacokinetics in south african children treated for multidrug-resistant tuberculosis. Antimicrobial Agents and Chemotherapy, 62(2). https://doi.org/10.1128/AAC.01521-17

Denti, P., Martinson, N., Cohn, S., Mashabela, F., Hoffmann, J., Msandiwa, R., Castel, S., Wiesner, L., Chaisson, R. E., McIlleron, H., & Dooley, K. E. (2016). Population Pharmacokinetics of Rifampin in Pregnant Women with Tuberculosis and HIV Coinfection in Soweto, South Africa. Antimicrobial Agents and Chemotherapy, 60(3), 1234–1241. https://doi.org/10.1128/AAC.02051-15

Denti, P., Wasmann, R. E., Francis, J., McIlleron, H., Sugandhi, N., Cressey, T. R., Mirochnick, M., Capparelli, E. V., & Penazzato, M. (2022). One dose does not fit all: revising the WHO paediatric dosing tool to include the non-linear effect of body size and maturation. In The Lancet Child and Adolescent Health (Vol. 6, Issue 1, pp. 9–10). Elsevier B.V. https://doi.org/10.1016/S2352-4642(21)00302-3

Denti, P., Wasmann, R. E., van Rie, A., Winckler, J., Bekker, A., Rabie, H., Hesseling, A. C., van der Laan, L. E., Gonzalez-Martinez, C., Zar, H. J., Davies, G., Wiesner, L., Svensson, E. M., & McIlleron, H. M. (2022). Optimizing Dosing and Fixed-Dose Combinations of Rifampicin, Isoniazid, and Pyrazinamide in Pediatric Patients With Tuberculosis: A Prospective Population Pharmacokinetic Study. Clinical Infectious Diseases : An Official Publication of the Infectious Diseases Society of America, 75(1), 141–151. https://doi.org/10.1093/cid/ciab908

Department of Health and Human Services. (2018). Panel on Antiretroviral Guidelines for Adults and Adolescents. Guidelines for the Use of Antiretroviral Agents in Adults and Adolescents with HIV. Department of Health and Human Services, USA, 40(Build 29393). https://aidsinfo.nih.gov/contentfiles/lvguidelines/adultandadolescentgl.pdf

Department of Health, & RSA. (2019). MANAGEMENT OF RIFAMPICIN-RESISTANT TUBERCULOSIS: A Clinical Reference Guide.

Desai, M., Iyer, G., & Dikshit, R. K. (2012). Antiretroviral drugs: Critical issues and recent advances. Indian Journal of Pharmacology, 44(3), 288–298. https://doi.org/10.4103/0253-7613.96296

Devanathan, A. S., Anderson, D. J. C., Cottrell, M. L., Burgunder, E. M., Saunders, A. C., & Kashuba, A. D. M. (2019a). Contemporary Drug–Drug Interactions in HIV Treatment. Clinical Pharmacology and Therapeutics, 105(6), 1362–1377. https://doi.org/10.1002/cpt.1393

Devanathan, A. S., Anderson, D. J. C., Cottrell, M. L., Burgunder, E. M., Saunders, A. C., & Kashuba, A. D. M. (2019b). Contemporary Drug-Drug Interactions in HIV Treatment. CLINICAL PHARMACOLOGY & THERAPEUTICS | VOLUME, 105(6). https://doi.org/10.1002/cpt.1393

Dewolf, F., Lukashov, V. V, Danner, S. A., Goudsmit, J., Lange, J. M. A., Gallicano, ; K, Sahai, J., Kravcik, S., Seguin, J., Bristow, N., & Cameron, D. W. (2000). BMS-232632, a Highly Potent Human Immunodeficiency Virus Protease Inhibitor That Can Be Used in Combination with Other Available Antiretroviral Agents (Vol. 44, Issue 8). https://journals.asm.org/journal/aac

Dickinson, L., Walimbwa, S., Singh, Y., Kaboggoza, J., Kintu, K., Sihlangu, M., Coombs, J. A., Malaba, T. R., Byamugisha, J., Pertinez, H., Amara, A., Gini, J., Else, L., Heiberg, C., Hodel, E. M., Reynolds, H., Myer, L., Waitt, C., Khoo, S., … Ssempija, E. (2021a). Infant Exposure to Dolutegravir through Placental and Breast Milk Transfer: A Population Pharmacokinetic Analysis of DolPHIN-1. Clinical Infectious Diseases, 73(5), E1200–E1207. https://doi.org/10.1093/cid/ciaa1861

Dickinson, L., Walimbwa, S., Singh, Y., Kaboggoza, J., Kintu, K., Sihlangu, M., Coombs, J. A., Malaba, T. R., Byamugisha, J., Pertinez, H., Amara, A., Gini, J., Else, L., Heiberg, C., Hodel, E. M., Reynolds, H., Myer, L., Waitt, C., Khoo, S., … Ssempija, E. (2021b). Infant Exposure to Dolutegravir through Placental and Breast Milk Transfer: A Population Pharmacokinetic Analysis of DolPHIN-1. Clinical Infectious Diseases, 73(5), E1200–E1207. https://doi.org/10.1093/cid/ciaa1861

Dickinson, & Mitchison. (1981). Experimental models to explain the high sterilizing activity of rifampin in the chemotherapy of tuberculosis. American Review of Respiratory Disease, 123(4), 367–371. https://doi.org/10.1164/arrd.1981.123.4.367

Diczfalusy, U., Nylén, H., Elander, P., & Bertilsson, L. (2011). 4β-hydroxycholesterol, an endogenous marker of CYP3A4/5 activity in humans. British Journal of Clinical Pharmacology, 71(2), 183–189. https://doi.org/10.1111/j.1365-2125.2010.03773.x

Donald, P. R. (2010). Cerebrospinal fluid concentrations of antituberculosis agents in adults and children. In Tuberculosis (Vol. 90, Issue 5, pp. 279–292). https://doi.org/10.1016/j.tube.2010.07.002

Donald, P. R., & Diacon, A. H. (2008). The early bactericidal activity of anti-tuberculosis drugs: a literature review. Tuberculosis, 88, S75–S83. https://doi.org/10.1016/S1472-9792(08)70038-6

Dooley, K. E., Kaplan, R., Mwelase, N., Grinsztejn, B., Ticona, E., Lacerda, M., Sued, O., Belonosova, E., Ait-Khaled, M., Angelis, K., Brown, D., Singh, R., Talarico, C. L., Tenorio, A. R., Keegan, M. R., Aboud, M., Dooley, K. E., Richard, K., Noluthando, M., … Anchalee, A. (2020). Dolutegravir-based Antiretroviral Therapy for Patients Coinfected with Tuberculosis and Human Immunodeficiency Virus: A Multicenter, Noncomparative, Open-label, Randomized Trial. Clinical Infectious Diseases, 70(4), 549–556. https://doi.org/10.1093/cid/ciz256

Dooley, K. E., Sayre, P., Borland, J., Purdy, E., Chen, S., Song, I., Peppercorn, A., Everts, S., Piscitelli, S., & Flexner, C. (2013). Safety, tolerability, and pharmacokinetics of the HIV integrase inhibitor dolutegravir given twice daily with rifampin or once daily with rifabutin: Results of a phase 1 study among healthy subjects. Journal of Acquired Immune Deficiency Syndromes, 62(1), 21–27. https://doi.org/10.1097/QAI.0b013e318276cda9

Dosne, A. G., Bergstrand, M., Harling, K., & Karlsson, M. O. (2016). Improving the estimation of parameter uncertainty distributions in nonlinear mixed effects models using sampling importance resampling. Journal of Pharmacokinetics and Pharmacodynamics, 43(6), 583–596. https://doi.org/10.1007/S10928-016-9487-8

Drozdzik, M., Drozdzik, M., & Oswald, S. (2021). Membrane Carriers and Transporters in Kidney Physiology and Disease. Biomedicines, 9(4), 426. https://doi.org/10.3390/biomedicines9040426

Dryden, M. S. (2011). Linezolid pharmacokinetics and pharmacodynamics in clinical treatment. In Journal of Antimicrobial Chemotherapy (Vol. 66, Issue SUPPL. 4). https://doi.org/10.1093/jac/dkr072

Ebrahim, I., Maartens, G., Wiesner, L., Orrell, C., Smythe, W., & McIlleron, H. (2020). Pharmacokinetic profile and safety of adjusted doses of darunavir/ritonavir with rifampicin in people living with HIV. Journal of Antimicrobial Chemotherapy, 75(4), 1019–1025. https://doi.org/10.1093/jac/dkz522

Eichbaum, C., Cortese, M., Blank, A., Burhenne, J., & Mikus, G. (2013). Concentration effect relationship of CYP3A inhibition by ritonavir in humans. European Journal of Clinical Pharmacology, 69(10), 1795–1800. https://doi.org/10.1007/s00228-013-1530-8

Farooq, M., Kelly, E. J., & Unadkat, J. D. (2016). CYP2D6 Is Inducible by endogenous and exogenous corticosteroids. Drug Metabolism and Disposition, 44(5), 750–757. https://doi.org/10.1124/dmd.115.069229

FDA. (2021, September 21). Pharmacometrics overview (2021). Https://Www.Fda.Gov/about-Fda/Center-Drug-Evaluation-and-Research-Cder/Division-Pharmacometrics .

FDA, & CDER. (2003). Reyataz (atazanavir sulfate) capsules: Highlights of prescribing information. www.fda.gov/medwatch

FDA, & CDER. (2010). RIFADIN ® (rifampin capsules USP) and RIFADIN ® IV (rifampin for injection USP): Highlights of prescribing information.

FDA, & CDER. (2013). Zyvox (linezolid): Highlights of prescribing information. www.fda.gov/medwatch.

FDA, & CDER. (2016a). Isoniazid Tablets, Label.

FDA, & CDER. (2016b). LAMPRENE (clofazimine): Highlights of prescribing information. www.fda.gov/medwatch.

FDA, & CDER. (2018). Levaquin (levofloxacin) oral tablets: Highlights of prescribing information. www.fda.gov/medwatch.

FDA, & CDER. (2019). NORVIR (ritonavir) for oral use: Highlights of prescribing information. www.fda.gov/medwatch.

FDA, CDER, Purdie, & Florine P. (2017). Waiver of In Vivo Bioavailability and Bioequivalence Studies for Immediate-Release Solid Oral Dosage Forms Based on a Biopharmaceutics Classification System Guidance for Industry. http://www.fda.gov/Drugs/GuidanceComplianceRegulatoryInformation/Guidances/default.htm

Fish, D. N., & Chow, A. T. (1997). The Clinical Pharmacokinetics of Levofloxacin. In PhOfmocokinet (Vol. 32, Issue 2).

Focà, E., Calcagno, A., Bonito, A., Simiele, M., Domenighini, E., D'Avolio, A., Roldan, E. Q., Trentini, L., Casari, S., Di Perri, G., Castelli, F., & Bonora, S. (2017). Atazanavir intracellular concentrations remain stable during pregnancy in HIV-infected patients. Journal of Antimicrobial Chemotherapy, 72(11), 3163–3166. https://doi.org/10.1093/jac/dkx274

Foissac, F., Blanche, S., Dollfus, C., Hirt, D., Firtion, G., Laurent, C., Treluyer, J. M., & Urien, S. (2011). Population pharmacokinetics of atazanavir/ritonavir in HIV-1-infected children and adolescents. British Journal of Clinical Pharmacology, 72(6), 940–947. https://doi.org/10.1111/j.1365-2125.2011.04035.x

Foti, R. S. (2024). Utility of PBPK Modeling in Predicting and Characterizing Clinical Drug Interactions . Drug Metabolism and Disposition, DMD-MR-2023-001384. https://doi.org/10.1124/dmd.123.001384

Fredrick M. Menger. (2006). Chapter 7 Nonlinear Mixed Effects Models: Theory. https://doi.org/doi.org/10.1007/0-387-27199-6_7

Fromm, M. F., Kauffmann, H. M., Fritz, P., Burk, O., Kroemer, H. K., Warzok, R. W., Eichelbaum, M., Siegmund, W., & Schrenk, D. (2000). The effect of rifampin treatment on intestinal expression of human MRP transporters. American Journal of Pathology, 157(5), 1575–1580. https://doi.org/10.1016/S0002-9440(10)64794-3

Gabay, M., & Spencer, S. H. (2021). Drug Interactions: Scientific and Clinical Principles. PSAP 2021 Book 3 • Chronic Conditions and Public Health.

Gammal, R., Court, M., Haidar, C., Iwuchukwu, O., Gaur, A., Alvarellos, M., Guillemette, C., Lennox, J., Whirl-Carrillo, M., Brummel, S., Ratain, M., Klein, T., Schackman, B., Caudle, K., & Haas, D. (2016). Clinical Pharmacogenetics Implementation Consortium (CPIC) Guideline for UGT1A1 and Atazanavir Prescribing. Clinical Pharmacology & Therapeutics, 99(4), 363–369. https://doi.org/10.1002/cpt.269

Garcia-Prats, A. J., Purchase, S. E., Osman, M., Draper, H. R., Simon Schaaf, H., Wiesner, L., Denti, P., & Hesseling, A. C. (2019). Pharmacokinetics, safety, and dosing of novel pediatric levofloxacin dispersible tablets in children with multidrug-resistant tuberculosis exposure. Antimicrobial Agents and Chemotherapy, 63(4). https://doi.org/10.1128/AAC.01865-18

Gardner, E. M., Burman, W. J., Steiner, J. F., Anderson, P. L., & Bangsberg, D. R. (2009). Antiretroviral medication adherence and the development of class-specific antiretroviral

resistance. In AIDS (Vol. 23, Issue 9, pp. 1035–1046). https://doi.org/10.1097/QAD.0b013e32832ba8ec

Gausi, K., Mugerwa, H., Siccardi, M., Montanha, M. C., Lamorde, M., Wiesner, L., D'Avolio, A., McIlleron, H., Wilkins, E., De Nicolò, A., Maartens, G., Khoo, S., Kityo, C., Denti, P., & Waitt, C. (2024). Pharmacokinetics and Safety of Twice-daily Ritonavir-boosted Atazanavir With Rifampicin. Clinical Infectious Diseases, 78(5), 1246–1255. https://doi.org/10.1093/cid/ciad700

Gausi, K., Wiesner, L., Norman, J., Wallis, C. L., Onyango-Makumbi, C., Chipato, T., Haas, D. W., Browning, R., Chakhtoura, N., Montepiedra, G., Aaron, L., Mccarthy, K., Bradford, S., Vhembo, T., Stranix-Chibanda, L., Masheto, G. R., Zimmer, B., Costello, D., Jean-Philippe, P., … Denti, P. (2021). Pharmacokinetics and Drug-Drug Interactions of Isoniazid and Efavirenz in Pregnant Women Living With HIV in High TB Incidence Settings: Importance of Genotyping Study Highlight WHAT IS THE CURRENT KNOWLEDGE ON THE TOPIC? CLINICAL PHARMACOLOGY & THERAPEUTICS, 109(4), 1034–1044. https://doi.org/10.1002/cpt.2044

Gianotti, N., & Lazzarin, A. (2007). Atazanavir/ritonavir: a valuable once-daily HIV protease inhibitor with little impact on lipid profile. Future Virology, 2(2), 131–143. https://doi.org/10.2217/17460794.2.2.131

Gibas, K. M., Kelly, S. G., Arribas, J. R., Cahn, P., Orkin, C., Daar, E. S., Sax, P. E., & Taiwo, B. O. (2022). Two-drug regimens for HIV treatment. In The Lancet HIV (Vol. 9, Issue 12, pp. e868–e883). Elsevier Ltd. https://doi.org/10.1016/S2352-3018(22)00249-1

Gill, M. M., Khumalo, P. N., Hoffman, H. J., Chouraya, C., Kunene, M., Dlamini, F., Tukei, V., Scheuerle, A. E., Nhlabatsi, B., & Mofenson, L. (2025). Birth Defects and Adverse Pregnancy Outcomes in Hospital-based Birth Surveillance in Eswatini. Pediatric Infectious Disease Journal. https://doi.org/10.1097/INF.0000000000004745

Glaeser, H., Drescher, S., Eichelbaum, M., & Fromm, M. F. (2005). Influence of rifampicin on the expression and function of human intestinal cytochrome P450 enzymes. British Journal of Clinical Pharmacology, 59(2), 199–206. https://doi.org/10.1111/j.1365-2125.2004.02265.x

Gobburu, J. V. S. (2010). Pharmacometrics 2020. The Journal of Clinical Pharmacology, 50(S9), 151S-157S. https://doi.org/10.1177/0091270010376977

Goldstein, B. P. (2014). Resistance to rifampicin: A review. In Journal of Antibiotics (Vol. 67, Issue 9, pp. 625–630). Nature Publishing Group. https://doi.org/10.1038/ja.2014.107

Gopal, M., Padayatchi, N., Metcalfe, J. Z., & O'Donnell, M. R. (2013). Systematic review of clofazimine for the treatment of drug-resistant tuberculosis. In International Journal of Tuberculosis and Lung Disease (Vol. 17, Issue 8, pp. 1001–1007). https://doi.org/10.5588/ijtld.12.0144

Gorski, J. (2003). The effect of age, sex, and rifampin administration on intestinal and hepatic cytochrome P450 3A activity. Clinical Pharmacology & Therapeutics, 74(3), 275–287. https://doi.org/10.1016/S0009-9236(03)00187-5

Greene, & Peterlin. (2002). Charting HIV ' s remarkable voyage through the cell : Basic. Nature Medicine Review, 673–680.

Greiner, B., Eichelbaum, M., Fritz, P., Kreichgauer, H.-P., Von Richter, O., Zundler, J., Kroemer, H. K., Pharmakologie, A. A., & Moritz-Arndt, E. (1999). Introduction The role of intestinal P-glycoprotein in the interaction of digoxin and rifampin. In The Journal of Clinical Investigation (Vol. 104, Issue 2).

Gumbo, T., Louie, A., Deziel, M. R., Liu, W., Parsons, L. M., Salfinger, M., & Drusano, G. L. (2007). Concentration-dependent Mycobacterium tuberculosis killing and prevention of resistance by rifampin. Antimicrobial Agents and Chemotherapy, 51(11), 3781–3788. https://doi.org/10.1128/AAC.01533-06

Gwitira, I., Murwira, A., Mberikunashe, J., & Masocha, M. (2018). Spatial overlaps in the distribution of HIV/AIDS and malaria in Zimbabwe. BMC Infectious Diseases, 18(1). https://doi.org/10.1186/s12879-018-3513-y

Hashemian, S. M. R., Farhadi, T., & Ganjparvar, M. (2018). Linezolid: A review of its properties, function, and use in critical care. In Drug Design, Development and Therapy (Vol. 12, pp. 1759–1767). Dove Medical Press Ltd. https://doi.org/10.2147/DDDT.S164515

Havlir, D. V, & O'marro, S. D. (2004). Atazanavir: New Option for Treatment of HIV Infection (Vol. 38, Issue 11). https://about.jstor.org/terms

Heidary, M., Shariati, S., Nourigheimasi, S., Khorami, M., Moradi, M., Motahar, M., Bahrami, P., Akrami, S., & Kaviar, V. H. (2024). Mechanism of action, resistance, interaction, pharmacokinetics, pharmacodynamics, and safety of fostemsavir. BMC Infectious Diseases, 24(1). https://doi.org/10.1186/s12879-024-09122-5

Heidary, M., Shirani, M., Moradi, M., Goudarzi, M., Pouriran, R., Rezaeian, T., & Khoshnood, S. (2022). Tuberculosis challenges: Resistance, co-infection, diagnosis, and treatment. In European Journal of Microbiology and Immunology. Akademiai Kiado ZRt. https://doi.org/10.1556/1886.2021.00021

Hein, D. W. (2009). N-acetyltransferase SNPs: Emerging concepts serve as a paradigm for understanding complexities of personalized medicine. In Expert Opinion on Drug Metabolism and Toxicology (Vol. 5, Issue 4, pp. 353–366). https://doi.org/10.1517/17425250902877698

Hein, D. W., & Doll, M. A. (2012). Accuracy of various human NAT2 SNP genotyping panels to infer rapid, intermediate and slow acetylator phenotypes. Pharmacogenomics, 13(1), 31–41. https://doi.org/10.2217/pgs.11.122

Hightower, K. E., Wang, R., DeAnda, F., Johns, B. A., Weaver, K., Shen, Y., Tomberlin, G. H., Carter, H. L., Broderick, T., Sigethy, S., Seki, T., Kobayashi, M., & Underwood, M. R. (2011). Dolutegravir (S/GSK1349572) exhibits significantly slower dissociation than raltegravir and elvitegravir from wild-type and integrase inhibitor-resistant HIV-1 integrase-DNA complexes. Antimicrobial Agents and Chemotherapy, 55(10), 4552–4559. https://doi.org/10.1128/AAC.00157-11

Hirigo, A. T., Gutema, S., Eifa, A., & Ketema, W. (2022). Experience of dolutegravir-based antiretroviral treatment and risks of diabetes mellitus. SAGE Open Medical Case Reports, 10. https://doi.org/10.1177/2050313X221079444

Hirigo, A. T., Yilma, D., Astatkie, A., & Debebe, Z. (2023). Effect of dolutegravir-based first-line antiretroviral therapy on weight and body mass index among adult people living with HIV on follow up at health facilities in Hawassa city administration, Southern Ethiopia: a retrospective cohort study. Annals of Medicine, 55(2). https://doi.org/10.1080/07853890.2023.2242250

Holdiness, M. R. (1989). Clinical Pharmacokinetics of Clofazimine. Clinical Pharmacokinetics, 16(2), 74–85. https://doi.org/10.2165/00003088-198916020-00002

Holford N. G. H., & Anderson B. J. (2017). Allometric size: The scientific theory and extension to normal fat mass. European Journal of Pharmaceutical Sciences, 109, S59–S64. https://doi.org/10.1016/j.ejps.2017.05.056

Holford, N. H. G., & Sheiner, L. B. (1982). Kinetics of pharmacologic response. Pharmacology & Therapeutics, 16(2), 143–166. https://doi.org/10.1016/0163-7258(82)90051-1

Holford, N., & Karlsson, M. (2005). Model Evaluation Visual Predictive Checks PAGE 2008 Marseille Slide 2 Outline. www.page-meeting.org/?abstract=1434

Horsfall, L. J., Zeitlyn, D., Tarekegn, A., Bekele, E., Thomas, M. G., Bradman, N., & Swallow, D. M. (2011). Prevalence of Clinically Relevant UGT1A Alleles and Haplotypes in African Populations. Annals of Human Genetics, 75(2), 236–246. https://doi.org/10.1111/J.1469-1809.2010.00638.X

Houben, R. M. G. J., & Dodd, P. J. (2016). The Global Burden of Latent Tuberculosis Infection: A Re-estimation Using Mathematical Modelling. PLoS Medicine, 13(10). https://doi.org/10.1371/journal.pmed.1002152

Hsu, A., Granneman, G. R., & Bertz, R. J. (1998). Ritonavir. Clinical Pharmacokinetics, 35(4), 275–291. https://doi.org/10.2165/00003088-199835040-00002

Hughes, D., & Andersson, D. I. (2015). Evolutionary consequences of drug resistance: Shared principles across diverse targets and organisms. In Nature Reviews Genetics (Vol. 16, Issue 8, pp. 459–471). Nature Publishing Group. https://doi.org/10.1038/nrg3922

Hull, M. W., & Montaner, J. S. G. (2011). Ritonavir-boosted protease inhibitors in HIV therapy. Annals of Medicine, 43(5), 375–388. https://doi.org/10.3109/07853890.2011.572905

Huszar, D., Lynch, C. A., Dunmore, J. H., Fang, Q., Berkemeier, L. R., Gu, W., circuits, ral, mechanisms Friedman, molecular, Kesterson, R. A., & Boston, B. A. (1997). Targeted Disruption of the Melanocortin-4 Receptor Results in Obesity in Mice. In Cell (Vol. 88).

Imaz, A., Martinez-Picado, J., Niubó, J., Kashuba, A. D. M., Ferrer, E., Ouchi, D., Sykes, C., Rozas, N., Acerete, L., Curto, J., Vila, A., & Podzamczer, D. (2016). HIV-1-RNA decay and dolutegravir concentrations in semen of patients starting a first antiretroviral regimen. Journal of Infectious Diseases, 214(10), 1512–1519. https://doi.org/10.1093/infdis/jiw406

Islam, M. M., Alam, M. S., Liu, Z., Khatun, M. S., Yusuf, B., Hameed, H. M. A., Tian, X., Chhotaray, C., Basnet, R., Abraha, H., Zhang, X., Khan, S. A., Fang, C., Li, C., Hasan, S., Tan, S., Zhong, N., Hu, J., & Zhang, T. (2023). Molecular mechanisms of resistance and treatment efficacy of clofazimine and bedaquiline against Mycobacterium tuberculosis. In Frontiers in Medicine (Vol. 10). Frontiers Media SA. https://doi.org/10.3389/fmed.2023.1304857

Janmahasatian, S., Duffull, S. B., Ash, S., Ward, L. C., Byrne, N. M., & Green, B. (2005). Quantification of Lean Bodyweight.

Joel S. Owen, & Jill Fiedler-Kelly. (2014). Introduction to Population Pharmacokinetic / Pharmacodynamic Analysis with Nonlinear Mixed Effects Models (First Edition). John Wiley & Sons, Inc.

Joerger, M. (2012). Covariate pharmacokinetic model building in oncology and its potential clinical relevance. In AAPS Journal (Vol. 14, Issue 1, pp. 119–132). https://doi.org/10.1208/s12248-012-9320-2

Josephson, F., Bertilsson, L., Böttiger, Y., Flamholc, L., Gisslén, M., Ormaasen, V., Sönnerborg, A., & Diczfalusy, U. (2008). CYP3A induction and inhibition by different antiretroviral regimens reflected by changes in plasma 4β-hydroxycholesterol levels. European Journal of Clinical Pharmacology, 64(8), 775–781. https://doi.org/10.1007/s00228-008-0492-8

Karlsson, M. O., & Savic, R. M. (2007). Diagnosing Model Diagnostics. Clinical Pharmacology & Therapeutics, 82(1), 17–20. https://doi.org/10.1038/sj.clpt.6100241

Karlsson, M. O., & Sheiner, L. B. (1993). The Importance of Modeling Interoccasion Variability in Population Pharmacokinetic Analyses. In Journal of Pharmacokinetics and Biopharmaceutics (Vol. 21, Issue 6).

Katzenmaier, S., Markert, C., Riedel, K. D., Burhenne, J., Haefeli, W. E., & Mikus, G. (2011). Determining the time course of CYP3A inhibition by potent reversible and irreversible CYP3A inhibitors using a limited sampling strategy. Clinical Pharmacology and Therapeutics, 90(5), 666–673. https://doi.org/10.1038/clpt.2011.164

Kawuma, A. N., Walimbwa, S. I., Pillai, G. (Colin), Khoo, S., Lamorde, M., Wasmann, R. E., & Denti, P. (2021). Dolutegravir pharmacokinetics during co-administration with either artemether/lumefantrine or artesunate/amodiaquine. Journal of Antimicrobial Chemotherapy. https://doi.org/10.1093/jac/dkab022

Kawuma, A. N., Wasmann, R. E., Dooley, K. E., Boffito, M., Maartens, G., & Denti, P. (2022). Population Pharmacokinetic Model and Alternative Dosing Regimens for Dolutegravir Coadministered with Rifampicin. Antimicrobial Agents and Chemotherapy, 66(6). https://doi.org/10.1128/aac.00215-22

Kearney, B. P., Flaherty, J. F., & Shah, J. (2004). Tenofovir Disoproxil Fumarate Clinical Pharmacology and Pharmacokinetics. In Clin Pharmacokinet (Vol. 43, Issue 9).

Keizer R. J, Karlsson M. O, & Hooker A. (2013). Modeling and simulation workbench for NONMEM: Tutorial on Pirana, PsN, and Xpose. CPT: Pharmacometrics and Systems Pharmacology, 2(6). https://doi.org/10.1038/psp.2013.24

Kengo, A., Gausi, K., Nabisere, R., Musaazi, J., Buzibye, A., Omali, D., Aarnoutse, R., Lamorde, M., Dooley, K. E., Sloan, D. J., Sekaggya-Wiltshire, C., & Denti, P. (2023). Unexpectedly low drug exposures among Ugandan patients with TB and HIV receiving high-dose rifampicin. Antimicrobial Agents and Chemotherapy, 67(11). https://doi.org/10.1128/aac.00431-23

Kengo, A., Kamunkhwala, G., Nabisere, R., Musaazi, J., Buzibye, A., Omali, D., Aarnoutse, R., Lamorde, M., Dooley, E. K., Sloan, J. D., Sekaggya-Wiltshire, C., & Denti, P. (n.d.). Unexpectedly low drug exposures among Ugandan patients with TB and HIV receiving high-dose rifampicin. Submitted for Publication (AAC00431-23).

Khoshnood, S., Goudarzi, M., Taki, E., Darbandi, A., Kouhsari, E., Heidary, M., Motahar, M., Moradi, M., & Bazyar, H. (2021). Bedaquiline: Current status and future perspectives. In Journal of Global Antimicrobial Resistance (Vol. 25, pp. 48–59). Elsevier Ltd. https://doi.org/10.1016/j.jgar.2021.02.017

Kim, R. B., Fromm, M. F., Wandel, C., Leake, B., Wood, A. J. J., Roden, D. M., & Wilkinson, G. R. (1998). P-glycoprotein Transport of HIV Protease Inhibitors Rapid Publication The Drug Transporter P-glycoprotein Limits Oral Absorption and Brain Entry of HIV-1 Protease Inhibitors Key words: P-glycoprotein • HIV-1 protease inhibitors • AIDS • membrane transport • pharma-cokinetics. In J. Clin. In-vest (Vol. 101, Issue 2). http://www.jci.org

Kis, O., Walmsley, S. L., & Bendayan, R. (2014). In vitro and in situ evaluation of ph-dependence of atazanavir intestinal permeability and interactions with acid-reducing agents. Pharmaceutical Research, 31(9), 2404–2419. https://doi.org/10.1007/s11095-014-1336-0

Kis, O., Zastre, J. A., Hoque, M. T., Walmsley, S. L., & Bendayan, R. (2013). Role of drug efflux and uptake transporters in atazanavir intestinal permeability and drug-drug interactions. Pharmaceutical Research, 30(4), 1050–1064. https://doi.org/10.1007/s11095-012-0942-y

Klein, D. J., Boukouvala, S., McDonagh, E. M., Shuldiner, S. R., Laurieri, N., Thorn, C. F., Altman, R. B., & Klein, T. E. (2016). PharmGKB summary: Isoniazid pathway, pharmacokinetics. Pharmacogenetics and Genomics, 26(9), 436–444. https://doi.org/10.1097/FPC.0000000000000232

Kumah, E., Boakye, D. S., Boateng, R., & Agyei, E. (2023). Advancing the Global Fight Against HIV/Aids: Strategies, Barriers, and the Road to Eradication. Annals of Global Health, 89(1). https://doi.org/10.5334/aogh.4277

Ladner, J., Besson, M. H., Rodrigues, M., Sams, K., Audureau, E., & Saba, J. (2013). Prevention of mother-to-child HIV transmission in resource-limited settings: Assessment of 99 Viramune Donation Programmes in 34 countries, 2000-2011. BMC Public Health, 13(1). https://doi.org/10.1186/1471-2458-13-470

Landersdorfer, C. B., Kirkpatrick, C. M. J., Kinzig, M., Bulitta, J. B., Holzgrabe, U., Jaehde, U., Reiter, A., Naber, K. G., Rodamer, M., & Sörgel, F. (2010). Competitive inhibition of renal tubular secretion of ciprofloxacin and metabolite by probenecid. British Journal of Clinical Pharmacology, 69(2), 167–178. https://doi.org/10.1111/j.1365-2125.2009.03564.x

Laurenzi, M., Ginsberg, A., & Spigelman, M. (2007). Challenges Associated with Current and Future TB Treatment. In Infectious Disorders-Drug Targets (Vol. 7).

Letendre, S. L., Mills, A. M., Tashima, K. T., Thomas, D. A., Min, S. S., Chen, S., Song, I. H., & Piscitelli, S. C. (2014). ING116070: A study of the pharmacokinetics and antiviral activity of dolutegravir in cerebrospinal fluid in HIV-1-infected, antiretroviral therapy-naive subjects. Clinical Infectious Diseases, 59(7), 1032–1037. https://doi.org/10.1093/cid/ciu477

Lin, T. Y., Yang, C. J., Liu, C. E., Tang, H. J., Chen, T. C., Chen, G. J., Hung, T. C., Lin, K. Y., Cheng, C. Y., Lee, Y. C., Lin, S. P., Tsai, M. S., Lee, Y. L., Cheng, S. H., Hung, C. C., & Wang, N. C. (2019). Clinical features of acute human immunodeficiency virus infection in Taiwan: A multicenter study. Journal of Microbiology, Immunology and Infection, 52(5), 700–709. https://doi.org/10.1016/j.jmii.2018.01.005

Lindbom, L., Ribbing, J., & Jonsson, E. N. (2004). Perl-speaks-NONMEM (PsN)—a Perl module for NONMEM related programming. Computer Methods and Programs in Biomedicine, 75(2), 85–94. https://doi.org/10.1016/j.cmpb.2003.11.003

Longmire, J., Albright, K., Lewis, A., Meincke, L., Hildebrand, C., Leadon, S., Cerutti, P., Dykes, D. D., Fondell, J., Watkins, P., & Polesky, H. F. (1987). A simple salting out procedure for extracting DNA from human nucleated cells. In Nucleic Acids Research (Vol. 15, Issue 2). C I R L Press Limited.

Loos, N. H. C., Beijnen, J. H., & Schinkel, A. H. (2022). The Mechanism-Based Inactivation of CYP3A4 by Ritonavir: What Mechanism? In International Journal of Molecular Sciences (Vol. 23, Issue 17). MDPI. https://doi.org/10.3390/ijms23179866

Loos, N. H. C., Beijnen, J. H., & Schinkel, A. H. (2023). The inhibitory and inducing effects of ritonavir on hepatic and intestinal CYP3A and other drug-handling proteins. In Biomedicine and Pharmacotherapy (Vol. 162). Elsevier Masson s.r.l. https://doi.org/10.1016/j.biopha.2023.114636

Lowther, J., Yard, B. A., Johnson, K. A., Carter, L. G., Bhat, V. T., Raman, M. C. C., Clarke, D. J., Ramakers, B., McMahon, S. A., Naismith, J. H., & Campopiano, D. J. (2010). Inhibition of the PLP-dependent enzyme serine palmitoyltransferase by cycloserine: Evidence for a novel decarboxylative mechanism of inactivation. Molecular BioSystems, 6(9), 1682–1693. https://doi.org/10.1039/c003743e

Lv, Z., Chu, Y., & Wang, Y. (2015). HIV protease inhibitors: A review of molecular selectivity and toxicity. HIV/AIDS - Research and Palliative Care, 7, 95–104. https://doi.org/10.2147/HIV.S79956

Maeda, T., Takahashi, K., Ohtsu, N., Oguma, T., Ohnishi, T., Atsumi, R., & Tamai, I. (2007). Identification of influx transporter for the quinolone antibacterial agent levofloxacin. Molecular Pharmaceutics, 4(1), 85–94. https://doi.org/10.1021/mp060082j

Maxwell, S. R. (2024). Pharmacodynamics and pharmacokinetics for the prescriber. In Medicine (United Kingdom) (Vol. 52, Issue 1, pp. 1–10). Elsevier Ltd. https://doi.org/10.1016/j.mpmed.2023.10.008

McDonagh, E. M., Boukouvala, S., Aklillu, E., Hein, D. W., Altman, R. B., & Klein, T. E. (2014). PharmGKB summary: Very important pharmacogene information for N-acetyltransferase 2. Pharmacogenetics and Genomics, 24(8), 409–425. https://doi.org/10.1097/FPC.0000000000000062

McIlleron, H., Hundt, H., Smythe, W., Bekker, A., Winckler, J., Van Der Laan, L., Smith, P., Zar, H. J., Hesseling, A. C., Maartens, G., & Wiesner, L. (2016a). Bioavailabilityoftwolicensed paediatric rifampicin suspensions: Implications for quality control programmes. International Journal of Tuberculosis and Lung Disease, 20(7), 915–919. https://doi.org/10.5588/ijtld.15.0833

McIlleron, H., Hundt, H., Smythe, W., Bekker, A., Winckler, J., Van Der Laan, L., Smith, P., Zar, H. J., Hesseling, A. C., Maartens, G., & Wiesner, L. (2016b). Bioavailabilityoftwolicensed paediatric rifampicin suspensions: Implications for quality control programmes. International Journal of Tuberculosis and Lung Disease, 20(7), 915–919. https://doi.org/10.5588/ijtld.15.0833

McIlleron, H., Rustomje, R., Vahedi, M., Mthiyane, T., Denti, P., Connolly, C., Rid, W., Pym, A., Smith, P. J., & Onyebujoh, P. C. (2012). Reduced antituberculosis drug concentrations in HIV-infected patients who are men or have low weight: Implications for international dosing guidelines. Antimicrobial Agents and Chemotherapy, 56(6), 3232–3238. https://doi.org/10.1128/AAC.05526-11

McIlleron, H., Wash, P., Burger, A., Folb, P., & Smith, P. (2002). Widespread distribution of a single drug rifampicin formulation of inferior bioavailability in South Africa. In INT J TUBERC LUNG DIS (Vol. 6, Issue 4).

McMahon, C., Trevaskis, J. L., Carter, C., Holsapple, K., White, K., Das, M., Collins, S., Martin, H., & Burns-Naas, L. A. (2020). Lack of an association between clinical INSTI-related body weight gain and direct interference with MC4 receptor (MC4R), a key central regulator of body weight. PLoS ONE, 15(2 February). https://doi.org/10.1371/JOURNAL.PONE.0229617

Min, S., Song, I., Borland, J., Chen, S., Lou, Y., Fujiwara, T., & Piscitelli, S. C. (2010). Pharmacokinetics and Safety of S/GSK1349572, a Next-Generation HIV Integrase Inhibitor, in Healthy Volunteers. Antimicrobial Agents and Chemotherapy, 54(1), 254–258. https://doi.org/10.1128/AAC.00842-09

Mirnejad, R., Asadi, A., Khoshnood, S., Mirzaei, H., Heidary, M., Fattorini, L., Ghodousi, A., & Darban-Sarokhalil, D. (2018). Clofazimine: A useful antibiotic for drug-resistant tuberculosis. In Biomedicine and Pharmacotherapy (Vol. 105, pp. 1353–1359). Elsevier Masson SAS. https://doi.org/10.1016/j.biopha.2018.06.023

Mirochnick, M., Best, B. M., Stek, A. M., Capparelli, E. V., Hu, C., Burchett, S. K., Rossi, S. S., Hawkins, E., Basar, M., Smith, E., & Read, J. S. (2011). Atazanavir pharmacokinetics with and without tenofovir during pregnancy. Journal of Acquired Immune Deficiency Syndromes, 56(5), 412–419. https://doi.org/10.1097/QAI.0b013e31820fd093

Mitchison. (2005a). Drug resistance in tuberculosis. European Respiratory Journal, 25(2), 376–379. https://doi.org/10.1183/09031936.05.00075704

Mitchison. (2005b). Shortening the treatment of tuberculosis. http://www.nature.com/naturebiotechnology

Mitchison, D. A. (2000). Role of individual drugs in the chemotherapy of tuberculosis.

Modongo, C., Wang, Q., Dima, M., Matsiri, O., Kgwaadira, B., Rankgoane-Pono, G., Shin, S. S., & Zetola, N. M. (2019). Clinical and Virological Outcomes of TB/HIV Coinfected Patients Treated With Dolutegravir-Based HIV Antiretroviral Regimens: Programmatic Experience From Botswana. www.jaids.com

Moir, S., Chun, T. W., & Fauci, A. S. (2011). Pathogenic mechanisms of HIV disease. Annual Review of Pathology: Mechanisms of Disease, 6, 223–248. https://doi.org/10.1146/annurev-pathol-011110-130254

Montanha, M. C., Fabrega, F., Howarth, A., Cottura, N., Kinvig, H., Bunglawala, F., Lloyd, A., Denti, P., Waitt, C., & Siccardi, M. (2022). Predicting Drug–Drug Interactions between Rifampicin and Ritonavir-Boosted Atazanavir Using PBPK Modelling. Clinical Pharmacokinetics, 61(3), 375–386. https://doi.org/10.1007/s40262-021-01067-1

Moses, O., Patrick, V., Muhammad, N., Jasper, O.-O., & Celestino, O. (2013). Substandard rifampicin based anti-tuberculosis drugs common in Ugandan drug market. In Journal Of Pharmacy And Pharmacological Research (Vol. 3, Issue 1). http://www.globalresearchjournals.org/journal/jppr

Mould, D., & Upton, R. (2012). Basic Concepts in Population Modeling, Simulation, and Model-Based Drug Development. CPT: Pharmacometrics & Systems Pharmacology, 1(9), 6. https://doi.org/10.1038/psp.2012.4

Mould, D., & Upton, R. (2013). Basic Concepts in Population Modeling, Simulation, and Model-Based Drug Development—Part 2: Introduction to Pharmacokinetic Modeling Methods. CPT: Pharmacometrics & Systems Pharmacology, 2(4), 1–14. https://doi.org/10.1038/psp.2013.14

Mukonzo, J., Aklillu, E., Marconi, V., & Schinazi, R. F. (2019). Potential drug–drug interactions between antiretroviral therapy and treatment regimens for multi-drug resistant tuberculosis: Implications for HIV care of MDR-TB co-infected individuals. In International Journal of Infectious Diseases (Vol. 83, pp. 98–101). Elsevier B.V. https://doi.org/10.1016/j.ijid.2019.04.009

Mulubwa, M., & Mugabo, P. (2019). Steady-state population pharmacokinetics of terizidone and its metabolite cycloserine in patients with drug-resistant tuberculosis. British Journal of Clinical Pharmacology, 85(9), 1946–1956. https://doi.org/10.1111/bcp.13975

Murphy, R. A., Marconi, V. C., Gandhi, R. T., Kuritzkes, D. R., & Sunpath, H. (2012). Coadministration of Lopinavir/Ritonavir and Rifampicin in HIV and Tuberculosis Co-Infected Adults in South Africa. In PLoS ONE (Vol. 7, Issue 9). https://doi.org/10.1371/journal.pone.0044793

Murray, J. F., Schraufnagel, D. E., & Hopewell, P. C. (2015). Treatment of tuberculosis: A historical perspective. In Annals of the American Thoracic Society (Vol. 12, Issue 12, pp. 1749–1759). American Thoracic Society. https://doi.org/10.1513/AnnalsATS.201509-632PS

Nabisere, R., Musaazi, J., Denti, P., Aber, F., Lamorde, M., Dooley, K. E., Aarnoutse, R., Sloan, D. J., & Sekaggya-Wiltshire, C. (2020). Pharmacokinetics, SAfety/tolerability, and EFficacy of high-dose RIFampicin in tuberculosis-HIV co-infected patients on efavirenz- or dolutegravir-based antiretroviral therapy: Study protocol for an open-label, phase II clinical trial (SAEFRIF). Trials, 21(1), 181. https://doi.org/10.1186/s13063-020-4132-7

Naga, & Kumar. (2024). Lenacapavir: A Novel Capsid Inhibitor in HIV-1 Treatment and Capsid Inhibitors Drugs. Int. J. of Pharm. Sci, 2(11), 961. https://doi.org/10.5281/zenodo.14208676

Namara, D., Schwartz, J. I., Tusubira, A. K., McFarland, W., Birungi, C., Semitala, F. C., & Muddu, M. (2022). The risk of hyperglycemia associated with use of dolutegravir among adults living with HIV in Kampala, Uganda: A case-control study. International Journal of STD and AIDS, 33(14), 1158–1164. https://doi.org/10.1177/09564624221129410

Ndjeka, N., Schnippel, K., Master, I., Meintjes, G., Maartens, G., Romero, R., Padanilam, X., Enwerem, M., Chotoo, S., Singh, N., Hughes, J., Variava, E., Ferreira, H., Te Riele, J., Ismail, N., Mohr, E., Bantubani, N., & Conradie, F. (2018). High treatment success rate for multidrug-resistant and extensively drug-resistant tuberculosis using a bedaquiline-containing treatment regimen. The European Respiratory Journal, 52(6). https://doi.org/10.1183/13993003.01528-2018

Neon Healthcare Ltd. (2023). Cycloserine. Summary of Product Characteristics. https://www.medicines.org.uk/emc/product/13280/smpc/print

Nguyen, L. (2016). Antibiotic resistance mechanisms in M. tuberculosis: an update. In Archives of Toxicology (Vol. 90, Issue 7, pp. 1585–1604). Springer Verlag. https://doi.org/10.1007/s00204-016-1727-6

Nguyen, T. H. T., Mouksassi, M. S., Holford, N., Al-Huniti, N., Freedman, I., Hooker, A. C., John, J., Karlsson, M. O., Mould, D. R., Perez Ruixo, J. J., Plan, E. L., Savic, R., Van Hasselt, J. G. C., Weber, B., Zhou, C., Comets, E., & Mentre, F. (2017). Model evaluation of continuous data pharmacometric models: Metrics and graphics. CPT: Pharmacometrics and Systems Pharmacology, 6(2), 87–109. https://doi.org/10.1002/psp4.12161

Ngwalero, P., Brust, J. C. M., van Beek, S. W., Wasserman, S., Maartens, G., Meintjes, G., Joubert, A., Norman, J., Castel, S., Gandhi, N. R., Denti, P., McIlleron, H., Svensson, E. M., & Wiesner, L. (2021). Relationship between plasma and intracellular concentrations of bedaquiline and its m2 metabolite in South African patients with rifampin-resistant tuberculosis. Antimicrobial Agents and Chemotherapy, 65(11). https://doi.org/10.1128/AAC.02399-20

Niemi, M., Backman, J. T., Fromm, M. F., Neuvonen, P. J., & Kivistö, K. T. (2003). Pharmacokinetic interactions with rifampicin : clinical relevance. Clinical Pharmacokinetics, 42(9), 819–850. https://doi.org/10.2165/00003088-200342090-00003

Nina Singh, Stephen M. Berman, Susan Swindells, Janice C. Justis, Jeffrey A. Mohr, Cheryl Squier, & Marilyn M. Wagener. (1999). Adherence of Human Immunodeficiency Virus-Infected Patients to Antiretroviral Therapy. Clinical Infectious Diseases, 29(4), 824–830. https://doi.org/https://doi.org/10.1007/0-387-27199-6_7

Nix, D. E., Adam, R. D., Auclair, B., Krueger, T. S., Godo, P. G., & Peloquin, C. A. (2004). Pharmacokinetics and relative bioavailability of clofazimine in relation to food, orange juice and antacid. Tuberculosis, 84(6), 365–373. https://doi.org/10.1016/j.tube.2004.04.001

Obach, R. S. (2022). Linezolid Metabolism Is Catalyzed by Cytochrome P450 2J2, 4F2, and 1B1. Drug Metabolism and Disposition, 50(4), 413–421. https://doi.org/10.1124/dmd.121.000776

Odone, A., Amadasi, S., White, R. G., Cohen, T., Grant, A. D., & Houben, R. M. G. J. (2014). The impact of antiretroviral therapy on mortality in hiv positive people during tuberculosis treatment: A systematic review and meta-analysis. In PLoS ONE (Vol. 9, Issue 11). Public Library of Science. https://doi.org/10.1371/journal.pone.0112017

Pai, M. P., Momary, K. M., & Rodvold, K. A. (2006). Antibiotic Drug Interactions. Medical Clinics of North America, 90(6), 1223–1255. https://doi.org/10.1016/j.mcna.2006.06.008

Palmisano L, & Vella S. (2011). A brief history of antiretroviral therapy of HIV infection: success and challenges. Ann Ist Super Sanità, 47(1), 44–48. https://doi.org/DOI: 10.4415/ANN_11_01_10

Panchagnula, R., & Agrawal, S. (2004). Biopharmaceutic and pharmacokinetic aspects of variable bioavailability of rifampicin. In International Journal of Pharmaceutics (Vol. 271, Issues 1–2, pp. 1–4). Elsevier. https://doi.org/10.1016/j.ijpharm.2003.11.031

Pang, K. S., & Rowland, M. (1977). Hepatic Clearance of Drugs. I. Theoretical Considerations of a “Well-Stirred” Model and a “Parallel Tube” Model. Influence of Hepatic Blood Flow, Plasma and Blood Cell Binding, and the Hepatocellular Enzymatic Activity on Hepatic Drug Clearance I. In Journal of Pharmacokinetics and Biopharmaceutics (Vol. 5, Issue 6).

Parant, F., Miailhes, P., Brunel, F., & Gagnieu, M.-C. (2019). Dolutegravir Population Pharmacokinetics in a Real-Life Cohort of People Living With HIV Infection: A Covariate Analysis. www.asqualab.com

Pasipanodya, J. G., McIlleron, H., Burger, A., Wash, P. A., Smith, P., & Gumbo, T. (2013). Serum Drug Concentrations Predictive of Pulmonary Tuberculosis Outcomes. Journal of Infectious Diseases, 208(9), 1464–1473. https://doi.org/10.1093/infdis/jit352

Paterson, D. L., Swindells, S., Mohr, J., Brester, M., Vergis, E. N., Squier, C., Wagener, M. M., & Singh, N. (2000). Adherence to Protease Inhibitor Therapy and Outcomes in Patients with HIV Infection Background: Combination antiretroviral therapy with protease. https://annals.org

Peloquin, C. A., Hadad, D. J., Molino, L. P. D., Palaci, M., Boom, W. H., Dietze, R., & Johnson, J. L. (2008). Population pharmacokinetics of levofloxacin, gatifloxacin, and moxifloxacin in adults with pulmonary tuberculosis. Antimicrobial Agents and Chemotherapy, 52(3), 852–857. https://doi.org/10.1128/AAC.01036-07

Peloquin, C. A., Phillips, P. P. J., Mitnick, C. D., Eisenach, K., Patienti, R. F., Lecc, L., Gotuzzo, E., Gandhi, N. R., Butler, D., Diacon, A. H., Martel, B., Santillan, J., Hunt, K. R., Vargas, D., Von Groote-Bidlingmaier, F., Seas, C., Dianis, N., Moreno-Martinez, A., Kaur, P., & Horsburgh, C. R.

(2018). Increased doses lead to higher drug exposures of levofloxacin for treatment of tuberculosis. Antimicrobial Agents and Chemotherapy, 62(10). https://doi.org/10.1128/AAC.00770-18

Philips, J. A., & Ernst, J. D. (2012). Tuberculosis pathogenesis and immunity. Annual Review of Pathology: Mechanisms of Disease, 7, 353–384. https://doi.org/10.1146/annurev-pathol-011811-132458

Piscitelli, S. C., & Rodvold, K. A. (2005). Drug Interactions in Infectious Diseases.

Podany, A. T., Scarsi, K. K., Pham, M. M., & Fletcher, C. V. (2020). Comparative Clinical Pharmacokinetics and Pharmacodynamics of HIV-1 Integrase Strand Transfer Inhibitors: An Updated Review. In Clinical Pharmacokinetics (Vol. 59, Issue 9, pp. 1085–1107). Adis. https://doi.org/10.1007/s40262-020-00898-8

Pommier, Y., Johnson, A. A., & Marchand, C. (2005). Integrase inhibitors to treat HIV/AIDS. In Nature Reviews Drug Discovery (Vol. 4, Issue 3, pp. 236–248). https://doi.org/10.1038/nrd1660

Poulton, N. C., Azadian, Z. A., DeJesus, M. A., & Rock, J. M. (2022). Mutations in rv0678 Confer Low-Level Resistance to Benzothiazinone DprE1 Inhibitors in Mycobacterium tuberculosis. Antimicrobial Agents and Chemotherapy, 66(9). https://doi.org/10.1128/aac.00904-22

Prosser, G. A., & De Carvalho, L. P. S. (2013). Reinterpreting the mechanism of inhibition of mycobacterium tuberculosis d -alanine: D -alanine ligase by d -cycloserine. Biochemistry, 52(40), 7145–7149. https://doi.org/10.1021/bi400839f

PSN 5.3.0. (2019). SIR_userguide.

Punyawudho, B., Thammajaruk, N., Ruxrungtham, K., & Avihingsanon, A. (2017). Population pharmacokinetics and dose optimisation of ritonavir-boosted atazanavir in Thai HIV-infected patients. International Journal of Antimicrobial Agents, 49(3), 327–332. https://doi.org/10.1016/j.ijantimicag.2016.11.019

Raja, A. (2004a). Immunology of tuberculosis. Indian Journal of Medical Research, 120(4), 213–232. https://doi.org/10.5005/jp/books/10992_7

Raja, A. (2004b). Immunology of tuberculosis. The Indian Journal of Medical Research, 120(4), 213–232. http://www.ncbi.nlm.nih.gov/pubmed/15520479

Rathbun, R. C., Lockhart, S. M., Miller, M. M., & Liedtke, M. D. (2014). Dolutegravir, a Second-Generation Integrase Inhibitor for the Treatment of HIV-1 Infection. In Annals of Pharmacotherapy (Vol. 48, Issue 3, pp. 395–403). https://doi.org/10.1177/1060028013513558

Reese, M. J., Savina, P. M., Generaux, G. T., Tracey, H., Humphreys, J. E., Kanaoka, E., Webster, L. O., Harmon, K. A., Clarke, J. D., & Polli, J. W. (2013). In vitro investigations into the roles of drug transporters and metabolizing enzymes in the disposition and drug interactions of dolutegravir, a hiv integrase inhibitor. Drug Metabolism and Disposition, 41(2), 353–361. https://doi.org/10.1124/dmd.112.048918

Rescigno, A. (2000). Area under the curve and bioavailability. Pharmacological Research, 42(6), 539–540. https://doi.org/10.1006/phrs.2000.0719

Resendiz-Galvan, J. E., Arora, P. R., Abdelwahab, M. T., Udwadia, Z. F., Rodrigues, C., Gupta, A., Denti, P., Ashavaid, T. F., & Tornheim, J. A. (2023). Pharmacokinetic analysis of linezolid for multidrug resistant tuberculosis at a tertiary care centre in Mumbai, India. Frontiers in Pharmacology, 13. https://doi.org/10.3389/fphar.2022.1081123

Ribera, E., Azuaje, C., Lopez, R. M., Domingo, P., Curran, A., Feijoo, M., Pou, L., Sánchez, P., Sambeat, M. A., Colomer, J., Lopez-Colomes, J. L., Crespo, M., Falcó, V., Ocaña, I., & Pahissa, A. (2007). Pharmacokinetic interaction between rifampicin and the once-daily combination of saquinavir and low-dose ritonavir in HIV-infected patients with tuberculosis. Journal of Antimicrobial Chemotherapy, 59(4), 690–697. https://doi.org/10.1093/jac/dkl552

Salim S.A.K, K. N. A. G. N. P. , C. B. A. G. T. G. G. N. S. B. A. S. M. K. J. P. W. E. G. F. and Q. A. K. (2010). Timing of Initiation of Antiretroviral Drugs during Tuberculosis Therapy. N Engl J Med, 362, 697–706.

Sangana, R., Gu, H., Chun, D. Y., & Einolf, H. J. (2018). Evaluation of clinical drug interaction potential of clofazimine using static and dynamic modeling approaches. Drug Metabolism and Disposition, 46(1), 26–32. https://doi.org/10.1124/dmd.117.077834

Santajit, S., & Indrawattana, N. (2016). Mechanisms of Antimicrobial Resistance in ESKAPE Pathogens. In BioMed Research International (Vol. 2016). Hindawi Limited. https://doi.org/10.1155/2016/2475067

Savarit, D., De Cock, K. M., Schutz, R., Konate, S., Lackritz, E., & Bondurand, A. (1992). Risk of HIV infection from transfusion with blood negative for HIV antibody in a west African city. British Medical Journal, 305(6852), 498–502. https://doi.org/10.1136/bmj.305.6852.498

Savic, R. M., Jonker, D. M., Kerbusch, T., & Karlsson, M. O. (2007). Implementation of a transit compartment model for describing drug absorption in pharmacokinetic studies. Journal of Pharmacokinetics and Pharmacodynamics, 34(5), 711–726. https://doi.org/10.1007/s10928-007-9066-0

Scarsi, K. K., Havens, J. P., Podany, A. T., Avedissian, S. N., & Fletcher, C. V. (2020). HIV-1 Integrase Inhibitors: A Comparative Review of Efficacy and Safety. In Drugs (Vol. 80, Issue 16, pp. 1649–1676). Adis. https://doi.org/10.1007/s40265-020-01379-9

Schalkwijk, S., Greupink, R., Colbers, A. P., Wouterse, A. C., Verweij, V. G. M., van Drongelen, J., Teulen, M., van den Oetelaar, D., Burger, D. M., & Russel, F. G. M. (2016). Placental transfer of the HIV integrase inhibitor dolutegravir in an ex vivo human cotyledon perfusion model. Journal of Antimicrobial Chemotherapy, 71(2), 480–483. https://doi.org/10.1093/jac/dkv358

Schatz, A., Bugie, E., & Waksman, S. A. (2005). Streptomycin, a substance exhibiting antibiotic activity against gram-positive and gram-negative bacteria. 1944. Clinical Orthopaedics and Related Research, 437, 3–6. https://doi.org/10.1097/01.blo.0000175887.98112.fe

Schipani, A., Dickinson, L., Boffito, M., Austin, R., Owen, A., Back, D., Khoo, S., & Davies, G. (2013). Simultaneous population pharmacokinetic modelling of atazanavir and ritonavir in HIV-

infected adults and assessment of different dose reduction strategies. Journal of Acquired Immune Deficiency Syndromes, 62(1), 60–66. https://doi.org/10.1097/QAI.0b013e3182737231

Scourfield Andrew, Waters Laura, & Nelson Mark. (2011). Drug combinations for HIV: what's new? Expert Review of Anti-Infective Therapy, 9(11), 1001–1011. https://doi.org/10.1586/eri.11.125

Seitz, R. (2016). Human Immunodeficiency Virus (HIV). Transfusion Medicine and Hemotherapy, 43(3), 203–222. https://doi.org/10.1159/000445852

Sekaggya-Wiltshire, C., Chirehwa, M., Musaazi, J., Von Braun, A., Buzibye, A., Muller, D., Gutteck, U., Motta, I., Calcagno, A., Fehr, J. S., Kambugu, A., Castelnuovo, B., Lamorde, M., & Denti, P. (2019). Low Antituberculosis Drug Concentrations in HIV-Tuberculosis-Coinfected Adults with Low Body Weight: Is It Time To Update Dosing Guidelines? https://doi.org/10

Sekaggya-Wiltshire, C., Nabisere, R., Musaazi, J., Otaalo, B., Aber, F., Alinaitwe, L., Nampala, J., Najjemba, L., Buzibye, A., Omali, D., Gausi, K., Kengo, A., Lamorde, M., Aarnoutse, R., Denti, P., Dooley, K. E., & Sloan, D. J. (2022). Decreased Dolutegravir and Efavirenz Concentrations With Preserved Virological Suppression in Patients With Tuberculosis and Human Immunodeficiency Virus Receiving High-Dose Rifampicin. Clinical Infectious Diseases. https://doi.org/10.1093/cid/ciac585

Self, T. H., Chrisman, C. R., Baciewicz, A. M., & Bronze, M. S. (1999). Isoniazid drug and food interactions. In American Journal of the Medical Sciences (Vol. 317, Issue 5, pp. 304–311). Lippincott Williams and Wilkins. https://doi.org/10.1016/S0002-9629(15)40533-6

Shean, K., Streicher, E., Pieterson, E., Symons, G., van Zyl Smit, R., Theron, G., Lehloenya, R., Padanilam, X., Wilcox, P., Victor, T. C., van Helden, P., Groubusch, M., Warren, R., Badri, M., & Dheda, K. (2013). Drug-Associated Adverse Events and Their Relationship with Outcomes in Patients Receiving Treatment for Extensively Drug-Resistant Tuberculosis in South Africa. In PLoS ONE (Vol. 8, Issue 5). https://doi.org/10.1371/journal.pone.0063057

Sidamo, T., Rao, P. S., Aklillu, E., Shibeshi, W., Park, Y., Cho, Y. S., Shin, J. G., Heysell, S. K., Mpagama, S. G., & Engidawork, E. (2022). Population Pharmacokinetics of Levofloxacin and Moxifloxacin, and the Probability of Target Attainment in Ethiopian Patients with Multidrug-Resistant Tuberculosis. Infection and Drug Resistance, 15, 6839–6852. https://doi.org/10.2147/IDR.S389442

Singh, R., Dwivedi, S. P., Gaharwar, U. S., Meena, R., Rajamani, P., & Prasad, T. (2020). Recent updates on drug resistance in Mycobacterium tuberculosis. In Journal of Applied Microbiology (Vol. 128, Issue 6, pp. 1547–1567). John Wiley and Sons Inc. https://doi.org/10.1111/jam.14478

Smith, T., Wolff, K. A., & Nguyen, L. (2012). Molecular Biology of Drug Resistance in Mycobacterium tuberculosis (pp. 53–80). https://doi.org/10.1007/82_2012_279

Smith, Zhao, X. Z., Passos, D. O., Lyumkis, D., Burke, T. R., & Hughes, S. H. (2021). Integrase Strand Transfer Inhibitors Are Effective Anti-HIV Drugs. Viruses, 13(2), 205. https://doi.org/10.3390/v13020205

Snyder, B., Polasek, T. M., & Doogue, M. P. (2012). Drug interactions: principles and practice. Australian Prescriber, 35(3), 85–88. https://doi.org/10.18773/austprescr.2012.037

Song, Borland, J., Arya, N., Wynne, B., & Piscitelli, S. (2015). Pharmacokinetics of dolutegravir when administered with mineral supplements in healthy adult subjects. Journal of Clinical Pharmacology, 55(5), 490–496. https://doi.org/10.1002/jcph.439

Song, Borland, J., Chen, S., Lou, Y., Peppercorn, A., Wajima, T., Min, S., & Piscitelli, S. C. (2011). Effect of atazanavir and atazanavir/ritonavir on the pharmacokinetics of the next-generation HIV integrase inhibitor, S/GSK1349572. British Journal of Clinical Pharmacology, 72(1), 103–108. https://doi.org/10.1111/j.1365-2125.2011.03947.x

Song, Borland, J., Chen, S., Patel, P., Wajima, T., Peppercorn, A., & Piscitelli, S. C. (2012). Effect of food on the pharmacokinetics of the integrase inhibitor dolutegravir. Antimicrobial Agents and Chemotherapy, 56(3), 1627–1629. https://doi.org/10.1128/AAC.05739-11

Song, Zong, J., Borland, J., Jerva, F., Wynne, B., Zamek-Gliszczynski, M. J., Humphreys, J. E., Bowers, G. D., & Choukour, M. (2016). The Effect of Dolutegravir on the Pharmacokinetics of Metformin in Healthy Subjects. http://links.lww.com/QAI/A800

Sonnenkalb, L., Carter, J. J., Spitaleri, A., Iqbal, Z., Hunt, M., Malone, K. M., Utpatel, C., Cirillo, D. M., Rodrigues, C., Nilgiriwala, K. S., Fowler, P. W., Merker, M., Niemann, S., Barilar, I., Battaglia, S., Borroni, E., Brandao, A. P., Brankin, A., Cabibbe, A. M., … Zhu, B. (2023). Bedaquiline and clofazimine resistance in Mycobacterium tuberculosis: an in-vitro and in-silico data analysis. The Lancet Microbe, 4(5), e358–e368. https://doi.org/10.1016/S2666-5247(23)00002-2

SSE user guide. (2018). https://uupharmacometrics.github.io/PsN/docs.html

Stadler, J. A. M., Maartens, G., Meintjes, G., & Wasserman, S. (2023). Clofazimine for the treatment of tuberculosis. Frontiers in Pharmacology, 14. https://doi.org/10.3389/fphar.2023.1100488

Stalker, D. J., & Jungbluth, G. L. (2003). Clinical Pharmacokinetics of Linezolid, a Novel Oxazolidinone Antibacterial. In Clin Pharmacokinet (Vol. 42, Issue 13).

Stevenson, M. (2003). HIV-1 pathogenesis. Nature Medicine, 9(7), 853–860. https://doi.org/10.1038/nm0703-853

Storch, C. H., Theile, D., Lindenmaier, H., Haefeli, W. E., & Weiss, J. (2007). Comparison of the inhibitory activity of anti-HIV drugs on P-glycoprotein. Biochemical Pharmacology, 73(10), 1573–1581. https://doi.org/10.1016/j.bcp.2007.01.027

Svensson, E. M., DIan, S., Te Brake, L., Ganiem, A. R., Yunivita, V., Van Laarhoven, A., Van Crevel, R., Ruslami, R., & Aarnoutse, R. E. (2020). Model-Based Meta-analysis of Rifampicin

Exposure and Mortality in Indonesian Tuberculous Meningitis Trials. Clinical Infectious Diseases, 71(8), 1817–1823. https://doi.org/10.1093/cid/ciz1071

Swainston Harrison, T., & Scott, L. J. (2005). Atazanavir. Drugs, 65(16), 2309–2336. https://doi.org/10.2165/00003495-200565160-00010

Taburet, A. M., Piketty, C., Chazallon, C., Vincent, I., Gérard, L., Calvez, V., Clavel, F., Aboulker, J. P., & Girard, P. M. (2004). Interactions between atazanavir-ritonavir and tenofovir in heavily pretreated human immunodeficiency virus-infected patients. Antimicrobial Agents and Chemotherapy, 48(6), 2091–2096. https://doi.org/10.1128/AAC.48.6.2091-2096.2004

Taha, H., Das, A., & Das, S. (2015). Clinical effectiveness of dolutegravir in the treatment of HIV/AIDS. Infection and Drug Resistance, 8, 339–352. https://doi.org/10.2147/IDR.S68396

Te Brake, L. H. M., de Jager, V., Narunsky, K., Vanker, N., Svensson, E. M., Phillips, P. P. J., Gillespie, S. H., Heinrich, N., Hoelscher, M., Dawson, R., Diacon, A. H., Aarnoutse, R. E., & Boeree, M. J. (2021). Increased bactericidal activity but dose-limiting intolerability at 50 mg·kg $^{-1}$ rifampicin. European Respiratory Journal, 58(1), 2000955. https://doi.org/10.1183/13993003.00955-2020

Te Brake, L. H. M., Russel, F. G. M., Van Den Heuvel, J. J. M. W., De Knegt, G. J., De Steenwinkel, J. E., Burger, D. M., Aarnoutse, R. E., & Koenderink, J. B. (2016). Inhibitory potential of tuberculosis drugs on ATP-binding cassette drug transporters. Tuberculosis, 96, 150–157. https://doi.org/10.1016/j.tube.2015.08.004

Ter Heine, R., Mulder, J. W., Van Gorp, E. C. M., Wagenaar, J. F. P., Beijnen, J. H., & Huitema, A. D. R. (2010). Intracellular and plasma steady-state pharmacokinetics of raltegravir, darunavir, etravirine and ritonavir in heavily pre-treated HIV-infected patients. British Journal of Clinical Pharmacology, 69(5), 475–483. https://doi.org/10.1111/j.1365-2125.2010.03634.x

The INSIGHT START Study Group. (2015). Initiation of Antiretroviral Therapy in Early Asymptomatic HIV Infection. The Lancet HIV, 2(9). https://doi.org/10.1056/NEJMoa1506816

Timmins, G. S., & Deretic, V. (2006). Mechanisms of action of isoniazid. Molecular Microbiology, 62(5), 1220–1227. https://doi.org/10.1111/j.1365-2958.2006.05467.x

Todd M. (1953). Treatment of primary pulmonary tuberculosis P.A.S. British Medical Journal, 1(4822), 1247–1249. https://doi.org/10.1136/bmj.1.4822.1247

Tsunoda, S. M., Velez, R. L., von Moltke, L. L., & Greenblatt, D. J. (1999). Differentiation of intestinal and hepatic cytochrome P450 3A activity with use of midazolam as an in vivo probe: effect of ketoconazole. Clinical Pharmacology and Therapeutics, 66(5), 461–471. https://doi.org/10.1016/S0009-9236(99)70009-3

UNAIDS. (2019). UNAIDS Data 2019. In Encyclopedia of Global Health. SAGE Publications, Inc. https://doi.org/10.4135/9781412963855.n665

UNAIDS. (2022). Country factsheets South Africa: HIV and AIDS Estimates.

UNAIDS. (2023a). Fact Sheet: Global HIV statistics.

UNAIDS. (2023b). THE PATH THAT ENDS AIDS 2023 UNAIDS GLOBAL AIDS UPDATE. http://www.wipo.int/amc/en/mediation/rules

Van Bambeke, F., Michot, J. M., Van Eldere, J., & Tulkens, P. M. (2005). Quinolones in 2005: An update. In Clinical Microbiology and Infection (Vol. 11, Issue 4, pp. 256–280). Blackwell Publishing Ltd. https://doi.org/10.1111/j.1469-0691.2005.01131.x

Van der Walt, M., & Moyo Sizulu. (2018). The First National TB Prevalence Survey South Africa Short Report.

Van Deun, A., Maug, A. K. J., Salim, M. A. H., Das, P. K., Sarker, M. R., Daru, P., & Rieder, H. L. (2010). Short, highly effective, and inexpensive standardized treatment of multidrug-resistant tuberculosis. American Journal of Respiratory and Critical Care Medicine, 182(5), 684–692. https://doi.org/10.1164/rccm.201001-0077OC

Van Lunzen, J., Maggiolo, F., Arribas, J. R., Rakhmanova, A., Yeni, P., Young, B., Rockstroh, J. K., Almond, S., Song, I., Brothers, C., & Min, S. (2012). Once daily dolutegravir (S/GSK1349572) in combination therapy in antiretroviral-naive adults with HIV: planned interim 48 week results from SPRING-1, a dose-ranging, randomised, phase 2b trial. Www.Thelancet.Com/Infection, 12, 111–129. https://doi.org/10.1016/S1473

Velásquez, G. E., Brooks, M. B., Coit, J. M., Pertinez, H., Vásquez, D. V., Garavito, E. S., Calderón, R. I., Jiménez, J., Tintaya, K., Peloquin, C. A., Osso, E., Tierney, D. B., Seung, K. J., Lecca, L., Davies, G. R., & Mitnick, C. D. (2018). Efficacy and safety of high-dose rifampin in pulmonary tuberculosis a randomized controlled trial. American Journal of Respiratory and Critical Care Medicine, 198(5), 657–666. https://doi.org/10.1164/rccm.201712-2524OC

Venuto, C. S., Mollan, K., Ma, Q., Daar, E. S., Sax, P. E., Fischl, M., Collier, A. C., Smith, K. Y., Tierney, C., Morse, G. D., Rosenkranz, S., Lu, D., Myers, L., & Bloom, A. (2014). Sex differences in atazanavir pharmacokinetics and associations with time to clinical events: AIDS Clinical Trials Group Study A5202. Journal of Antimicrobial Chemotherapy, 69(12), 3300–3310. https://doi.org/10.1093/jac/dku303

ViiV Healthcare. (2021). Tivicay, INN-dolutegravir—Europa EU. Summary of Product characteristics (SPC). www.fda.gov/medwatch.

Vilchèze, & Jacobs. (2014). Resistance to Isoniazid and Ethionamide in Mycobacterium tuberculosis : Genes, Mutations, and Causalities . Microbiology Spectrum, 2(4). https://doi.org/10.1128/microbiolspec.mgm2-0014-2013

Von Hentig, N., Dauer, B., Haberl, A., Klauke, S., Lutz, T., Staszewski, S., & Harder, S. (2007). Tenofovir comedication does not impair the steady-state pharmacokinetics of ritonavir-boosted atazanavir in HIV-1-infected adults. European Journal of Clinical Pharmacology, 63(10), 935–940. https://doi.org/10.1007/s00228-007-0344-y

Vukovic, M., Radlovic, N., Lekovic, Z., Vucicevic, K., Maric, N., Kotur, N., Gasic, V., Ugrin, M., Stojiljkovic, M., Dokmanovic, L., Zukic, B., & Pavlovic, S. (2018). UGT1A1 (TA)n promoter genotype: Diagnostic and population pharmacogenetic marker in Serbia. Balkan Journal of Medical Genetics, 21(1), 59–68. https://doi.org/10.2478/bjmg-2018-0012

Wählby, U., Jonsson, E. N., & Karlsson, M. O. (2002). Comparison of Stepwise Covariate Model Building Strategies in Population Pharmacokinetic-Pharmacodynamic Analysis. In AAPS PharmSci (Vol. 4, Issue 4). http://www.aapspharmsci.org

Walensky, R. P., Paltiel, A. D., Losina, E., Mercincavage, L. M., Schackman, B. R., Sax, P. E., Weinstein, M. C., & Freedberg, K. A. (2006). The Survival Benefits of AIDS Treatment in the United States. In Survival Benefits of AIDS Treatment • JID. https://academic.oup.com/jid/article/194/1/11/794287

Wallis, R. S. (2016). Cardiac safety of extensively drug-resistant tuberculosis regimens including bedaquiline, delamanid and clofazimine. In European Respiratory Journal (Vol. 48, Issue 5, pp. 1526–1527). European Respiratory Society. https://doi.org/10.1183/13993003.01207-2016

Wang, X., Cerrone, M., Ferretti, F., Castrillo, N., Maartens, G., McClure, M., & Boffito, M. (2019). Pharmacokinetics of dolutegravir 100 mg once daily with rifampicin. International Journal of Antimicrobial Agents, 54(2), 202–206. https://doi.org/10.1016/j.ijantimicag.2019.04.009

Wasserman, S., Davis, A., Stek, C., Chirehwa, M., Botha, S., Daroowala, R., Bremer, M., Maxebengula, M., Koekemoer, S., Goliath, R., Jackson, A., Crede, T., Naude, J., Szymanski, P., Vallie, Y., Moosa, M. S., Wiesner, L., Black, J., Meintjes, G., … Wilkinson, R. J. (2021). Plasma pharmacokinetics of high-dose oral versus intravenous rifampicin in patients with tuberculous meningitis: a randomized controlled trial. Antimicrobial Agents and Chemotherapy, 65(8). https://doi.org/10.1128/AAC.00140-21

Weber, W. W., & Hein, D. W. (1979). Clinical Pharmacokinetics of Isoniazid. Clinical Pharmacokinetics, 4(6), 401–422. https://doi.org/10.2165/00003088-197904060-00001

Weber, W. W., & Hein, D. W. (1985). N.-Acetylation Pharmacogenetics.

Wehrli, W. (1983). Rifampin: Mechanisms of Action and Resistance. Clinical Infectious Diseases, 5(Supplement_3), S407–S411. https://doi.org/10.1093/clinids/5.Supplement_3.S407

Wen, X., Wang, J. S., Neuvonen, P. J., & Backman, J. T. (2002). Isoniazid is a mechanism-based inhibitor of cytochrome P450 1A2, 2A6, 2C19 and 3A4 isoforms in human liver microsomes. European Journal of Clinical Pharmacology, 57(11), 799–804. https://doi.org/10.1007/s00228-001-0396-3

WHO. (2022). Global Tuberculosis report 2022. http://apps.who.int/bookorders.

Wimer, S. M., Schoonover, L., & Garrison, M. W. (1998). Levofloxacin: a therapeutic review. Clinical Therapeutics, 20(6), 1049–1070. https://doi.org/10.1016/S0149-2918(98)80104-5

World Health Organization. (2021a). Consolidated guidelines on HIV prevention, testing, treatment, service delivery and monitoring : recommendations for a public health approach.

World Health Organization. (2021b). Guidelines of HIV prevention, testing, treatment, service delivery and monitoring: (Issue July).

World Health Organization. (2022a). WHO consolidated guidelines on tuberculosis Module 4: Treatment Drug-resistant tuberculosis treatment 2022 update.

World Health organization. (2022). WHO operational handbook on tuberculosis Module 4: Treatment Drug-susceptible tuberculosis treatment.

World Health Organization. (2023). Global tuberculosis report 2023. https://iris.who.int/.

World Health Organization. (2024). 2024 Global tuberculosis report.

Wright, P. M. C. (1998). Population based pharmacokinetic analysis: why do we need it; what is it; and what has it told us about anaesthetics? In British Journal of Anaesthesia (Vol. 80).

Xu, Y., Zhou, Y., Hayashi, M., Shou, M., & Skiles, G. L. (2011). Simulation of clinical drug-drug interactions from hepatocyte CYP3A4 induction data and its potential utility in trial designs. Drug Metabolism and Disposition, 39(7), 1139–1148. https://doi.org/10.1124/dmd.111.038067

Yagura, H., Watanabe, D., Kushida, H., Tomishima, K., Togami, H., Hirano, A., Takahashi, M., Hirota, K., Ikuma, M., Kasai, D., Nishida, Y., Yoshino, M., Yamazaki, K., Uehira, T., & Shirasaka, T. (2017). Impact of UGT1A1 gene polymorphisms on plasma dolutegravir trough concentrations and neuropsychiatric adverse events in Japanese individuals infected with HIV-1. BMC Infectious Diseases, 17(1), 622. https://doi.org/10.1186/s12879-017-2717-x

Yang, J., Jamei, M., Yeo, K. R., Rostami-Hodjegan, A., & Tucker, G. T. (2007). Misuse of the well-stirred model of hepatic drug clearance. In Drug Metabolism and Disposition (Vol. 35, Issue 3, pp. 501–502). https://doi.org/10.1124/dmd.106.013359

Yano Ikuko, Ito Tatsuya, Takano Mikihisa, & Inui Ken-ichi. (1997). Evaluation of renal tubular secretion and reabsorption of levofloxacin in rats. Pharmaceutical Research, 14(4), 508–511. https://doi.org/10.1023/a:1012111902798

Zhang, C., Denti, P., Decloedt, E., Maartens, G., Karlsson, M. O., Simonsson, U. S. H., & Mcilleron, H. (2012a). Model-based approach to dose optimization of lopinavir/ritonavir when co-administered with rifampicin. British Journal of Clinical Pharmacology, 73(5), 758–767. https://doi.org/10.1111/j.1365-2125.2011.04154.x

Zhang, C., Denti, P., Decloedt, E., Maartens, G., Karlsson, M. O., Simonsson, U. S. H., & Mcilleron, H. (2012b). Model-based approach to dose optimization of lopinavir/ritonavir when co-administered with rifampicin. British Journal of Clinical Pharmacology, 73(5), 758–767. https://doi.org/10.1111/j.1365-2125.2011.04154.x

Zhang, J., Hayes, S., Sadler, B. M., Minto, I., Brandt, J., Piscitelli, S., Min, S., & Song, I. H. (2015). Population pharmacokinetics of dolutegravir in HIV-infected treatment-naive patients. British Journal of Clinical Pharmacology, 80(3), 502–514. https://doi.org/10.1111/bcp.12639

Zhang, Wei, C., Hop, C. E. C. A., Wright, M. R., Hu, M., Lai, Y., Khojasteh, S. C., & Humphreys, W. G. (2021). Intestinal Excretion, Intestinal Recirculation, and Renal Tubule Reabsorption Are Underappreciated Mechanisms That Drive the Distribution and Pharmacokinetic Behavior of Small Molecule Drugs. In Journal of Medicinal Chemistry (Vol. 64, Issue 11, pp. 7045–7059). American Chemical Society. https://doi.org/10.1021/acs.jmedchem.0c01720

Zhu, J.-Y., Leng, X.-S., Nan, D., Qi, G.-Y., & Ru-Yu, D. U. (1999). Measurement of liver volume and its clinical significance in cirrhotic portal hypertensive patients. World Journal of Gastroenterology, 5(6), 525–526. www.wjgnet.com

Zhu, P., Liu, J., Bess, J., Chertova, E., Lifson, J. D., Grisé, H., Ofek, G. A., Taylor, K. A., & Roux, K. H. (2006). Distribution and three-dimensional structure of AIDS virus envelope spikes. Nature, 441(7095), 847–852. https://doi.org/10.1038/nature04817

Zítková, L., & Toušek, J. (1974). Pharmacokinetics of Cycloserine and Terizidone. Chemotherapy, 20(1), 18–28. https://doi.org/10.1159/000221787

Appendix 1: Ethical approval

UNIVERSITY OF CAPE TOWN

FACULTY OF HEALTH SCIENCES
Human Research Ethics Committee

FHS017: Annual Progress Report / Renewal

Record Reviews/Audits/Collection of Biological Specimens/Repositories/Databases/Registries

HREC office use only (FWA00001637; IRB00001938)			
This serves as notification of annual approval, including any documentation described below.			
☐ Approved	Annual progress report	Approved until/next renewal date	30.8.2025
☐ Not approved	See attached comments		
Signature Chairperson of the HREC/ Designee		Date Signed	23/7/2024

Note: Please note that incomplete submitted will not be reviewed.
Our website address: **https://health.uct.ac.za/hothe/human-research-ethics**

HUMAN RESEARCH ETHICS COMMITTEE
23 JUL 2024
HEALTH SCIENCES FACULTY
UNIVERSITY OF CAPE TOWN

Please email this form and supporting documents (if applicable) in a combined pdf-file to hrec-enquiries@uct.ac.za.

Principal Investigator to complete the following:

1. Protocol information

Date (when submitting this form)	18-Jul-2024		
HREC REF Number	288/2022	Current Ethics Approval was granted until	30-Aug-2024
Protocol title	NONLINEAR MIXED EFFECTS MODELING OF DRUG INTERACTIONS BETWEEN ANTIRETROVIRAL THERAPY AND TUBERCULOSIS TREATMENT - Mr Allan Kengo		
Principal Investigator	Professor Paolo Denti		
Department and email address	Division of Clinical Pharmacology, K45, Old Main Building, Groote Schuur Hospital		
1.1 Does this protocol receive US Federal funding?		☐ Yes	✓ No

2. Protocol status (tick ✓)

✓	Research-related activities are ongoing
☐	Data collection is complete, data analysis only
☐	Publication or thesis submitted and final completion?
Please indicate (in the block below) the titles and HREC reference numbers of any projects currently making use of the Database/registry/repository	
Ongoing MSc student research.	

3. Protocol summary

Total number of records or specimens collected, reviewed or stored since the original approval		N/A
Total number of records or specimens collected, reviewed or stored since last progress report		N/A
Have any research-related outputs (e.g. publications, abstracts, conference presentations) resulted from this research? If yes, please list and attach with this report.	✓ Yes	☐ No
Please complete the Closure form (FHS019) if the study is completed within the approval period		

UNIVERSITY OF CAPE TOWN

FACULTY OF HEALTH SCIENCES
Human Research Ethics Committee

4. Signature

Signature of PI				Date	22 July 2024

Appendix 2: NONMEM scripts

SAEFRIF

Rifampicin

```
;; 1. Based on: run396f
;; 2. Description: SAEM, all participants
;; x1. Author: Allan
;------------------------------------------------------------------------
$SIZES PD=-1000 LVR=-150 LTH=-200 MAXFCN=10000000 LNP4=-150000
;------------------------------------------------------------------------
$PROBLEM RIF_MODEL
;------------------------------------------------------------------------
$INPUT ID DAT2=DROP TIME OCC WHAT=DROP EVID AMT DV ODV=DROP MDV
VPC_TIME BMI SEX AGE ART HT=DROP WT FFM FAT HIGHRIF SPARSE
TMAX=DROP BLQ CENS FLAG=DROP SWAP=DROP EFV PROP_ONLY_RIF
DRUG PROB
;------------------------------------------------------------------------
$DATA RIF_DATA_NM23e.csv IGNORE=@ IGNORE=(PROB.EQ.1)
;------------------------------------------------------------------------
$SUBROUTINE ADVAN15 TRANS1 TOL=5 ATOL=5 ;SSTOL=5 SSATOL=4
;------------------------------------------------------------------------
$ABBREVIATED DERIV2=NO ;COMRES=2 ; For Cmax
;------------------------------------------------------------------------
$MODEL NCOMPARTMENTS=3
COMP=(ABS DEFDOSE)
COMP=(CENTRAL DEFOBSERVATION)
COMP=(Liver)
;------------------------------------------------------------------------
$PK
; ------- BSV
BSVCL = ETA(1)
BOVKA = 0
IF (OCC==1)BOVKA = ETA(11)
IF (OCC==2)BOVKA = ETA(12)
BOVBIO = 0
IF (OCC==1)BOVBIO = ETA(13)
IF (OCC==2)BOVBIO = ETA(14)

BOVMTT = 0
IF (OCC==1)BOVMTT = ETA(15)
IF (OCC==2)BOVMTT = ETA(16)
; ------- Typical values of covariates use MEDIAN WEIGHT OF MY PPN
TVWT = 53
TVFAT = 11
TVFFM = 42
;--------- Allometric scaling and covariates
ALLMCL_WT = (WT/TVWT)**0.75
ALLMV_WT = (WT/TVWT)
ALLMCL_FAT = (FAT/TVFAT)**0.75
ALLMV_FAT = (FAT/TVFAT)
ALLMCL_FFM = (FFM/TVFFM)**0.75
ALLMV_FFM = (FFM/TVFFM)
;---liver
ALLMCL_WT_HEP = (WT/70)**0.75
ALLMV_WT_HEP = (WT/70)
ALLMCL_FFM_HEP = (FFM/56.1)**0.75
ALLMV_FFM_HEP = (FFM/56.1)
;----------------------log of allometric scaling
L_ALLMCL_WT = LOG(WT/TVWT)*0.75
L_ALLMV_WT = LOG(WT/TVWT)
;ALLMCL_FAT = (FAT/TVFAT)**0.75
;ALLMV_FAT = (FAT/TVFAT)
L_ALLMCL_FFM = LOG(FFM/TVFFM)*0.75
L_ALLMV_FFM = LOG(FFM/TVFFM)
;---liver
;ALLMCL_WT_HEP = (WT/70)**0.75
;ALLMV_WT_HEP = (WT/70)
L_ALLMCL_FFM_HEP = LOG(FFM/56.1)*0.75
L_ALLMV_FFM_HEP = LOG(FFM/56.1)
;---------Typical values--------------------------------------------------
;TVCL = THETA(1)*ALLMCL_FFM
MU_1 = THETA(1) + L_ALLMCL_FFM
;TVV = THETA(2)*ALLMV_FFM
MU_2 = THETA(2) + L_ALLMV_FFM
;TVKA = THETA(3)
MU_12 = THETA(3)
;;----proportion in FDC
PROP_FDC = 1 - PROP_ONLY_RIF
;;------splitting BIO
;----FOR BIO
BIO_RIF = 1
IF (HIGHRIF.EQ.1) BIO_RIF = PROP_FDC + (THETA(11)*PROP_ONLY_RIF)
L_BIO = LOG(BIO_RIF)
MU_14 = THETA(4) + L_BIO
MU_16 = THETA(5)
MU_6 = THETA(6)
;---------------------------HEPATIC CL-----------------------------------
-------;
MU_7 = THETA(7) + L_ALLMCL_FFM_HEP ;QH
MU_8 = THETA(8) ;FU
MU_9 = THETA(9)+ L_ALLMV_FFM_HEP ;VH
MU_10 = THETA(10) ;KM
eBOV = THETA(12) ;extra bioavailability on all absorption parameters
;----FOR BOVS
OCC1=0
IF(OCC.EQ.1)OCC1=eBOV
;-----------Define parameters-----------------------------------------------
-------------------------------------------------
CLINT = EXP(MU_1 + ETA(1))
 V = EXP(MU_2 + ETA(2))
KA = EXP(MU_12 + ETA(12)) * EXP(OCC1*ETA(11))
BIO = EXP(MU_14 + ETA(14)) * EXP(OCC1*ETA(13))
MTT = EXP(MU_16 + ETA(16)) * EXP(OCC1*ETA(15))
NN = EXP(MU_6 + ETA(6)) ; Number of transit compartments
QH = EXP(MU_7 + ETA(7))
FU = EXP(MU_8 + ETA(8))
VH = EXP(MU_9 + ETA(9))
;------saturation
KM = EXP(MU_10 + ETA(10))
VMAX = CLINT*KM
;------------------------------------------------------------------------
-------------------------------------------------
```

```
; Transit compartment absorption
F1=0 ;
KTR = (NN+1)/MTT ;
IF (NEWIND/=2.OR.EVID>=3) THEN ; new individual, or reset event
   ; The values read here will be stored in TDOS and PD in this very PK call.
        TNXD=TIME ; Time of the dose
        PNXD=AMT ; Amount. If it's zero, the DE is deactivated.
ENDIF
TDOS=TNXD ;
PD=PNXD
IF(AMT>0) THEN
; IF(AMT.GT.0.AND.ALAG1.EQ.0) THEN ;
        TNXD=TIME
        PNXD=AMT
ENDIF
PIZZA = LOG(BIO*PD*KTR + 1E-12) - GAMLN(NN+1)
;;;-----------------------------------------------------------------
A_0(1) = 1E-12 ; abs
A_0(2) = 1E-12 ; central
A_0(3) = 1E-12  ; liver
;;;-----------------------------------------------------------------

$DES
CH = A(3)/VH ; drug conc in liver
SAT_CL = VMAX / (CH + KM) ;C
EH = (SAT_CL*FU)/((SAT_CL*FU)+QH) ; fraction undergoing first pass extraction
FH  = 1 - EH ;fraction available after 1st pass to go to systemic circulation
; re-parameterization
K30 = (QH*EH/VH);(rate constant of elimination)
K32 = (QH*FH/VH)  ; (rate constant from central to peripheral 1)
K23 = (QH/V)
TEMPO = T-TDOS ; this is time after dose for the transit, it should always be >= 0
KTT = 0
TRANSIT = 0
IF(PD.GT.0.AND.TEMPO.GT.0) THEN
        KTT = KTR*(TEMPO)
        TRANSIT = EXP(PIZZA+NN*LOG(KTT)-KTT)
ENDIF
DADT(1) = TRANSIT - KA*A(1)  ; Abs
DADT(2) = K32*A(3) - K23*A(2)  ; central
DADT(3) = KA*A(1) + K23*A(2) - K30*A(3) - K32*A(3) ; liver
;-----------------------------------------------------------------
$ERROR
IPRED=A(2)/V
LLOQ = 0.25 ; DEFINE YOUR OWN LLOQ HERE
CENS_THR = LLOQ
PROP = IPRED*THETA(13)
ADD = THETA(14)+(CENS_THR*0.2)
IF (ICALL/=4.AND.CENS==1) THEN
        ADD = ADD +(CENS_THR*0.5)
ENDIF
NO_FIT = 0
IF (ICALL/=4.AND.CENS==2) THEN
        PROP = 0
        ADD = 10000000000
        NO_FIT = 1
ENDIF
W = SQRT(ADD**2+PROP**2)
IF (W.LE.0.000001) W=0.000001
IRES=DV-IPRED
IWRES=IRES/W
Y = IPRED + W*ERR(1)
IF (ICALL==4.AND.Y<=CENS_THR) Y = CENS_THR/2
IF(AMT>0) THEN
        TIMEDOSE = TIME
        AMOUNTDOSE = AMT
ENDIF
TAD = TIME-TIMEDOSE
VARCL = BSVCL ;+ BOVCL
VARBIO = BOVBIO
VARAUC = BOVBIO - BSVCL
;----------RETRIEVE AMOUNT IN EACH COMPARTMENT----------
AA1 = A(1)
AA2 = A(2)
AA3 = A(3)
;-----------------------------------------------------------------
$THETA
(-13.8, 4.91,7.5) ; 1 CLINT [log] [L/h]
(-13.8, 3.9,7) ; 2 V [log] [L]
(-13.8, 0.662,1.609) ; 3 KA [log][1/h]
(0) FIX ; 4 BIO [log]
(-3, -0.677,1.609) ; 5 MTT [log]
(-13.8, 2.68,3) ; 6 NN [log]
(4.5) FIX ; 7 QH [log]
(-1.61) FIX ; 8 FU [log]
(0) FIX ; 9 VH [log]
(-13.8, 1.9699) ; 10 KM [log] [mg/L]
(0, 0.675) ; 11 BIO_RIFcaps
(0, 2.2,10) ; 12 eBOV()
(0, 0.2245,1) ; 13 PROP []
(0, 0,1) FIX ; 14 ADD [mg/L]
;-----------------------------------------------
$OMEGA  BLOCK(1)
 0.0665 ;   1 BSV CL
$OMEGA  BLOCK(1) FIX
 0.001  ;   2 BSV V
$OMEGA  BLOCK(1) FIX
 0  ;  3 BSV KA
$OMEGA  BLOCK(1) FIX
 0  ;  4 BSV BIO
$OMEGA  BLOCK(1) FIX
 0.001  ;  5 BSVMTT
$OMEGA  BLOCK(1) FIX
 0.001  ;   6 BSVNN
$OMEGA  BLOCK(1) FIX
 0  ;   7 BSVQH
$OMEGA  BLOCK(1) FIX
 0  ;   8 BSVFU
$OMEGA  BLOCK(1) FIX
 0  ;   9 BSVVH
$OMEGA  BLOCK(1) FIX
 0.001  ;  10 BSVKM
;-----------------------------------------------------------------
$OMEGA  BLOCK(1)
 0.913 ;   11 BOVKA
```

```
$OMEGA  BLOCK(1) SAME
$OMEGA  BLOCK(1)
 0.0646 ;  13 BOVBIO
$OMEGA  BLOCK(1) SAME
$OMEGA  BLOCK(1)
0.649 ;  15 BOVMTT
$OMEGA  BLOCK(1) SAME
;-------------------------------------------------------------------------------
-----------------------------------------------
$SIGMA 1 FIX
;-------------------------------------------------------------------------------
-----------------------------------------------
$ESTIMATION METHOD=SAEM INTER NBURN=5000
NITER=2500 CTYPE=3 PRINT=1
AUTO=1 NOPRIOR=0
MUM=M(1,2,3,4,5,6,7,8,9,10):N(11,12):D(13,14) ; IF YOU
MU REFERENCE
GRD=TG(1-12):TS(13-14) ; MUST HAVE
$ESTIMATION METHOD=IMP INTER NITER=500
ISAMPLE=5000 EONLY=1 NOPRIOR=0
PRINT=1 MAPITER=0 CTYPE=3
MUM=M(1,2,3,4,5,6,7,8,9,10):N(11,12):D(13,14) ; IF YOU
MU REFERENCE
GRD=TG(1-12):TS(13-14) ; MUST HAVE
;-------------------------------------------------------------------------------
-----------------------------------------------
$TABLE WRESCHOL ID OCC
MDV TIME TAD AA1 AA2 AA3 ;AA4
Y DV PRED RES WRES IPRED IRES IWRES CWRES CWRESI
OBJI NPDE
VPC_TIME NOPRINT NOAPPEND ONEHEADER FORMAT=,
ESAMPLE=1000
FILE=sdtab400.csv
;-------------------------------------------------------------------------------
-----------------------------------------------
$TABLE ID OCC
MDV CLINT V KA BIO MTT NN ;AUC ;FU QH;V3 Q V4 Q2
BSVCL ;BSVV BSVKA BSVBIO BSVV3 BSVQ BSVV4 BSVQ2
BOVKA BOVBIO BOVMTT ;BOVCL
VARCL VARBIO VARAUC NOPRINT NOAPPEND
ONEHEADER FORMAT=,
FILE=patab400.csv
;-------------------------------------------------------------------------------
-----------------------------------------------
$TABLE ID OCC
HIGHRIF EFV SEX ART SPARSE NOPRINT NOAPPEND
ONEHEADER FORMAT=, FILE=catab400.csv
;-------------------------------------------------------------------------------
-----------------------------------------------
$TABLE ID OCC
MDV WT AGE FFM FAT VPC_TIME NOPRINT NOAPPEND
ONEHEADER FORMAT=, FILE=cotab400.csv
;-------------------------------------------------------------------------------
-----------------------------------------------
$TABLE ID OCC
MDV TIME TAD AA1 AA2 AA3 ;AA4
Y DV PRED RES WRES IPRED IRES IWRES CWRES CWRESI
OBJI NPDE
CLINT V KA BIO MTT NN ;FU QH;V3 Q V4 Q2
BSVCL ;BSVV BSVKA BSVBIO BSVV3 BSVQ BSVV4 BSVQ2
BOVKA BOVBIO BOVMTT ;BOVCL
VARCL VARBIO VARAUC WT AGE FFM FAT VPC_TIME SEX
HIGHRIF
EFV ;
NOPRINT NOAPPEND ONEHEADER FORMAT=,
FILE=mytab400.csv
;-------------------------------------------------------------------------------
-----------------------------------------------
;-------------------------------------------------------------------------------
-----------------------------------------------
```

Dolutegravir

```
;; 1. Based on: run353
;; 2. Description: AUC_RIF effect
;; x1. Author: Allan
;-------------------------------------------------------------------------------
$SIZES PD=-1000 LVR=-150 LTH=-200
MAXFCN=10000000 LNP4=-150000
;-------------------------------------------------------------------------------
$PROBLEM    DTG_MODEL
;-------------------------------------------------------------------------------
$INPUT      ID DAT2=DROP TIME OCC WHAT=DROP EVID
AMT DV ODV=DROP MDV
        VPC_TIME BMI SEX AGE ART HT WT FFM=DROP
FAT=DROP HIGHRIF HERBAL
        ALCOHOL MULTIVIT FERROUS ANTIACID VOMITED
DIARRHEA
        JOINTPAIN SKINRASH NEUROPATHY SPARSE
TMAX=DROP BLQ CENS
        FLAG MISS SWAP=DROP FIXED_IN_R=DROP PROB
UGT GENE AUC_RIF3
;-------------------------------------------------------------------------------
$DATA     DTG_DATA_NM14.csv IGNORE=@
IGNORE=(FLAG==3) ; will not see 3.0!!!
IGNORE=(FLAG==4)
IGNORE=(FLAG==1)
IGNORE=(PROB==1)
;-------------------------------------------------------------------------------
$SUBROUTINE ADVAN13 TRANS1 TOL=9 ATOL=9 SSTOL=3
SSATOL=3
;-------------------------------------------------------------------------------
$ABBREVIATED COMRES=2 ; For Cmax
;-------------------------------------------------------------------------------
$MODEL     NCOMPARTMENTS=3 ; 4
        COMP=(ABS DEFDOSE)
                                    COMP=(CENTRAL
DEFOBSERVATION)
        COMP=(AUC) ; you make an extra compartment
which fills up from the central to calculate AUC
;-------------------------------------------------------------------------------
---
$PK
SMALL =  1E-6
; ------- BSV
BSVCL   = ETA(1)
BSVV   = ETA(2)
BSVKA   = ETA(3)
BSVBIO = ETA(4)
BSVV3 = ETA(5)
BSVQ = ETA(6)
BSVV4 = ETA(7)
BSVQ2 = ETA(8)
BSVMTT = ETA(9)
; ---------- BOV
BOVCL = 0
IF (OCC==1)BOVCL = ETA(10)
```

```
IF (OCC==2)BOVCL=ETA(11)
BOVBIO = 0
IF (OCC==1)BOVBIO = ETA(12)
IF (OCC==2)BOVBIO=ETA(13)
BOVKA = 0
IF (OCC==1)BOVKA = ETA(14)
IF (OCC==2)BOVKA=ETA(15)
BOVLAG = 0
IF (OCC==1)BOVLAG = ETA(16)
IF (OCC==2)BOVLAG=ETA(17)
BOVMTT = 0
IF (OCC==1)BOVMTT = ETA(18)
IF (OCC==2)BOVMTT=ETA(19)
;--------------------------------------
eBOV = THETA(12)  ;extra bioavailability on all absorption
parameters
IF (SPARSE.EQ.1) THEN
BOVKA=eBOV*BOVKA
BOVMTT=eBOV*BOVMTT
BOVBIO=eBOV*BOVBIO
ENDIF
;------ Typical values of covariates use MEDIAN WEIGHT
OF MY PPN
TVWT = 56
TVFAT = 13
TVFFM = 43
;--------- Allometric scaling and covariates
; ---------- Calculation of Fat-free Mass
; These formulas require WT in KG and HT in m !!!
; Conversion from cm to m
HTM = HT/100
IF (SEX.EQ.0) THEN  ; female
              WHSMAX=37.99
              WHS50=35.98
ELSE       ;males
              WHSMAX=42.92
              WHS50=30.93
ENDIF
HTM2 = HTM**2
FFM = (WHSMAX*HTM2*WT)/(WHS50*HTM2+WT)
FAT = WT-FFM
ALLMCL_WT = (WT/TVWT)**0.75
ALLMV_WT = (WT/TVWT)
 ALLMCL_FAT = (FAT/TVFAT)**0.75
ALLMV_FAT = (FAT/TVFAT)
 ALLMCL_FFM = (FFM/TVFFM)**0.75
ALLMV_FFM = (FFM/TVFFM)
;-------------------------------------------------
;---------testing AUC

RIF_AUC_M = 32.29

RIF_AUC_EFF = 1 + (THETA(15)*(AUC_RIF3-RIF_AUC_M))

;---------Typical values-------------------------------------------------
-------------
; Covariate test: HIGHRIF on CL
TVCL = THETA(1)*ALLMCL_FFM ;Reference 10mg/kg
TVV = THETA(2)*ALLMV_FFM
TVKA = THETA(3)
TVBIO = THETA(4)*RIF_AUC_EFF
TVLAG = THETA(7)
TVV3 = THETA(8);*ALLMV_WT
TVQ = THETA(9);*ALLMCL_WT
TVV4 = THETA(10);*ALLMV_WT
TVQ2 = THETA(11);*ALLMCL_WT
TVMTT = THETA(13)
TVNN = THETA(14)
;-----------Define parameters-----------------------------
CL  = TVCL*EXP(BSVCL+BOVCL) ; CLEARANCE
V   = TVV*EXP(BSVV) ; CENTRAL VOL.
KA  = TVKA*EXP(BSVKA+BOVKA) ; ABS. RATE CONSTANT
BIO = TVBIO*EXP(BSVBIO+BOVBIO) ; BIOAVAILABILITY
LAG =TVLAG*EXP(BOVLAG) ; LAG TIME
V3 = TVV3*EXP(BSVV3) ; PERIPH VOL
Q = TVQ*EXP(BSVQ) ; INTER COMPT CL
V4 = TVV4*EXP(BSVV4) ; PERIPH VOL
Q2 = TVQ2*EXP(BSVQ2) ; INTER COMPT CL
MTT =TVMTT*EXP(BSVMTT+BOVMTT)
NN = TVNN


;-------------------------------------------------------------------------
---------------------------
;---------------------- re-parameterization
K = CL/V ;(rate constant of elimination)
K23 = Q/V   ; (rate constant from central to peripheral 1)
K32 = Q/V3 ;(rate constant from peripheral 1 to central)
K24 = Q2/V ;(rate constant from central to peripheral 2)
K42 = Q2/V4 ; (rate constant from peripheral 2 to central)
S2 = V
F1=0
KTR = (NN+1)/MTT
IF (NEWIND/=2.OR.EVID>=3) THEN
TNXD=TIME
PNXD=AMT
ENDIF
TDOS=TNXD
PD=PNXD
IF(AMT>0) THEN
TNXD=TIME
PNXD=AMT
ENDIF
PIZZA = LOG(BIO*PD*KTR + 1E-12) - GAMLN(NN+1)
;-------------------------------------------------------------------------
--
A_0(1) = SMALL
A_0(2) = SMALL
;-------------------------------------------------------------------------
--
;-----AUC calculation------
IF (NEWIND.NE.2.OR.EVID.GE.3) THEN ; Each time I have
a new subject, or a reset
              COM(1)=0
              COM(2)=0
              TDOS = 0
ENDIF
;-------------------------------------------------------------------------
-------
$DES
TEMPO = T-TDOS
KTT = 0
TRANSIT = 0
IF(PD.GT.0.AND.TEMPO.GT.0) THEN
KTT = KTR*(TEMPO)
TRANSIT = EXP(PIZZA+NN*LOG(KTT)-KTT)
```

```
ENDIF
DADT(1) = TRANSIT -KA*A(1)
DADT(2) = KA*A(1) -K*A(2)
;-------------------------------------------------------------------------------
--
;------------AUC and Cmax----------
CC = A(2)/V   ; v or v2?
IF(TIME.GT.0.AND.CC.GT.COM(1)) THEN ; This will only look at the Cmax after 0h, e.g. steady state in my case (the patients are already at SS due to imputed doses. AUC cmt from dose + 23.99 h)
COM(1) = CC
ENDIF
;COM resflects the central compartent (concentration)
TSS1 = 0
IF(T.GT.0) TSS1=1 ; This will open up the A(4) cmt at 0h, you can change these times to the AUC period you want
IF(T.GT.11.99) TSS1=0 ;This will close the A(4) cmt at 23.99 hours later
DADT(3) = CC*TSS1
;-------------------------------------------------------------------------------
---
$ERROR
AUC = A(3) ; You need to save the AUC. The amount in this cmt will keep increasing as long as TSS1 is still 1. When TSS1=0 the amount in the AUC cmt will remain the same.
CMAX = COM(1) ; You need this to save the Cmax
AUCINF = BIO*50/CL ; Check your code where your DOSE/AMT is in
IPRED=A(2)/V
LLOQ = 0.05 ; DEFINE YOUR OWN LLOQ HERE
CENS_THR = LLOQ
PROP = IPRED*THETA(5)
ADD = THETA(6)+(CENS_THR*0.2)
IF (ICALL/=4.AND.CENS==1) THEN
        ADD = ADD +(CENS_THR*0.5)
ENDIF
NO_FIT = 0
IF (ICALL/=4.AND.CENS==2) THEN
        PROP = 0
        ADD = 10000000000
        NO_FIT = 1
ENDIF
W = SQRT(ADD**2+PROP**2)
IF (W.LE.0.000001) W=0.000001
IRES=DV-IPRED
IWRES=IRES/W
Y = IPRED + W*ERR(1)
IF (ICALL==4.AND.Y<=CENS_THR) Y = CENS_THR/2
IF(AMT>0) THEN
        TIMEDOSE = TIME
        AMOUNTDOSE = AMT
ENDIF
TAD = TIME-TIMEDOSE
VARCL = BSVCL + BOVCL
VARBIO = BSVBIO + BOVBIO
VARAUC = BSVBIO + BOVBIO - BSVCL - BOVCL
VARABS = BOVKA + BSVKA-BSVMTT - BOVMTT
;-----------------------------------------RETRIEVE AMOUNT IN EACH COMPARTMENT----------
AA1 = A(1)
AA2 = A(2)
;----------
```

```
$THETA  (0,1.82432,90) ; 1 CL [L/h]
 (0,12.1293,800) ; 2 V [L]
 (0,1.41849,5) ; 3 KA [1/h]
 1 FIX ; 4 BIO
 (0,0.100404,0.5) ; 5 PROP []
 (0,0.205657,1) ; 6 ADD [mg/L]
 0 FIX ; 7 LAG
 (0,0,800) FIX ; 8 V3 [L]
 (0,0,90) FIX ; 9 Q [L/h]
 (0,0,800) FIX ; 10 V4 [L]
 (0,0,90) FIX ; 11 Q2 [L/h]
 (0,1.55283,10) ; 12 eBOV
 (0,0.580239,5) ; 13 TVMTT [L]
 (0,21.4516,50) ; 14 TVNN [L/h]
 (-0.00499,-0.00237992,0.15197) ; 15  RIF_AUC_EFF
 ;-----------------------------------
$OMEGA  BLOCK(1)
 0.0175156  ;   1 BSV CL
$OMEGA  BLOCK(1) FIX
 0  ;    2 BSV V
$OMEGA  BLOCK(1) FIX
 0  ;   3 BSV KA
$OMEGA  BLOCK(1) FIX
 0  ;  4 BSV BIO
$OMEGA  BLOCK(1) FIX
 0  ;    5 BSVV3
$OMEGA  BLOCK(1) FIX
 0  ;     6 BSVQ
$OMEGA  BLOCK(1) FIX
 0  ;   7 BSVV4
$OMEGA  BLOCK(1) FIX
 0  ;   8 BSVQ2
$OMEGA  BLOCK(1) FIX
 0  ;  9 BSVMTT
;-------------------------------------------
$OMEGA  BLOCK(1) FIX
 0  ;   10 BOVCL
$OMEGA  BLOCK(1) SAME
;---------------------------------------
$OMEGA  BLOCK(1)
 0.170507  ;  12 BOVBIO
$OMEGA  BLOCK(1) SAME
;-----------------------------------------
$OMEGA  BLOCK(1)
 1.07642  ;   14 BOVKA
$OMEGA  BLOCK(1) SAME
;-------------------------------------------------
$OMEGA  BLOCK(1) FIX
 0  ;  16 BOVLAG
$OMEGA  BLOCK(1) SAME
;-------------------------------------------------
$OMEGA  BLOCK(1)
 0.226506  ;  18 BOVMTT
$OMEGA  BLOCK(1) SAME
;-------------------------------------------------
$SIGMA  1  FIX
;-------------------------------------------------
$ESTIMATION  MSFO=run354.msf  MAXEVAL=0  PRINT=1 METHOD=1 INTER NOABORT
NSIG=3  NONINFETA=1  ETASTYPE=1  MCETA=1000 RANMETHOD=4P ; REPEAT
$ESTIMATION  MSFO=run354.msf  MAXEVAL=9999 PRINT=1 METHOD=1 INTER
```

```
NOABORT NSIG=3 NONINFETA=1 ETASTYPE=1 MCETA=10
RANMETHOD=4P ; REPEAT
$COVARIANCE PRINT=E ; MATRIX=S
;-------------------------------------------------------------------------
-----
$TABLE WRESCHOL ID OCC TIME TAD AA1 AA2 ; AA3 AA4
Y DV PRED RES WRES IPRED IRES IWRES CWRES CWRESI
OBJI
VPC_TIME SPARSE MDV NOPRINT NOAPPEND
ONEHEADER FORMAT=,
FILE=sdtab354.csv
;--------------------------------------
$TABLE ID OCC CL V KA BIO MTT NN AUC ;V3 Q V4 Q2
BSVCL ;BSVKA BSVBIO BSVV3 BSVQ BSVV4 BSVQ2
BOVKA BOVBIO BOVMTT ;BOVCL
VARCL VARBIO VARAUC NOPRINT NOAPPEND
ONEHEADER FORMAT=,
FILE=patab354.csv
;-----------------------------------------
$TABLE ID OCC WT HT AGE FFM FAT V BMI VPC_TIME AUC
CMAX AUCINF CC
NOPRINT NOAPPEND ONEHEADER FORMAT=,
FILE=cotab354.csv
;-----------------------------------------
$TABLE ID OCC UGT GENE SEX HIGHRIF HERBAL ALCOHOL
ART MULTIVIT FERROUS
ANTIACID VOMITED DIARRHEA JOINTPAIN SKINRASH
NEUROPATHY
SPARSE NOPRINT NOAPPEND ONEHEADER FORMAT=,
FILE=catab354.csv
;-----------------------------------------
$TABLE ID OCC TIME TAD AA1 AA2 ; AA3 AA4
Y DV PRED RES WRES IPRED IRES IWRES CWRES CWRESI
OBJI UGT GENE
SPARSE MDV CL V KA BIO MTT NN ;V3 Q V4 Q2
BSVCL ;BSVKA BSVBIO ;BSVV3 BSVQ BSVV4 BSVQ2
BOVKA BOVBIO BOVMTT ;BOVCL
VARCL VARBIO VARAUC WT HT AGE FFM FAT VPC_TIME
AUC CMAX
AUCINF CC BMI SEX HIGHRIF HERBAL ALCOHOL MULTIVIT
FERROUS
ANTIACID VOMITED DIARRHEA JOINTPAIN SKINRASH
NEUROPATHY
ART NOPRINT NOAPPEND ONEHEADER FORMAT=,
FILE=mytab354.csv
;-------------------------------------------------------------------------
-----------------------------------------------
;-------------------------------------------------------------------------
-----------------------------------------------
```

DERIVE
Atazanavir

```
;; 1. Based on: 090
;; 2. Description: + Unfix plasma
;; x1. Author: allan
;; 2022-09-23
; Settings for the memory of NONMEM
;-------------------------------------------------------------------------------
$SIZES      PD=-1000 LVR=-150 LTH=-200
MAXFCN=10000000 LNP4=-150000
;-------------------------------------------------------------------------------
$PROBLEM    VIRTUAL_ATV
;-------------------------------------------------------------------------------
$ABBREVIATED DERIV2=NO
;-----------------------------------------------
$ABBREVIATED COMRES=2
;-------------------------------------------------------------------------------
$INPUT      ID VISIT OCC DAT2=DROP TIME EVID AMT
PK_HR=DROP EVENING
        MDV OBS DV ATV_PBMC RTV_PBMC DVID BLQ
CENS FLAG PROB
        CMT=DROP VPC_TIME WEIGHT HEIGHT SEXM
AGE VIRAL_LOAD
        CONCOMITANT_MEDS DTG RIF FASTING_3H
FOOD_X3 FOOD_X2
        FOOD_X1 DOSE_SKIPPED_X3 DOSE_SKIPPED_X2
DOSE_SKIPPED_X1
        ATV DV_RTV=DROP RTV DV_DTG=DROP
DV_RIF=DROP COMMENT=DROP
        ID_VISIT=DROP CONCOMITANT
CONC_DRUG=DROP
        CONC_DRUG_TIME=DROP ALT AST GGT
BILIRUBIN_TOTAL
        SERUM_CREATININE ALBUMIN TOTAL_PROTEIN
AUC_RTV AUC_RTV2
        AUC_RTV3 CHOLESTEROL BETA_CHOLESTEROL
BETA_TO_CHOL
        CHOL_TO_BETA BACK_BONE ABC TDF AZT
REG=DROP REGIMEN=DROP
;-------------------------------------------------------------------------------
$DATA      VIRTUAL_data_ATV_12.csv IGNORE=#
IGNORE=(PROB==1)

;IGNORE=(DVID==2)

;-----------------------------------------------
$SUBROUTINE ADVAN13 TRANS1 ; 2 compartment
        TOL=9 ATOL=9
;-------------------------------------------------------------------------------
$MODEL      NCOMPARTMENTS=4 COMP=(ABS DEFDOSE)
        COMP=(CENTRAL DEFOBSERVATION) ;
COMP=(CENTRAL DEFOBSERVATION)
        COMP=(PERIPH) ; you make an extra
compartment which fills up from the central to calculate
AUC
        COMP=(PBMC)
; ;-------------------------------------------------------------------------------
$PK
SMALL = 1E-6
; ------- BSV
BSVCL   = ETA(1)
BSVV    = ETA(2)
BSVKA   = ETA(3)
BSVBIO  = ETA(4)
BSVV3   = ETA(5)
BSVQ = ETA(6)
BSVV4 = ETA(7)
BSVQ2 = ETA(8)
BSVMTT = ETA(9)
;------for effect cmpt
BSVKE0  = ETA(46)
BSVPPC  = ETA(47)
; ---------- BOV
BOVCL = 0
IF (OCC==1)BOVCL = ETA(10)
IF (OCC==2)BOVCL = ETA(11)
IF (OCC==3)BOVCL = ETA(12)
IF (OCC==4)BOVCL = ETA(13)
IF (OCC==5)BOVCL = ETA(14)
IF (OCC==6)BOVCL = ETA(15)
IF (OCC==7)BOVCL = ETA(16)
IF (OCC==8)BOVCL = ETA(17)

BOVBIO = 0
IF (OCC==1)BOVBIO = ETA(18)
IF (OCC==2)BOVBIO = ETA(19)
IF (OCC==3)BOVBIO = ETA(20)
IF (OCC==4)BOVBIO = ETA(21)
IF (OCC==5)BOVBIO = ETA(22)
IF (OCC==6)BOVBIO = ETA(23)
IF (OCC==7)BOVBIO = ETA(24)
IF (OCC==8)BOVBIO = ETA(25)
BOVKA = 0
IF (OCC==1)BOVKA = ETA(26)
IF (OCC==2)BOVKA = ETA(27)
IF (OCC==3)BOVKA = ETA(28)
IF (OCC==4)BOVKA = ETA(29)
IF (OCC==5)BOVKA = ETA(30)
IF (OCC==6)BOVKA = ETA(31)
IF (OCC==7)BOVKA = ETA(32)
IF (OCC==8)BOVKA = ETA(33)
BOVMTT = 0
IF (OCC==1)BOVMTT = ETA(34)
IF (OCC==2)BOVMTT = ETA(35)
IF (OCC==3)BOVMTT = ETA(36)
IF (OCC==4)BOVMTT = ETA(37)
IF (OCC==5)BOVMTT = ETA(38)
IF (OCC==6)BOVMTT = ETA(39)
IF (OCC==7)BOVMTT = ETA(40)
IF (OCC==8)BOVMTT = ETA(41)

;----------between visit variability
BVVCL = 0
IF (VISIT == 1)BVVCL = ETA(42)
IF (VISIT == 2)BVVCL = ETA(43)
IF (VISIT == 3)BVVCL = ETA(44)
IF (VISIT == 4)BVVCL = ETA(45)
;----------------
SCALE_BOV = THETA(10)  ;extra bioavailability on all
absorption parameters
IF (OBS.EQ.0) THEN
```

```
BOVKA=SCALE_BOV*BOVKA
BOVMTT=SCALE_BOV*BOVMTT
BOVBIO=SCALE_BOV*BOVBIO
ENDIF

; ---------- Calculation of Fat-free Mass
; These formulas require WT in KG and HT in m !!!
HTM = HEIGHT/100
WT = WEIGHT
SEX = SEXM

IF (SEX.EQ.0) THEN  ; female
 WHSMAX=37.99
 WHS50=35.98
ELSE       ;males
 WHSMAX=42.92
 WHS50=30.93
ENDIF
HTM2 = HTM**2
FFM = (WHSMAX*HTM2*WT)/(WHS50*HTM2+WT)
FAT = WT-FFM

IF (FAT.LT.0) FAT = 0
; ------- Typical values of covariates use MEDIAN WEIGHT
OF MY PPN
TVWT = 67
TVFAT = 25
TVFFM = 42
;--------- Allometric scaling and covariates
ALLMCL_WT = (WT/TVWT)**0.75
ALLMV_WT = (WT/TVWT)
ALLMCL_FAT = (FAT/TVFAT)**0.75
ALLMV_FAT = (FAT/TVFAT)
ALLMCL_FFM = (FFM/TVFFM)**0.75
ALLMV_FFM = (FFM/TVFFM)
;----------Allometry for liver
ALLMCL_WT_HEP = (WT/70)**0.75
ALLMV_WT_HEP = (WT/70)
ALLMCL_FFM_HEP = (FFM/56.1)**0.75
ALLMV_FFM_HEP = (FFM/56.1)
;----------covariates
;;Covariate test: RTV_CL
MEDIAN_AUC24_RTV = 7.0923

; RTV_CL =1;no RTV
; IF(RTV.EQ.1)
RTVAUC_CL = 1 + THETA(11)*(AUC_RTV2 -
MEDIAN_AUC24_RTV) ;Inter

;   Min. 1st Qu.  Median    Mean 3rd Qu.    Max.
 ; 0.874   3.380   7.240   7.095   9.680  23.200
;For stratifying VPC
VISIT_DVID = VISIT + 10*DVID

;;Different CL for every visit:
CL_VISIT = 1;no RTV
IF(VISIT.EQ.2) CL_VISIT = 1 + THETA(12);Inter
IF(VISIT.GE.3) CL_VISIT = 1 + THETA(13);Inter
;IF(VISIT.EQ.4) CL_VISIT = THETA(14);Inter

 BIO_VISIT = THETA(4);
IF(VISIT.EQ.2) BIO_VISIT = THETA(14);v2

;;Different KA for visits with RIF
RIF_KA = 1;no RTV
IF(RIF.EQ.1) RIF_KA = 1 + THETA(16);Inter



;---------Typical values----------------------------------------------
-------------------------------------------------------------------------
------------------------------
TVCL = THETA(1) * ALLMCL_FFM * CL_VISIT *
RTVAUC_CL;*NAT2_CL*CFZ_CL ;
TVV = THETA(2) * ALLMV_FFM
TVKA = THETA(3) * RIF_KA
TVBIO = BIO_VISIT
TVMTT = THETA(7) ;* MTT_VISIT
TVNN = THETA(15)
TVV3 = THETA(8)*ALLMV_FFM
TVQ = THETA(9)*ALLMCL_FFM
;------for effect cmpt
TVKE0 = THETA(17)
TVPPC = THETA(18)
;----------Define parameters-------------------------------------
-------------------------------------------------------------------------
-------------------------
CL  = TVCL*EXP(BSVCL+BOVCL+BVVCL) ; CLEARANCE
V   = TVV*EXP(BSVV) ; CENTRAL VOL.
KA  = TVKA*EXP(BSVKA+BOVKA) ; ABS. RATE CONSTANT
BIO = TVBIO*EXP(BSVBIO+BOVBIO) ; BIOAVAILABILITY
MTT = TVMTT*EXP(BSVMTT+BOVMTT) ; MTT TIME
NN = TVNN ; Number of transit compartments
V3 = TVV3*EXP(BSVV3) ; PERIPH VOL
Q = TVQ*EXP(BSVQ) ; INTER COMPT CL

;-------for effect compartment
KE0 = TVKE0 * EXP(BSVKE0)
PPC = TVPPC * EXP(BSVPPC)



;-------------------------------------------------------------------------
-------------------------------------------------------------------------
; re-parameterization
K = CL/V ;(rate constant of elimination)
K23 = Q/V   ; (rate constant from central to peripheral 1)
K32 = Q/V3 ;(rate constant from peripheral 1 to central)

; Transit compartment absorption
F1=0 ; I need to set bioavailability in compartment 1 to 0
for this implementation of the transit compartment
absorption

KTR = (NN+1)/MTT ; The number of actual transit
compartments is NN+1, so this number can never be 0

IF (NEWIND/=2.OR.EVID>=3) THEN ; new individual, or
reset event
   ; The values read here will be stored in TDOS and PD in
this very PK call.
            TNXD=TIME ; Time of the dose
```

```
        PNXD=AMT ; Amount. If it's zero, the DE is
deactivated.
ENDIF

TDOS=TNXD ; This will either save here the temporary
values if it's a new individual...
PD=PNXD ; ...or the values which were read one record
ahead during the execution of the previous record.

IF(AMT>0) THEN ; This reads one record ahead and
stores the data to be used when running the following
record
        TNXD=TIME
        PNXD=AMT
ENDIF

; To speed up the computation, I calculate here all the
non-time-varying quantities used in $DES
PIZZA = LOG(BIO*PD*KTR + 1E-12) - GAMLN(NN+1)  ;
without +0.00001, it won't work with ETAs in
bioavailability




;;--------------------------------------------------------------------
A_0(1) = SMALL
A_0(2) = SMALL
A_0(3) = SMALL
A_0(4) = SMALL; PBMC



;;;--------------------------------------------------------------------
$DES

C2 = A(2)/V ; state this as it is used for the DE of pbmc
CMT
TEMPO = T-TDOS ; this is time after dose for the transit,
it should always be >= 0
KTT = 0
TRANSIT = 0
IF(PD.GT.0.AND.TEMPO.GT.0) THEN ; This happens only
id PD>0, so only if a dose has been detected
        KTT = KTR*(TEMPO)
        TRANSIT = EXP(PIZZA+NN*LOG(KTT)-KTT)
ENDIF

DADT(1) = TRANSIT - KA*A(1)

DADT(2) = KA*A(1) - K*A(2) + K32*A(3) - K23*A(2)
DADT(3) = K23*A(2) - K32*A(3)

DADT(4) = KE0*(PPC*C2 - A(4)) ;A(4) IS ACTUALLY CONC
IN EFFECT CMT

$ERROR
IPRED_P=A(2)/V
HALF_L = LOG(2)/KE0

; DEFINE LLOQ VALUE
LLOQ_P = 0.03 ; DEFINE YOUR OWN LLOQ HERE
LLOQ_C = 0.015 ; DEFINE YOUR OWN LLOQ HERE

CENS_THR_P = LLOQ_P
;CENS_THR =0.3*LLOQ ; check the readme section


PROP_P = IPRED_P*THETA(5)
ADD_P = THETA(6)+(CENS_THR_P*0.2)
; For CENS==1 (i.e. first CENSORED value in a series,
which was imputed to CENS_THR/2), we add extra
additive error on the concentrations,
; since the value in DV has been imputed and therefore
more uncertain.
IF (ICALL/=4.AND.CENS==1) THEN
 ADD_P = ADD_P +(CENS_THR_P*0.5)
ENDIF

NO_FIT = 0
; For CENS==2 (i.e. the trailing CENSORED values in a
series that were imputed to CENS_THR/2), we don't
want these to influence the fit,

IF (ICALL/=4.AND.CENS==2) THEN
 PROP_P = 0
 ADD_P = 10000000000
 NO_FIT = 1
ENDIF

W_P = SQRT(ADD_P**2+PROP_P**2)

;------PBMC
CC = A(4)
CENS_THR_C = LLOQ_C

IPRED_C = CC
PROP_C  = IPRED_C * THETA(19)
ADD_C   = THETA(20) + (0.2*CENS_THR_C)

IF(ICALL/=4.AND.CENS==1.AND.DVID==4) THEN
 ADD_C = ADD_C + (LLOQ_C*0.5)
 ENDIF

IF (ICALL/=4.AND.CENS==2.AND.DVID==4) THEN
 PROP_C = 0
 ADD_C = 10000000000
 NO_FIT = 1
ENDIF

W_C = SQRT(ADD_C**2+PROP_C**2)

  ERROR_P = W_P * ERR(1)
  ERROR_C = W_C * ERR(1)

;Redefine IPRED & weighting-----------------------------------
--------------------------------------------------------------------
-------------------------
  IPRED = IPRED_P
  W = W_P
  ERROR_TERM = ERROR_P

  IF(DVID==2) THEN
  IPRED = IPRED_C
 W = W_C
  ERROR_TERM = ERROR_C
```

```
  ENDIF

; Protective code
IF (W.LE.0.000001) W=0.000001

IRES=DV-IPRED
IWRES=IRES/W

Y = IPRED + ERROR_TERM
; To prevent simulation (ICALL==4) of negative values. It
set a positive lower bound for Y, so that VPCs in the log-
scale can be plotted
IF (DVID==1.AND.ICALL==4.AND.Y<=LLOQ_P)
Y=LLOQ_P/2
IF (DVID==2.AND.ICALL==4.AND.Y<=LLOQ_C)
Y=LLOQ_C/2
; To calculate time after dose.
IF(AMT>0) THEN
 TIMEDOSE = TIME
 AMOUNTDOSE = AMT
ENDIF

TAD = TIME-TIMEDOSE
IF(VISIT==1.AND.DVID==2) TAD = 25.5
IF(VISIT==2.AND.DVID==2) TAD = 15
IF(VISIT==3.AND.DVID==2) TAD = 15
IF(VISIT==4.AND.DVID==2) TAD = 15

VARCL = BSVCL + BOVCL
VARBIO = BSVBIO + BOVBIO
VARAUC = BSVBIO + BOVBIO - BSVCL - BOVCL
VARABS = BOVKA + BSVKA - BSVMTT - BOVMTT
;----------RETRIEVE AMOUNT IN
EACH COMPARTMENT----------
AA1 = A(1)
AA2 = A(2)
AA3 = A(3)
AA4 = A(4)

;----------
$THETA  (0,7.55,50)  ; 1 CL_1 [L/h]
 (0,79.0582,300)  ; 2 V [L]
 (0,6,10)  FIX; 3 KA [1/h]
 1 FIX ; 4 BIO
 (0,0.188663,0.5)  ; 5 PROP []
 0 FIX ; 6 ADD [mg/L]
 (0,0.514785,10)  ; 7 MTT
 (0,46.7027,300)  ; 8 V3 [L]
 (0,3.21354,50)  ; 9 Q [L/h]
 (0,1.70998,5)  ; 10 SCALE_BOV
 (-0.0616,0,1502) FIX ; 11 RTVAUC_CL
 (-0.99,2.08781,10)  ; 12 CL_2 [L/h]
 (-0.99,1.01864,10)  ; 13 CL_3/4 [L/h]
 (0,0.480537)  ; 14 BIO_VISIT2
 (0,10,50) FIX ; 15 NN
 (-0.99,-0.784495,10)  ; 16 RIF_KA
 (0,0.700687,10) ; 17 KE0
 (0,0.647886) ; 18 PPC
 (0,0.753099,1) ; 19 PROP_E []
 (0,0,5) FIX ; 20 ADD_C [mg/L]

$OMEGA  BLOCK(1)
 0.0734386  ;   1 BSV CL
$OMEGA  BLOCK(1) FIX
 0  ;    2 BSV V
$OMEGA  BLOCK(1) FIX
 0  ;   3 BSV KA
$OMEGA  BLOCK(1) FIX
 0  ;  4 BSV BIO
$OMEGA  BLOCK(1) FIX
 0  ;    5 BSVV3
$OMEGA  BLOCK(1) FIX
 0  ;     6 BSVQ
$OMEGA  BLOCK(1) FIX
 0  ;    7 BSVV4
$OMEGA  BLOCK(1) FIX
 0  ;    8 BSVQ2
$OMEGA  BLOCK(1) FIX
 0  ;   9 BSVMTT
;----------
----------
----------
$OMEGA  BLOCK(1) FIX
 0  ;   10 BOVCL
$OMEGA  BLOCK(1) SAME
$OMEGA  BLOCK(1) SAME
$OMEGA  BLOCK(1) SAME
$OMEGA  BLOCK(1) SAME
$OMEGA  BLOCK(1) SAME
$OMEGA  BLOCK(1) SAME
$OMEGA  BLOCK(1) SAME
;----------
$OMEGA  BLOCK(1)
 0.237034  ;  14 BOVBIO
$OMEGA  BLOCK(1) SAME
$OMEGA  BLOCK(1) SAME
$OMEGA  BLOCK(1) SAME
$OMEGA  BLOCK(1) SAME
$OMEGA  BLOCK(1) SAME
$OMEGA  BLOCK(1) SAME
$OMEGA  BLOCK(1) SAME
;----------
$OMEGA  BLOCK(1)
 0.861212  ;   18 BOVKA
$OMEGA  BLOCK(1) SAME
$OMEGA  BLOCK(1) SAME
$OMEGA  BLOCK(1) SAME
$OMEGA  BLOCK(1) SAME
$OMEGA  BLOCK(1) SAME
$OMEGA  BLOCK(1) SAME
$OMEGA  BLOCK(1) SAME
;----------
$OMEGA  BLOCK(1)
 0.357417  ;  22 BOVMTT
$OMEGA  BLOCK(1) SAME
$OMEGA  BLOCK(1) SAME
$OMEGA  BLOCK(1) SAME
$OMEGA  BLOCK(1) SAME
$OMEGA  BLOCK(1) SAME
$OMEGA  BLOCK(1) SAME
$OMEGA  BLOCK(1) SAME
;----------
$OMEGA  BLOCK(1)
```

```
 0.0339448 ;     BVVCL
$OMEGA  BLOCK(1) SAME
$OMEGA  BLOCK(1) SAME
$OMEGA  BLOCK(1) SAME
;-------------------------------------------------------------------------
-------------------------------------------------------------------------
---
$OMEGA  BLOCK(1) FIX
 0  ;  46 BSVKE0
$OMEGA  BLOCK(1) FIX
 0  ;  47 BVVPPC
$OMEGA  BLOCK(1) SAME
$OMEGA  BLOCK(1) SAME
$OMEGA  BLOCK(1) SAME
;-------------------------------------------------------------------------
-------------------------------------------------------------------------
---
$SIGMA  1  FIX
;-------------------------------------------------------------------------
-------------------------------------------------------------------------
--
$ESTIMATION MSFO=run090_3.msf MAXEVAL=9999
PRINT=1 METHOD=1 INTER
        NOABORT NSIG=3 NONINFETA=1 ETASTYPE=1
;MCETA=1000 RANMETHOD=4P ; REPEAT
$COVARIANCE UNCONDITIONAL PRECOND=1 PRINT=E
MATRIX=R
;-------------------------------------------------------------------------
-------------------------------------------------------------------------
--
$TABLE     ID OCC TIME TAD AA1 AA2 AMT DVID ; AA3
AA4
        Y DV MDV PRED RES WRES IPRED IRES IWRES
CWRES CWRESI OBJI
        NOPRINT NOAPPEND ONEHEADER FORMAT=,
FILE=sdtab090_3.csv
;-------------------------------------------------------------------------
-------------------------------------------------------------------------
--
$TABLE     ID OCC CL V KA BIO MTT V3 Q ;
        HALF_L PPC KE0 ;
        BSVCL ;BSVV BSVKA BSVBIO BSVV3 BSVQ BSVV4
BSVQ2
        BVVCL BOVCL BOVKA BOVBIO BOVMTT ;BOVMTT
        VARCL VARBIO VARAUC NOPRINT NOAPPEND
ONEHEADER FORMAT=,
        FILE=patab090_3.csv
;-------------------------------------------------------------------------
-------------------------------------------------------------------------
--
$TABLE     ID OCC WT HTM AGE FFM FAT AUC_RTV
AUC_RTV2 AUC_RTV3
        VIRAL_LOAD NOPRINT NOAPPEND ONEHEADER
FORMAT=,
        FILE=cotab090_3.csv
;-------------------------------------------------------------------------
-------------------------------------------------------------------------
--
$TABLE     ID OCC VISIT SEXM EVENING OBS RIF
VISIT_DVID ABC AZT TDF
        BACK_BONE CONCOMITANT_MEDS FOOD_X1
FOOD_X2 FOOD_X3
        DOSE_SKIPPED_X1 DOSE_SKIPPED_X2
DOSE_SKIPPED_X3 FASTING_3H
        BLQ CENS FLAG PROB NOPRINT NOAPPEND
ONEHEADER FORMAT=,
        FILE=catab090_3.csv
;-------------------------------------------------------------------------
-------------------------------------------------------------------------
--
$TABLE     ID OCC TIME TAD AA1 AA2 AMT DVID ; AA3
AA4
        Y DV MDV PRED RES WRES IPRED IRES IWRES
CWRES CWRESI OBJI
        CL V KA BIO MTT V3 Q BSVCL ;
        VPC_TIME HALF_L PPC KE0 VISIT_DVID ;
        BVVCL BOVCL BOVKA BOVBIO BOVMTT ;
        VARCL VARBIO VARAUC VISIT SEXM EVENING OBS
RIF ABC AZT TDF
        BACK_BONE CONCOMITANT_MEDS FOOD_X1
FOOD_X2 FOOD_X3
        DOSE_SKIPPED_X1 DOSE_SKIPPED_X2
DOSE_SKIPPED_X3 FASTING_3H
        BLQ CENS FLAG PROB NOPRINT NOAPPEND
ONEHEADER FORMAT=,
        FILE=mytab090_3.csv
;-------------------------------------------------------------------------
-----------------------------------------------
```

Ritonavir

```
;; 1. Based on: 070
;; 2. Description: + FIX ADD_C to 0
;; x1. Author: Allan
;; 2022-09-23
; Settings for the memory of NONMEM
$SIZES                  PD=-1000    LVR=-150    LTH=-200
MAXFCN=10000000 LNP4=-150000
$PROBLEM    VIRTUAL_RTV
$ABBREVIATED DERIV2=NO
;-------------------------------------------------------------------------
-----------------------------
$INPUT       ID VISIT OCC DAT2=DROP TIME EVID AMT
PK_HR=DROP EVENING DV
        MDV RTV_PBMC DVID OBS BLQ CENS FLAG PROB
VPC_TIME WEIGHT
        HEIGHT      SEXM      AGE      VIRAL_LOAD=DROP
CONCOMITANT_MEDS DTG RIF
        FASTING_3H    FOOD_X3    FOOD_X2    FOOD_X1
DOSE_SKIPPED_X3
        DOSE_SKIPPED_X2 DOSE_SKIPPED_X1 ATV=DROP
DV_RTV=DROP
        DV_ATV=DROP      RTV=DROP      DV_DTG=DROP
DV_RIF=DROP COMMENT=DROP
        ID_VISIT=DROP                  CONCOMITANT
CONC_DRUG=DROP
        CONC_DRUG_TIME=DROP     ALT     AST     GGT
BILIRUBIN_TOTAL
        SERUM_CREATININE ALBUMIN TOTAL_PROTEIN
AUC24 AUC24_RIF
        BETA_TO_CHOL BETA_CHOLESTEROL BACK_BONE
ABC TDF AZT
        CHOLESTEROL
;-------------------------------------------------------------------------
-----------------------------
```

```
$DATA VIRTUAL_data_RTV_7.csv IGNORE=#
IGNORE=(PROB==1)
      IGNORE=(PROB==2) ;IGNORE=(DVID==2)
$SUBROUTINE ADVAN13 TRANS1 ; 2 compartment
TOL=9 ATOL=9
;-------------------------------------------------------------------------
$MODEL NCOMPARTMENTS=4 COMP=(ABS DEFDOSE)
      COMP=(CENTRAL DEFOBSERVATION) ;
COMP=(CENTRAL DEFOBSERVATION)
      COMP=(PERIPH) ;
      COMP=(PBMC) ; for the PBMC
; ;-------------------------------------------------------------------------
$PK
SMALL = 1E-12
; ------- BSV
BSVCL   = ETA(1)
BSVV    = ETA(2)
BSVKA   = ETA(3)
BSVBIO  = ETA(4)
BSVV3   = ETA(5)
BSVQ = ETA(6)
BSVV4 = ETA(7)
BSVQ2 = ETA(8)
BSVMTT = ETA(9)
;------for effect cmpt
BSVKE0  = ETA(46)
BSVPPC  = ETA(47)
; ---------- BOV
BOVCL = 0
IF (OCC==1) BOVCL = ETA(10)
IF (OCC==2) BOVCL = ETA(11)
IF (OCC==3) BOVCL = ETA(12)
IF (OCC==4) BOVCL = ETA(13)
IF (OCC==5) BOVCL = ETA(14)
IF (OCC==6) BOVCL = ETA(15)
IF (OCC==7) BOVCL = ETA(16)
IF (OCC==8) BOVCL = ETA(17)
BOVBIO = 0
IF (OCC==1)  BOVBIO = ETA(18)
IF (OCC==2) BOVBIO = ETA(19)
IF (OCC==3) BOVBIO = ETA(20)
IF (OCC==4) BOVBIO = ETA(21)
IF (OCC==5) BOVBIO = ETA(22)
IF (OCC==6) BOVBIO = ETA(23)
IF (OCC==7) BOVBIO = ETA(24)
IF (OCC==8) BOVBIO = ETA(25)
BOVKA = 0
IF (OCC==1) BOVKA = ETA(26)
IF (OCC==2) BOVKA = ETA(27)
IF (OCC==3) BOVKA = ETA(28)
IF (OCC==4) BOVKA = ETA(29)
IF (OCC==5) BOVKA = ETA(30)
IF (OCC==6) BOVKA = ETA(31)
IF (OCC==7) BOVKA = ETA(32)
IF (OCC==8) BOVKA = ETA(33)
BOVMTT = 0
IF (OCC==1) BOVMTT = ETA(34)
IF (OCC==2) BOVMTT = ETA(35)
IF (OCC==3) BOVMTT = ETA(36)
IF (OCC==4) BOVMTT = ETA(37)
IF (OCC==5) BOVMTT = ETA(38)
IF (OCC==6) BOVMTT = ETA(39)
IF (OCC==7) BOVMTT = ETA(40)
IF (OCC==8) BOVMTT = ETA(41)
;----------between visit variability
BVVCL = 0
IF (VISIT == 1) BVVCL = ETA(42)
IF (VISIT == 2) BVVCL = ETA(43)
IF (VISIT == 3) BVVCL = ETA(44)
IF (VISIT == 4) BVVCL = ETA(45)
;----------between visit variability in PPC
BVVPPC = 0
IF (VISIT == 1) BVVPPC = ETA(48)
IF (VISIT == 2) BVVPPC = ETA(49)
IF (VISIT == 3) BVVPPC = ETA(50)
IF (VISIT == 4) BVVPPC = ETA(51)


;----------------
SCALE_BOV = THETA(10)  ;extra bioavailability on all
absorption parameters
IF (OBS.EQ.0) THEN
; BOVKA=SCALE_BOV*BOVKA
; BOVMTT=SCALE_BOV*BOVMTT
BOVBIO=SCALE_BOV*BOVBIO
ENDIF
; ---------------- Calculation of Fat-free Mass
HTM = HEIGHT/100
WT = WEIGHT
SEX = SEXM
IF (SEX.EQ.0) THEN  ; female
 WHSMAX=37.99
 WHS50=35.98
ELSE       ;males
 WHSMAX=42.92
 WHS50=30.93
ENDIF
HTM2 = HTM**2
FFM = (WHSMAX*HTM2*WT)/(WHS50*HTM2+WT)
FAT = WT-FFM
IF (FAT.LT.0) FAT = 0
; ------- Typical values of covariates use MEDIAN WEIGHT
OF MY PPN
TVWT = 67
TVFAT = 25
TVFFM = 42
;--------- Allometric scaling and covariates
ALLMCL_WT = (WT/TVWT)**0.75
ALLMV_WT = (WT/TVWT)
ALLMCL_FAT = (FAT/TVFAT)**0.75
ALLMV_FAT = (FAT/TVFAT)
ALLMCL_FFM = (FFM/TVFFM)**0.75
ALLMV_FFM = (FFM/TVFFM)
;----------Allometry for liver
ALLMCL_WT_HEP = (WT/70)**0.75
ALLMV_WT_HEP = (WT/70)
ALLMCL_FFM_HEP = (FFM/56.1)**0.75
ALLMV_FFM_HEP = (FFM/56.1)
;-----------------------covariates
;;Covariate test: RTV_CL
RIF_CL =1 ;no RTV
IF(RIF.EQ.1) RIF_CL =(1+THETA(11)) ;Inter
;;Covariate test: RTV_CL
BIO_VISIT2 = 1;no RTV
IF(VISIT.EQ.2) BIO_VISIT2 =(1+THETA(12)) ;Inter
;;Evening doses
```

```
BIO_EFFECT = THETA(4)
IF(VISIT.EQ.2) BIO_EFFECT = THETA(14)
IF(VISIT.GE.3) BIO_EFFECT = THETA(15)
;IF(VISIT.EQ.4) BIO_EFFECT = THETA(16)
VISIT_DVID = VISIT + 10*DVID
;------for effect cmpt
TVKE0 = THETA(16)
TVPPC = THETA(17)

;---------Typical values--------------------------
TVCL                                                    =
THETA(1)*ALLMCL_WT*RIF_CL;*NAT2_CL*ALLMCL_FFM
*CFZ_CL ;
TVV = THETA(2)*ALLMV_WT;*ALLMV_FFM
TVKA = THETA(3);
TVBIO = BIO_EFFECT * BIO_VISIT2
TVMTT = THETA(7)
TVNN = THETA(13)
TVV3 = THETA(8)*ALLMV_WT
TVQ = THETA(9)*ALLMCL_WT
;-----------Define parameters------------
CL  = TVCL*EXP(BSVCL+BOVCL+BVVCL) ; CLEARANCE
V   = TVV*EXP(BSVV) ; CENTRAL VOL.
KA  = TVKA*EXP(BSVKA+BOVKA) ; ABS. RATE CONSTANT
BIO = TVBIO*EXP(BSVBIO+BOVBIO) ; BIOAVAILABILITY
MTT = TVMTT*EXP(BSVMTT+BOVMTT) ; MTT TIME
NN = TVNN ; Number of transit compartments
V3 = TVV3*EXP(BSVV3) ; PERIPH VOL
Q = TVQ*EXP(BSVQ) ; INTER COMPT CL
;-------for effect compartment
KE0 = TVKE0 * EXP(BSVKE0)
PPC = TVPPC * EXP(BSVPPC+BVVPPC)

;---------------------------------------------------------------
; re-parameterization
K = CL/V ;(rate constant of elimination)
K23 = Q/V   ; (rate constant from central to peripheral 1)
K32 = Q/V3 ;(rate constant from peripheral 1 to central)
;KA (rate constant of absorption)
F1=0 ;
KTR = (NN+1)/MTT ; The number of actual transit
compartments is NN+1
IF (NEWIND/=2.OR.EVID>=3) THEN ; new individual, or
reset event
   ; The values read here will be stored in TDOS and PD in
this very PK call.
        TNXD=TIME ; Time of the dose
        PNXD=AMT ; Amount. If it's zero, the DE is
deactivated.
ENDIF
TDOS=TNXD ; This will either save here the temporary
values if it's a new individual...
PD=PNXD ; ...or the values which were read one record
ahead during the execution of the previous record.
IF(AMT>0) THEN ; This reads one record ahead and stores
the data to be used when running the following record
; IF(AMT.GT.0.AND.ALAG1.EQ.0) THEN ; Use this INSTEAD
if there is ALAG, as it will also checks if the ALAG is not 0.
Note that you normally do not want to include both ALAG
and transit, this is a very exceptional case
        TNXD=TIME
        PNXD=AMT
ENDIF
; Uncomment this if you have ALAG or if you use ADDL
; IF (DOSTIM>0) THEN ; This will account for the ADDL or
lagged doses. It will overwrite the time, if it a non-event
record
;       TNXD=DOSTIM
;       PNXD=AMT
; ENDIF
;---------------------------------------------------------------
$DES
PIZZA = LOG(BIO*PD*KTR + 1E-12) - GAMLN(NN+1)  ;
without +0.00001, it won't work with ETAs in
bioavailability
;;---------------------------------------------------------------
A_0(1) = SMALL
A_0(2) = SMALL
A_0(3) = SMALL
A_0(4) = SMALL; PBMC

;;;---------------------------------------------------------------
$DES
C2 = A(2)/V ; state this as it is used for the DE of pbmc
CMT
TEMPO = T-TDOS ; this is time after dose for the transit, it
should always be >= 0
KTT = 0
TRANSIT = 0
IF(PD.GT.0.AND.TEMPO.GT.0) THEN ; This happens only id
PD>0, so only if a dose has been detected
        KTT = KTR*(TEMPO)
        TRANSIT = EXP(PIZZA+NN*LOG(KTT)-KTT)
ENDIF
DADT(1) = TRANSIT - KA*A(1)
DADT(2) = KA*A(1) - K*A(2) + K32*A(3) - K23*A(2)
DADT(3) = K23*A(2) - K32*A(3)
DADT(4) = KE0*(PPC*C2 - A(4)) ;A(4) IS ACTUALLY CONC
IN EFFECT CMT
;;;---------------------------------------------------------------
$ERROR
HALF_L = LOG(2)/KE0


IPRED_P = A(2)/V
 ; DEFINE LLOQ VALUE
LLOQ_P = 0.005 ; Plasma
LLOQ_C = 0.015 ; PBMC
CENS_THR_P = LLOQ_P
;prop and ADD error for plasma
PROP_P = IPRED_P*THETA(5)
ADD_P = THETA(6)+(CENS_THR_P*0.2)
; For CENS==1 (i.e. first CENSORED value in a series, which
was imputed to CENS_THR/2), we add extra additive error
on the concentrations,
; since the value in DV has been imputed and therefore
more uncertain.
IF (ICALL/=4.AND.CENS==1) THEN
 ADD_P = ADD_P +(CENS_THR_P*0.5)
ENDIF
NO_FIT = 0
; For CENS==2 (i.e. the trailing CENSORED values in a
series that were imputed to CENS_THR/2), we don't want
these to influence the fit,
IF (ICALL/=4.AND.CENS==2) THEN
 PROP_P = 0
```

```
 ADD_P = 10000000000
 NO_FIT = 1
ENDIF
W_P = SQRT(ADD_P**2+PROP_P**2)
;------PBMC
CC = A(4)
CENS_THR_C = LLOQ_C
 IPRED_C = CC
PROP_C  = IPRED_C * THETA(18)
ADD_C   = THETA(19) + (0.2*CENS_THR_C)
IF(ICALL/=4.AND.CENS==1.AND.DVID==4) THEN
 ADD_C = ADD_C + (LLOQ_C*0.5)
 ENDIF
IF (ICALL/=4.AND.CENS==2.AND.DVID==4) THEN
 PROP_C = 0
 ADD_C = 10000000000
 NO_FIT = 1
ENDIF
W_C = SQRT(ADD_C**2+PROP_C**2)

  ERROR_P = W_P * ERR(1)
  ERROR_C = W_C * ERR(1)

;Redefine IPRED & weighting----------
  IPRED = IPRED_P
  W = W_P
  ERROR_TERM = ERROR_P
  IF(DVID==2) THEN
  IPRED = IPRED_C
 W = W_C
  ERROR_TERM = ERROR_C
  ENDIF
 ; Protective code
IF (W.LE.0.000001) W=0.000001
IRES=DV-IPRED
IWRES=IRES/W
Y = IPRED + ERROR_TERM
; To prevent simulation (ICALL==4) of negative values. It
set a positive lower bound for Y, so that VPCs in the log-
scale can be plotted
IF              (DVID==1.AND.ICALL==4.AND.Y<=LLOQ_P)
Y=LLOQ_P/2
IF              (DVID==2.AND.ICALL==4.AND.Y<=LLOQ_C)
Y=LLOQ_C/2
; To calculate time after dose.
IF(AMT>0) THEN
 TIMEDOSE = TIME
 AMOUNTDOSE = AMT
ENDIF
TAD = TIME-TIMEDOSE
IF(VISIT==1.AND.DVID==2) TAD = 25.5
IF(VISIT==2.AND.DVID==2) TAD = 15
IF(VISIT==3.AND.DVID==2) TAD = 15
IF(VISIT==4.AND.DVID==2) TAD = 15
VARCL = BSVCL + BOVCL
VARBIO = BSVBIO + BOVBIO
VARAUC = BSVBIO + BOVBIO - BSVCL - BOVCL
VARABS = BOVKA + BSVKA - BSVMTT - BOVMTT

;--RETRIEVE AMOUNT IN EACH COMPARTMENT------
AA1 = A(1)
AA2 = A(2)
AA3 = A(3)
AA4 = A(4)
;-----------------------------------------
$THETA
0,9.67,50) FIX ; 1 CL [L/h]
 (0,55.4,300) FIX ; 2 V [L]
 (0,1.02,10) FIX ; 3 KA [1/h]
 1 FIX ; 4 BIO
 (0,0.256,0.5) FIX ; 5 PROP []
 (0,0,1) FIX ; 6 ADD [mg/L]
 (0,0.483,10) FIX ; 7 MTT
 (0,70.1,500) FIX ; 8 V3 [L]
 (0,1.56,50) FIX ; 9 Q [L/h]
 1 FIX ; 10 SCALE_BOVBIO
 (-0.99,1.12,5) FIX ; 11 RIF_CL
 (-0.99,0,5) FIX ; 12 BIO_VISIT2
 (0,12.3,50) FIX ; 13 NN
 (0,0.312) FIX ; 14 BIO_VISIT2
 (0,0.666) FIX ; 15 BIO_VISIT3/4
 (0,0.525554,10) ; 16 KE0
 (0,1.66352, 20) ; 17 PPC
 (0,0.693445,1) ; 18 PROP_E []
 0 FIX ; 19 ADD_C [mg/L]
$OMEGA  BLOCK(1) FIX
 0.0268  ;   1 BSV CL
$OMEGA  BLOCK(1) FIX
 0  ;    2 BSV V
$OMEGA  BLOCK(1) FIX
 0  ;   3 BSV KA
$OMEGA  BLOCK(1) FIX
 0  ;  4 BSV BIO
$OMEGA  BLOCK(1) FIX
 0  ;    5 BSVV3
$OMEGA  BLOCK(1) FIX
 0  ;     6 BSVQ
$OMEGA  BLOCK(1) FIX
 0  ;    7 BSVV4
$OMEGA  BLOCK(1) FIX
 0  ;    8 BSVQ2
$OMEGA  BLOCK(1) FIX
 0  ;   9 BSVMTT
;---------------------------------------
$OMEGA  BLOCK(1) FIX
 0  ;   10 BOVCL
$OMEGA  BLOCK(1) SAME
$OMEGA  BLOCK(1) SAME
$OMEGA  BLOCK(1) SAME
$OMEGA  BLOCK(1) SAME
$OMEGA  BLOCK(1) SAME
$OMEGA  BLOCK(1) SAME
$OMEGA  BLOCK(1) SAME
;-------------------------
$OMEGA  BLOCK(1) FIX
 0.308  ;  14 BOVBIO
$OMEGA  BLOCK(1) SAME
$OMEGA  BLOCK(1) SAME
$OMEGA  BLOCK(1) SAME
$OMEGA  BLOCK(1) SAME
$OMEGA  BLOCK(1) SAME
$OMEGA  BLOCK(1) SAME
$OMEGA  BLOCK(1) SAME
;-------------------------
$OMEGA  BLOCK(1) FIX
 0.678  ;   18 BOVKA
```

```
$OMEGA  BLOCK(1) SAME
$OMEGA  BLOCK(1) SAME
$OMEGA  BLOCK(1) SAME
$OMEGA  BLOCK(1) SAME
$OMEGA  BLOCK(1) SAME
$OMEGA  BLOCK(1) SAME
$OMEGA  BLOCK(1) SAME
;------------------------
$OMEGA  BLOCK(1) FIX
 0.19  ;  22 BOVMTT
$OMEGA  BLOCK(1) SAME
$OMEGA  BLOCK(1) SAME
$OMEGA  BLOCK(1) SAME
$OMEGA  BLOCK(1) SAME
$OMEGA  BLOCK(1) SAME
$OMEGA  BLOCK(1) SAME
$OMEGA  BLOCK(1) SAME
;------------------------
$OMEGA  BLOCK(1) FIX
 0  ;     BVVCL
$OMEGA  BLOCK(1) SAME
$OMEGA  BLOCK(1) SAME
$OMEGA  BLOCK(1) SAME
;-----------------------------------------------
$OMEGA  BLOCK(1) FIX
 0  ;  46 BSVKE0
$OMEGA  BLOCK(1) FIX
 0  ;  47 BSVPPC
;------------------------
$OMEGA  BLOCK(1) FIX
 0  ;  48 BVVPPC
$OMEGA  BLOCK(1) SAME
$OMEGA  BLOCK(1) SAME
$OMEGA  BLOCK(1) SAME
$SIGMA  1  FIX
;---------------------------------------------------------------
$ESTIMATION     MSFO=run070a.msf     MAXEVAL=9999
PRINT=1 METHOD=1 INTER
        NOABORT  NSIG=3  NONINFETA=1  ETASTYPE=1
;MCETA=1000 RANMETHOD=4P ; REPEAT
;---------------------------------------------------------
$TABLE      ID OCC TIME TAD AA1 AA2 AMT AA3 ; AA4
        Y  DV  MDV  PRED  RES  WRES  IPRED  IRES  IWRES
CWRES CWRESI OBJI
        NOPRINT  NOAPPEND  ONEHEADER  FORMAT=,
FILE=sdtab070a.csv
;-------------------------------------------------------------------------
$TABLE      ID OCC CL V KA BIO MTT V3 Q ;V4 Q2 ;
        HALF_L  PPC  KE0  BSVCL  ;BSVV  BSVKA  BSVBIO
BSVV3 BSVQ BSVV4 BSVQ2
        BVVCL BOVCL BOVKA BOVBIO BOVMTT ;BOVMTT
        VARCL  VARBIO  VARAUC  NOPRINT  NOAPPEND
ONEHEADER FORMAT=,
        FILE=patab070a.csv
;-------------------------------------------------------------------------
--------
$TABLE        ID OCC WT HTM AGE FFM FAT AUC24_RIF
BETA_TO_CHOL
        BETA_CHOLESTEROL  CHOLESTEROL  NOPRINT
NOAPPEND ONEHEADER
        FORMAT=, FILE=cotab070a.csv
;-------------------------------------------------------------------------
--------
$TABLE      ID OCC VISIT SEXM OBS RIF BACK_BONE ABC
TDF AZT VISIT_DVID
        CONCOMITANT_MEDS  FOOD_X1  FOOD_X2
FOOD_X3 DOSE_SKIPPED_X1
        DOSE_SKIPPED_X2  DOSE_SKIPPED_X3
FASTING_3H NOPRINT
        NOAPPEND  ONEHEADER  FORMAT=,
FILE=catab070a.csv
;-------------------------------------------------------------------------
----------
$TABLE      ID OCC TIME TAD AA1 AA2 AMT AA3 ; AA4
        Y  DV  MDV  PRED  RES  WRES  IPRED  IRES  IWRES
CWRES CWRESI OBJI
        CL V KA BIO MTT V3 Q ;V4 Q2 ;
        HALF_L  PPC  KE0  BSVCL  ;BSVV  BSVKA  BSVBIO
BSVV3 BSVQ BSVV4 BSVQ2
        BVVCL BOVCL BOVKA BOVBIO BOVMTT ;BOVMTT
        VARCL  VARBIO  VARAUC  WT  HTM  AGE  FFM  FAT
AUC24_RIF
        BETA_TO_CHOL  BETA_CHOLESTEROL
CHOLESTEROL VISIT SEXM OBS
        RIF  BACK_BONE  ABC  TDF  AZT  VISIT_DVID
CONCOMITANT_MEDS FOOD_X1 FOOD_X2
        FOOD_X3  DOSE_SKIPPED_X1  DOSE_SKIPPED_X2
DOSE_SKIPPED_X3
        FASTING_3H BLQ CENS FLAG PROB DVID NOPRINT
NOAPPEND
        ONEHEADER FORMAT=, FILE=mytab070a.csv
;-------------------------------------------------------------------------
--------
```

ISA_DRPK
Isoniazid

```
;; 1. Based on: 040a
;; 2. Description: Final INH model
;; x1. Author: allan
;; 2022-09-23
; Settings for the memory of NONMEM
;-------------------------------------------------------------------------------
$SIZES PD=-1000 LVR=-150 LTH=-200 MAXFCN=10000000 LNP4=-150000
$PROBLEM ISA_INH
$ABBREVIATED DERIV2=NO
$INPUT ID OCC WHAT=DROP EVID MDV AMT DAT2=DROP TIME VPC_TIME DV
       ADDL=DROP II=DROP AGE SEXM HIVP HTM WTKG RACEB NAT2=DROP
       BLQ PROB CENS BDQ_DOSE=DROP CFZ_DOSE=DROP INH_DOSE=DROP
       VISIT_WK PREDOSE=DROP DV_INH ID_VISIT=DROP SWAP
       OLD_DV_INH=DROP FLAG INH EFV EFV_DAYS LPV LPV_DAYS RPV
       RPV_DAYS TDF TDF_DAYS OBS BLQ2=DROP WT2 CREATININE=DROP
       CREATMGDL CRCL NAT_STATUS=DROP NAT_2
$DATA ISA_INH_data5.csv IGNORE=# IGNORE=(INH==0) IGNORE=(PROB==1)
       IGNORE=(SWAP==1) IGNORE=(FLAG==1) IGNORE=(FLAG==2)
       IGNORE=(FLAG==3) IGNORE=(PROB==2)
$SUBROUTINE ADVAN14 TRANS1 TOL=6 ATOL=6
;-------------------------------------------------------------------------
$MODEL NCOMPARTMENTS=3
COMP=(ABS DEFDOSE)
 COMP=(CENTRAL DEFOBSERVATION) ;
COMP=(CENTRAL DEFOBSERVATION)
  COMP=(PERIPH)
; ;-------------------------------------------------------------------------
$PK
SMALL = 1E-6
; ------- BSV
BSVCL   = ETA(1)
BSVV    = ETA(2)
BSVKA   = ETA(3)
BSVBIO  = ETA(4)
BSVV3   = ETA(5)
BSVQ = ETA(6)
BSVV4 = ETA(7)
BSVQ2 = ETA(8)
BSVMTT = ETA(9)

; ---------- BOV

BOVCL = 0
IF (OCC==1)BOVCL = ETA(10)
IF (OCC==2)BOVCL = ETA(11)
IF (OCC==5)BOVCL = ETA(12)
IF (OCC==6)BOVCL = ETA(13)
BOVBIO = 0
IF (OCC==1)BOVBIO = ETA(14)
IF (OCC==2)BOVBIO = ETA(15)
IF (OCC==5)BOVBIO = ETA(16)
IF (OCC==6)BOVBIO = ETA(17)
BOVKA = 0
IF (OCC==1)BOVKA = ETA(18)
IF (OCC==2)BOVKA = ETA(19)
IF (OCC==5)BOVKA = ETA(20)
IF (OCC==6)BOVKA = ETA(21)

BOVMTT = 0
IF (OCC==1)BOVMTT = ETA(22)
IF (OCC==2)BOVMTT = ETA(23)
IF (OCC==5)BOVMTT = ETA(24)
IF (OCC==6)BOVMTT = ETA(25)
;----------VISIT_WK to CFZ
CFZ = 0
IF (VISIT_WK == 6) CFZ = 1
;----------between visit variability
BVVCL = 0
IF (CFZ == 0)BVVCL = ETA(26)
IF (CFZ == 1)BVVCL = ETA(27)
;----------------
E_BOV = THETA(10)  ;extra bioavailability on all absorption parameters
IF (OBS.EQ.0) THEN
BOVKA=E_BOV*BOVKA
BOVMTT=E_BOV*BOVMTT
BOVBIO=E_BOV*BOVBIO
ENDIF
;----------------CFZ_NAT
CFZ_NAT = CFZ + 10*NAT_2
; -------------- Calculation of Fat-free Mass
WT = WT2
SEX = SEXM
IF (SEX.EQ.0) THEN  ; female
        WHSMAX=37.99
        WHS50=35.98
ELSE    ;males
        WHSMAX=42.92
        WHS50=30.93
ENDIF
HTM2 = HTM**2
FFM = (WHSMAX*HTM2*WT)/(WHS50*HTM2+WT)
FAT = WT-FFM
IF (FAT.LT.0) FAT = 0
; ------- Typical values of covariates
TVWT = 52
TVFAT = 10
TVFFM = 42
;--------- Allometric scaling and covariates
ALLMCL_WT = (WT/TVWT)**0.75
ALLMV_WT = (WT/TVWT)
ALLMCL_FAT = (FAT/TVFAT)**0.75
ALLMV_FAT = (FAT/TVFAT)
ALLMCL_FFM = (FFM/TVFFM)**0.75
ALLMV_FFM = (FFM/TVFFM)
;----------Allometry for liver
ALLMCL_WT_HEP = (WT/70)**0.75
ALLMV_WT_HEP = (WT/70)
 ALLMCL_FFM_HEP = (FFM/56.1)**0.75
ALLMV_FFM_HEP = (FFM/56.1)
;----------------------covariates
;Covariate test: NAT2 on CL
NAT2_CL = THETA(1);slow
```

```
IF(NAT_2.EQ.2) NAT2_CL = THETA(11)  ;Inter

IF(NAT_2.EQ.3) NAT2_CL = THETA(12)  ;rapid
;Covariate test: NAT2 on CL
CFZ_CL =1;week 2
IF(CFZ.EQ.1) CFZ_CL =(1+THETA(16)) ;Week 6

;---------Typical values----------------------------------------------
-------------------------------------------------------------------------
------------------------------
TVCL = NAT2_CL * ALLMCL_FFM * CFZ_CL ;
TVV = THETA(2)*ALLMV_FFM
TVKA = THETA(3);
TVBIO = THETA(4)
TVMTT = THETA(7)
TVNN = THETA(13)
TVV3 = THETA(8)*ALLMCL_FFM
TVQ = THETA(9)*ALLMCL_FFM
;-------------------------HEPATIC  CL-------------------------------
-------;
TVQH=THETA(14)*ALLMCL_FFM_HEP    ; PLASMA FLOW
RATE recommended to be fixed to 90L/h but also test
50L/h
TVFU=THETA(15)  ; UNBOUND PLASMA FRACTION OF RIF
;-----------Define parameters-------------------------------------------
-------------------------------------------------------------------------
------------------------
CLINT  = TVCL*EXP(BSVCL+BOVCL+BVVCL) ; CLEARANCE
V   = TVV*EXP(BSVV) ; CENTRAL VOL.
KA  = TVKA*EXP(BSVKA+BOVKA) ; ABS. RATE CONSTANT
BIO = TVBIO*EXP(BSVBIO+BOVBIO) ; BIOAVAILABILITY
MTT = TVMTT*EXP(BSVMTT+BOVMTT) ; MTT TIME
NN = TVNN ; Number of transit compartments
V3 = TVV3*EXP(BSVV3) ; PERIPH VOL
Q = TVQ*EXP(BSVQ) ; INTER COMPT CL
QH=TVQH
FU=TVFU
;-------------------------------------------------------------------------
-------------------------------------------------
;--------  Transfer constants for liver model ---------
; define hepatic extraction
EH  = (CLINT*FU)/((CLINT*FU)+QH) ; fraction undergoing
first pass extraction
FH  = 1 - EH ; fraction available after 1st pass to go to
systemic circulation
K20 = QH*EH /V ; liver elimination rate constant
; re-parameterization
K23 = Q/V   ; (rate constant from central to peripheral 1)
K32 = Q/V3 ;(rate constant from peripheral 1 to central)
; ; Transit compartment absorption
F1=0 ;
KTR = (NN+1)/MTT
IF (NEWIND/=2.OR.EVID>=3) THEN
        TNXD=TIME
        PNXD=AMT
ENDIF
TDOS=TNXD
PD=PNXD
IF(AMT>0) THEN
        TNXD=TIME
        PNXD=AMT
ENDIF
PIZZA = LOG(BIO*PD*KTR + 1E-12) - GAMLN(NN+1)
;;;-------------------------------------------------------------
A_0(1) = SMALL
A_0(2) = SMALL
A_0(3) = SMALL
;;;-------------------------------------------------------------

$DES
TEMPO = T-TDOS
KTT = 0
TRANSIT = 0
IF(PD.GT.0.AND.TEMPO.GT.0) THEN
        KTT = KTR*(TEMPO)
        TRANSIT = EXP(PIZZA+NN*LOG(KTT)-KTT)
ENDIF
DADT(1) = TRANSIT - KA*A(1)
DADT(2) = KA*A(1)*FH - K20*A(2) + K32*A(3) - K23*A(2)
DADT(3) = K23*A(2) - K32*A(3)
;;;-------------------------------------------------------------
$ERROR
CL = CLINT*FU
IPRED=A(2)/V
LLOQ = 0.105 ; DEFINE YOUR OWN LLOQ HERE
CENS_THR = LLOQ
PROP = IPRED*THETA(5)
ADD = THETA(6)+(LLOQ*0.2)
IF (ICALL/=4.AND.CENS==1) THEN
        ADD = ADD +(CENS_THR*0.5)
ENDIF
NO_FIT = 0
IF (ICALL/=4.AND.CENS==2) THEN
        PROP = 0
        ADD = 10000000000
        NO_FIT = 1
ENDIF
W = SQRT(ADD**2+PROP**2)

IF (W.LE.0.000001) W=0.000001
IRES=DV-IPRED
IWRES=IRES/W
Y = IPRED + W*ERR(1)
IF (ICALL==4.AND.Y<=CENS_THR) Y = CENS_THR/2
IF(AMT>0) THEN
        TIMEDOSE = TIME
        AMOUNTDOSE = AMT
ENDIF
TAD = TIME-TIMEDOSE
VARCL = BSVCL + BOVCL
VARBIO = BSVBIO + BOVBIO
VARAUC = BSVBIO + BOVBIO - BSVCL - BOVCL
VARABS = BOVKA - BSVMTT - BOVMTT
;----------------------------------------RETRIEVE  AMOUNT  IN
EACH COMPARTMENT-------------------
AA1 = A(1)
AA2 = A(2)
AA3 = A(3)
; AA4 = A(4)
;----------------------------------Initial estimates-----------------
-------------------------------------------------
$THETA  (0,12.0151,50) ; 1 CL [L/h]
 (0,56.1749,300) ; 2 V [L]
 (0,3.28,10) FIX ; 3 KA [1/h]
 1 FIX ; 4 BIO
 (0,0.255145,0.5) ; 5 PROP []
```

```
 (0,0,1) FIX ; 6 ADD [mg/L]
 (0,0.112,10) FIX ; 7 MTT
 (0,44.1111,100) ; 8 V3 [L]
 (0,1.18456,50) ; 9 Q [L/h]
 (0,1,10) FIX; 10 E_BOV
 (0,24.1722,50) ; 11 Inter
 (0,46.6151,70) ; 12 Rapid
 (0,2.32,50) FIX ; 13 NN
 90 FIX ; 14 QH (L/h)
 0.95 FIX ; 15 FU (%)
 (-0.99,0,5) FIX ; 16 CFZ_CL
$OMEGA  BLOCK(1)
 0.0292283  ;   1 BSV CL
$OMEGA  BLOCK(1) FIX
 0  ;    2 BSV V
$OMEGA  BLOCK(1) FIX
 0  ;   3 BSV KA
$OMEGA  BLOCK(1) FIX
 0  ;  4 BSV BIO
$OMEGA  BLOCK(1) FIX
 0  ;    5 BSVV3
$OMEGA  BLOCK(1) FIX
 0  ;     6 BSVQ
$OMEGA  BLOCK(1) FIX
 0  ;    7 BSVV4
$OMEGA  BLOCK(1) FIX
 0  ;    8 BSVQ2
$OMEGA  BLOCK(1) FIX
 0  ;   9 BSVMTT
;----------------------------------------------------------------------
----------------------------------------------------------------------
----------
$OMEGA  BLOCK(1) FIX
 0  ;   10 BOVCL
$OMEGA  BLOCK(1) SAME
$OMEGA  BLOCK(1) SAME
$OMEGA  BLOCK(1) SAME
$OMEGA  BLOCK(1)
 0.113145  ;  14 BOVBIO
$OMEGA  BLOCK(1) SAME
$OMEGA  BLOCK(1) SAME
$OMEGA  BLOCK(1) SAME
$OMEGA  BLOCK(1)
 0.602651  ;   18 BOVKA
$OMEGA  BLOCK(1) SAME
$OMEGA  BLOCK(1) SAME
$OMEGA  BLOCK(1) SAME
$OMEGA  BLOCK(1)
 1.70328  ;  22 BOVMTT
$OMEGA  BLOCK(1) SAME
$OMEGA  BLOCK(1) SAME
$OMEGA  BLOCK(1) SAME
;---------------------------------------
$OMEGA  BLOCK(1)
 0.0385361  ;     BVVCL
$OMEGA  BLOCK(1) SAME
;----------------------------------------------------------------------
----------------------------------------------------------------------
---
$SIGMA  1  FIX
;-----------------------------
$ESTIMATION MSFO=run040d.msf MAXEVAL=0 PRINT=1
METHOD=1 INTER NOABORT
        NSIG=2 NONINFETA=1 ETASTYPE=1 MCETA=1000
RANMETHOD=4P ; REPEAT
$ESTIMATION MSFO=run040d.msf MAXEVAL=9999
PRINT=1 METHOD=1 INTER
        NOABORT NSIG=2 NONINFETA=1 ETASTYPE=1
MCETA=10
        RANMETHOD=4P ; REPEAT
;---------------------
$TABLE     ID OCC TIME TAD AA1 AA2 AMT ; AA3 AA4
        Y DV MDV PRED RES WRES IPRED IRES IWRES
CWRES CWRESI OBJI
        NOPRINT NOAPPEND ONEHEADER FORMAT=,
FILE=sdtab040d.csv
;-----------------------
$TABLE     ID OCC CL V KA BIO NN MTT V3 Q ;V4 Q2 ;
        BSVCL ;BSVV BSVKA BSVBIO BSVV3 BSVQ BSVV4
BSVQ2
        BOVCL BOVKA BOVBIO BOVMTT BVVCL ;BOVLAG
        VARCL VARBIO VARAUC NOPRINT NOAPPEND
ONEHEADER FORMAT=,
        FILE=patab040d.csv
;-------------------------
$TABLE       ID OCC WT HTM AGE FFM FAT VPC_TIME
CREATMGDL CRCL EFV_DAYS
        LPV_DAYS RPV_DAYS TDF_DAYS NOPRINT
NOAPPEND ONEHEADER
        FORMAT=, FILE=cotab040d.csv
;---------------------
$TABLE     ID OCC NAT_2 HIVP SEXM RACEB PROB CFZ EFV
LPV RPV TDF
        CFZ_NAT NOPRINT NOAPPEND ONEHEADER
FORMAT=,
        FILE=catab040d.csv
;---------------------
$TABLE     ID OCC TIME TAD AA1 AA2 AMT ; AA3 AA4
        Y DV MDV PRED RES WRES IPRED IRES IWRES
CWRES CWRESI OBJI
        CL V KA BIO NN MTT V3 Q ; NN V4 Q2
        BSVCL BVVCL ;BSVV BSVKA BSVBIO BSVV3 BSVQ
BSVV4 BSVQ2
        BOVCL BOVKA BOVBIO BOVMTT VARCL VARBIO
VARAUC WT HTM AGE
        FFM FAT VPC_TIME CREATMGDL CRCL EFV_DAYS
LPV_DAYS RPV_DAYS
        TDF_DAYS NAT_2 HIVP SEXM RACEB PROB CFZ EFV
LPV RPV TDF
        CFZ_NAT NOPRINT NOAPPEND ONEHEADER
FORMAT=,
        FILE=mytab040d.csv
;------------------
```

Linezolid

```
;; 1. Based on: 042b
;; 2. Description: Final Linezolid model
;; x1. Author: Allan
;; 2022-09-23
; Settings for the memory of NONMEM
;----------------------------------------------------------------------
------------------------------
$SIZES                  PD=-1000   LVR=-150   LTH=-200
MAXFCN=10000000 LNP4=-150000
$PROBLEM    ISA_LINEZOLID
$ABBREVIATED DERIV2=NO
```

```
$INPUT ID OCC WHAT=DROP EVID MDV AMT DAT2=DROP TIME VPC_TIME DV
ADDL=DROP II=DROP AGE SEXM HIVP HTM WTKG RACEB NAT2 BLQ
PROB CENS LINEZOLID_DOSE=DROP VISIT_WK PREDOSE
ID_VISIT=DROP SWAP=DROP OLD_DV_LIN=DROP LIN FLAG
CREATININE=DROP WT2 OBS CREATMGDL=DROP CRCL EFV EFV_DAYS
LPV LPV_DAYS RPV RPV_DAYS TDF TDF_DAYS
;-------------------------------------------------------------------------------
$DATA ISA_Lin_data10.csv IGNORE=# IGNORE=(LIN.EQ.0)
IGNORE=(PROB.EQ.1) IGNORE=(FLAG.EQ.5) IGNORE=(FLAG.EQ.7)
IGNORE=(FLAG.EQ.1) IGNORE=(FLAG.EQ.2) IGNORE=(FLAG.EQ.3)
IGNORE=(FLAG.EQ.8) ;IGNORE=(FLAG.EQ.9)
$SUBROUTINE ADVAN14 TRANS1 TOL=9 ATOL=9
$MODEL NCOMPARTMENTS=2
COMP=(ABS DEFDOSE)
COMP=(CENTRAL DEFOBSERVATION) ;
COMP=(CENTRAL DEFOBSERVATION) COMP=(PERIPH)
; ;-------------------------------------------------------------------------------
$PK
SMALL = 1E-6
; ------- BSV
BSVCL = ETA(1)
BSVV = ETA(2)
BSVKA = ETA(3)
BSVBIO = ETA(4)
BSVV3 = ETA(5)
BSVQ = ETA(6)
BSVV4 = ETA(7)
BSVQ2 = ETA(8)
BSVMTT = ETA(9)

; ---------- BOV

BOVCL = 0
IF (OCC==1)BOVCL = ETA(10)
IF (OCC==2)BOVCL = ETA(11)
IF (OCC==3)BOVCL = ETA(12)
IF (OCC==4)BOVCL = ETA(13)
BOVBIO = 0
IF (OCC==1)BOVBIO = ETA(14)
IF (OCC==2)BOVBIO = ETA(15)
IF (OCC==3)BOVBIO = ETA(16)
IF (OCC==4)BOVBIO = ETA(17)
BOVKA = 0
IF (OCC==1)BOVKA = ETA(18)
IF (OCC==2)BOVKA = ETA(19)
IF (OCC==3)BOVKA = ETA(20)
IF (OCC==4)BOVKA = ETA(21)

BOVMTT = 0
IF (OCC==1)BOVMTT = ETA(22)
IF (OCC==2)BOVMTT = ETA(23)
IF (OCC==3)BOVMTT = ETA(24)
IF (OCC==4)BOVMTT = ETA(25)
;----------VISIT_WK to CFZ
CFZ = 0
IF (VISIT_WK == 6) CFZ = 1
;----------between visit variability
BVVCL = 0
IF (CFZ == 0)BVVCL = ETA(26)
IF (CFZ == 1)BVVCL = ETA(27)
;----------
E_BOV = THETA(10) ;extra bioavailability on all absorption parameters
IF (OBS.EQ.0) THEN
BOVKA=E_BOV*BOVKA
BOVMTT=E_BOV*BOVMTT
BOVBIO=E_BOV*BOVBIO
ENDIF
; ---------- Calculation of Fat-free Mass
WT = WT2
SEX = SEXM
IF (SEX.EQ.0) THEN ; female
WHSMAX=37.99
WHS50=35.98
ELSE ;males
WHSMAX=42.92
WHS50=30.93
ENDIF
HTM2 = HTM**2
FFM = (WHSMAX*HTM2*WT)/(WHS50*HTM2+WT)
FAT = WT-FFM
IF (FAT.LT.0) FAT = 0
; ------- Typical values of covariates use MEDIAN WEIGHT OF MY PPN
TVWT = 52
TVFAT = 10
TVFFM = 42
;--------- Allometric scaling and covariates
ALLMCL_WT = (WT2/TVWT)**0.75
ALLMV_WT = (WT2/TVWT)
ALLMCL_FAT = (FAT/TVFAT)**0.75
ALLMV_FAT = (FAT/TVFAT)
ALLMCL_FFM = (FFM/TVFFM)**0.75
ALLMV_FFM = (FFM/TVFFM)
;----------Allometry for liver
ALLMCL_WT_HEP = (WT2/70)**0.75
ALLMV_WT_HEP = (WT2/70)
ALLMCL_FFM_HEP = (FFM/56.1)**0.75
ALLMV_FFM_HEP = (FFM/56.1)
;-----------------------covariates
;---------Typical values-------------------------
TVCL = THETA(1)*ALLMCL_FFM ;
TVV = THETA(2)*ALLMV_FFM
TVKA = THETA(3);
TVBIO = THETA(4)
TVMTT = THETA(7)
TVNN = THETA(11)
TVV3 = THETA(8)*ALLMCL_FFM
TVQ = THETA(9)*ALLMCL_WT
;-----------Define parameters-------------
CL = TVCL*EXP(BSVCL+BOVCL+BVVCL) ; CLEARANCE
V = TVV*EXP(BSVV) ; CENTRAL VOL.
KA = TVKA*EXP(BSVKA+BOVKA) ; ABS. RATE CONSTANT
BIO = TVBIO*EXP(BSVBIO+BOVBIO) ; BIOAVAILABILITY
MTT = TVMTT*EXP(BSVMTT+BOVMTT) ; MTT TIME
NN = TVNN ; Number of transit compartments
V3 = TVV3*EXP(BSVV3) ; PERIPH VOL
```

```
Q = TVQ*EXP(BSVQ) ; INTER COMPT CL
;----------------------
; re-parameterization
K = CL/V ;(rate constant of elimination)
K23 = Q/V   ; (rate constant from central to peripheral 1)
K32 = Q/V3 ;(rate constant from peripheral 1 to central)
;  Transit compartment absorption
F1=0 ;
KTR = (NN+1)/MTT ;
IF (NEWIND/=2.OR.EVID>=3) THEN ;
        TNXD=TIME ;
        PNXD=AMT ;
ENDIF
TDOS=TNXD ;
PD=PNXD ;
IF(AMT>0) THEN ;
        TNXD=TIME
        PNXD=AMT
ENDIF

PIZZA = LOG(BIO*PD*KTR + 1E-12) - GAMLN(NN+1)  ;
;;;-------------------------------------------------------------
A_0(1) = SMALL
A_0(2) = SMALL
;;;----------------------

$DES
TEMPO = T-TDOS
KTT = 0
TRANSIT = 0
IF(PD.GT.0.AND.TEMPO.GT.0) THEN ;
        KTT = KTR*(TEMPO)
        TRANSIT = EXP(PIZZA+NN*LOG(KTT)-KTT)
ENDIF
;-----DEs
DADT(1) = TRANSIT-KA*A(1)
DADT(2) = KA*A(1)-K*A(2)
;;;-------------------------------------------------------------
$ERROR
IPRED=A(2)/V
LLOQ = 0.1 ;
CENS_THR = LLOQ
PROP = IPRED*THETA(5)
ADD = THETA(6)+(LLOQ*0.2)
IF (ICALL/=4.AND.CENS==1) THEN
        ADD = ADD +(CENS_THR*0.5)
ENDIF
NO_FIT = 0
IF (ICALL/=4.AND.CENS==2) THEN
        PROP = 0
        ADD = 10000000000
        NO_FIT = 1
ENDIF
W = SQRT(ADD**2+PROP**2)
IF (W.LE.0.000001) W=0.000001
IRES=DV-IPRED
IWRES=IRES/W
Y = IPRED + W*ERR(1)
IF (ICALL==4.AND.Y<=CENS_THR) Y = CENS_THR/2
IF(AMT>0) THEN
        TIMEDOSE = TIME
        AMOUNTDOSE = AMT
ENDIF
TAD = TIME-TIMEDOSE
VARCL = BSVCL + BOVCL
VARBIO = BSVBIO + BOVBIO
VARAUC = BSVBIO + BOVBIO - BSVCL - BOVCL
VARABS = BOVKA - BSVMTT - BOVMTT
;-----------------------------------------RETRIEVE   AMOUNT   IN
EACH COMPARTMENT--------
AA1 = A(1)
AA2 = A(2)
;AA3 = A(3)
; AA4 = A(4)
;---------------------------------------Initial estimates
$THETA
(0,3.05884,50) ; 1 CL [L/h]
 (0,38.8589,300) ; 2 V [L]
 (0,1.13526,10) ; 3 KA [1/h]
 1 FIX ; 4 BIO
 (0,0.0762417,0.5) ; 5 PROP []
 (0,0.2064,1) ; 6 ADD [mg/L
 (0,0.964945,2) ; 7 MTT
 0 FIX ; 8 V3 [L]
 0 FIX ; 9 Q [L/h]
 (0,1.71024,10) ; 10 E_BOV
 (0,12.8013,50) ; 11 NN
$OMEGA  BLOCK(1)
 0.0954025  ;   1 BSV CL
$OMEGA  BLOCK(1) FIX
 0  ;    2 BSV V
$OMEGA  BLOCK(1) FIX
 0  ;   3 BSV KA
$OMEGA  BLOCK(1) FIX
 0  ;  4 BSV BIO
$OMEGA  BLOCK(1) FIX
 0  ;    5 BSVV3
$OMEGA  BLOCK(1) FIX
 0  ;     6 BSVQ
$OMEGA  BLOCK(1) FIX
 0  ;    7 BSVV4
$OMEGA  BLOCK(1) FIX
 0  ;    8 BSVQ2
$OMEGA  BLOCK(1) FIX
 0  ;   9 BSVMTT
;--------------------------------------
$OMEGA  BLOCK(1) FIX
 0  ;   10 BOVCL
$OMEGA  BLOCK(1) SAME
$OMEGA  BLOCK(1) SAME
$OMEGA  BLOCK(1) SAME
$OMEGA  BLOCK(1)
 0.0151055  ;  14 BOVBIO
$OMEGA  BLOCK(1) SAME
$OMEGA  BLOCK(1) SAME
$OMEGA  BLOCK(1) SAME
$OMEGA  BLOCK(1)
 1.06071  ;   18 BOVKA
$OMEGA  BLOCK(1) SAME
$OMEGA  BLOCK(1) SAME
$OMEGA  BLOCK(1) SAME
$OMEGA  BLOCK(1)
 0.475772  ;  22 BOVMTT
$OMEGA  BLOCK(1) SAME
$OMEGA  BLOCK(1) SAME
$OMEGA  BLOCK(1) SAME
```

```
;----------------------------------------
$OMEGA  BLOCK(1)
 0.1114 ;     BVVCL
$OMEGA  BLOCK(1) SAME
;----------------------------------------
$SIGMA  1  FIX
;----------------------------------------
$ESTIMATION MSFO=run045.msf MAXEVAL=0 PRINT=1
METHOD=1 INTER NOABORT
        NSIG=2 NONINFETA=1 ETASTYPE=1 MCETA=1000
RANMETHOD=4P ; REPEAT
$ESTIMATION MSFO=run045.msf MAXEVAL=9999
PRINT=1 METHOD=1 INTER
        NOABORT NSIG=2 NONINFETA=1 ETASTYPE=1
MCETA=10
        RANMETHOD=4P ; REPEAT
;----------------------------------------------------------------------------
-----------------------------------------------
$TABLE     ID OCC TIME TAD AA1 AA2 AMT ; AA3 AA4
        Y DV MDV PRED RES WRES IPRED IRES IWRES
CWRES CWRESI OBJI
        NOPRINT NOAPPEND ONEHEADER FORMAT=,
FILE=sdtab045.csv
;----------------------------------------------------------------------------
-----------------------------------------------
$TABLE     ID OCC CL V KA BIO MTT NN ;V3 Q ;V4 Q2 ;
        BSVCL ;BSVV BSVKA BSVBIO BSVV3 BSVQ BSVV4
BSVQ2
        BOVCL BOVKA BOVBIO BOVMTT ;BOVLAG
        BVVCL VARCL VARBIO VARAUC NOPRINT
NOAPPEND ONEHEADER
        FORMAT=, FILE=patab045.csv
;----------------------------------------------------------------------------
-----------------------------------------------
$TABLE     ID OCC WT2 HTM AGE FFM FAT CRCL VPC_TIME
EFV_DAYS,LPV_DAYS
        RPV_DAYS TDF_DAYS NOPRINT NOAPPEND
ONEHEADER FORMAT=,
        FILE=cotab045.csv
;----------------------------------------------------------------------------
-----------------------------------------------
$TABLE     ID OCC NAT2 HIVP SEXM RACEB PROB CFZ EFV
LPV RPV TDF
        NOPRINT NOAPPEND ONEHEADER FORMAT=,
FILE=catab045.csv
;----------------------------------------------------------------------------
-----------------------------------------------
$TABLE     ID OCC TIME TAD AA1 AA2 AMT ; AA3 AA4
        Y DV MDV PRED RES WRES IPRED IRES IWRES
CWRES CWRESI OBJI
        CL V KA BIO MTT NN ; V3 Q ; V4 Q2
        BSVCL BVVCL ;BSVV BSVKA BSVBIO BSVV3 BSVQ
BSVV4 BSVQ2
        BOVCL BOVKA BOVBIO BOVMTT VARCL VARBIO
VARAUC WT2 HTM AGE
        FFM FAT CRCL VPC_TIME EFV_DAYS,LPV_DAYS
RPV_DAYS TDF_DAYS
        NAT2 HIVP SEXM RACEB PROB CFZ EFV LPV RPV
TDF NOPRINT
        NOAPPEND ONEHEADER FORMAT=,
FILE=mytab045.csv
;----------------------------------------------------------------------------
-----------------------------------------------
```

Levofloxacin

```
;; 1. Based on: 067
;; 2. Description: + renal function
;; x1. Author: allan
;; 2022-09-23
; Settings for the memory of NONMEM
;----------------------------------------------------------------------------
-----------------------------
$SIZES                PD=-1000 LVR=-150 LTH=-200
MAXFCN=10000000 LNP4=-150000
$PROBLEM    ISA_LEVO
$INPUT          ID OCC WHAT=DROP EVID MDV AMT
DAT2=DROP TIME VPC_TIME DV
        ADDL=DROP II=DROP AGE SEXM HIVP HTM
WTKG=DROP RACEB NAT2
        BLQ PROB CENS LINEZOLID_DOSE=DROP VISIT_WK
PREDOSE
        ID_VISIT=DROP SWAP=DROP FLAG
CREATININE=DROP WT2 OBS
        CREATMGDL=DROP CRCL LEVO
$DATA                 ISA_Levo_data.csv IGNORE=#
IGNORE=(LEVO==0)
        IGNORE=(PROB.EQ.1)          IGNORE=(PROB.EQ.2)
IGNORE=(FLAG.EQ.3)
        IGNORE=(FLAG.EQ.4) IGNORE=(FLAG.EQ.5)
$SUBROUTINE ADVAN14 TRANS1 TOL=9 ATOL=9
$MODEL     NCOMPARTMENTS=2 COMP=(ABS DEFDOSE)
        COMP=(CENTRAL DEFOBSERVATION)
; ;----------------------------------------------------------------------------
$PK
SMALL = 1E-6
; ------ BSV
BSVCL   = ETA(1)
BSVV    = ETA(2)
BSVKA   = ETA(3)
BSVBIO  = ETA(4)
BSVV3   = ETA(5)
BSVQ = ETA(6)
BSVV4 = ETA(7)
BSVQ2 = ETA(8)
BSVMTT = ETA(9)

; ---------- BOV

BOVCL = 0
IF (OCC==1)BOVCL = ETA(10)
IF (OCC==2)BOVCL = ETA(11)
IF (OCC==3)BOVCL = ETA(12)
IF (OCC==4)BOVCL = ETA(13)
BOVBIO = 0
IF (OCC==1)BOVBIO = ETA(14)
IF (OCC==2)BOVBIO = ETA(15)
IF (OCC==3)BOVBIO = ETA(16)
IF (OCC==4)BOVBIO = ETA(17)
BOVKA = 0
IF (OCC==1)BOVKA = ETA(18)
IF (OCC==2)BOVKA = ETA(19)
IF (OCC==3)BOVKA = ETA(20)
IF (OCC==4)BOVKA = ETA(21)

BOVMTT = 0
IF (OCC==1)BOVMTT = ETA(22)
```

```
IF (OCC==2)BOVMTT = ETA(23)
IF (OCC==3)BOVMTT = ETA(24)
IF (OCC==4)BOVMTT = ETA(25)
;----------------
BVVCL = 0
IF (VISIT_WK==6)BVVCL = ETA(26)
IF (VISIT_WK==6)BVVCL = ETA(27)
E_BOV = THETA(10)
IF (OBS.EQ.0) THEN
BOVKA=E_BOV*BOVKA
BOVMTT=E_BOV*BOVMTT
BOVBIO=E_BOV*BOVBIO
ENDIF
; ---------- Calculation of Fat-free Mass
WT = WT2
SEX = SEXM
IF (SEX.EQ.0) THEN  ; female
            WHSMAX=37.99
            WHS50=35.98
ELSE       ;males
            WHSMAX=42.92
            WHS50=30.93
ENDIF
HTM2 = HTM**2
FFM = (WHSMAX*HTM2*WT)/(WHS50*HTM2+WT)
FAT = WT-FFM
IF (FAT.LT.0) FAT = 0
; ------- Typical values of covariates use MEDIAN WEIGHT
OF MY PPN
TVWT = 52
TVFAT = 10
TVFFM = 42
;--------- Allometric scaling and covariates
ALLMCL_WT = (WT2/TVWT)**0.75
ALLMV_WT = (WT2/TVWT)
ALLMCL_FAT = (FAT/TVFAT)**0.75
ALLMV_FAT = (FAT/TVFAT)
ALLMCL_FFM = (FFM/TVFFM)**0.75
ALLMV_FFM = (FFM/TVFFM)
;----------Allometry for liver
ALLMCL_WT_HEP = (WT2/70)**0.75
ALLMV_WT_HEP = (WT2/70)
 ALLMCL_FFM_HEP = (FFM/56.1)**0.75
ALLMV_FFM_HEP = (FFM/56.1)
;----------covariates
CFZ_CL = 1
IF(VISIT_WK==6) CFZ_CL = 1 + THETA(12)
;;----------renal function
eGFR_STD = CRCL*52/WT2
RF = 1 + THETA(13)*(eGFR_STD-85.7) ; 85.7 being my
median eGFR_STD
;---------Typical values--------
TVCL = THETA(1)*ALLMCL_FFM*CFZ_CL*RF ;
TVV = THETA(2)*ALLMV_FFM
TVKA = THETA(3);
TVBIO = THETA(4)
TVMTT = THETA(7)
TVNN = THETA(11)
TVV3 = THETA(8)*ALLMCL_FFM
TVQ = THETA(9)*ALLMCL_WT
;-----------Define parameters---------------
CL  = TVCL*EXP(BSVCL+BOVCL+BVVCL) ; CLEARANCE
V   = TVV*EXP(BSVV) ; CENTRAL VOL.
KA  = TVKA*EXP(BSVKA+BOVKA) ; ABS. RATE CONSTANT
BIO = TVBIO*EXP(BSVBIO+BOVBIO) ; BIOAVAILABILITY
MTT = TVMTT*EXP(BSVMTT+BOVMTT) ; MTT TIME
NN = TVNN ; Number of transit compartments
V3 = TVV3*EXP(BSVV3) ; PERIPH VOL
Q = TVQ*EXP(BSVQ) ; INTER COMPT CL
;-------------------------------------------------------------------
; re-parameterization
K = CL/V ;(rate constant of elimination)
K23 = Q/V   ; (rate constant from central to peripheral 1)
K32 = Q/V3 ;(rate constant from peripheral 1 to central)
;---------- Transit compartment absorption
F1=0
KTR = (NN+1)/MTT
IF (NEWIND/=2.OR.EVID>=3) THEN
            TNXD=TIME
            PNXD=AMT
ENDIF

TDOS=TNXD
PD=PNXD
IF(AMT>0) THEN
            TNXD=TIME
            PNXD=AMT
ENDIF
PIZZA = LOG(BIO*PD*KTR + 1E-12) - GAMLN(NN+1)
;;;-------------------------------------------------------------------
A_0(1) = SMALL
A_0(2) = SMALL
;A_0(3) = SMALL

$DES
TEMPO = T-TDOS
KTT = 0
TRANSIT = 0
IF(PD.GT.0.AND.TEMPO.GT.0) THEN
            KTT = KTR*(TEMPO)
            TRANSIT = EXP(PIZZA+NN*LOG(KTT)-KTT)
ENDIF

DADT(1) = TRANSIT -KA*A(1)
DADT(2) = KA*A(1) -K*A(2)

$ERROR
IPRED=A(2)/V
LLOQ = 0.078 ; DEFINE YOUR OWN LLOQ HERE
CENS_THR = LLOQ
PROP = IPRED*THETA(5)
ADD = THETA(6)+(LLOQ*0.2)
IF (ICALL/=4.AND.CENS==1) THEN
            ADD = ADD +(CENS_THR*0.5)
ENDIF
NO_FIT = 0
IF (ICALL/=4.AND.CENS==2) THEN
            PROP = 0
            ADD = 10000000000
            NO_FIT = 1
ENDIF
W = SQRT(ADD**2+PROP**2)
IRES=DV-IPRED
IWRES=IRES/W
Y = IPRED + W*ERR(1)
IF(AMT>0) THEN
```

```
        TIMEDOSE = TIME
        AMOUNTDOSE = AMT
ENDIF
TAD = TIME-TIMEDOSE
VARCL = BSVCL + BOVCL
VARBIO = BSVBIO + BOVBIO
VARAUC = BSVBIO + BOVBIO - BSVCL - BOVCL
VARABS = BOVKA - BSVMTT - BOVMTT

;-------------------------------------------RETRIEVE  AMOUNT  IN
EACH COMPARTMENT---
AA1 = A(1)
AA2 = A(2)

;--------------------Initial estimates
$THETA
(0,6.6998,50) ; 1 CL [L/h]
 (0,98.4989,300) ; 2 V [L]
 (0,1.99575,10) ; 3 KA [1/h]
 1 FIX ; 4 BIO
 (0,0.0502668,0.5) ; 5 PROP []
 (0.0156,0.235403,1) ; 6 ADD [mg/L]
 (0,1.31016,2) ; 7 MTT
 0 FIX ; 8 V3 [L]
 0 FIX ; 9 Q [L/h]
 (0,1.985,10) ; 10 E_BOV
 (0,16.7729,100) ; 11 NN
 (-0.99, -0.146, 10) ; 12 CFZ_CL
 (-0.0588,-0.01,0.0658) ; 13 CR_CL`
$OMEGA  BLOCK(1)
 0.0509292  ;   1 BSV CL
$OMEGA  BLOCK(1) FIX
 0  ;    2 BSV V
$OMEGA  BLOCK(1) FIX
 0  ;   3 BSV KA
$OMEGA  BLOCK(1) FIX
 0  ;  4 BSV BIO
$OMEGA  BLOCK(1) FIX
 0  ;    5 BSVV3
$OMEGA  BLOCK(1) FIX
 0  ;     6 BSVQ
$OMEGA  BLOCK(1) FIX
 0  ;    7 BSVV4
$OMEGA  BLOCK(1) FIX
 0  ;    8 BSVQ2
$OMEGA  BLOCK(1) FIX
 0  ;   9 BSVLAG
;------------------------------
$OMEGA  BLOCK(1) FIX
 0  ;   10 BOVCL
$OMEGA  BLOCK(1) SAME
$OMEGA  BLOCK(1) SAME
$OMEGA  BLOCK(1) SAME
$OMEGA  BLOCK(1)
 0.0424656  ;  14 BOVBIO
$OMEGA  BLOCK(1) SAME
$OMEGA  BLOCK(1) SAME
$OMEGA  BLOCK(1) SAME
$OMEGA  BLOCK(1)
 1.45592  ;   18 BOVKA
$OMEGA  BLOCK(1) SAME
$OMEGA  BLOCK(1) SAME
$OMEGA  BLOCK(1) SAME
$OMEGA  BLOCK(1)
 0.196686  ;  22 BOVLAG
$OMEGA  BLOCK(1) SAME
$OMEGA  BLOCK(1) SAME
$OMEGA  BLOCK(1) SAME
$OMEGA  BLOCK(1)
 0.0275387  ;   26 BVVCL
$OMEGA  BLOCK(1) SAME
;------------------------------------
$SIGMA  1  FIX
;-----------------------------
$ESTIMATION  MSFO=run070.msf  MAXEVAL=0  PRINT=1
METHOD=1 INTER NOABORT
        NSIG=4 NONINFETA=1 ETASTYPE=1 ;MCETA=1000
RANMETHOD=4P ; REPEAT
$ESTIMATION      MSFO=run070.msf      MAXEVAL=9999
PRINT=1 METHOD=1 INTER
        NOABORT  NSIG=3  NONINFETA=1  ETASTYPE=1
;MCETA=10
;----------------------------
$TABLE     ID OCC TIME TAD AA1 AA2 AMT ; AA3 AA4
        Y DV MDV PRED RES WRES IPRED IRES IWRES
CWRES CWRESI OBJI
        NOPRINT NOAPPEND ONEHEADER FORMAT=,
FILE=sdtab070.csv
;-------------------------
$TABLE     ID OCC CL V KA BIO MTT NN V3 Q ;V4 Q2 ;
        BSVCL ;BSVV BSVKA BSVBIO BSVV3 BSVQ BSVV4
BSVQ2
        BOVCL BOVKA BOVBIO BOVMTT ;BOVLAG
        VARCL VARBIO VARAUC NOPRINT NOAPPEND
ONEHEADER FORMAT=,
        FILE=patab070.csv
;----------------------------
$TABLE       ID OCC WT2 HTM AGE FFM FAT VPC_TIME
NOPRINT NOAPPEND
        ONEHEADER FORMAT=, FILE=cotab070.csv
;----------------------------
$TABLE    ID OCC NAT2 HIVP SEXM RACEB PROB VISIT_WK
NOPRINT NOAPPEND
        ONEHEADER FORMAT=, FILE=catab070.csv
;----------------------------
$TABLE     ID OCC TIME TAD AA1 AA2 AMT ; AA3 AA4
        Y DV MDV PRED RES WRES IPRED IRES IWRES
CWRES CWRESI OBJI
        CL V KA BIO MTT NN V3 Q ; NN V4 Q2
        BSVCL ;BSVV BSVKA BSVBIO BSVV3 BSVQ BSVV4
BSVQ2
        BOVCL BOVKA BOVBIO BOVMTT VARCL VARBIO
VARAUC WT2 HTM AGE
        FFM FAT VPC_TIME NAT2 HIVP SEXM RACEB PROB
VISIT_WK
        NOPRINT NOAPPEND ONEHEADER FORMAT=,
FILE=mytab070.csv
;-------------------------
```

Terizidone

```
;; 1. Based on: 007b
;; 2. Description: Restart at Maxwel's model
;; x1. Author: Allan
;; 2022-09-23
; Settings for the memory of NONMEM
```

```
;-------------------------------------------------------------------------------
$SIZES PD=-1000 LVR=-150 LTH=-200 MAXFCN=10000000 LNP4=-150000
;-------------------------------------------------------------------------------
$PROBLEM ISA_Terizidone
;-------------------------------------------------------------------------------
$INPUT ID OCC WHAT=DROP EVID MDV AMT_OLD AMT DAT2=DROP TIME
VPC_TIME DV AGE SEXM HIVP HTM WTKG=DROP RACEB NAT2=DROP
BLQ PROB CENS VISIT_WK PREDOSE DV_CYCLO=DROP ID_VISIT=DROP
SWAP=DROP OLD_DV_CYCLO=DROP FLAG CYC EFV EFV_DAYS OBS WT2
CREATININE CREATMGDL CRCL NAT_2 NAT_STATUS=DROP TOBACCO
CIGARETTE
;-------------------------------------------------------------------------------
$DATA ISA_cyc_data4.csv IGNORE=# IGNORE=(PROB==1)
IGNORE=(FLAG==1) IGNORE=(FLAG==3) IGNORE=(FLAG==4)

;-------------------------------------------------------------------------------
$SUBROUTINE ADVAN15 TRANS1 TOL=9 ATOL=9
;-------------------------------------------------------------------
$ABBREVIATED COMRES=2 ; For AUC and CMAX

;-----------------------------------------------------------
$MODEL NCOMPARTMENTS=3 COMP=(ABS DEFDOSE)
COMP=(CENTRAL DEFOBSERVATION) ; COMP=(CENTRAL DEFOBSERVATION)
COMP=(AUC)
; ;-------------------------------------------------------------------------
$PK
SMALL = 1E-6
; ------- BSV
BSVCL = ETA(1)
BSVV = ETA(2)
BSVKA = ETA(3)
BSVBIO = ETA(4)
BSVV3 = ETA(5)
BSVQ = ETA(6)
BSVV4 = ETA(7)
BSVQ2 = ETA(8)
BSVMTT = ETA(9)

; ---------- BOV

BOVCL = 0
IF (OCC==1)BOVCL = ETA(10)
IF (OCC==2)BOVCL = ETA(11)
IF (OCC==3)BOVCL = ETA(12)
IF (OCC==4)BOVCL = ETA(13)
BOVBIO = 0
IF (OCC==1)BOVBIO = ETA(14)
IF (OCC==2)BOVBIO = ETA(15)
IF (OCC==3)BOVBIO = ETA(16)
IF (OCC==4)BOVBIO = ETA(17)
BOVKA = 0
IF (OCC==1)BOVKA = ETA(18)
IF (OCC==2)BOVKA = ETA(19)
IF (OCC==3)BOVKA = ETA(20)
IF (OCC==4)BOVKA = ETA(21)

BOVMTT = 0
IF (OCC==1)BOVMTT = ETA(22)
IF (OCC==2)BOVMTT = ETA(23)
IF (OCC==3)BOVMTT = ETA(24)
IF (OCC==4)BOVMTT = ETA(25)
;----------VISIT_WK to CFZ
CFZ = 0
IF (VISIT_WK == 6) CFZ = 1
;----------between visit variability
BVVCL = 0
IF (CFZ == 0)BVVCL = ETA(26)
IF (CFZ == 1)BVVCL = ETA(27)
;----------------
E_BOV = THETA(10) ;extra bioavailability on all absorption parameters
IF (OBS.EQ.0) THEN
BOVKA=E_BOV*BOVKA
BOVMTT=E_BOV*BOVMTT
BOVBIO=E_BOV*BOVBIO
ENDIF
; ---------- Calculation of Fat-free Mass
WT = WT2
SEX = SEXM
IF (SEX.EQ.0) THEN ; female
WHSMAX=37.99
WHS50=35.98
ELSE ;males
WHSMAX=42.92
WHS50=30.93
ENDIF
HTM2 = HTM**2
FFM = (WHSMAX*HTM2*WT)/(WHS50*HTM2+WT)
FAT = WT-FFM
IF (FAT.LT.0) FAT = 0
; ------- Typical values of covariates
TVWT = 52
TVFAT = 10
TVFFM = 42
;--------- Allometric scaling and covariates
ALLMCL_WT = (WT/TVWT)**0.75
ALLMV_WT = (WT/TVWT)
ALLMCL_FAT = (FAT/TVFAT)**0.75
ALLMV_FAT = (FAT/TVFAT)
ALLMCL_FFM = (FFM/TVFFM)**0.75
ALLMV_FFM = (FFM/TVFFM)
;----------Allometry for liver
ALLMCL_WT_HEP = (WT/70)**0.75
ALLMV_WT_HEP = (WT/70)
ALLMCL_FFM_HEP = (FFM/56.1)**0.75
ALLMV_FFM_HEP = (FFM/56.1)
;-----------------------covariates
;Covariate test: CFZ_CL
CFZ_CL =1;slow
IF(CFZ.EQ.1) CFZ_CL =(1+THETA(12)) ;Inter
;Covariate test: smoking
CIG_CL =1;no smoking currently
```

```
IF(CIGARETTE.EQ.1) CIG_CL =(1+THETA(14)) ;Inter
; creatinine on renal clearance
IF(SEX==1) CRCLSTD = 1.23*(140-AGE)*WT/CREATININE
IF(SEX==0) CRCLSTD = 1.04*(140-AGE)*WT/CREATININE  ;
FEMALES
CRCLSTD47=100  ; ML/MIN
RF = CRCLSTD/CRCLSTD47
;---------Typical values----------

TVCLNR = THETA(1)*ALLMCL_FFM*CIG_CL;*CFZ_CL ;
TVCLR  = THETA(13)*RF
TVCL   = TVCLNR + TVCLR
TVV = THETA(2)*ALLMV_FFM
TVKA = THETA(3);
TVBIO = THETA(4)
TVMTT = THETA(7)
TVNN = THETA(11)
TVV3 = THETA(8)*ALLMCL_FFM
TVQ = THETA(9)*ALLMCL_WT
;----------Define parameters----------
CL  = TVCL*EXP(BSVCL+BOVCL+BVVCL) ; CLEARANCE
V   = TVV*EXP(BSVV) ; CENTRAL VOL.
KA  = TVKA*EXP(BSVKA+BOVKA) ; ABS. RATE CONSTANT
BIO = TVBIO*EXP(BSVBIO+BOVBIO) ; BIOAVAILABILITY
MTT = TVMTT*EXP(BSVMTT+BOVMTT) ; MTT TIME
NN = TVNN ; Number of transit compartments
V3 = TVV3*EXP(BSVV3) ; PERIPH VOL
Q = TVQ*EXP(BSVQ) ; INTER COMPT CL
;---
; re-parameterization
K = CL/V ;(rate constant of elimination)
K23 = Q/V   ; (rate constant from central to peripheral 1)
K32 = Q/V3 ;(rate constant from peripheral 1 to central)
; ; Transit compartment absorption
F1=0
KTR = (NN+1)/MTT
IF (NEWIND/=2.OR.EVID>=3) THEN
        TNXD=TIME
        PNXD=AMT
ENDIF
TDOS=TNXD
PD=PNXD
IF(AMT>0) THEN
        TNXD=TIME
        PNXD=AMT
ENDIF
PIZZA = LOG(BIO*PD*KTR + 1E-12) - GAMLN(NN+1)
;;;-------------------------------------------------------------
A_0(1) = SMALL
A_0(2) = SMALL
A_0(3) = SMALL
;;;-------------------------------------------------------------
IF (NEWIND.NE.2.OR.EVID.GE.3) THEN ; Each time I have
a new subject, or a reset
        COM(1)=0
        COM(2)=0
        TDOS = 0
ENDIF
;----------------------

$DES
TEMPO = T-TDOS ; this is time after dose for the transit, it
should always be >= 0
KTT = 0
TRANSIT = 0
IF(PD.GT.0.AND.TEMPO.GT.0) THEN
        KTT = KTR*(TEMPO)
        TRANSIT = EXP(PIZZA+NN*LOG(KTT)-KTT)
ENDIF
DADT(1) = TRANSIT -KA*A(1)
DADT(2) = KA*A(1) -K*A(2)
;-------------------------------
$ERROR
IPRED=A(2)/V
LLOQ = 0.313 ; DEFINE YOUR OWN LLOQ HERE
CENS_THR = LLOQ
PROP = IPRED*THETA(5)
ADD = THETA(6)+(LLOQ*0.2)
IF (ICALL/=4.AND.CENS==1) THEN
        ADD = ADD +(CENS_THR*0.5)
ENDIF
NO_FIT = 0
IF (ICALL/=4.AND.CENS==2) THEN
        PROP = 0
        ADD = 10000000000
        NO_FIT = 1
ENDIF
W = SQRT(ADD**2+PROP**2)
IF (W.LE.0.000001) W=0.000001
IRES=DV-IPRED
IWRES=IRES/W
Y = IPRED + W*ERR(1)
IF (ICALL==4.AND.Y<=CENS_THR) Y = CENS_THR/2
IF(AMT>0) THEN
        TIMEDOSE = TIME
        AMOUNTDOSE = AMT
ENDIF
TAD = TIME-TIMEDOSE
VARCL = BSVCL + BOVCL
VARBIO = BSVBIO + BOVBIO
VARAUC = BSVBIO + BOVBIO - BSVCL - BOVCL
VARABS = BOVKA - BSVMTT - BOVMTT
;-----------------------------------------RETRIEVE   AMOUNT   IN
EACH COMPARTMENT---
AA1 = A(1)
AA2 = A(2)
AA3 = A(3)
;----------------------------------Initial estimates
$THETA
(0,0.346,50) ; 1 CLNR [L/h]
 (0,23.2,300) ; 2 V [L]
 (0,0.832,10) ; 3 KA [1/h]
 1 FIX ; 4 BIO
 (0,0.0893,0.5) ; 5 PROP []
 (0,1.58,10) ; 6 ADD [mg/L]
 (0,0.785,2) ; 7 MTT
 0 FIX ; 8 V3 [L]
 0 FIX ; 9 Q [L/h]
 (0,0,10) FIX ; 10 E_BOV
 (0,4,100) FIX ; 11 NN
 0 FIX ; 12 CFZ_CL
 (0,0.43,5) ; 13 CLR
 (-0.99,0.411,5) ; 14 smking_CLNR
$OMEGA  BLOCK(1)
 0.106929  ;   1 BSV CL
$OMEGA  BLOCK(1) FIX
```

```
 0  ;    2 BSV V
$OMEGA  BLOCK(1) FIX
 0  ;   3 BSV KA
$OMEGA  BLOCK(1) FIX
 0  ;  4 BSV BIO
$OMEGA  BLOCK(1) FIX
 0  ;    5 BSVV3
$OMEGA  BLOCK(1) FIX
 0  ;     6 BSVQ
$OMEGA  BLOCK(1) FIX
 0  ;    7 BSVV4
$OMEGA  BLOCK(1) FIX
 0  ;    8 BSVQ2
$OMEGA  BLOCK(1) FIX
 0  ;   9 BSVMTT
;----------------------------------------
$OMEGA  BLOCK(1) FIX
 0  ;   10 BOVCL
$OMEGA  BLOCK(1) SAME
$OMEGA  BLOCK(1) SAME
$OMEGA  BLOCK(1) SAME
$OMEGA  BLOCK(1)
 0.022201  ;  14 BOVBIO
$OMEGA  BLOCK(1) SAME
$OMEGA  BLOCK(1) SAME
$OMEGA  BLOCK(1) SAME
$OMEGA  BLOCK(1)
 0.257049  ;   18 BOVKA
$OMEGA  BLOCK(1) SAME
$OMEGA  BLOCK(1) SAME
$OMEGA  BLOCK(1) SAME
$OMEGA  BLOCK(1)
 0.461041  ;  22 BOVMTT
$OMEGA  BLOCK(1) SAME
$OMEGA  BLOCK(1) SAME
$OMEGA  BLOCK(1) SAME
;----------------------------------------
$OMEGA  BLOCK(1)
 0.0324  ;     BVVCL
$OMEGA  BLOCK(1) SAME
;----------------------
$SIGMA  1  FIX
;----------------------
$ESTIMATION  MSFO=run015.msf  MAXEVAL=0  PRINT=1
METHOD=1 INTER NOABORT
        NSIG=3  NONINFETA=1  ETASTYPE=1  ;MCETA=1000
RANMETHOD=4P ; REPEAT

;----------------------
$TABLE     ID OCC TIME TAD AA1 AA2 AMT ; AA3 AA4
        Y  DV  MDV  PRED  RES  WRES  IPRED  IRES  IWRES
CWRES CWRESI OBJI
        NOPRINT  NOAPPEND  ONEHEADER  FORMAT=,
FILE=sdtab015.csv
;--------------------
$TABLE     ID OCC CL V KA BIO MTT NN AUC ;V4 Q2 ;
        BSVCL  BVVCL  ;BSVV  BSVKA  BSVBIO  BSVV3  BSVQ
BSVV4 BSVQ2
        BOVCL BOVKA BOVBIO BOVMTT ;BOVLAG
        VARCL  VARBIO  VARAUC  NOPRINT  NOAPPEND
ONEHEADER FORMAT=,
        FILE=patab015.csv
;----------------------
$TABLE       ID OCC WT2 HTM AGE FFM FAT VPC_TIME
NOPRINT NOAPPEND
        ONEHEADER FORMAT=, FILE=cotab015.csv
;----------------------
$TABLE       ID OCC HIVP SEXM RACEB PROB VISIT_WK
NOPRINT NOAPPEND
        ONEHEADER FORMAT=, FILE=catab015.csv
;------------------------
$TABLE     ID OCC TIME TAD AA1 AA2 AMT ; AA3 AA4
        Y  DV  MDV  PRED  RES  WRES  IPRED  IRES  IWRES
CWRES CWRESI OBJI
        CL V KA BIO MTT NN AUC ; NN V4 Q2
        BSVCL  BVVCL  ;BSVV  BSVKA  BSVBIO  BSVV3  BSVQ
BSVV4 BSVQ2
        BOVCL BOVKA BOVBIO BOVMTT VARCL VARBIO
VARAUC WT2 HTM AGE
        FFM  FAT  VPC_TIME  HIVP  SEXM  RACEB  PROB
VISIT_WK NOPRINT
        NOAPPEND  ONEHEADER  FORMAT=,
FILE=mytab015.csv
;--------------------------------------------------------------------------
-------------------------------------------
;--------------------------------------------------------------------------
-------------------------------------------
```